



HAL
open science

Predicting the response of the oceanic carbon cycle to climate change: eco-evolutionary modeling of the microbial loop and the role of viruses

Philippe Cherabier

► To cite this version:

Philippe Cherabier. Predicting the response of the oceanic carbon cycle to climate change: eco-evolutionary modeling of the microbial loop and the role of viruses. Ecology, environment. Sorbonne Université, 2022. English. NNT : 2022SORUS184 . tel-03828259

HAL Id: tel-03828259

<https://theses.hal.science/tel-03828259>

Submitted on 25 Oct 2022

HAL is a multi-disciplinary open access archive for the deposit and dissemination of scientific research documents, whether they are published or not. The documents may come from teaching and research institutions in France or abroad, or from public or private research centers.

L'archive ouverte pluridisciplinaire **HAL**, est destinée au dépôt et à la diffusion de documents scientifiques de niveau recherche, publiés ou non, émanant des établissements d'enseignement et de recherche français ou étrangers, des laboratoires publics ou privés.

Sorbonne Université

ED227 - Sciences de la nature et de l'Homme : évolution et écologie

préparée à l'Institut de biologie de l'École Normale Supérieure (IBENS)

Predicting the response of the oceanic carbon cycle to climate change: eco-evolutionary modeling of the microbial loop and the role of viruses

Philippe Cherabier

Thèse de doctorat en écologie et évolution

Dirigée par Régis Ferrière

Présentée et soutenue publiquement le 24 juin 2022.

COMPOSITION DU JURY

Elena Litchman Professeure	<i>Rapportrice</i>
Jean-Christophe Poggiale Professeur	<i>Rapporteur</i>
Marina Lévy Directrice de recherche CNRS (DR1)	<i>Examinatrice</i>
Ingrid Obernosterer Directrice de recherche CNRS (DR2)	<i>Examinatrice</i>
Joshua Weitz Professeur	<i>Examineur</i>
Régis Ferrière Professeur	<i>Directeur de thèse</i>



Acknowledgements

‘The most important thing in life will always be the people in this room. Right here, right now. *Salud mi familia.*’

Dominic Toretto, *Fast Five* (2011)

Joe Pesci knew the value of a short and impactful thank you. When accepting the Oscar in 1991 for his role in *The Goodfellas*, his speech was the following: ‘It was my privilege, thank you’. I am no Joe Pesci though, so allow me to paraphrase a little bit and develop what I am sure he meant to say: this thesis was the result of many interactions with a great deal of wonderful people, and it truly was my privilege to have them by my side during this journey.

First and foremost, I am grateful to my advisor Régis Ferrière for guiding me through these three years of research. Your insights, fresh ideas and most importantly your kindness meant a lot to me, and I wanted to thank you for our collaboration. I don’t think I would have enjoyed my thesis half as much if it weren’t for you! I also wish to thank Elena Litchman and Jean-Christophe Poggiale for accepting to review my thesis, and Marina Lévy, Ingrid Obernosterer and Joshua Weitz for being part of my jury.

Thank you to everyone in the Eco-Evolutionary Mathematics lab for being so kind and welcoming, it was always a pleasure to chat and discuss with you all. To current teammates Antonin, Mathieu, Boris, Elie, Jacopo, Jérémy, Sophia, Mathilde, Nathanaël, Laura and Philippine but also past ones Benjamin, Guillaume, Phuong, thank you for all the lunches, coffees and beer sessions. These times were a breath of fresh air when work was just too much! To everyone in Tucson at iGlobes, I am sad that COVID shortened my stay and that I wasn’t able to come back: thank you especially to Ruth Gosset who made sure my trip and stay were as smooth as possible, and for inviting me to my first (and only) rodeo.

I owe much of the work I did to the people I worked with: thank you very much to Sylvie Méléard, Olivier Aumont and Anh Le-Duy Pham for the projects we did together. A big part of this thesis relies on the use of bioclust, and I would not have been able to make it work if it were not for the great team managing it and helping its user: I would like to thank in particular Maël for his work, it really was a life saver to have him. To Laurent Bopp and

Acknowledgements

everyone in the biogeochemistry team, I am truly grateful for the talks in which I learned so much about your field.

Ces remerciements ne pourraient pas être complets sans mentionner la multitude d'amis qui m'ont soutenu pendant ma thèse, et que je ne peux hélas que citer par groupes par souci de place. À tous mes camarades et amis Conversationnaires, mille mercis pour la conversation, les mots gentils sur mes figures, les discussions politiques, les verres et les soirées jeux. Aux vieux de Barbey, que dire si ce n'est que la distance géographique qui nous sépare est trop grande, et les occasions de se retrouver trop rares, mais que j'ai bon espoir que cela change ! Pour la crème de la crème du MSV, un simple « bonne continuation » devrait suffire. Philou, Loulou et Loulou (quel nom de groupe choisir ?), merci pour les bonnes bouteilles partagées. À tous mes camarades IPEF thésards, je pense à vous, on en a vu le bout. Deux personnes méritent une petite mention tout de même : merci à Lugdiwine pour nos nombreux échanges de galères administratives, ils m'ont permis de naviguer (presque) sereinement dans le cycle de mobilité du ministère, et merci Agnès, qui m'a fait commencer à rédiger mon manuscrit : nos sessions piscine me manqueront ainsi que celles d'écriture, mais peut-être trouverai-je le temps de revenir à l'escalade ?

Dans ces moments, savoir qu'on a une famille sur laquelle on peut compter vaut plus que tout, et je peux dire avec sincérité que c'est mon cas. Dans tous les pays où elle se trouve, de la Grèce aux États-Unis, et dans toutes les villes, de Quincampoix à Londres, merci. À Ian et Caroline, je regrette de ne pas avoir trouvé de citation collant à ma thèse dans l'un des nombreux chefs d'œuvre que nous avons vus ensemble (ce n'est pas faute d'avoir essayé). Merci Caroline pour tous les gifs Buffy, les fils twitter, les messages insta quotidiens (qui n'ont pas duré longtemps) – l'autoroute de l'information a un nouvel axe grâce à toi. À Ian, merci à toi pour nos appels qui m'ont permis de prendre du recul sur ma thèse, mais aussi et surtout pour nos parties de PS4 qui m'ont permis de « m'échapper » très littéralement le temps d'une soirée. À mes parents enfin, pour toujours avoir été présents et m'avoir accompagné pas seulement le temps d'une thèse mais toute ma vie : Papa, Maman, merci du fond du cœur.

Emeline, comment exprimer toute ma reconnaissance envers toi en si peu de mots ? J'espère que tu sais déjà tout l'amour et l'admiration que je te porte, mais je ne pense pas que tu réalises à quel point tu m'étais vitale pendant ma thèse, et combien tu m'as soutenu. Te savoir à mes côtés était plus qu'un baume au cœur, c'était l'assurance de savoir que tout irait bien. Merci pour tout, mon amour.

Malgré tout le travail et le temps qu'elle a représenté, cette thèse n'arrive qu'à la deuxième place des grandes nouvelles de cette année. Comment ne pas terminer ces remerciements par celle qui a chamboulé notre vie, à sa maman et à moi ? Amalia, pour être le bébé chou le plus gentil de la terre, pour être celle qui par un seul regard me permet d'oublier tous mes soucis et qui arrive à me faire fondre avec un simple sourire du coin des lèvres, pour m'avoir surveillé pendant que j'écrivais ce manuscrit, merci. Ton papa t'aime très fort.

Abstract / Résumé

‘What are you doing here? Five words, or less.’

Buffy Summers, *Buffy the vampire slayer* (1997)

Abstract

Human activities are affecting ocean health dramatically. Climate change caused by anthropogenic greenhouse gas emission results in sea-surface warming, polar ice caps melting, ocean acidification, and changes in circulation and mixing regimes leading to stratification. All life forms in the ocean are impacted, primarily microorganisms which dominate ocean biodiversity and play a major role in global ecosystem function. Microbial communities have a capacity for rapid adaptation because of their large population sizes and short generation times, potentially altering the global cycles of carbon and nutrients in response to climate change, but these feedbacks are largely unresolved.

In this thesis, we focus on heterotrophic bacteria and their ability to remineralize dissolved organic matter into inorganic nutrients. This ‘microbial loop’ fuels a carbon recycling pathway, but its response to climate change is still poorly understood. Through eco-evolutionary modeling, we resolve the potential feedback loop resulting from bacterial adaptation in different oceanic regions, both at the surface and deep in the water column. We find that bacterial adaptation tends to mitigate the negative effect climate change has on dissolved organic matter regeneration, with varying degrees depending on the biogeographical region. In order to generate predictions of our model at the global scale, we develop a novel framework for integrating eco-evolutionary processes with Earth system models. We find that bacterial adaptation in the microbial loop adds uncertainty to global ocean ecosystem forecasts, and call for further eco-evolutionary studies at this scale. Finally, we extend our eco-evolutionary modeling framework to address the effect of bacteriophages – arguably a major demographic factor of bacterial populations. We present preliminary analyses of bacteriophages’ influence on the carbon cycle and how they may alter the speed and dynamics of bacterial adaptation to changing environments.

Overall, this thesis emphasizes two current 'blind spots' of Earth system models: an explicit representation of the microbial loop and the integration of eco-evolutionary processes that are mediated by ocean microorganisms.

Résumé

Les activités humaines ont un impact considérable sur la santé des océans. Le changement climatique causé par les émissions anthropiques de gaz à effet de serre entraîne un réchauffement de la surface de la mer, la fonte des calottes polaires, l'acidification des océans et des changements dans les régimes de circulation et de mélange conduisant à une stratification de la colonne d'eau. Toutes les formes de vie dans l'océan sont touchées, principalement les micro-organismes qui dominent la biodiversité des océans et jouent un rôle majeur dans la fonction des écosystèmes marins. Les communautés microbiennes ont une capacité d'adaptation rapide en raison de la taille importante de leurs populations et de la brièveté de leur temps de génération, ce qui peut potentiellement modifier les cycles globaux du carbone et des nutriments en réponse au changement climatique, mais ces rétroactions sont encore peu comprises.

Dans cette thèse, nous nous concentrons sur les bactéries hétérotrophes et leur capacité à reminéraliser la matière organique dissoute en nutriments inorganiques. Cette "boucle microbienne" alimente une voie de recyclage du carbone, mais sa réponse au changement climatique est encore mal déterminée. Grâce à une modélisation éco-évolutive, nous quantifions la boucle de rétroaction potentielle résultant de l'adaptation bactérienne dans différentes régions océaniques, tant à la surface qu'en profondeur dans la colonne d'eau. Nous constatons que l'adaptation bactérienne tend à atténuer l'effet négatif du changement climatique sur la régénération de la matière organique dissoute, avec des degrés variables selon la région biogéographique. Afin de tester les prédictions de notre modèle dans un contexte global, nous développons un nouveau cadre pour intégrer les processus éco-évolutifs aux modèles de circulation océanique. Nous constatons que l'adaptation bactérienne dans la boucle microbienne peut ajouter de l'incertitude à nos prévisions, et appelons à de nouvelles études éco-évolutives à cette échelle. Enfin, nous incluons les bactériophages dans notre modèle et étudions à la fois leur influence biogéochimique sur le cycle du carbone et la façon dont ils pourraient influencer la vitesse d'adaptation des bactéries aux environnements changeants.

Dans son ensemble, cette thèse met l'accent sur deux "angles morts" actuels des modèles du système terrestre : une représentation explicite de la boucle microbienne et l'intégration des processus éco-évolutifs dans l'analyse de sa dynamique en réponse aux changements globaux.

Keywords *Microbial loop, Eco-evolutionary processes, Natural selection, Adaptive dynamics, Oceans, Climate change.*

Mots clés *Boucle microbienne, Processus éco-évolutifs, Sélection naturelle, Dynamique adaptative, Océans, Changement climatique.*

Table of contents

Acknowledgements	i
Abstract / Résumé	iii
Table of contents	vii
1 The ocean, climate change and microbes	1
1.1 Ocean ecosystems and the flow of carbon	2
1.1.1 The global ocean, a major carbon trap	2
1.1.2 Microorganisms and biogeochemical cycles	3
1.2 Climate change and the carbon pump	7
1.2.1 Climate change and ocean feedback	9
1.2.2 Earth system models, a relevant tool for predictions	10
1.2.3 The underestimated importance of adaptation by natural selection	13
1.3 Thesis overview	16
2 Modeling the microbial loop	19
2.1 Design philosophy	20
2.1.1 General considerations and aim	20
2.1.2 An ecological representation of the microbial loop	24
2.1.3 The evolutionary framework	26
2.2 A mathematical description of the module	28
2.2.1 Temporal dynamics of the population	28
2.2.2 Integrating bacterial adaptation	29
2.2.3 Deriving the evolutionary equilibrium	30
2.3 Microbial loop adaptation in the aphotic zone	33
2.3.1 Initial state of the ecosystem	34
2.3.2 Effect of ocean warming and stratification on the ecosystem	36
2.3.3 Bacterial adaptation and its impact	38
2.4 Conclusion and perspectives	39
3 Predicting the response of primary production to climate change	41
3.1 A sea-surface ecosystem model for ocean productivity	42

3.1.1	Predicting the future of primary production	42
3.1.2	Ecosystem model	43
3.1.3	Initial state of the system	47
3.2	Eco-evolutionary responses of the system and impact on productivity	51
3.2.1	The direction of primary production variation is controlled by ecophysiological changes in the microbial loop	52
3.2.2	Bacterial adaptation in the microbial loop drives primary production	54
3.2.3	Warming causes different eco-evolutionary responses in different biogeographic regions	56
3.3	Conclusion and perspectives	58
3.3.1	Ecophysiological vs. eco-evolutionary predictions	58
3.3.2	Bridging eco-evolutionary modeling and sequence data	60
3.3.3	Model extensions and conclusion	61
4	Natural selection in Earth system models	63
4.1	Eco-evolutionary processes in ESMs, a current blindspot	64
4.1.1	The importance of adaptation for climate forecasting	64
4.1.2	State of the art	65
4.2	A proposed alternative: the selection gradient equations	67
4.2.1	Keeping the basic structure of current ESMs	67
4.2.2	Defining the selection gradient	69
4.2.3	Pros and cons of the method	72
4.2.4	Theoretical evaluation in a chemostat model	72
4.3	Bacterial growth efficiency in NEMO-PISCES	77
4.3.1	Methods	77
4.3.2	Results	81
4.4	Conclusions	88
5	Bacteriophages and the microbial loop	91
5.1	Viruses, players at the heart of the microbial loop	91
5.1.1	The biogeochemical importance of viral life cycles	91
5.1.2	Integrating bacteriophages in the microbial loop module	93
5.1.3	The NB-V model in the aphotic zone	97
5.2	Bacteriophage influence in a constant environment	99
5.2.1	Shifting the evolutionary stable strategy	99
5.2.2	Phages increase DOM recycling	102
5.3	Bacteriophage influence under ocean stratification	104
5.3.1	Eco-evolutionary response of the system	104
5.3.2	Can ocean stratification lead to phage extinction?	107
5.4	Conclusion and perspectives	109

6	Transduction, a viral mechanism influencing bacterial adaptation	111
6.1	Introduction	111
6.2	A mathematical model for transduction	113
6.2.1	Individual-level model of infection and transduction	113
6.2.2	Phage-bacteria population dynamics with mutation and transduction	116
6.2.3	Mutant invasion, Trait Substitution Sequence, and canonical equation of adaptive dynamics	117
6.2.4	Simulations	119
6.3	Results	119
6.3.1	Dynamics of bacterial adaptation without transduction	119
6.3.2	Mutant invasion with transduction	121
6.3.3	Rate of adaptation with transduction	123
6.3.4	Effect of transduction on bacterial adaptive diversification	126
6.4	Conclusions	128
A	Deriving the invasion fitness with transduction	132
B	Deriving the invasion probability with transduction	134
C	Convergence towards the stochastic canonical equation	141
	Concluding remarks	143
	Bibliography	147
	A Acronyms	169
	B Résumé long	171

Chapter 1

The ocean, climate change and microbes

‘Is it not a strange fate that we should suffer so much
fear and doubt for so small a thing? So small a thing!’

Boromir, *The Fellowship of the Ring* (1954)

‘The Blue Planet’, such is the name often given by people to Earth. From outer space, our planet does indeed look blue because of the vastness of the oceans, spanning across a majority of Earth’s surface. The importance of the global ocean goes beyond its size: thought to be the cradle of life, it still holds an important connection to humanity to this day. One third of the population lives within 100 km from the ocean, and much of the health and well-being of communities around the world rely on the state of the ocean. Human activities pose a serious threat to ocean health and its ecosystems, which could directly impact all ecosystem services provided by the ocean.

In this introductory chapter, we give a broad description of the context and detail the oceans’ role in global climate regulation. More specifically, we delve into the realm of marine ecosystems, which are at the foundation of a crucial biological carbon pump. We then describe the potential consequences of climate change on the ocean, particularly on the adaptation of microorganisms to environmental shifts, and underline the potential eco-evolutionary feedbacks resulting thereof. Finally, we present current modeling efforts to predict the scope of climate change, with the potential shortcoming induced by not taking eco-evolutionary processes into account.

1.1 Ocean ecosystems and the flow of carbon

1.1.1 The global ocean, a major carbon trap

The ocean plays a major role in regulating the global climate. In school, we learn that the water cycle originates in the ocean [259]: water from the surface evaporates, creating the clouds from which the rain falls, potentially hundreds if not thousands of kilometers away. But the ocean's role in climate goes beyond that: in particular, it is a key actor in the Earth's carbon cycle. It acts as a major carbon reservoir, second only to the lithosphere [235], and holds more than 50 times the amount of carbon present in the atmosphere (Figure 1.1).

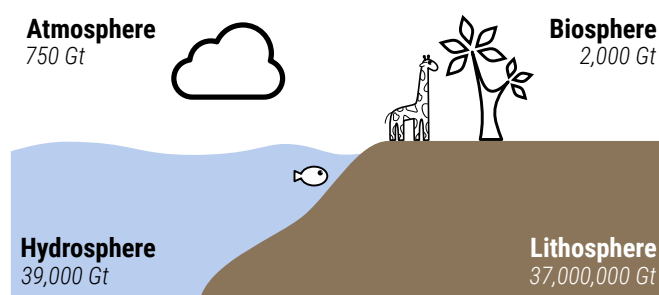


FIGURE 1.1: Carbon reservoirs of the Earth

The difference in partial pressures between atmospheric and aqueous CO_2 drives the dissolution of the former in the ocean [236]. On the timescale of millennia, the global ocean acts as a control on atmospheric CO_2 , and is expected to remove up to 90% of all anthropogenic carbon dioxide from the atmosphere [8]. On shorter timescales, it can also act as a strong buffer of variations in atmospheric CO_2 levels [88], with about a third of yearly man-made emissions estimated to be captured by the ocean [232, 124].

Ocean mixing can lead to large concentrations of carbon sinking to deeper layers of the sea [160], effectively trapping it. This pathway for trapping carbon in the ocean relies purely on physical properties (the 'solubility pump' [266] or 'physical pump'), but other mechanisms can trap carbon for geological times relying on oceanic ecosystems; this is the 'biological pump' [211].

To understand how efficient the biological pump really is, let us look at the distribution of a very important nutrient for life in the ocean: nitrate (Figure 1.2). We note a huge discrepancy between the poles and the tropics, with the difference spanning several orders of magnitude. Compare this to salinity, which lies roughly between 34 and 37 parts per thousand [32]: its value varies approximately by $\pm 10\%$. What makes one practically constant across the ocean while the other varies so much? Because of ocean mixing, we could expect nitrate to be as uniformly distributed as salt, but it is not. Nitrate, unlike salt, is what we call a 'nutrient', for it can be used by phytoplankton as a resource for fueling photosynthesis. Some oceanic regions are poor in nitrate because biological processes strip it from the surface at

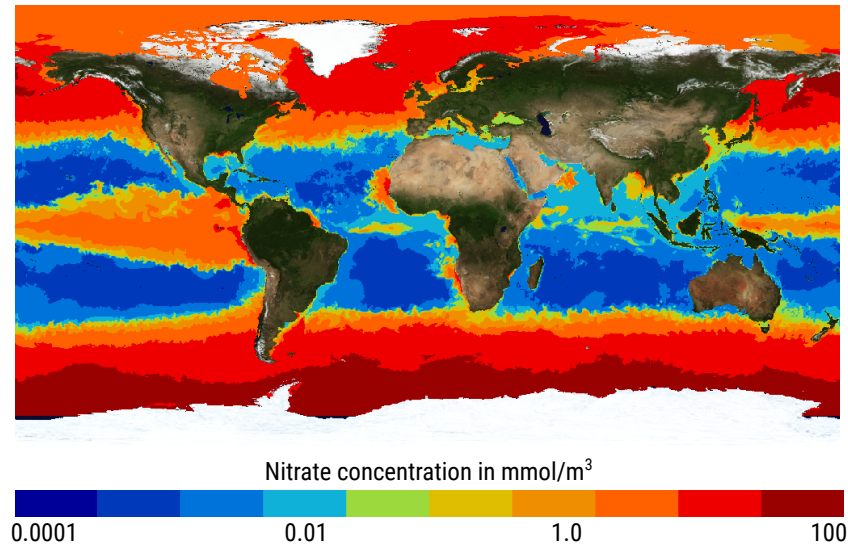


FIGURE 1.2: Nitrate distribution at the surface of the ocean. Source: Copernicus Marine Service Information [136].

a much faster rate than ocean mixing [236], leading to different biogeographical regions. By stripping the surface ocean from nutrients, oceanic ecosystems can lead to moving carbon from the surface to the bottom of the water column. But how exactly does this mechanism work?

Everything starts with CO₂ dissolution at the surface of the ocean, generating dissolved inorganic carbon (DIC). In this dissolved form, carbon can then be used by phytoplankton to create organic matter through photosynthesis. Phytoplankton are then grazed by zooplankton, and both are consumed by higher trophic level animals such as fishes and whales. Through death and egestion, all those individuals create particulate organic matter (POM), which then sinks to the bottom of the ocean (Figure 1.3). Once part of the sediment floor, carbon is considered locked and won't return to the atmosphere before up to millenia [211, 126].

Up until the mid 1970's, this pathway from small to large organisms (the 'food chain') was considered the only of importance for carbon in the ocean. But the food chain gradually became the food web [218], and more focus was given to microorganisms and their importance in biogeochemical cycles.

1.1.2 Microorganisms and biogeochemical cycles

The scientific community then realized that microorganisms dominate ocean biodiversity: as Falkowski, Fenchel, and Delong [94] aptly phrase it, the Earth's biogeochemical cycles are driven by microbial engines. Microbes may not seem like much at first glance (some you wouldn't even see with the naked eye!), but they amount to a lot when it comes to cli-

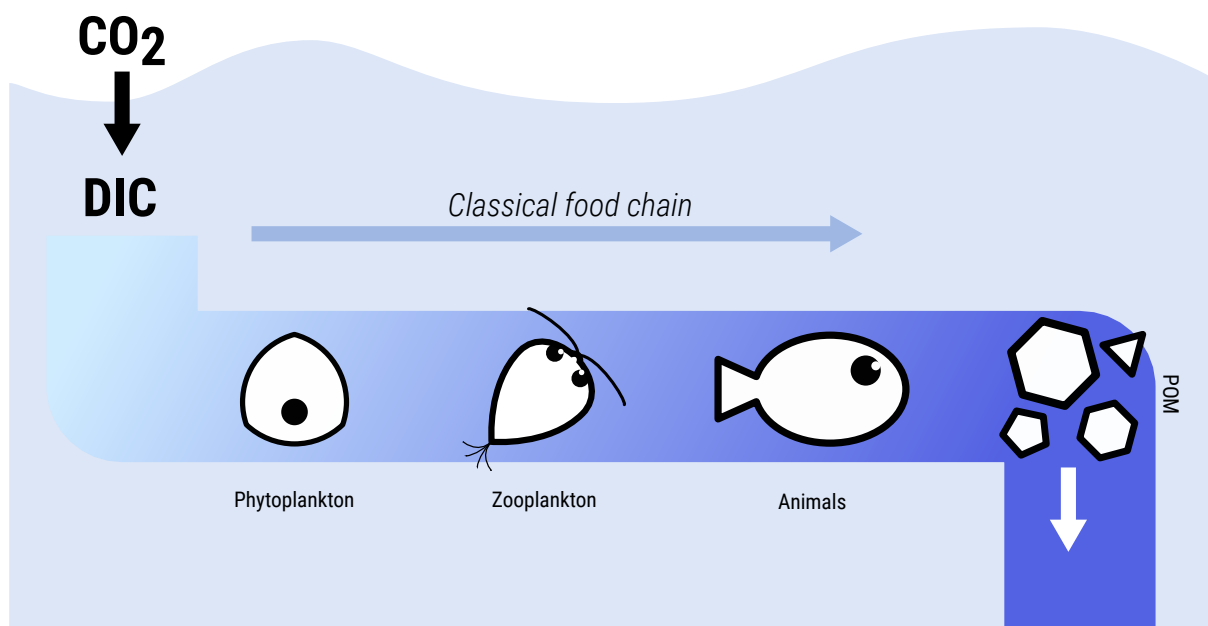


FIGURE 1.3: A representation of the main export pathway for organic carbon. The classical food chain: phytoplankton perform photosynthesis and move up carbon in the food chain to zooplankton and bigger animals through grazing and predation. Particulate organic matter (POM) is created through death and egestion, and sinks to the oceanic floor, trapping carbon over several millenia.

mate [134]. In order to comprehend just how influential these organisms can be, we first need to grasp how ubiquitous they are. For that, let us do the following experiment: we take a spoonful¹ of ocean water and see what we find in it.

First, how likely are we to catch the biggest animal there is on Earth with our spoon? Optimistic estimates² and a small calculation gives us just a little under 1 in 1 billion chance to end up fishing a blue whale that way. Compare that to the tiniest animals in the ocean, zooplankton: you would have 1 in 200 chance [207] to find one in your small ocean water sample.

Now let's turn to even smaller organisms: phytoplankton. Diatoms are amongst the largest phytoplankton species in the ocean, and you would find about 35 of them in your spoon [155]. They are a major actor in global biogeochemical cycles, as they perform about 20% of all primary production on Earth [171]. That means that 1 in every 5 breaths we take is directly attributable to diatoms, and this ratio goes up to 1 in every 2 breaths when taking into account all species of phytoplankton [99]. The most abundant type of phytoplankton are cyanobacteria, with about 500,000 cells ending up in your spoon [104]. Like their name suggests, cyanobacteria are a type of bacteria, meaning that unlike diatoms they are prokaryotic. Prokaryotes are way older than their nucleated counterparts, and photosynthesis is

¹ 1 tea spoon = 5ml.

² Considering a population of 25,000 whales [105] of length 30m and height 4m [81] in the first 500m of the ocean.

likely to have appeared in that group.

Cyanobacteria are not the only prokaryotes of the oceans, and other heterotrophic bacteria abound. Our spoonful contains no less than 5,000,000 bacteria in total [33]. Heterotrophic bacteria do not perform photosynthesis, and as such rely on organic matter to generate energy. By consuming organic matter produced by others, they remineralize otherwise lost carbon into nutrients: this pathway was dubbed the ‘microbial loop’ [17], and will be the focus of the next subsection.

Bacteria, numerous as they may be, are dwarfed in number by viruses. Dubbed by some as the ‘puppet masters of the ocean’ [33], bacteriophages³ outnumber bacteria by a ratio of 10:1. Practically speaking, your spoon contains no less than 50,000,000 of them right now! In addition to applying a strong ecological and evolutionary pressure on bacterial populations, bacteriophages exert a control over the nutrient cycle by short-circuiting both the classical food chain and the microbial loop through the viral shunt [277], which will be the subject of a following subsection.

The microbial loop

With the seminal work of Azam et al. [17] came the term ‘microbial loop’ to represent a different path for carbon in ocean ecosystems. The relationship between organic matter and heterotrophic bacteria is at the heart of this loop [194]. To understand the role of the microbial loop, remember that the classical food chain ends with POM sinking to the sediment floor, effectively trapping it over very long periods of time (Figure 1.3). However, only an estimated 1% of this flux reaches the bottom of the ocean [175, 261]: what happens to the 99% of the particles that don’t make it all the way down?

Sinking particles form a particular type of ecological niche, the ‘marine snow’ [4]. Marine snow is best described as a macroscopic aggregate of organic and inorganic matter sinking slowly to the depths of the ocean (as the name would suggest). It provides a hot spot for marine life, among which attached heterotrophic bacteria, which degrade POM [248]. Through the activity of hydrolytic exoenzymes [12], these microorganisms break down POM to lighter components in order to consume them.

If some of the POM is then turned into bacterial biomass or respired, this is not the case for the majority of the particles. Part of the result of POM degradation stays as particles, but too small to sink: together they form the dissolved organic matter (DOM) pool [130]. Do not let the name fool you as ‘dissolved’ organic matter is not dissolved in the chemical sense, but in an operational sense: any organic matter that passes a filter of a certain size (usually 0.7 μm) is considered part of the DOM category. This broad definition of DOM makes it a very diverse group, both organically and chemically [209]. In order to specify its nature,

³The specific name for bacterial viruses.

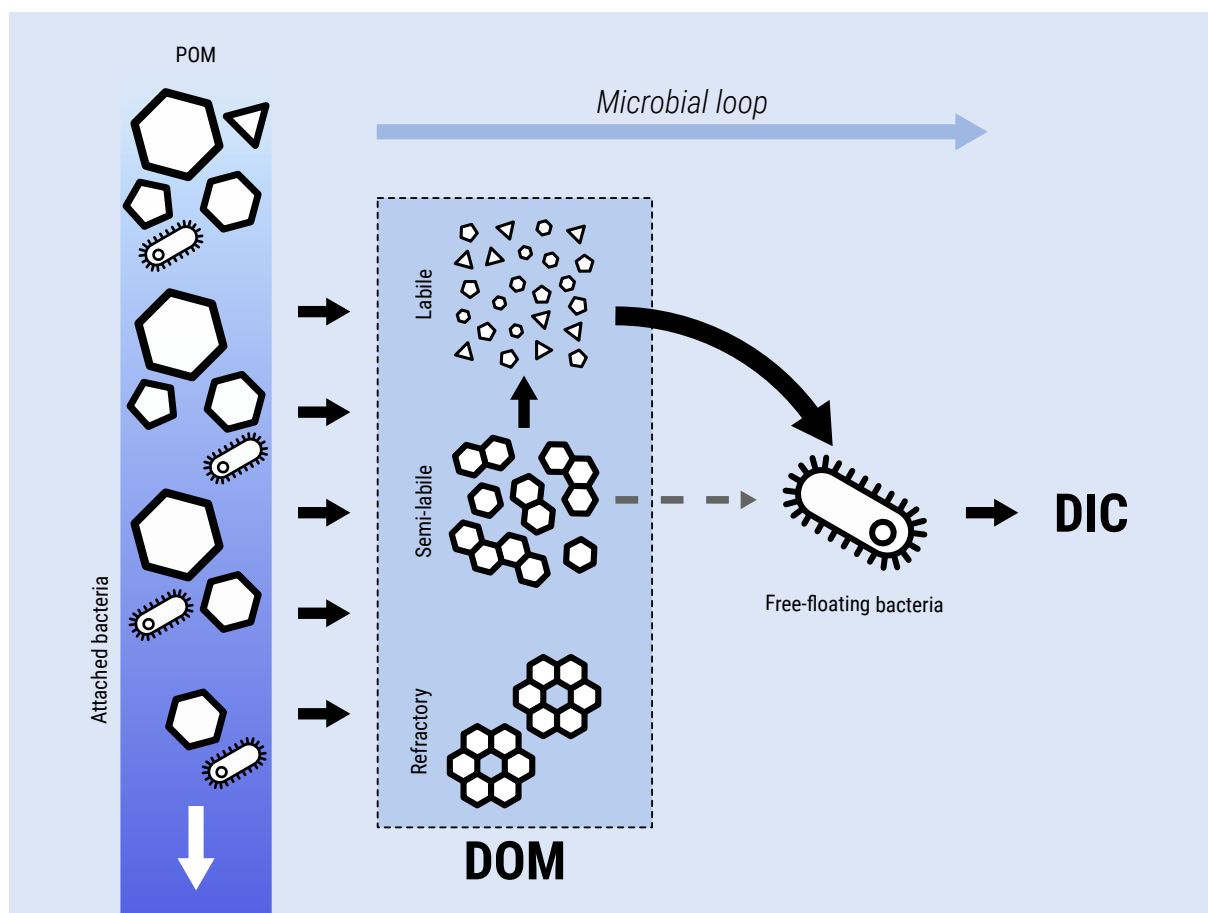


FIGURE 1.4: A representation of the microbial loop. Particles sinking are broken down by attached bacteria into dissolved organic matter (DOM), which is usually described by its chemical availability: labile, semi-labile and refractory. Labile and semi-labile DOM are consumed by free-floating bacteria which release carbon in its inorganic form through respiration, thus recycling nutrients.

DOM is categorized with regards to its reactivity to free-floating heterotrophic bacteria: this type of bacteria feeds on DOM and remineralize it to DIC, thus completing the recycling of nutrients. Generally, three DOM compartments are defined, from the most reactive to bacterial decomposition to the least: labile DOM, which has a turnover rate of just a few days, semi-labile DOM, which can have a turnover rate as high as a few months, and refractory DOM, which can stay in the ocean for several years.

In summary, the microbial loop represents the pathway that regenerates organic matter and carbon that should have exited the ecosystem (POM) into inorganic nutrients (Figure 1.4)

The viral shunt

The influence of viruses in the microbial loop and the biological pump has gained a lot of attention in the last twenty years [33]. On top of acting as a selecting pressure on bacteria [229]

and potentially directly tinkering with their metabolism [34], viruses affect the flow of carbon in marine ecosystem by triggering the direct release of DOM through lysis. When infecting a bacterial cell, bacteriophages have two broad phases they can enter: the lysogenic phase or the lytic phase [168, 165]. In the lysogenic phase, viruses integrate their DNA to their host, allowing them to reproduce when the host reproduces. On the contrary, when viruses enter the lytic phase, they induce a ‘viral burst’ of the host cell, which releases more virions in the environment. During this literal burst of the host cell, all matter not turned into viral biomass is by definition DOM. This ‘viral shunt’ [277] short-circuits the traditional food web and redirects carbon directly to the DOM pool.

Recent studies have shown a strong correlation between certain bacterial-phage communities (*Synechococcus* and their phages⁴) and carbon export in oligotrophic waters [126], and theoretical models show that the presence of viruses can increase primary production [274]. While underlying mechanisms are still to be fully determined, this suggests the importance of the viral shunt for global carbon cycling in the ocean, and calls for their inclusion in biogeochemical models.

A first general view of the biological carbon pump

The biological pump can be summarized by three components: the classical food web leading to carbon being trapped in the ocean floor for geological timescales, the microbial loop recycling part of the organic carbon into nutrients and the viral shunt moving carbon directly to the DOM pool and short-circuiting the entire food web (Figure 1.5).

These three components of the carbon pump work in unison to create a complex flow of carbon in the ecosystems in which microorganisms play a central role. In order to understand how the carbon cycle works in the ocean, and how it responds to climate change, it is necessary to focus on microbial communities and their relation to carbon.

1.2 Climate change and the carbon pump

Human activities and the emission of greenhouse gases (GHGs) have affected the climate in a major way, leading us to a new geological era: the Anthropocene [281]. The effects of these activities are already being felt today, with an increase in extreme climatic events [222] and a major biodiversity loss [20]. Climate change is bound to have dramatic effects on ocean ecosystems and the carbon pump, which is why being able to predict those effects has become an important research focus.

⁴Short for ‘bacteriophages’.

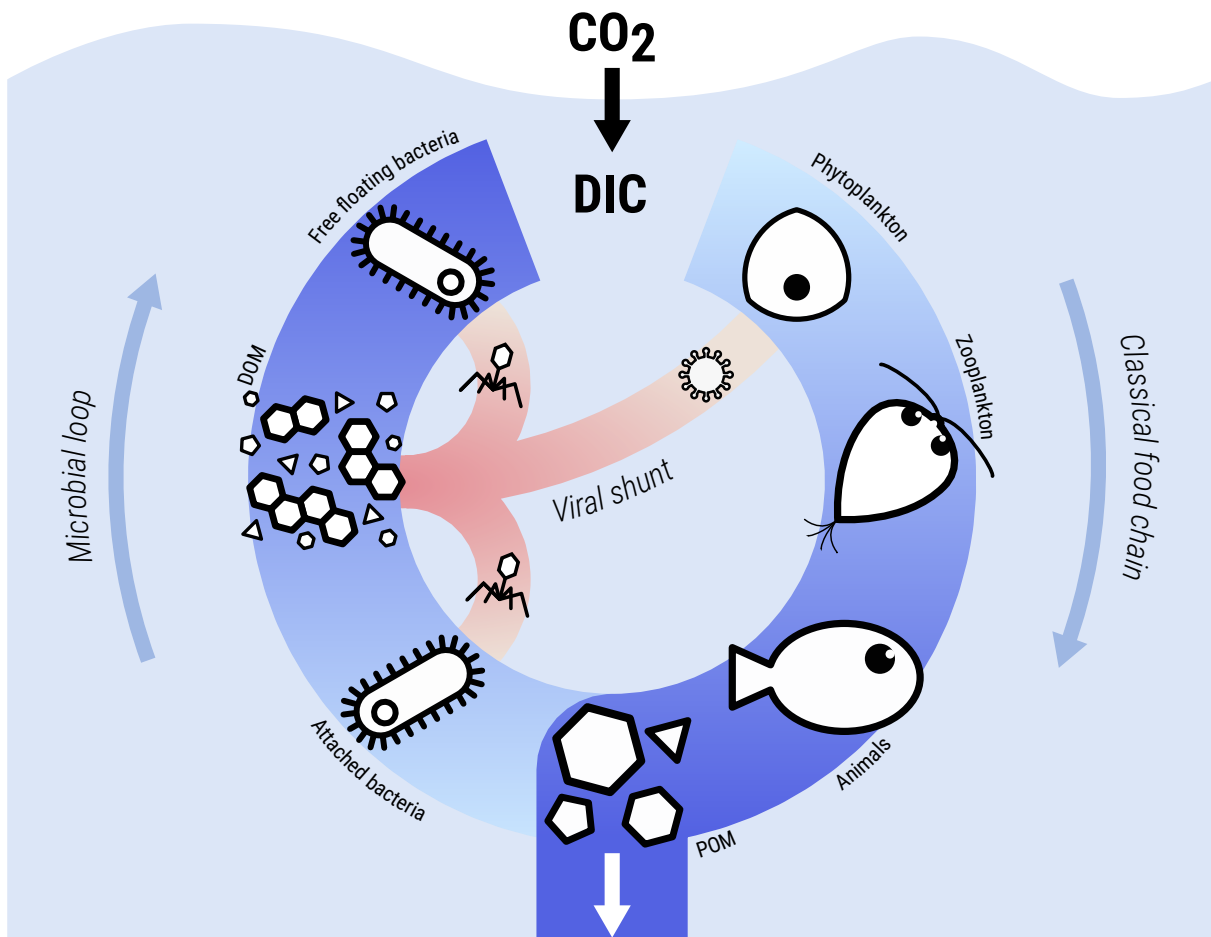


FIGURE 1.5: A representation of the biological carbon pump and carbon flow in the ocean. On the right side, the classical food chain: phytoplankton perform photosynthesis and move up carbon in the food chain to zooplankton and bigger animals through grazing and predation. Particulate organic matter (POM) is created through death and egestion, and sinks to the oceanic floor, trapping carbon over several millenia. On the left side, the microbial loop: through the action of attached bacteria living in marine snow, POM is degraded to dissolved organic matter (DOM), which is then remineralized into dissolved inorganic carbon (DIC) by free floating bacteria. In the center, the viral shunt: through lysis, marine viruses short-circuit the regular flow of carbon and move nutrients directly from unicellular organisms to the DOM pool.

1.2.1 Climate change and ocean feedback

Climate and the ocean are deeply intertwined. Changes to the climate brought by human activities will impact the ocean [28], and those changes will eventually feed back to climate. The different oceanic responses can either increase the rate of climate change (a ‘positive feedback loop’) or mitigate it (a ‘negative feedback loop’), and the difference between the two are bound to shape public policies around the world.

The ocean absorbs about a third of all yearly anthropogenic emissions of carbon [232, 124], which alters its chemical composition. This has led to strong acidification of the ocean [83], which could have dire consequences on marine life. For instance, many calcifying species will be impacted in their capacity to form shells, from phytoplankton to corals, leading to reduced primary production and more coral bleaching. The microbial loop will also be impacted, as nitrification rates decline as oceans acidify [24]. Decreasing nitrification results in reduced nutrient recycling, leading to lower oceanic productivity. This feedback is positive, as the effects favor a ‘snowball effect’ of the accumulation of carbon in the ocean.

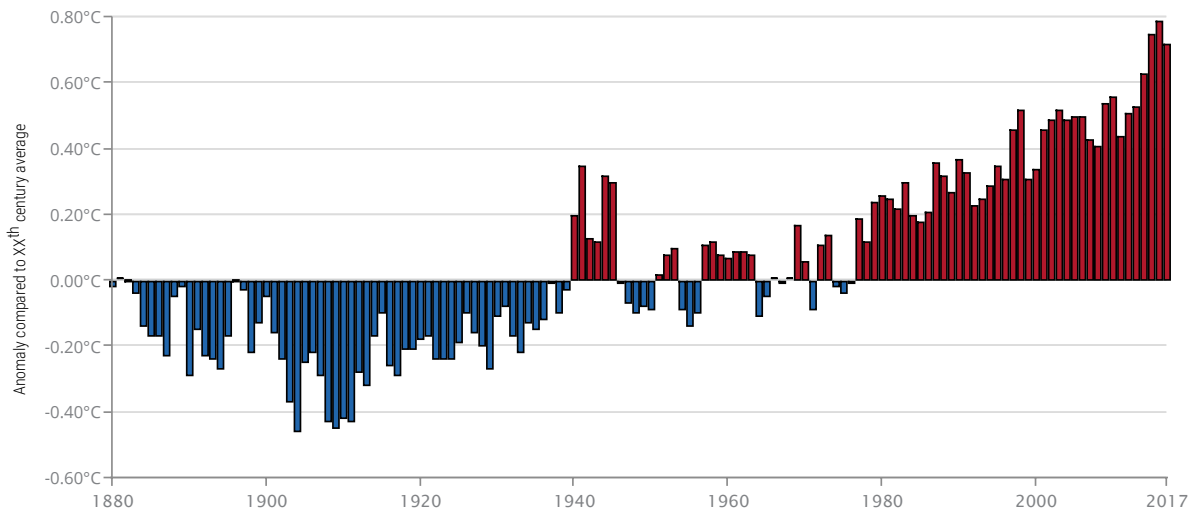


FIGURE 1.6: Sea-surface temperature anomalies. Annual sea-surface temperature anomalies are represented compared to the average temperature of the XXth century. Source: NOAA [89].

Numerous reports have concluded that the Earth is warming due to human activities, most notably the last IPCC report [177]. This includes the ocean, which has seen a surface temperature increase of roughly 0.7°C since 1880 [89] (Figure 1.6). This warming alters the ecological niches of many species as well as their metabolism, which leads to contrasting effects on ocean productivity, with higher individual growth rates for phytoplankton but more oligotrophic oceans [234]. Hence the difficulty when it comes to predicting how primary production will vary in the future [251, 150], even if the global trend seems to be towards a decline of primary production [177, 108]. While the confidence in these predictions is not 100%, it is likely that warming oceans feed back positively to climate change.

An increase in water temperature also has a direct consequence on physical properties of the ocean: in addition to sea-level rising [39], the ocean becomes more stratified [164], which has global climate consequences. Stratification leads to reduced convection from the deep sea [69], lowering nutrient influxes for surface ecosystems [108] and possibly altering heat and carbon storage capacity of the ocean [76]. All these effects reinforce the negative effects of climate change in a positive feedback loop.

Finally, increased stratification and a warmer ocean result in deoxygenation of the water column [244, 205]. Oxygen minimum zones are expanding, changing ecosystem structure and reducing potential fisheries catches [28], but they also have important climatic consequences: these regions are indeed linked to high emissions of nitrous oxide (N₂O), a potent GHG [9]. Once again, the feedback loop from oxygen depletion to climate change is positive.

Quantifying and predicting these potential feedbacks to the climate is a central topic for both scientist and public authorities [222]. Predicting how the climate will change by the end of the century is central to policy decisions, and the accuracy of these predictions can impact everyone's life. But how exactly do we proceed to make these life-changing predictions?

1.2.2 Earth system models, a relevant tool for predictions

This big question raises an even bigger one: how do we predict anything? From how long the commute from your home to your workplace might take tomorrow, to the future of climate, every prediction relies on the same basic tool, a model.

What is a model?

Oftentimes, the word 'model' sparks images of miniature trains and ships in bottles before numbers and equations. While the focus of this thesis will be on mathematical modeling, the two kinds of models are not unrelated. Indeed, just as a hobbyist modeler takes a complex object, downsizes it and simplifies it until it can fit miniature train tracks or a bottle, a mathematical modeler takes complex events, downsizes them and simplifies them using mathematical language and symbolism.

For instance, describing the dynamics of population growth over time can be modeled by the following differential equation:

$$\frac{dN}{dt} = r \times N \times \left(1 - \frac{N}{K}\right). \quad (1.1)$$

This is the 'logistic growth model' [260], and it aims at describing key ecological principles with just one equation. N represents the population size, r the population growth rate, and

K the carrying capacity of the environment (i.e., the largest population that can be sustained by a given environment). With just three parameters, we are able to describe the dynamics of a simple ecosystem in a way that matches observations reasonably well.

Before jumping into a specific model, we need to keep in mind what the end goal is. Models can be used for three general types of purposes:

- **Description:** The models used to describe are sometimes referred to as *phenomenological*, as they aim to reproduce observed phenomena without delving into mechanistic details. Models describing the relationship between bacterial growth rate and resource concentration such as the Monod equation [186] fall in this category.
- **Explanation:** Models can also be used to understand the emergence of certain properties. Contrary to descriptive models, the models used here try to focus on the basic building blocks of a mechanism so that key properties emerge from simpler interactions. For instance, the Lotka-Volterra cycles [270] emerge from the simple predator-prey interactions, but are not modeled *a priori*.
- **Prediction:** Models can be used to predict the behavior of a system in different settings. By taking a mechanistic model, and placing it in a new setting, we can predict what would happen in the real world. This is the case for general circulation models (GCM) and more broadly Earth system models (ESM), which will be a particular focus of this thesis [172].

Of course, the lines between description, explanation and prediction are not clearly drawn. Models used for prediction are not inherently different from models used for explanation: a model used for explanation in a novel setting provides a useful basis for predictions, and the building blocks of these models are often descriptive. The type of models used to predict the future of the ocean and climate are complex and intricate, and fall under the category of Earth system models.

Earth system models

Earth system models (ESM) are general models designed to represent the interactions between the different ‘systems’ of the planet: physical evolution of climate, biogeochemistry, and anthropogenic influence [103].

The first building block of ESMs is the modeling of climate itself and the physical laws governing its evolution. This is done by general circulation models (GCM) [169, 3], which describe how fluids move and interact through the Navier-Stokes equations [254]. This allows us to predict the movement and physical transformations of both the atmosphere and the hydrosphere on very large scales. When applied to the oceans, these models predict the

movements of water masses, the dynamics of currents and physical properties at the scale of the Earth.

GCMs can then be coupled to biogeochemical models to include the influence of biology on climate [15, 132]. Biogeochemistry is eloquently defined by the Encyclopedia Britannica as *'the study of the behaviour of inorganic chemical elements in biological systems of geologic scope'*. For instance, the study of the carbon cycle in ocean ecosystems from the previous section was a biogeochemical study. By implementing the dynamics of biotic components of the ocean (usually through differential equations between interacting compartments), ESMs are able to model the influence of climate on the biological carbon pump and assess the corresponding feedback.

The last piece of the puzzle necessary to predict the future of climate with ESMs is the inclusion of anthropogenic influence. This can be done by using Representative Concentration Pathways (RCPs) [252], which represent the trajectory of GHG concentration under different scenarios. For instance, RCP2.6 is an optimistic scenario in which global action is taken to insure global temperatures do not increase by more than 2°C by the end of the century; conversely, RCP8.5 is sometimes called the 'business as usual' scenario, in which no effort is made to lower GHG emissions. This could lead to an increase of temperature close to 4°C by the end of the century. To make the predictions, the climate models start from a climate state close to its contemporary state and run until the end of the century while we control the GHG concentration according to the chosen RCP.

In order to have the most accurate predictions possible, relying on one model is not enough. In order to evaluate climate models and compare them, a common framework was developed: the Coupled Model Intercomparison Project (CMIP). In its latest phase (CMIP Phase 6), 23 models using a common set of forcings are compared to address the Earth response to forcing, the origin and consequence of model biases and the assessment of future climate change [91].

ESMs integrate more and more complex mechanisms as they are developed in order to provide accurate assessments and predictions. For instance, the first climate models did not even include the biogeochemical cycles and only relied on physical components [172]. Notably, the microbial loop was rarely included even recently and bacteria treated implicitly [15], but this is starting to change [132, 87].

One component that is lacking from all current ESMs is biological adaptation by natural selection and the feedback it can provide to climate. Biogeochemical models used in ESMs are calibrated to represent the current state of the ocean, including ecosystems. They assume that the living communities present in the ocean a hundred year from now will not be sensibly different from contemporary ones [137]. While this may be the case for large organisms such as fishes and sea mammals, microorganisms are known to evolve rapidly to changing environments [111, 282]. As microbes are central to biogeochemical cycles [94],

taking into account their adaptive capacities is a central point of interest in order to provide a more accurate depiction of the potential future of the oceans under climate change [137, 187].

1.2.3 The underestimated importance of adaptation by natural selection

When talking about adaptation by natural selection, it is easy to picture dramatic changes in a species that gives it a definite advantage over its competitors. Such dramatic changes come about as rare ‘evolutionary innovations’, such as the apparition of citrate metabolism in bacteria [29]. In this thesis, we focus on ‘common’ evolution, whereby natural selection fine-tunes existing functions of a population.

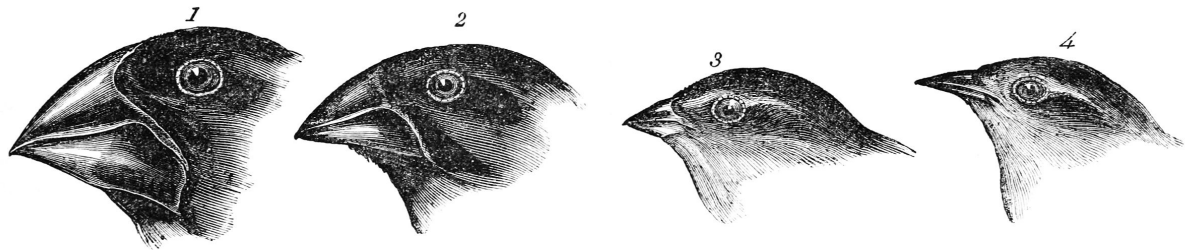


FIGURE 1.7: Darwin’s finches. (1) *Geospiza magnirostris*; (2) *Geospiza fortis*; (3) *Geospiza parvula*; (4) *Certhidea olivacea*. Source: *Journal and Remarks* [64].

Take Darwin’s finches for instance (Figure 1.7). These birds were first collected by Darwin in the early 1830’s during the second voyage of the HMS Beagle in the Galàpagos, surveying sea routes and completing nautical charts [64]. Darwin noted the remarkable diversity of beak form, which seemed perfectly adapted for different food sources. This observation helped him develop his theory of natural selection in his seminal work *On the Origin of species* [65].

For natural selection to take place, three conditions need to be met [162, 84]:

1. **Phenotypic variation:** in a population, individuals are intrinsically different.
2. **Differential fitness:** the differences in phenotype lead to different probabilities of survival and reproduction.
3. **Heritable variation:** phenotypic variation can be passed down between generations.

The strength of this framework is that it can be applied at any scale for which the conditions are met. For instance, we can study the evolution of beak form in the Galàpagos finches through this lense: to simplify, we focus on how natural selection lead to the coexistence of

finches with large beaks feeding on seeds and nuts (e.g. *Geospiza magnirostris*) and finches with small beaks feeding on small insects and worms (e.g. *Certhidea olacea*).

Let us go back to a time when all finches had similar beaks of intermediate size which allowed them to feed on both sources, though not as efficiently. One day⁵, a finch is born with a slightly larger beak (efficient for seeds and nuts) and another with a slightly smaller beak (efficient for insects and worms). By being more specialized in a certain type of food, these two new phenotypes thrive, and the ancestral finch is driven to extinction by the competition on both nuts and worms. This process can be iterated and repeated over many generations, eventually leading to the differentiation of beak forms (Figure 1.8).

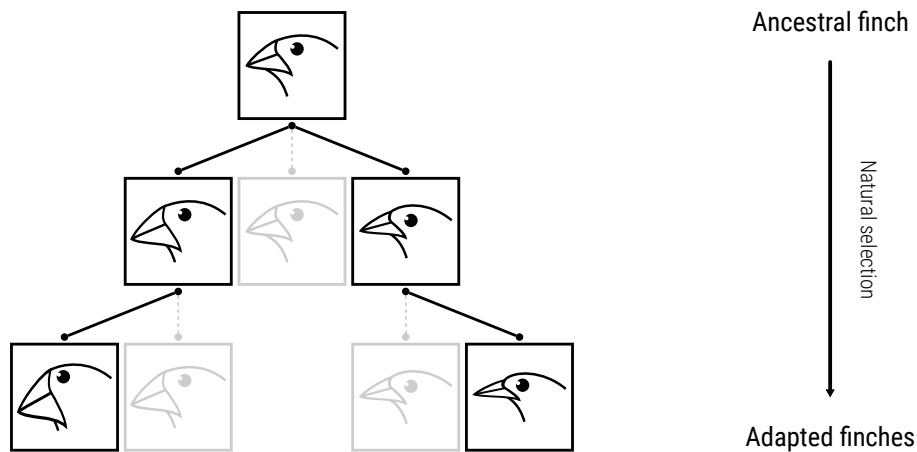


FIGURE 1.8: Adaptation of finches' beaks. From top to bottom, the different generations of finches with varying beak sizes. Extinction events are symbolized by grey boxes, and lineage is expressed by connecting lines.

With this simple example, we saw how the environment could induce the adaptation of a population. In return, populations act on the environment and modify it, leading to an eco-evolutionary feedback loop [97]. In the case of Darwin's finches, we could imagine that the population feeding on nuts will favor the spread of nut trees by eating and sowing seeds, thus changing the general landscape of the island. Eventually, this loop may converge towards a steady-state: in this situation, the population has reached the evolutionary stable strategy (see Toolbox 1.1).

⁵Naturally, in the real world these events happen over a long period of time and not simultaneously.

Toolbox 1.1 *The evolutionary stable strategy (ESS)*

When natural selection leads to a state where the resident population can no longer be replaced by fitter populations, we say that the resident has reached an *evolutionary stable strategy* (ESS) [249].

In this thesis, we focus on evolutionary stable strategies as ‘outcomes’ of natural selection to assess its importance on climate change, but we need to keep in mind that it is not the only possible outcome. For instance, natural selection can lead to evolutionary branching, a state where selection actually leads to coexistence of multiple phenotypes [73].

Oceanic microorganisms have a strong potential for rapid adaptation through selection, a fact that has long been hinted at by laboratory experiments [26], and recently been confirmed *in vivo*: adaptation to increased temperature in the zooplankton *Daphnia magna* occurred in as little as 2 years, resulting in an increase in thermal tolerance of 3.5°C [113], and adaptation to increased temperature has been documented in the phytoplankton *Chlorella vulgaris* in as little as 100 generations [206]. These examples illustrate the potential for evolution at speed comparable to plastic and ecological responses to climate change.

The adaptation of functional traits involved in the carbon cycle (‘C cycling traits’ [187]) has the potential to feed back to climate change in ways that could upset current predictions of future atmospheric CO₂ predictions [137]. Relevant traits include C fixation rates in phytoplankton [140], nitrogen fixation and growth rates in cyanobacteria [135, 268]. A decade-long mesocosm experiment found that, under increased temperatures, populations of the algae *Chlamydomonas reinhardtii* evolved 3.5-fold greater net photosynthesis compared with populations evolved under ambient temperatures [240]. Likewise, under experimentally increased CO₂ and acidification, *Gephyrocapsa oceanica* evolved higher photosynthetic C fixation and growth rates [140]. These experiments suggest that autotrophic adaptive trait evolution driven by climate change can increase photosynthesis relative to respiration – a potentially negative feedback to atmospheric CO₂. Altogether, such studies suggest that selection caused by increased temperature or acidification acts in directions that increase the net flux of C from the atmosphere to biotic and abiotic storage pools and produce a negative feedback loop to atmospheric CO₂. Generalization, however, is premature. Under experimentally increased CO₂ and acidification, *Phaeodactylum tricorutum* evolved reduced photosynthesis, respiration, and growth rates [163]. Moreover, adaptive evolution can occur in the opposite direction of plastic responses. For example, under ocean acidification, phytoplankton often decrease rates of photosynthesis plastically, in the opposite direction to evolutionary increase in photosynthetic rates [59].

In addition to phytoplankton adaptation, the feedback induced by heterotrophic bacteria has the potential to alter global biogeochemical cycles. Bacterial biomass may not be a major carbon reservoir, but the carbon fluxes going through heterotrophic bacteria are

amongst the most important [189]: bacterial respiration in particular represents most of the respiration occurring in the oceans [228] and could determine whether the global ocean is a source or a sink of carbon [71]. Heterotrophic bacterial C cycling traits include bacterial carbon demand [263], enzyme temperature sensitivity [6] or bacterial growth efficiency [233]. Heterotrophic bacterial adaptation in terrestrial environment is likely to aggravate carbon loss to the atmosphere [2], establishing a positive feedback to atmospheric CO₂, but similar results in the ocean have yet to be established.

Such complexities speak to the need for greater understanding of eco-evolutionary feedbacks emerging from the individual and population responses of functional traits across whole ecosystems.

1.3 Thesis overview

The general aim of this thesis is to assess the impact of microorganism adaptation on biogeochemical cycles and the potential feedback to climate change. A particular point of interest was the influence of viruses on climate change, both on biogeochemical cycles (through the viral shunt) and on bacterial adaptation (through transduction). In both their action through the viral shunt and transduction, viruses affect heterotrophic bacteria and the microbial loop. In order to understand phage role in global biogeochemical cycles, a detailed study of heterotrophic bacteria and their adaptation in the microbial loop was needed. Indeed, whereas a body of theory exists for phytoplankton adaptation [241] in response to the rise of sea surface temperature, microbial loop function and its response to climate change are still poorly understood. Working at the scale of the global ocean is necessary to properly assess the impact of microbial adaptation on global biogeochemical cycles. In this thesis, we propose a novel framework to integrate adaptation by natural selection in the current generation of ESMs and apply it to the study of heterotrophic bacteria adaptation.

In **Chapter 2**, we explain the philosophy behind our modeling of the microbial loop in absence of viruses. We use an ecological compartments describing bacterial biomass and DOM concentration, coupled with a trait-based model of bacterial metabolism. The resulting microbial loop model is designed to be easily coupled with larger classes of models, from toy-models of the water column to complex Earth system models. General results are derived regarding the bacterial evolutionary stable strategy, and the model is applied to the study of DOM remineralization deep in the water column under ocean warming and stratification.

We apply our framework to an extensive study of a sea-surface ecosystem in **Chapter 3**. We aim to understand the response of both new and regenerated production to increased temperatures, and how bacterial adaptation shifts microbial loop function. We divide biogeographical regions according to their richness in nutrients and to their initial temperatures and quantify the relative strengths of the ecophysiological response and the effect of bacte-

rial adaptation.

In order to test the predictions of our theoretical model, we develop a novel framework for integrating eco-evolutionary processes in ESMs in **Chapter 4**. Future climate forecasts fail to take microbial adaptation into account, which may have important consequences on biogeochemical cycle. To make the computation biologically reliable and computationally cheap, we implement bacterial adaptation as the dynamical optimization of a community trait through a phenomenological description of adaptation: the selection gradient. We apply it to the study of the microbial loop adaptation in the NEMO-PISCES ESM to assess the uncertainty brought by taking bacterial adaptation into account.

In **Chapter 5**, we introduce a viral compartment to the microbial loop model. Through increased bacterial mortality and the viral shunt, bacteriophages influence microbial loop function and thus biogeochemical cycles. We resolve the effect they have on bacterial adaptation and the remineralization power of the microbial loop in a constant environment, and compute the ecosystem response to ocean stratification. We discuss the potential for bacterial adaptation to drive bacteriophages to extinction and the potential consequences for biogeochemical cycles in the ocean.

Chapter 6 focuses on the influence of transduction on bacterial adaptation. Transduction - horizontal gene transfer by viruses - is an important macroevolutionary force in prokaryotes, contributing to functional innovation and lineage diversification. In contrast, the role that transduction play in bacterial microevolutionary adaptation is poorly known. By facilitating the transfer of beneficial alleles between host cells, transduction may accelerate adaptation. But transduction also carries the risk of transferring deleterious alleles, which, in addition to the ecological cost of viral infection, may hinder adaptation. Here we resolve the conflicting effects of transduction on bacterial adaptation in a simple eco-evolutionary model for large populations characterized by a quantitative (resource-use) trait with a single evolutionary optimum.

Chapter 2

Modeling the microbial loop

‘- Once more let’s go over the entire plan and layout. I apologize for the crudity of this model but I just...

‘- Yeah Doc’ I know, it’s not to scale.’

Dr. Emmett Brown & Marty McFly, *Back to the future III* (1990)

Modeling aims at striking a balance between having detailed enough models to represent reality, yet simple enough to study and understand their underlying mechanisms. The most important question to ask ourselves when modeling is ‘*why?*’ Why do we want to model the microbial loop? In the context of this thesis, modeling the microbial loop will allow us to understand and predict the response of nutrient recycling to climate change and the impact it might have on the ocean carbon cycle. The goal is thus to design a model of the microbial loop that could easily fit a larger class of models, from theoretical sea-surface ecosystems to ESMs.

In this chapter, we first explain the aim of the microbial loop module and lay out the eco-evolutionary analysis scheme of the thesis. We then design the ecological module representing the microbial loop in an abstract setting, where inputs and outputs can be tuned to represent different ecosystems of varying complexity. We then describe the eco-evolutionary framework used for this thesis, focusing on the traits and trade-offs. Finally, we focus on a simple application of the module by applying our module to the study of the microbial loop in the aphotic zone of the ocean. In this part of the water column that isn’t reached by sunlight, the system has the advantage of being mainly comprised of bacteria and sinking organic matter, which provides an interesting case-study for our model.

2.1 Design philosophy

In this section, we explain the goal of the model as well as the design philosophy and modeling choices leading to it. We try asking ourselves the simple question ‘*why?*’ at every step of the way, and see how it can lead to a number of choices that should be discussed and analyzed.

2.1.1 General considerations and aim

The model determined in this chapter will be used throughout the thesis (with the exception of Chapter 6), so the choice was made to develop a ‘module’ that could easily fit different classes of models depending on the study. We talk about a ‘module’ and not a model, because we intentionally leave parts of the larger model undetermined (Figure 2.1). Our microbial loop module has a set of inputs and outputs that can be ‘connected’ to a larger model \mathcal{M} depending on the study. This approach allows us to perform base analysis of the microbial loop in the most general cases, and apply the results to the different models implementing the module.

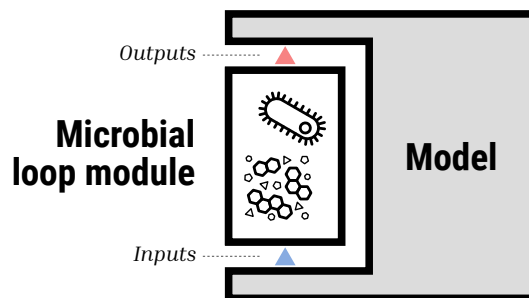


FIGURE 2.1: General representation of the modeling framework. The microbial loop module described in this chapter can be ‘connected’ to a larger model depending on the research question.

Assessing the effect of bacterial adaptation on an ecosystem

The first goal of the theoretical models built and analyzed in this thesis is to compute and assess the effects of bacterial adaptation on an ecosystem under climate change. To do so, we need a general analysis framework, which we describe here. Environmental change is supposed to be gradual, and on a timescale orders of magnitude longer than eco-evolutionary processes. This allows us to consider bacterial populations at eco-evolutionary equilibrium at all time, which enables us to isolate the effect of adaptation on the system.

Let us consider an environmental variable e that represents the state of the environment in one point in time. Metabolic functions such as bacterial growth rate or waste production can depend on the variable e , allowing us to quantify the effect of environmental changes

on the ecosystem. What e represents depends on the research question we aim to answer: it could simply be the temperature of the system or something more complicated such as a multi-dimensional variable representing ocean acidity, atmospheric carbon concentration and temperature all together.

To isolate the effect of bacterial adaptation of a trait x , we use and extend the analysis scheme developed in Abs and Ferrière [1]. We compare ecological and evolutionary steady states under three distinct scenarios:

1. **Initial adaptation.** Initially, the system is locally adapted to a given environment e_0 . The corresponding bacterial evolutionary stable strategy is denoted by x_0 .
2. **Ecophysiological scenario.** Here, the environment has shifted from its initial value e_0 to its final value e_1 . Environment-dependant parameters of the ecosystem respond to this environmental change, but we control the model to prevent bacterial adaptation: trait value remains at $x = x_0$.
3. **Eco-evolutionary scenario.** As the environment gradually shifts from e_0 to e_1 , the adaptive capacity of heterotrophic bacteria is included, and the trait evolves from x_0 in an environment e_0 to the new evolutionary stable value x_1 at e_1 .

By comparing the ecophysiological scenario to the initial adaptation, we can compute the broad ecophysiological response of the system in absence of bacterial adaptation. Similarly, comparing the eco-evolutionary scenario to the initial adaptation gives us the eco-evolutionary response of the system. Then, the difference between the ecophysiological and eco-evolutionary responses provides us with a measure of the effect of bacterial adaptation on ecosystem function (Figure 2.2). An example of this analysis scheme will be given later in this chapter, and the studies of Chapters 3 and 5 rely on this method.

The nature of environmental changes considered in this thesis depends on the ecosystem. The water column, in which all our studies take place, can be divided into two broad categories: the surface ocean and the deep ocean. The limit between the two can be defined from physical properties, with the surface layer being the ‘mixed layer’ in which biogeochemical properties are considered homogenized by active turbulence [62] whereas deeper layers are more stratified; or through light penetration, with the surface layer being the ‘euphotic zone’ where light is sufficient for phytoplankton to perform photosynthesis, and the deeper layer being the ‘aphotic zone’, where no photosynthesis can be achieved [157]. We do not make the distinction between ‘mixed layer’ and ‘euphotic zone’ in this thesis, as for the level of detail we’re focusing on both definitions can be considered roughly equal [212].

The warming of the atmosphere directly induces sea-surface warming [89], which in turn impacts the ecosystems of the mixed layer. The metabolic response of bacterial communities to a temperature increase has been thoroughly studied and modeled [263, 167, 197], but

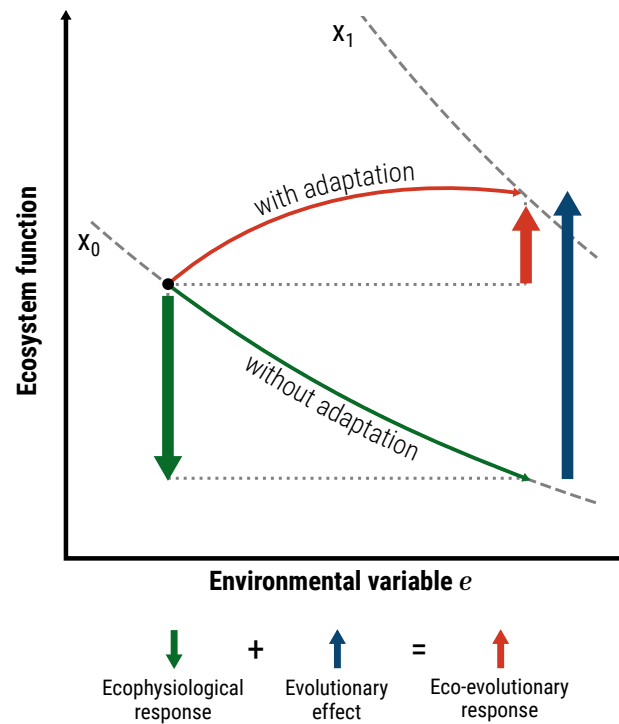


FIGURE 2.2: Untangling eco-evolutionary effects of environmental change on the ecosystem. Ecosystem variations in absence of bacterial adaptation are represented in green, ecosystem variations in presence of bacterial adaptation are represented in red, and the isolated effect of bacterial adaptation is represented in blue.

the ecosystem-wide response is still to be determined. For models focusing on sea-surface ecosystems, the variable e chosen to represent environmental change shall thus be temperature.

Because of the physical barrier between the mixed layer and deeper in the water column, sea-surface warming would not immediately increase deep water temperatures, but actually increase the physical and biogeochemical differences between the layers, resulting in a more stratified ocean [164]. This stratification would result in a decrease in particles sinking [204], which translates as a decrease in nutrient input in deep-water ecosystems. For models focusing on deep-water ecosystems, the variable e chosen to represent environmental change shall thus be the external nutrient input.

Choosing the right type of model

Translating biological realities to mathematical concepts can be done in a number of ways, and a wide variety of model types can be considered for our module, both for the ecological side and the evolutionary side. Individual-based models [22] have the advantage of allowing ecosystem-wide functions to emerge from individual interactions, but on the other hand global compartment models [55] are simpler to simulate and study. Modeling bacterial metabolism can be done through precise thermodynamic considerations [256, 237], more general considerations of energy budgets [156] or even relying on environmental conditions alone through resource concentrations considerations [186].

Keeping in mind that the end goal of our module is ESM integration, we need to look at how these types of models represent ecosystems. The ocean biogeochemistry model NEMO-PISCES [15] chosen for this thesis (see Chapter 4) works with a compartment model, and this seems to be a common choice for large scale studies [132, 86]. Our module should fit this larger class of models, so we choose to model all populations and resources as compartments. Here, each compartment is represented by its concentration (for resources) or its total biomass (for populations), and temporal dynamics are determined by differential equations. Similarly, all metabolic functions rely on external concentration of nutrients rather than internal energy budgets.

Eco-evolutionary processes can be integrated through a direct quantitative genetic approach [241, 58], by focusing on taxons and phylogeny [190] or by focusing on phenotype and individual functions through *traits* [141]. In a trait-based model, different metabolic functions of the individuals are represented by numerical values called traits, which define the phenotype of the individual. Theoretically, one could differentiate between different species solely through trait values [122, 280], but we choose to have a mix of the two philosophies and introduced trait variation within the bacterial population. This is a classical approach to integrating adaptation in ecological models [1, 120, 127], and is useful for studying evolution as the ‘optimization’ of a given function rather than the apparition of novel features.

2.1.2 An ecological representation of the microbial loop

What compartments do we model?

If we look back at the first general look at the microbial loop (Figure 1.4 from Chapter 1), we can see that we can divide the microbial loop according to two distinct biomes:

1. **Marine snow ecosystem:** In this environment, heterotrophic bacteria are attached to particulate organic matter (POM) forming biofilms [67]. Their enzymatic activity hydrolyzes POM into dissolved organic matter (DOM) [130, 85], which then stops sinking.
2. **Free-floating ecosystem:** In this environment, free-floating bacteria interact with DOM as separated individuals [14]. In order to consume DOM, they first need to hydrolyze it through the action of exoenzymes [12, 11].

In global circulation models, only free-floating individuals are represented, and the marine snow environments in which bacteria are attached to sinking particles are treated implicitly through a density-dependant flux from POM to DOM [25, 132, 15]. For this reason, our model should focus on free-floating ecosystems, and as such treat first and foremost the relationship between heterotrophic bacteria and DOM, leaving POM out of the system.

An important actor in this relationship is the exoenzyme pool produced by bacteria. Similar studies in soil environments include an exoenzyme pool as a relevant compartment [5, 114, 1], but the current generation of microbial loop models in the ocean omit them [25, 87]. We can ask ourselves the following questions: why such a discrepancy between terrestrial and marine environments, and should we include an exoenzyme pool to our microbial loop module?

Marine bacteria can produce two types of exoenzymes [10]: they either release them in the ocean to become free-floating, or they can keep them attached to their cellular walls. The distinction is important here, as the inclusion of a separate exoenzyme pool in our model would be warranted only if the bacteria we study release them in the environment as ‘common goods’. If the exoenzymes are attached to the bacteria, a single bacterial pool would better represent the combined bacteria-enzyme ensemble. Studying exoenzyme production *in situ* is a difficult endeavour, especially in pelagic environments [10, 13], but theories have been developed arguing that this production depends on the environment’s richness [53, 192, 14]:

- In **marine snow ecosystems**, the environment is very rich in nutrients, and individual bacteria have a very low risk of not gathering resource even if they release their enzymes. As such, we expect free-floating exoenzymes to be found in this environment.

- In **free-floating ecosystems**, releasing ones enzymes runs the risk of not having a return on the ‘investment’, and cheaters could benefit from the common goods of exoenzyme pools without contributing. Even if it is costlier to keep the exoenzymes attached, it gives an advantage on resource acquisition.

The difference with soil ecosystems comes from the fact that ocean environments are much more diluted [53]. Where releasing exoenzymes in the soil assures proximity and thus easier access to nutrients, it is much more difficult to say so in the ocean, where diffusion and currents could take enzymes very far from their production location. modeling studies have led further credibility to this theory [258], and we will work under the assumption that exoenzymes are attached to bacterial walls: a specific enzyme pool will not be included in our model.

How many DOM compartments?

In the previous chapter, we have seen that DOM can be categorized in multiple classes depending on their expected turnover rates. The number of classes is generally three, namely labile, semi-labile and refractory, but sometimes a fourth class can be added dubbed semi-refractory [130].

This begs the question of whether we should include all three or four classes in our model. In order to answer it, we need to remind ourselves of what exactly the aim of this model is: we are trying to represent a general model of the microbial loop that could then be fitted to different scenarios of varying complexity. Modeling only one compartment has multiple advantages:

- Having only one resource for our adapting population of bacteria allows us to consider one of the most general classes of trade-offs between yield and resource acquisition [170]. Focusing on specific mechanisms that transform semi-labile DOM to labile DOM for instance would open the door to that many more potential trade-offs, blurring the central goal which is to focus on biogeochemical cycles on the large scale.
- In theoretical toy models such as the NPZ model [106, 95, 236] (see Chapter 3), compartments are very general, with all populations of phytoplankton being grouped in one class for instance. In this case, having a detailed pool of DOM would introduce a level of details not found in other compartments, which is not warranted.
- In ESMs including the microbial loop [132, 87], bacteria usually only feed on the labile class of DOM, even though the flux of semi-labile DOM to labile DOM can depend on bacterial biomass [25]. The input of DOM in our model can depend on bacterial biomass if we choose to, which means that we could fit our model with one compartment to ESMs by adapting the input.

Because of all these reasons, we choose to model DOM as one general pool, with the possibility to add more DOM pools in the larger model \mathcal{M} .

A simple representation of the microbial loop

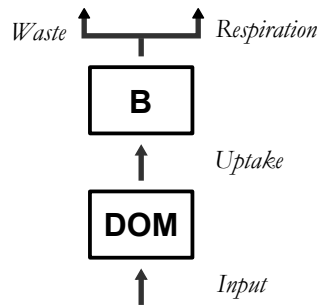


FIGURE 2.3: General representation of the microbial loop module. B: bacterial biomass; DOM, dissolved organic matter concentration.

All of these modeling choices left us with a simple representation of the microbial loop comprised of a bacterial pool and a DOM pool (Figure 2.3), which can then be adapted to a multitude of scenarios. This module has one input of DOM and two outputs, bacterial respiration and waste production. Cell death, egestion, nutrient overflow are all globally categorized as 'waste production' in this module, but all those cases can be parametrized as needed in a more complex model without modifying this module (Figure 2.4).

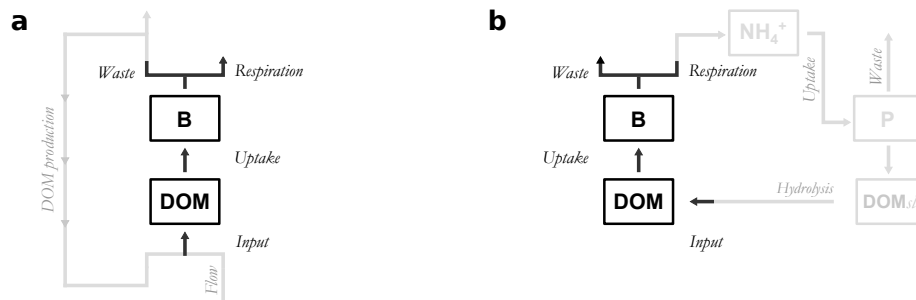


FIGURE 2.4: Examples of simple adaptations of the microbial loop module to complex cases. (a) Ecosystem in the aphotic zone of the water column; (b) Ecosystem with two classes of DOM, labile (DOM) and semi-labile ($DOM_{s,l}$), as well as ammonium (NH_4^+) and phytoplankton (P).

2.1.3 The evolutionary framework

Designing a robust eco-evolutionary framework in a trait-based model requires the definition of two important aspects: the *trait* and the *trade-offs*. Defining the bacterial function or characteristic most relevant for our biogeochemical study will give us the trait, and understanding how variations in this trait influence bacterial life-history determines the trade-offs

we consider. This is the most crucial yet complex step in integrating eco-evolutionary processes in an ecological model.

Microbial communities are likely to play a central role in shaping the Earth's response to climate change [38]. A wide variety of traits are relevant for studying their impact on the carbon cycle (C-cycling traits [187]), from phytoplankton cell size [238] to global nutrient stoichiometry [245]. Regarding heterotrophic bacteria, a very general framework for bacteria was developed in Malik et al. [170] called the Y-A-S framework. It states that bacteria have a limited amount of resource to divide between three general strategies: maximizing yield ('Y'), maximizing resource acquisition ('A') or maximizing stress tolerance ('S'). This framework mirrors the plant-based framework of C-S-R strategies defined in Grime [121], in which plants can adopt three strategies based on competition ('C'), stress tolerance ('S') or resource gathering ('R').

Yield is most commonly referred to as bacterial growth efficiency (BGE) in marine ecology [70], and is defined as the ratio between bacterial production and bacterial carbon demand (i.e. the sum of bacterial production and bacterial respiration). Different BGE values will result in different partitions of organic and inorganic fluxes through the microbial loop, making it a relevant trait for our biogeochemical study. BGE has been shown to be at least partially genetically determined [193, 230, 217] and its genetic variations to be under intense selection [233]: BGE adaptation through selection to be a significant factor of variation between populations exposed to different environments [230, 233]. Such variation could determine the strength of the recycling pathway and impact the carbon cycle in the oceans.

The Y-A-S framework is well-suited to a two-dimensional trait-space because of the three competing strategies it describes, but we choose to keep the space unidimensional and focus on the 'yield' strategy. In addition to the biogeochemical importance of BGE, it also acts as a metabolic master trait [187] from which others can be inferred, much like phytoplankton size [238]. Respiration is a vital part of creating energy for a bacterial cell, and can be seen as a proxy for all processes involved in maintaining cell functions [37]. This includes processes that are central to resource acquisition and uptake, such as hydrolysis exoenzymes production [13], ATP production [214] or rRNA copy number [193], but also stress tolerance, such as accumulating carbon reserves when in risk of starvation [146] or producing fluid membranes to avert freezing [179]. As a consequence, we can conclude that a cell that invests more in bacterial growth will be less efficient in acquiring nutrients or defending itself: this is the basis of evolutionary trade-offs (see Toolbox 2.1).

Toolbox 2.1 *Evolutionary trade-offs*

Evolutionary trade-offs are an integral part of evolutionary biology since its inception [250]. Charles Darwin refers to them as ‘correlation of growth’, and defines it in the following manner:

I mean by this expression that the whole organisation is so tied together during its growth and development, that when slight variations in any one part occur, and are accumulated through natural selection, other parts become modified. This is a very important subject, most imperfectly understood.

A more intuitive way to look at it is to notice that you can’t be good at everything at once [110], and a good example of this is the classical r/K strategies in animals [216]. We can observe to general antagonist strategies when it comes to reproduction in animals: they either spawn a lot of offsprings with low life-expectancy (the r strategy) or few with high life-expectancy (the K strategy). Intuitively, a species spawning numerous offsprings with high life-expectancy would outcompete both these strategies, but this has never been observed in nature. You can’t be good at everything at once!

2.2 A mathematical description of the module

In this section, we translate the general considerations and design philosophy into mathematical terms. We first describe the temporal dynamics of the ecological system, and then integrate eco-evolutionary processes. We derive a general expression of the eco-evolutionary stable strategy when the general model \mathcal{M} fits simple assumptions.

2.2.1 Temporal dynamics of the population

Now that we know the general shape of our ecosystem, we need to describe its dynamics. The input and waste fluxes depend on the global model \mathcal{M} in which the module is implemented. All fluxes are modeled as follows:

- $In(\mathcal{M})$ is the total influx of DOM. Its dependence on the global model \mathcal{M} could represent steady fluxes of DOM from outside the model, egestion and waste from individual bacteria or sloppy feeding by zooplankton amongst others.
- U_B is the total bacterial uptake of DOM. We use a Monod representation [186] with maximal growth rate λ_B and half-velocity constant K_B . This representation was chosen for its mathematical simplicity and wide variety of studies using it:

$$U_B = \lambda_B \frac{DOM}{K_B + DOM} B \quad (2.1)$$

- Bacterial production BP is then determined by the bacterial growth efficiency (BGE), i.e. the fraction of the uptake that is eventually transformed in biomass. BGE is thought to be partially genetically determined [233] and as such can be taken constant at the scale of our bacterial population [263]. We note it ω , and thus have:

$$BP = \omega U_B \quad (2.2)$$

- Bacterial respiration BR represents the fraction $(1 - \omega)$ of the uptake not transformed into biomass, with:

$$BR = (1 - \omega) U_B \quad (2.3)$$

- $W(\mathcal{M})$ is the bacterial waste production term. It can depend on the global model \mathcal{M} in multiple ways a regroups a wide variety of cases: grazing by zooplankton, infection by bacteriophages and linear mortality are potential terms, but others could be used.

The dynamical evolution of the system can then be described by the following system of ordinary differential equations:

$$\begin{cases} \frac{dDOM}{dt} = In(\mathcal{M}) - U_B \\ \frac{dB}{dt} = \omega U_B - W(\mathcal{M}) \end{cases} \quad (2.4)$$

2.2.2 Integrating bacterial adaptation

BGE ω has been defined as being the evolutionary trait of the system. In the spirit of the Y-A-S framework, we need to implement trade-offs such as when BGE decreases, stress tolerance and resource acquisition both increase and vice-versa. As the saying goes, ‘a rising tide lifts all boats’.

The trade-off between yield and stress tolerance is implemented in the waste production term $W(\mathcal{M})$. This term being the ‘loss’ of bacterial biomass, we can assume that stress-resistant strains on average lose less biomass than others. On the first order, we can define an individual waste term $w(\mathcal{M})$ for bacterial individual such that:

$$W(\mathcal{M}) = w(\mathcal{M}) \times B + o(B). \quad (2.5)$$

If there is no bacterial biomass, there is no waste, so linearizing the system always leads to this expression for waste production. We can implement the trade-off between yield and stress tolerance by varying w with ω , i.e.:

$$w(\mathcal{M}) := w(\omega, \mathcal{M}). \quad (2.6)$$

In this context, w would be an increasing function of ω , since higher yield implies lower resistance, hence higher individual waste production.

To represent the trade-off between BGE ω and resource acquisition, we use bacteria-DOM specific affinity [36], defined as the initial rate of DOM uptake per capita per unit of DOM concentration. In our model, the specific affinity α is defined as:

$$\alpha := \frac{\lambda_B}{K_B} \quad (2.7)$$

Specific affinity is an increasing function of the respired fraction $(1 - \omega)$, so that a bacterium that invests quasi exclusively into growth (i.e. ω close to one) will be almost unable to perform DOM uptake (i.e. an uptake rate nearing zero). Conversely, a bacterium that invests quasi exclusively into uptake (i.e. ω close to zero) will not grow efficiently. The optimal value for BGE must then lie between these two extremes.

In the general case, both λ_B and K_B are functions of ω , the former being increasing and the latter decreasing. In effect, we use the following relationship between half-velocity constant K_B and BGE ω to represent the trade-off in this thesis, with θ_A being the resource acquisition trade-off constant:

$$K_B(\omega) := \frac{K_B^0}{(1 - \omega)^{\theta_A}} \quad (2.8)$$

2.2.3 Deriving the evolutionary equilibrium

In this section, we want to compute the evolutionary stable strategy of our bacterial population regarding their resource allocation.

For now, the general model \mathcal{M} has no constraints, which makes working on it impractical and unrealistic. To be able to compute the evolutionary equilibrium state of the system, we need to make some assumptions on the model \mathcal{M} , which are simple enough to be met by all models we aim to study yet still allow us to derive an evolutionary equilibrium.

The evolutionary framework of adaptive dynamics assumes that ecological and evolutionary timescales are separate: populations are considered at their ecological equilibrium at all times. As such, for most of the thesis (with the exception of Chapters 4 and 6), we expect the model \mathcal{M} to have a stable ecological equilibrium¹. Under this equilibrium, we note bacterial biomass, DOM concentration and relevant fluxes respectively \bar{B} , \overline{DOM} , $\bar{I}n(\mathcal{M})$ and $\bar{W}(\mathcal{M})$.

In order to determine the evolutionary stable strategy, we will consider successive discrete trait change in the bacterial population, as successive invasions of new strains of bacteria unfold until the equilibrium is reached.

The first step towards this computation is to calculate the invasion fitness (see Toolbox 2.2) of a mutant population with trait ω' over a resident population with trait ω . Then, by iterating invasion events, we'll eventually end up with a stable strategy that won't be invaded by its neighbors. Calculating the invasion fitness for this system starts by assuming the apparition of a mutant bacterial population bearing the trait ω' while the resident population is at equilibrium. Its initial growth rate is the following:

Toolbox 2.2 *Invasion fitness*

The invasion fitness $S(\omega', \omega)$ of a mutant population ω' over a resident ω is a measure of the ability of an invading species to replace the resident. A positive invasion fitness implies a fitter mutant, and conversely a negative invasion fitness implies a fitter resident. If both populations are phenotypically close, the competitive exclusion principle [112] allows us to conclude that only one population will prevail in this scenario. This measure can be defined the following manner:

$$S(\omega', \omega) := \begin{array}{l} \text{Per capita growth rate of an} \\ \text{infinitesimal mutant population } \omega' \\ \text{with the resident population } \omega \\ \text{at ecological equilibrium} \end{array} \quad (2.9)$$

We can intuitively understand why this measure works for our purpose: if the mutant population is fit enough to thrive in an environment already invested by the resident population, then it means that it must be fitter. We can then conclude the outcome of the invasion event thanks to the competitive exclusion principle.

$$\frac{dB'}{dt} = \omega' \cdot \lambda_B(\omega') \frac{\overline{DOM}}{K_B(\omega') + \overline{DOM}} B' - w(\omega', \mathcal{M}) B' + o(B') \quad (2.10)$$

¹Working with periodic models would have been possible [227], but fixed environments with stable equilibria allow us to work on the interannual scale rather than interseasonal more easily.

From this equation, we can derive the invasion fitness $S(\omega', \omega)$:

$$S(\omega', \omega) = \omega' \cdot \lambda_B(\omega') \frac{\overline{DOM}}{K_B(\omega') + \overline{DOM}} - w(\omega', \mathcal{M}). \quad (2.11)$$

Using the fact that the resident population is at ecological equilibrium, we can rewrite the invasion fitness in the following fashion:

$$\begin{aligned} S(\omega', \omega) = & \underbrace{\left(\frac{\omega'}{\omega} - 1 \right) \cdot w(\omega, \mathcal{M})}_{\text{competitive advantage of higher yield}} \\ & + \omega' \cdot \underbrace{\left(\lambda_B(\omega') \frac{\overline{DOM}}{K_B(\omega') + \overline{DOM}} - \lambda_B(\omega) \frac{\overline{DOM}}{K_B(\omega) + \overline{DOM}} \right)}_{\text{competitive advantage of higher resource acquisition}} \\ & + \underbrace{(w(\omega, \mathcal{M}) - w(\omega', \mathcal{M}))}_{\text{competitive advantage of higher stress tolerance}}. \end{aligned} \quad (2.12)$$

The structure of the invasion fitness follows the classical framework of the Yield-Resource Acquisition-Stress Tolerance life history strategies defined in Malik et al. [170]. The first term represents the competitive advantage of having a high yield strategy (i.e. high values of BGE): it is positive for $\omega' > \omega$ and negative otherwise. Similarly, the second term represents the competitive advantage of having a resource acquisition strategy and the third the competitive advantage of having a stress tolerance strategy. Both these terms are positive for $\omega' < \omega$ and negative otherwise.

We can derive the selection gradient $dS(\omega)$ from the invasion fitness by taking the derivative with regards to ω' , and computing the result on the value of resident trait ω :

$$dS(\omega) = \partial_1 S(\omega', \omega)|_{\omega'=\omega} \quad (2.13)$$

We then find:

$$\begin{aligned} dS(\omega) = & \frac{w(\omega, \mathcal{M})}{\omega} \\ & + \left(\frac{\lambda'_B(\omega)}{\lambda_B(\omega)} - \frac{K'_B(\omega)}{K_B(\omega) + \overline{DOM}} \right) \omega \lambda_B(\omega) \frac{\overline{DOM}}{K_B(\omega) + \overline{DOM}} \\ & - \partial_1 w(\omega, \mathcal{M}). \end{aligned} \quad (2.14)$$

Following the selection gradient until a point ω^* such as $dS(\omega^*) = 0$ then leads us to a locally stable evolutionary strategy.

2.3 Microbial loop adaptation in the aphotic zone

We begin with the simplest ecosystem in which we could integrate our module, that is the microbial loop in the water column under the limit of the photic zone. In this zone spanning the limit of the ocean surface to the sediment floors, most of the remineralization of nutrients takes place thanks to the work of heterotrophic bacteria [25].

We study two main risks threatening the water column: ocean warming [166] and stratification [164]. Ocean warming is expected to increase carbon demand and respiration rates for heterotrophic bacteria [263], changing the microbial loop's capacity to remineralize nutrients, and ocean stratification may result in lower particle sinking rates, lowering carbon export [143, 204]. In this section, we model the response of the microbial loop to increased temperatures and stratification, and analyze the consequence for bacterial respiration and carbon stock. The simplicity of the model allows us to perform most of the analysis by hand.

Fitting the module in the aphotic zone ecosystem

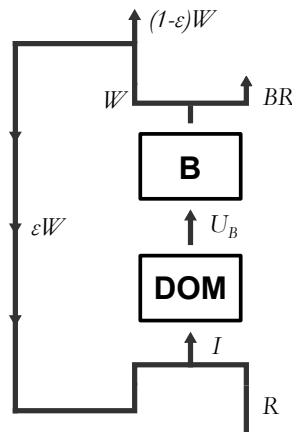


FIGURE 2.5: Model \mathcal{M}_{NB} of the microbial loop in the aphotic zone. B, bacterial biomass; DOM, dissolved organic matter. All fluxes are described in the main text.

We fit the module into a model \mathcal{M}_{NB} of the microbial loop in the aphotic zone (Figure 2.5). Only resources (N) and bacteria (B) are considered, hence the name NB. Here, waste production represents egestion and bacterial mortality, which will be modeled linearly. The individual rate μ_B is considered constant for all environments and across bacterial strains, meaning there will be no difference in stress tolerance between populations:

$$W(\mathcal{M}_{\text{NB}}) = \mu_B \cdot B \quad (2.15)$$

A fraction ϵ of this waste directly feeds the DOM pool, and the dissolution of POM to DOM (external to the system) is represented by an influx of DOM R constant for a given depth [175]. The sum of both DOM fluxes equals the total influx of the system:

$$\text{In}(\mathcal{M}_{\text{NB}}) = R + \epsilon \cdot W(\mathcal{M}_{\text{NB}}). \quad (2.16)$$

The ecosystem model is then given by the following system of ordinary differential equations:

$$\begin{cases} \frac{dDOM}{dt} = R + \epsilon \cdot \mu_B B - U_B \\ \frac{dB}{dt} = \omega U_B - \mu_B B \end{cases} \quad (2.17)$$

We introduce temperature-dependency in the system in order to study the impact of a temperature increase on microbial loop activity. In this system, only bacterial maximum growth rate λ_B is likely to strongly depend on temperature, so we apply the following Arrhenius relationship:

$$\lambda_B^0(T) := \lambda_B^{T_0} \exp\left(\frac{E_A}{k} \left(\frac{1}{T_0} - \frac{1}{T}\right)\right). \quad (2.18)$$

In this relationship, E_A represents the activation energy, k the Boltzmann constant, T_0 the baseline temperature and $\lambda_B^{T_0}$ the constant value at T_0 .

2.3.1 Initial state of the ecosystem

Deriving the ecological equilibrium

In order to derive the expression of the ecological equilibrium from equation (2.17), we simply need to find the values $(\bar{B}, \overline{DOM})$ for which the time derivatives are equal to zero.

Using the bacterial biomass dynamics, we can derive the uptake rate U_B at equilibrium, which can then be used in the DOM dynamics equation to find the following bacterial biomass at equilibrium \bar{B} :

$$\bar{B} = \frac{\omega R}{(1 - \omega\epsilon) \cdot \mu_B}. \quad (2.19)$$

This can then be used to derive the DOM concentration at equilibrium \overline{DOM} :

$$\overline{DOM} = \frac{\mu_B}{\omega \lambda_B - \mu_B} \cdot K_B(\omega). \quad (2.20)$$

These equilibrium values only make sense if $\omega \lambda_B > \mu_B$, which is logical: for bacteria to thrive, they need to produce biomass faster than they die. In this case, the equilibrium is stable and attractive. We assume this condition is met for the rest of the section.

The remineralization ratio r informs us on the strength of bacterial recycling of organic matter to inorganic nutrients. Here, it is the ratio between bacterial respiration BR and external input of DOM R :

$$r = \frac{1 - \omega}{1 - \omega \epsilon} \quad (2.21)$$

The remineralization ratio is determined by two system parameters: the fraction of bacterial waste directly recycled as DOM ϵ and the BGE ω . For a fixed waste recycling constant $\epsilon < 1$, the remineralization ratio r is decreasing when ω is increasing: in such a simple system, nutrient remineralization is directly correlated to the fraction $(1 - \omega)$ invested in respiration by a single bacteria. The relationship between remineralization and BGE is only linear for $\epsilon = 0$. For all other values of ϵ , the relationship between r and ω is concave: the remineralization rate of the whole system is higher than the remineralization of a single bacterial cell – thanks to waste recycling, the system as a whole is more efficient than the sum of the individuals. By definition, total remineralization is $r \times R$, so we can draw the same conclusions.

The turnover rate τ of DOM can inform us on how long carbon can stay locked in the system [21]. We can calculate this by dividing the equilibrium concentration \overline{DOM} by the total uptake rate U_B at equilibrium. We find:

$$\tau = \frac{1 - \omega \epsilon}{\left(\frac{\lambda_B}{\mu_B} \omega - 1\right) (1 - \omega)_A^\theta} \cdot \frac{K_B^0}{R} \quad (2.22)$$

The DOM turnover rate is inversely proportionnal to the external input in DOM R , showing that oligotrophic environments have longer turnover rates than copiotrophic ones.

Computing the evolutionary stable strategy

To compute the selection gradient in this model, we use equation (2.14) with the trade-off defined in equation (2.8). We find that:

$$dS(\omega) = \frac{\mu_B}{\omega} - \frac{\theta_A}{1 - \omega} \frac{K_B(\omega)}{K_B(\omega) + \overline{DOM}} \cdot \omega \lambda_B \frac{\overline{DOM}}{K_B(\omega) + \overline{DOM}} \quad (2.23)$$

Using the fact that the system is at ecological equilibrium, we can simplify the selection gradient in order to find the following expression for ESS ω^* :

$$\omega^* = \frac{1 + \frac{\mu_B}{\lambda_B} \cdot \theta_A}{1 + \theta_A}. \quad (2.24)$$

In this system and under the proposed trade-off, BGE is entirely determined by the death-to-birth ratio and trade-off constant θ_A . We can easily check that $\omega\lambda_B - \mu_B > 0$. The closer the intrinsic death rate μ_B is to maximal growth rate λ_B , the closer ω is to 1 to sustain the system. In a system limited by its nutrients, having a high mortality rate forces bacterial population to be efficient with their resource.

The trade-off constant θ_A potentially has a range of all positive real numbers. On this range, BGE decreases with increasing values of θ_A , with a lower limit of $\frac{\mu_B}{\lambda_B}$. This dependence can be interpreted by looking at the more general equation (2.14): a higher trade-off dependency favors the resource acquisition strategy, which mechanically lowers the value of BGE.

Finally, we can easily check that ω^* is the point for which DOM concentration is at its lowest: this is a form of the ‘pessimization principle’ which states that natural selection will select populations that utilize the resource the most [80, 180].

2.3.2 Effect of ocean warming and stratification on the ecosystem

In this section, we independently vary environmental parameters to represent ocean warming and stratification. Ocean warming is represented by a temperature increase while ocean stratification is represented by a decrease in external DOM input R . Indeed, since ocean stratification lowers the amount of particles sinking, the hydrolysis of POM to DOM is likely to decrease in the aphotic zone, which is represented by a decrease in R in our model.

Ecophysiological response of the ecosystem to temperature increase

The effect of a temperature increase on the system is to increase the maximum growth rate λ_B , which will change the structure of the system. If we look at the temperature dependency of equilibrium values from equations (2.19) and (2.20) with ω fixed, we find that bacterial biomass stays constant while DOM concentration decreases when temperature increases (Figure 2.6).

When temperature increases, the uptake rate increases per capita, but not the total DOM input from bacterial waste and outside source. Since at equilibrium, both fluxes are equal, a temperature increase mechanically decreases DOM concentration. The remineralization ratio is independent from temperature when adaptation is not taken into account, since

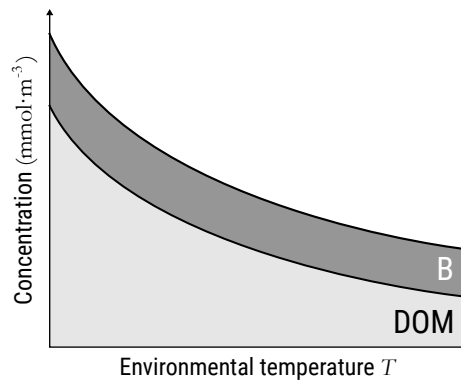


FIGURE 2.6: Carbon distribution variations to a temperature increase. B, bacterial biomass; DOM, dissolved organic matter; R , external DOM input.

it only depends on temperature-independent terms (BGE ω and waste recycling constant ϵ). As expected, higher temperatures imply faster fluxes between compartments, and DOM turnover τ decreases with increasing temperatures.

Ecophysiological response to ocean stratification

Looking at DOM input dependency of the equilibrium state from equations (2.19) and (2.20), we find that in this case bacterial biomass decreases and DOM concentration stays constant when the input decreases (Figure 2.7).

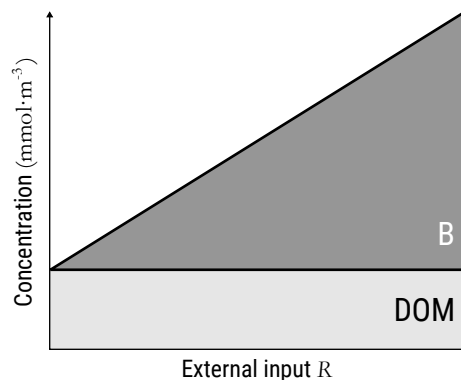


FIGURE 2.7: Carbon distribution between compartments at equilibrium. B, bacterial biomass; DOM, dissolved organic matter; R , external DOM input.

The fact that nutrient depletion impacts bacterial biomass and not DOM concentration is a hallmark of a ‘bottom-up’ limited system, meaning that bacterial growth is limited by the availability of resource, and not by external causes of death. Remineralization ratio is once again unaffected by the environmental change, but total remineralization rates are de-

creased. Finally, the decrease in bacterial biomass releases the pressure on DOM, decreasing its turnover.

2.3.3 Bacterial adaptation and its impact

Bacterial adaptation is driven by the ecophysiological response of the system

Changes in environmental parameters will result in a shift in trait value due to natural selection, as pressure to adapt comes from a mismatch between the bacterial population and the environment state. If we assume that ecological times are faster than evolutionary times, environmental variation first results in the ecophysiological response of the system, and this ecophysiological response then creates the mismatch between population and environment, inducing the pressure to adapt. We can understand ‘why’ bacteria adapt by looking at the ecophysiological response of the system.

Increasing the temperature results in a decrease in DOM concentration. Resource is becoming scarcer, so bacteria investing in resource acquisition will be fitter than their ancestral counterparts. Mechanically, decreasing the resource results in increasing the need for efficient resource acquisition mechanisms. The temperature sensitivity of BGE ω depends on the trade-off constant θ_A , as the more sensitive bacteria are to resource acquisition pressure, the more they will have to adapt to a DOM concentration decrease. In this simple model, decreasing the DOM input results in no variation of the ESS ω^* , since DOM concentrations at equilibrium don’t depend on R .

Effect of bacterial adaptation on the system

The effect of bacterial adaptation is equal to the effect of varying the trait value from ω_0 to ω_1 when the environment is at its final state e_1 (be it temperature, DOM input, etc...). In more complex cases, this effect can be numerically determined by comparing ecophysiological and eco-evolutionary responses of the system, but the \mathcal{M}_{NB} offers us the opportunity to study bacterial adaptation impact analytically by studying how key ecosystem functions vary with regards to BGE.

Regardless of the direction of bacterial adaptation, its effect on the DOM reservoir is negative. Indeed, using the pessimization principle that was established earlier, we show that BGE evolves towards minimizing DOM concentration in any environment. This allows us to conclude that any predictions for the future of DOM in the oceans that doesn’t take bacterial adaptation into account may overestimate the size of the reservoir.

To illustrate the other effects bacterial adaptation has on the system, let’s focus on a BGE

decrease in the case of ocean warming². Bacterial biomass decreases with ω , leading to even more oligotrophic oceans. The effect of bacterial biomass decrease on the recycling power of the microbial loop is mitigated by the increase in remineralization ratio. DOM turnover time is proportionnal to $(1 - \omega\epsilon)\overline{DOM}$, so it is possible to actually see a slight increase in DOM turnover times despite the decrease in DOM concentration if BGE decreases when the fraction ϵ of waste redirected to the DOM pool is high enough. In those cases, DOM uptake decreases faster than DOM equilibrium concentration.

2.4 Conclusion and perspectives

In this chapter, we have developed the basic eco-evolutionary module of the microbial loop that will allow us to study its adaptation under climate change. The reasoning behind the simplicity of the final module has been carefully explained, and the way to integrate it in more complex models detailed.

This simple model studied shows that the eco-evolutionary response of the microbial loop depends on the nature of environmental variations: ocean stratification implies an ecological response of the system, while ocean warming could influence bacterial adaptation more. It also provided proof that the recycling power of the microbial loop directly depends on bacterial growth efficiency, and that eco-evolutionary feedback could both increase or mitigate the effects of climate change. The relative power of the microbial loop is increased in the case of BGE decrease, which could potentially stimulate new production in the surface. On the other hand, this would also increase total DIC in the ocean. Changes in DIC concentrations have a direct effect on the interaction between the atmosphere and the ocean through the Revelle factor [88]. An increase in DIC could lead to a decrease of the Revelle factor, which would mean a decrease in the capacity for the ocean to extract carbon from the atmosphere. In conclusion, bacterial adaptation could have different consequences for different components of the Earth system.

A drawback of the model is the lack of limiting nutrients for the bacteria other than DOM. The focus of the thesis is indeed DOM recycling by heterotrophic bacteria, but they can be limited by other nutrients, most notably iron (Fe) in some regions of the surface ocean [201]. Other factors can influence bacterial metabolism that can not be captured by our model, such as the oxygen (O₂) dependency deep in the water column [138].

After having focused on the water column, the next logical step for this thesis is to implement the microbial loop module in a sea-surface ecosystem. How does the microbial loop adaptation influence major ecosystem functions such as primary production and carbon export? In the next chapter, we take a classical NPZ model in which we integrate the microbial

²All results can then be adapted for other environmental shifts leading to a BGE increase.

loop to answer this question.

Chapter 3

Predicting the response of primary production to climate change

With Régis Ferrière, published in The ISME Journal [48]. Presented at AGU Fall Meeting 2021 [49].

‘You want a prediction about the weather, you’re asking the wrong Phil. I’ll give you a winter prediction: It’s gonna be cold, it’s gonna be grey, and it’s gonna last you for the rest of your life.’

Phil Connors, *Groundhog Day* (1993)

In this chapter, we implement the microbial loop module in a larger ecosystem of the ocean surface. We compare two scenarios of a warming ocean, one with bacterial adaptation and one without. In both scenarios, temperatures are increased by 5°C, but bacterial populations adapt their BGE in only one of the two. The comparison of variations will allow us to conclude on the relevance of including eco-evolutionary processes in ESMs. Indeed, if the variations induced by bacterial adaptation are comparable to the variations induced by the temperature increase alone, then it must mean that adaptation is a key process that needs to be taken into account for more accurate predictions.

First, we describe the model $\mathcal{M}_{\text{NPZ-B}}$ in which we implement the microbial loop module from the previous chapter. Then we perform the eco-evolutionary analysis and compare scenarios in presence and absence of bacterial adaptation. Finally, we discuss the implications and opportunities of this study for a more comprehensive study in larger models.

3.1 A sea-surface ecosystem model for ocean productivity

3.1.1 Predicting the future of primary production

Microorganisms dominate ocean biodiversity and play a major role in global ecosystem function. As Falkowski, Fenchel, and Delong [94] aptly phrased it, Earth's biogeochemical cycles are driven by microbial engines. The ocean microbes' response to current climate changes has the potential to alter the global cycles of carbon and nutrients with likely feedbacks to the climate system [226, 134]. To improve our projections of ecosystem function such as primary production and better understand the future of climate, we need to assess both how ocean microorganisms respond to climate change and how their response impacts to the global environment [38].

The rise of sea surface temperature causes dramatic changes in the oceanic environment, such as increased stratification resulting in weaker nutrient fluxes from the deep sea [30], deoxygenation [205], and sea-level rise [39]. How ocean microorganisms are affected, and how these potential effects might propagate through the ocean ecological web is poorly known. In particular, primary production response to warming is hard to predict, even on short temporal horizons [107]. In some regions, not only the magnitude but even the very direction of these responses remains uncertain [251, 150], notably because of complex interactions between temperature, nutrient supply, and light.

Among ocean microorganisms, heterotrophic bacteria are key actors of nutrient cycling. They remineralize dissolved organic matter into nutrients (the 'recycling pathway'), and redirect otherwise lost organic matter to higher trophic links via grazing. Even though this microbial loop is estimated to process about half of all primary production [96, 142], an explicit recycling pathway is often missing in models of global carbon and nutrient cycles, and instead heterotrophic bacteria are treated implicitly [15]. Models that represent the microbial loop explicitly [264, 132] point to complex interaction effects between recycling and sea-surface warming: at a given temperature, models that include the microbial loop often predict a reduction in net primary production (NPP) [132]; however, when warming is predicted to decrease NPP by models without a microbial loop, inclusion of the microbial loop can reverse that prediction [151]. It thus seems that the direction of changes in primary production can in part be explained by the microbial loop and the balance between new and regenerated production. Our work aims at providing a mechanistic explanation for the direction of primary production variations by focusing on the microbial loop response to sea-surface warming.

A potentially important component of this response that is completely missing from previous models is bacterial adaptation through selection, i.e., the selection of different, more adapted bacterial strains. Bacterial adaptation may have important consequences for the future of primary production: as individual cells respond physiologically to warm-

ing, population- and ecosystem-level effects may feed back to the microbial community and drive the selection of different bacterial strains. In return, such bacterial adaptation may alter the ecological state of the system, thus entangling ecological and evolutionary dynamics in a closed eco-evolutionary feedback loop [187]. Because of heterotrophic bacteria's large population sizes and short generation time [219] relative to the timescale of climate change, we expect bacterial adaptation to play a role in their response to ocean warming [269], potentially altering the balance between new and regenerated primary production. How much and where then become key questions.

3.1.2 Ecosystem model

The ecosystem model in which the microbial loop module is integrated is adapted from biogeochemical modules of global circulation models, mainly Hasumi and Nagata [132] and Aumont et al. [15]. The backbone structure of our model is a standard 'NPZ' model with three pools: nitrogen N (often the common currency in models with only one nutrient, as stated in Sarmiento and Gruber [236]), phytoplankton P , and zooplankton Z . We design our model to accommodate a 0D setting to study the balance between new and regenerated production by dividing the nitrogen pool into three: nitrate tracks new production, ammonium tracks regenerated production, and DOM is expressed in its nitrogen content dissolved organic nitrogen (DON). Phytoplankton species are grouped into one compartment, and so are heterotrophic bacteria; both share zooplankton as one compartment of a common predator, allowing for both emergent bottom-up and top-down limitations. The outcome is a 6-compartment model $\mathcal{M}_{\text{NPZ-B}}$ called NPZ-B (Figure 3.1).

As is done classically, we assume a type II (Monod) response of all uptake rates, U , to nutrient concentrations. To keep the model mathematically tractable, we assume that the response of grazing rates, G , to population densities is type I: phytoplankton consumption by zooplankton is seldom at saturation. Maximum rates of uptake and grazing are temperature-dependent through an Arrhenius relationship, with different activation energies between autotrophic and heterotrophic organisms, ca. 0.3 eV for phytoplankton and 0.6 eV for bacteria and zooplankton [45].

The additional fluxes from $\mathcal{M}_{\text{NPZ-B}}$ can then be described as follow. c_0 denotes the deep ocean concentration of nutrients (expressed in its nitrogen content), which is mixed with the euphotic layer with flux rate ϕ ([236]), for the following exterior input of nitrate from mixing *Mix*:

$$\text{Mix} = \phi \cdot (c_0 - \text{NO}_3^-). \quad (3.1)$$

$U_{P,\text{new}}$ represents the new gross primary production from nitrate NO_3^- :

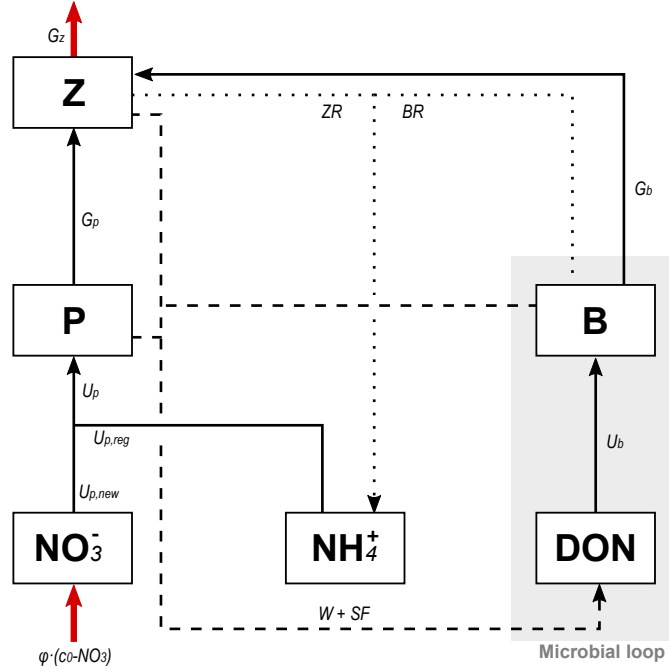


FIGURE 3.1: \mathcal{M}_{NPZ-B} model for sea-surface ecosystems. B, bacterial biomass. P phytoplankton biomass, Z zooplankton biomass, DON dissolved organic nitrogen. Fluxes driven by mortality are represented with dashed lines and all end up in the DON pool. Respiration fluxes are represented with dotted lines, ending in the ammonium pool. Red lines represent the incoming and outgoing fluxes of the system.

$$U_{P,new} = \lambda_P \frac{NO_3^-}{K_{P,new} + NO_3^-} P \quad (3.2)$$

where λ_P is the phytoplankton maximum growth rate and $K_{P,new}$ is the half-saturation constant for nitrate uptake.

$U_{P,reg}$ is the regenerated gross primary production of phytoplankton from ammonium NH_4^+ :

$$U_{P,reg} = \lambda_P \frac{NH_4^+}{K_{P,reg} + NH_4^+} P \quad (3.3)$$

where $K_{P,reg}$ is the half-saturation constant for ammonium uptake.

U_P is the total gross primary production:

$$U_P = U_{P,new} + U_{P,reg} \quad (3.4)$$

μ_B , μ_P , and μ_Z denote the mortality rates of bacteria, phytoplankton, and zooplankton, respectively. Overall, cell mortality represents ‘waste production’ W :

$$W = \mu_B B + \mu_P P + \mu_Z Z. \quad (3.5)$$

G_B , G_P , and G_Z measure grazing of bacteria, phytoplankton, and zooplankton, modeled with type-I function response:

$$G_B = g_B B Z \quad (3.6)$$

$$G_P = g_P P Z \quad (3.7)$$

$$G_Z = g_Z Z^2. \quad (3.8)$$

A fraction γ_B (resp. γ_P) of bacterial (resp. phytoplankton) grazing is then converted to zooplankton biomass, so that zooplankton production ZP can be written:

$$ZP = \gamma_B G_B + \gamma_P G_P. \quad (3.9)$$

Another fraction σ_B (resp. σ_P) is lost to the DON pool due to ‘sloppy feeding’. We can then express sloppy feeding SF as such:

$$SF = \sigma_B G_B + \sigma_P G_P. \quad (3.10)$$

In this model, the input of DON $In(\mathcal{M}_{NPZ-B})$ is then taken equal to the sum of waste production and sloppy feeding:

$$In(\mathcal{M}_{NPZ-B}) = W + SF. \quad (3.11)$$

ZR measures zooplankton respiration. Energy consumed that is not used for growth or lost to sloppy feeding is assumed to be respired. This leads to:

$$ZR = (1 - \gamma_B - \sigma_B) G_B + (1 - \gamma_P - \sigma_P) G_P. \quad (3.12)$$

The ecosystem model is then given by the following system of ordinary differential equations:

$$\left\{ \begin{array}{l} \frac{dB}{dt} = \omega U_B - G_B - \mu_B B \\ \frac{dP}{dt} = U_P - G_P - \mu_P P \\ \frac{dZ}{dt} = \gamma_B G_B + \gamma_P G_P - G_Z - \mu_Z Z \\ \frac{dDON}{dt} = W + SF - U_B \\ \frac{dNO_3^-}{dt} = \phi(c_0 - NO_3^-) - U_{P,new} \\ \frac{dNH_4^+}{dt} = BR + ZR - U_{P,reg} \end{array} \right. \quad (3.13)$$

The following parameters follow an Arrhenius-type relationship to temperature:

$$\lambda_P, \lambda_B, g_B, g_P, g_Z. \quad (3.14)$$

The analysis scheme follows the layout described in Chapter 2: three sets of simulations were run with the same parameters, corresponding to the computation of the system's steady state in three scenarios:

1. **Initial adaptation:** the system is at initial temperature T_0 .
2. **Ecophysiological scenario:** the system is at temperature $T_1 = T_0 + \Delta T$, with $\Delta T = 5^\circ\text{C}$, and the model is controlled to prevent bacterial adaptation.
3. **Eco-evolutionary scenario:** the system is at temperature $T_1 = T_0 + \Delta T$, with $\Delta T = 5^\circ\text{C}$, and bacteria are adapted to this new temperature.

Comparing the three scenarios allows us to derive the ecophysiological response of the system and to isolate the effect of bacterial adaptation.

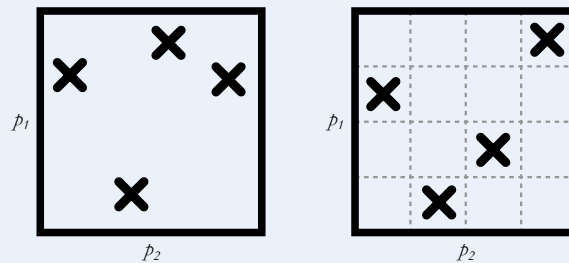
To analyze the responses of the microbial loop to warming, we focus on BGE, ω , and the microbial loop efficiency (MLE), which represents the fraction of primary production that cycles through bacteria and contributes to bacterial growth or respiration. To analyze the responses of primary production to warming, we focus on both new and regenerated production; we refer to the f-ratio as the ratio of new production over total primary production. The f-ratio is relevant for the study of the balance of new and regenerated production, but also export production: at ecological equilibrium, it is equal to the export ratio, or e-ratio [236], which can be denoted by the ef-ratio.

Due to the complexity of the system, a numerical approach was used to compare different biogeographical regions and their responses to sea-surface warming. A set of credible

ranges was determined for each parameter to represent different regions of the ocean (from nutrient-poor and warm regions such as the subtropical gyres to nutrient-rich and cold regions such as the Arctic Ocean) and a latin hypercube sampling was used to run 1,000 simulations (see Toolbox 3.1).

Toolbox 3.1 *Latin Hypercube Sampling*

When sampling high dimensional parameter spaces randomly, one runs the risk to sample some regions significantly more than others. To circumvent this difficulty, one may divide the parameter space along each axis according to the number of simulations needed and sample each subregion once, ensuring no 2 simulations will share a parameter value.



In the example above we sample four pairs of parameters (p_1, p_2) with random sampling for the left example and latin hypercube sampling for the right example. A simple way to understand latin hypercube sampling is to consider that we try to place rooks in a chess game such as no two rooks threaten each other.

Parameter range estimation (Table 3.1) was done by drawing from two main resources, with Bendtsen et al. [25] used for microbial loop parameters and Aumont et al. [15] for the rest of the ecosystem. Where modeling differences occurred (such as the type of response for zooplankton grazing), parameters were estimated for low saturation of resource, and overall the model was tuned for obtaining an ecosystem where the concentrations had the orders of magnitude found in Aumont et al. [15].

3.1.3 Initial state of the system

Ecological equilibrium

The first step is to compute the ecosystem equilibrium state at any given temperature. We first express equilibrium steady-state in terms of the nitrate pool concentration N through algebra on the dynamical system, and numerically derive the final solution.

Parameter	Minimum	Maximum	Unit
T	0.0	25.0	$^{\circ}\text{C}$
c_0	3.0	10.0	$\text{mmol}\cdot\text{m}^{-3}$
ϕ	0.01	0.1	day^{-1}
λ_P^0	2.0	5.0	day^{-1}
$K_{P,new}$	10.0	30.0	$\text{mmol}\cdot\text{m}^{-3}$
$K_{P,reg}$	0.5	5.0	$\text{mmol}\cdot\text{m}^{-3}$
μ_P	0.01	0.02	day^{-1}
g_P	0.2	1.0	$\text{day}^{-1}(\text{mmol}\cdot\text{m}^{-3})^{-1}$
σ_P	0.2	0.4	
γ_P	0.3	0.5	
λ_B^0	0.5	1.5	day^{-1}
K_B^0	0.5	1.0	$\text{mmol}\cdot\text{m}^{-3}$
θ	2.0	4.0	
μ_B	0.01	0.02	day^{-1}
g_B	0.05	0.15	$\text{day}^{-1}(\text{mmol}\cdot\text{m}^{-3})^{-1}$
σ_B	0.2	0.4	
γ_B	0.3	0.5	
μ_Z	0.01	0.02	day^{-1}
g_Z	0.8	1.0	$\text{day}^{-1}(\text{mmol}\cdot\text{m}^{-3})^{-1}$
E_A^P	0.3	0.4	ev
E_A^Z	0.5	0.6	ev
E_A^B	0.5	0.6	ev

TABLE 3.1: Parameter range of the $\mathcal{M}_{\text{NPZ-B}}$ model.

First, we use the dynamics of total nitrogen content of the system to express zooplankton biomass concentration in terms of nitrate N , dubbed $z(N)$:

$$z(N) = \sqrt{\frac{\phi}{g_Z}(c_0 - N)} \quad (3.15)$$

Then, looking at nitrate dynamics at equilibrium, we find phytoplankton biomass $p(N)$:

$$p(N) = \frac{\phi}{\lambda} \left(\frac{K_{P,new}}{N} + 1 \right) (c_0 - N). \quad (3.16)$$

Zooplankton dynamics allow us to compute bacterial biomass at equilibrium $b(N)$:

$$b(N) = \frac{1}{\gamma_B g_B} (\mu_Z + g_Z z(N) - \gamma_P g_P p(N)) \quad (3.17)$$

DON dynamics then allow us to find the expression of DON uptake by bacteria in terms of nitrate $u_B(N)$, with waste production $w(N)$ and sloppy feeding $sf(N)$ also expressed in terms of nitrate:

$$u_B(N) = w(N) + sf(N) \quad (3.18)$$

Finally, using bacterial dynamics we find the following equation which is verified when nitrate concentration N is at equilibrium:

$$\omega \cdot u_B(N) = g_B b(N) z(N) + \mu_B b(N) \quad (3.19)$$

Solving this equation numerically allows us to compute the equilibrium value of nitrate concentration. We can then deduce the biomass concentrations of bacteria, phytoplankton and zooplankton. DON dynamics then enables us to compute the equilibrium value of DON concentration, and finally ammonium dynamics helps us find ammonium equilibrium concentration. We performed a large number of quality checks by comparing these results with the long-term values of the numerical solutions of the system of differential equations (equation (3.13)).

Evolutionary equilibrium

Using equation (2.14) with the \mathcal{M}_{NPZ-B} model yields the following selection gradient:

$$dS(\omega) = \frac{\mu_B + g_B \cdot \bar{Z}}{\omega} - \theta \frac{\omega}{1 - \omega} \cdot \frac{K_B(\omega)}{K_B(\omega) + \overline{DOM}} \cdot \lambda_B \frac{\overline{DOM}}{K_B(\omega) + \overline{DOM}}. \tag{3.20}$$

The equation $dS(\omega) = 0$ was numerically solved to find the ESS ω^* .

Initial adaptation analysis

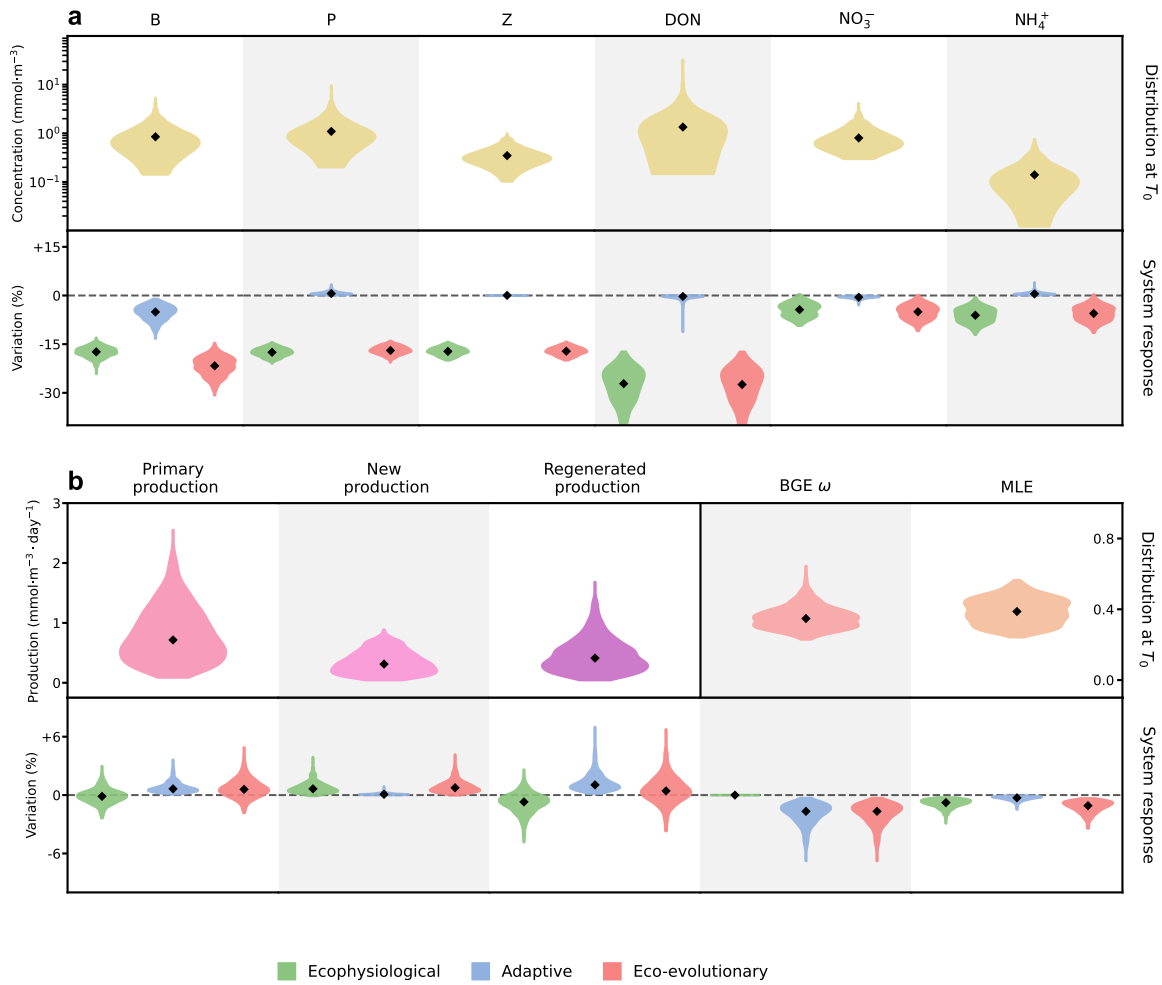


FIGURE 3.2: Distributions of model outputs at initial temperature T_0 (top rows) and corresponding ecophysiological (green), adaptive (blue) and the combined eco-evolutionary (red) responses (bottom rows). The adaptive effect represents variation in the ecosystem state driven by bacterial adaptation through selection after a temperature increase. Black dots indicate median values. a Equilibrium biomass and concentrations. See Fig. 1 for notations. b Microbial loop and ecosystem production outputs (separated by the black vertical line). BGE bacterial growth efficiency. MLE microbial loop efficiency. All parameters vary in the default parameter ranges.

Following adaptation to the initial temperature T_0 (Figure 3.2), all equilibrium state variables correlate negatively with T_0 , except for inorganic nutrients (Figure 3.3). Warmer temperatures accelerate fluxes between ecosystem compartments but do not increase nutrient input: this acceleration is thus made at the expense of equilibrium concentrations and biomass, which decrease across the temperature gradient (Figure 3.2a). Conversely, higher nutrient input correlates with higher nutrient concentrations and population biomass.

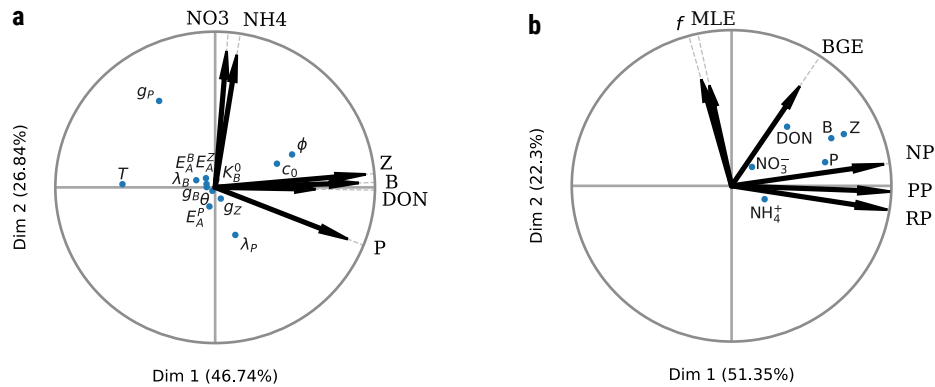


FIGURE 3.3: Principal component analysis for ecosystem equilibrium values at T_0 . (a) Equilibrium state at T_0 ; (b) Key outputs at T_0 . All parameter values are described in Table 3.1.

Correlations across state variables at equilibrium bear the signatures of top-down controls, with strong, negative correlations between inorganic nutrients concentrations and phytoplankton growth rate, and between phytoplankton biomass and grazing by zooplankton.

The f-ratio positively correlates with both BGE ω_0 , and MLE . By re-injecting in the trophic chain a fraction of the primary production that would otherwise be lost in the DON pool, the microbial loop acts as a recycling process, thus driving the export ratio up.

3.2 Eco-evolutionary responses of the system and impact on productivity

As temperatures increases, environmental parameters shift due to the ecosystem response. This shift then drives bacterial adaptation, which in return influences the environment. In this section, we resolve the ecophysiological response of the system and quantify the effect of bacterial adaptation on the system.

3.2.1 The direction of primary production variation is controlled by ecophysiological changes in the microbial loop

An increase in temperature changes multiple physiological parameters, causing a shift in the ecosystem equilibrium even in the absence of bacterial adaptation (green distributions in Figure 3.2). The biomass of all populations (heterotrophic bacteria, phytoplankton, zooplankton) and all nutrients concentrations tend to decrease. Even though individual process rates tend to increase with temperature, the overall effect on the ecosystem equilibrium is negative because nutrient consumption by phytoplankton and grazing both increase.

The general decrease in phytoplankton biomass observed across the parameter space (Figure 3.2a) is to be contrasted with the distribution of primary production. In some cases, primary production increases despite phytoplankton biomass decreasing (Figure 3.2b). This decoupling is explained by faster phytoplankton metabolism, which increases per capita primary production. Whether the effect of faster metabolism outweighs the decrease in biomass and yields a gain of primary production depends on the balance between new and regenerated production. While new production always increases with temperature, this is not the case of regenerated production (Figure 3.2b). Total primary production increases when the decrease in regenerated production is smaller than the increase in new production.

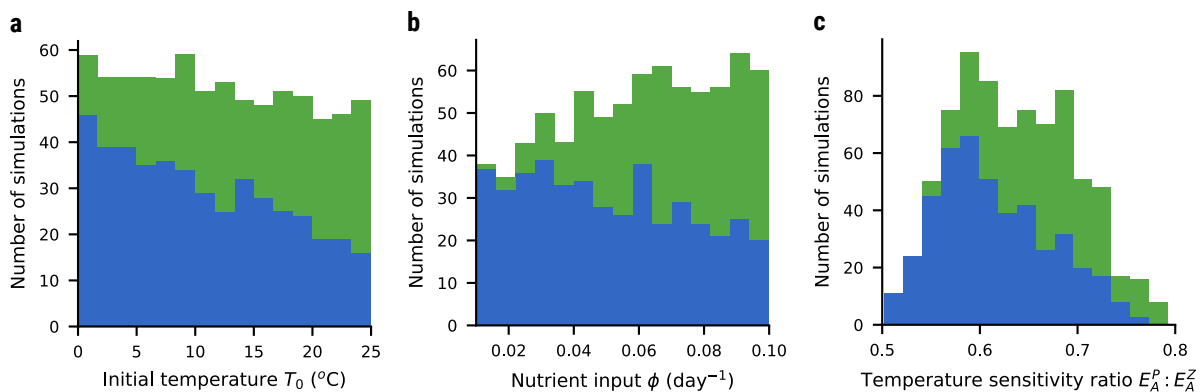


FIGURE 3.4: Key parameters influencing the ecophysiological response of primary production to warming. The number of simulations resulting in a negative (resp. positive) ecophysiological effect on primary production are represented in blue (resp. green), with respect to (a) nutrient input ϕ ; (b) initial temperature; (c) ratio of temperature sensitivities (i.e., activation energies of uptake for phytoplankton, grazing for zooplankton). These figures show that both nutrient limitation and temperature limitation are at play to explain the decrease in primary production, but that the effect of nutrient limitation is stronger.

Both nutrient limitation and the relative temperature sensitivities of phytoplankton and zooplankton are at play in this balance (Figure 3.4) with the effect of nutrient limitation being stronger. Indeed, total dissolved inorganic nitrogen (DIN) concentration (i.e., the sum of ni-

trate and ammonium concentrations) at initial temperature T_0 is a key factor of the response of primary production to warming (Figure 3.5a): positive in nutrient-rich ecosystems, negative in nutrient-poor ecosystems. Nutrient-rich ecosystems can sustain faster metabolism of phytoplankton in warmer conditions, driving primary production up. In nutrient-poor ecosystems, the increased maximum uptake rates result in stronger nutrient limitation, driving primary production down.

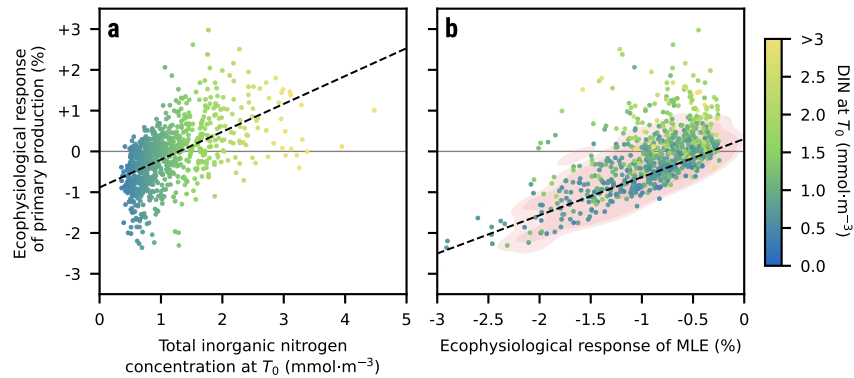


FIGURE 3.5: Ecophysiological response of primary production to warming. (a) Influence of nutrient availability. (b) Influence of microbial loop efficiency. Distribution of 1,000 simulation outputs with parameters sampled in the ranges given in Table 3.1. In (a), the dashed line is the linear regression through the whole set of simulation outputs. In (b), the red region indicates the kernel density of outputs for the resampled set of simulations that yielded dissolved inorganic nitrogen concentrations (DIN) lower than $1.5 \text{ mmol}\cdot\text{m}^{-3}$ (see Table 3.2). The dashed line represents the linear regression for the resampled simulations.

In the case of nutrient-poor ecosystems, the negative effect of warming on primary production can be directly traced to a decrease in microbial loop efficiency (Figure 3.5b). By resampling the set of parameters corresponding to nutrient-poor ecosystems (Table 3.2), we find a significant positive correlation between MLE and the ecophysiological response of primary production to warming, which approaches zero in ecosystems where little to no change occurs in MLE. This pattern is due to the fact that in nutrient-poor ecosystems, the main component of primary production is regenerated production, which strongly depends on microbial loop efficiency. In nutrient-rich ecosystems, primary production is driven mainly by new production, and ammonium production relies equally on bacterial and zooplankton respiration, thus causing a decoupling between primary production and microbial loop efficiency. In other words, only in nutrient-poor ecosystems does primary production hinge on the microbial loop.

Parameter	Minimum	Maximum	Unit
ϕ	0.01	0.05	day ⁻¹
$K_{P,new}$	10.0	15.0	mmol·m ⁻³

TABLE 3.2: Resampled parameter space for simulations yielding low DIN concentrations. All other parameters are taken from the standard run in Table 3.1.

3.2.2 Bacterial adaptation in the microbial loop drives primary production

We now assume that heterotrophic bacterial population can adapt to warming through selection. In response to a temperature increase ΔT , the adapted BGE shifts from the ω_0 value adapted to the initial sea-surface temperature T_0 to the new optimal value ω_1 adapted to temperature $T_1 = T_0 + \Delta T$. The concurrent change in ecosystem equilibrium state is the eco-evolutionary response of the system to the ΔT warming increment (red distributions in Figure 3.2). By measuring the difference between the ecophysiological response (without bacterial adaptation) and the eco-evolutionary response (with bacterial adaptation) on the ecosystem state variables we can quantify the ecosystem impact of bacterial adaptation to warming (blue distributions in Figure 3.2).

Bacterial strains with BGE lower than the initially adapted value turn out to be competitively superior in a warming ocean; as they replace the initial strain, BGE measured at the scale of the bacterial population decreases (Figure 3.2b). This occurs in response to the change in ecosystem state following from the ecophysiological response to warming. The selection gradient of BGE (equation 3.20) reveals the two main controls of selection on bacteria: top-down control by mortality (including grazing), and bottom-up control by DON-

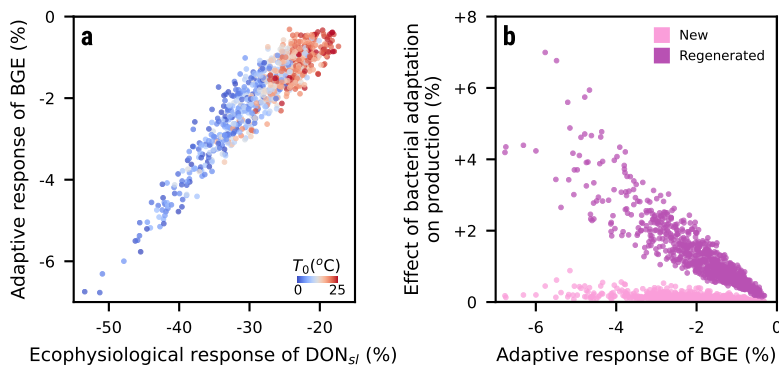


FIGURE 3.6: Eco-evolutionary feedbacks mediated by bacterial growth efficiency (BGE), ω . (a) From ecology to evolution: BGE adaptation as a function of the ecophysiological response of bacterial resource (DON) to warming. Individual simulations are color-coded according to the initial temperature. (b) From evolution to ecology: ecological impact of BGE adaptation on new and regenerated production. All parameters vary in the default parameter ranges.

limitation. Because the eco-physiological response of mortality to warming is always positive, the corresponding top-down agent of selection on BGE always intensifies with warming, which favors bacterial strains with higher BGE. Yet the result of adaptation is a decrease in BGE, showing that the system is under a stronger bottom-up limitation. Indeed, there is a strong correlation between the decrease in DON concentration and the adaptive response of bacteria (Figure 3.6a). In ecosystems with higher initial temperature, the increased mortality and relatively low decrease in DON concentrations results in weaker adaptive responses. In ecosystems with lower initial temperature, the decrease in DON concentration is stronger, resulting in a decrease in BGE. This is a consequence of the growth efficiency—resource acquisition trade-off, which favors resource acquisition when resource availability (here, DON concentration) drops.

The effect of bacterial adaptation then ripples through the whole ecosystem in a trophic cascade (Figure 3.7): the decrease in BGE drives bacterial production and microbial loop efficiency down while increasing ammonium concentrations. This nutrient increase drives phytoplankton biomass up, which adds pressure to the nitrate pool, thus decreasing the nitrate concentration. These variations in nutrient concentrations cause an increase in new and regenerated production, but not evenly so, resulting in a decrease in f-ratio.

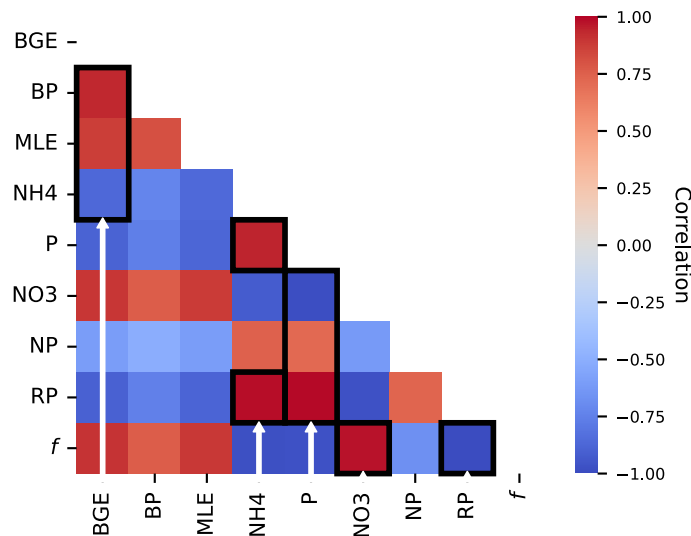


FIGURE 3.7: Correlation matrix of bacterial adaptation effects. Correlations underlying a potential causality are framed, and white arrows show causality link. BP, bacterial production; MLE, microbial loop efficiency; P, phytoplankton biomass; NP, new production; RP, regenerated production.

The adaptation of BGE to warming causes both new and regenerated production to increase (Figure 3.6b). Importantly, the net primary production variation due to bacterial adaptation to warming is of the same magnitude, or even greater than the ecophysiological response of the system (Figure 3.2b). This underscores the importance of the microbial loop and its evolutionary adaptative capacity to predict the response of primary production and other ecosystem functions to warming.

While the ecophysiological response to warming is controlled primarily by the availability of nutrients (Figure 3.5), the initial temperature of the system is also a major determinant of the eco-evolutionary response. In cold waters, warming causes a strong ecophysiological decrease in DON concentration, which selects for lower BGE. In warmer environments, the ecophysiological decrease in DON concentration is weaker, leading to a smaller adaptive response of BGE (Figure 3.6a). Thus, we expect a two-dimensional gradient of temperature and nutrient availability to shape the pattern of microbial adaptation (Figure 3.6a) and eco-evolutionary responses (Figure 3.6b).

3.2.3 Warming causes different eco-evolutionary responses in different biogeographic regions

To further evaluate the ecosystem impact of bacterial adaptation to warming, we focus on four hypothetical biogeographic regions characterized by two different initial temperatures, $T_0 = 5^\circ\text{C}$ (cold) or 20°C (warm), and nutrient input rates, $\phi = 0.03 \text{ day}^{-1}$ (poor) or 0.1 day^{-1} (rich).

The temperature difference captures the expected contrast between tropical zones and high-latitude areas. The difference in nutrient input was chosen so that the low ϕ value yields nitrate concentrations around $0.5 \text{ mmol} \cdot \text{m}^{-3}$, which is typical of oligotrophic zones; and the high ϕ value yields intermediate nutrient concentrations, ca. $2.0 \text{ mmol} \cdot \text{m}^{-3}$. Warm and poor environments are typical of subtropical gyres, while high latitude ecosystems are typically cold and nutrient-rich.

For each of these four hypothetical bioregions, we performed 1,000 simulations with parameters sampled from the default parameter ranges as before while T_0 and ϕ are fixed at values assigned to the region. Hereafter we focus on the responses of the microbial loop and primary production (Figure 3.8).

The initially adapted value of BGE tends to be larger in cold and/or nutrient-rich regions (Figure 3.8a). With warming, these regions are also the ones where the adaptive change in BGE is the largest (Figure 3.8b). As expected, primary production is in general much larger in nutrient-rich regions (Figure 3.8c), with little influence of the initial temperature. In nutrient-poor regions, ecophysiological effects of warming tend to be negative, whereas the effect of bacterial adaptation is positive (Figure 3.8d). Thus, in nutrient-poor regions, the decrease in primary production driven by the ecophysiological response to warming may be compensated by bacterial adaptation. In regions that are both nutrient-poor and cold, the positive effect of bacterial adaptation may even exceed the negative ecophysiological effect, causing an increase in primary production (Figure 3.8d).

Primary production shows contrasted ecophysiological and eco-evolutionary responses to warming. This pattern can be understood from the responses of new and regenerated

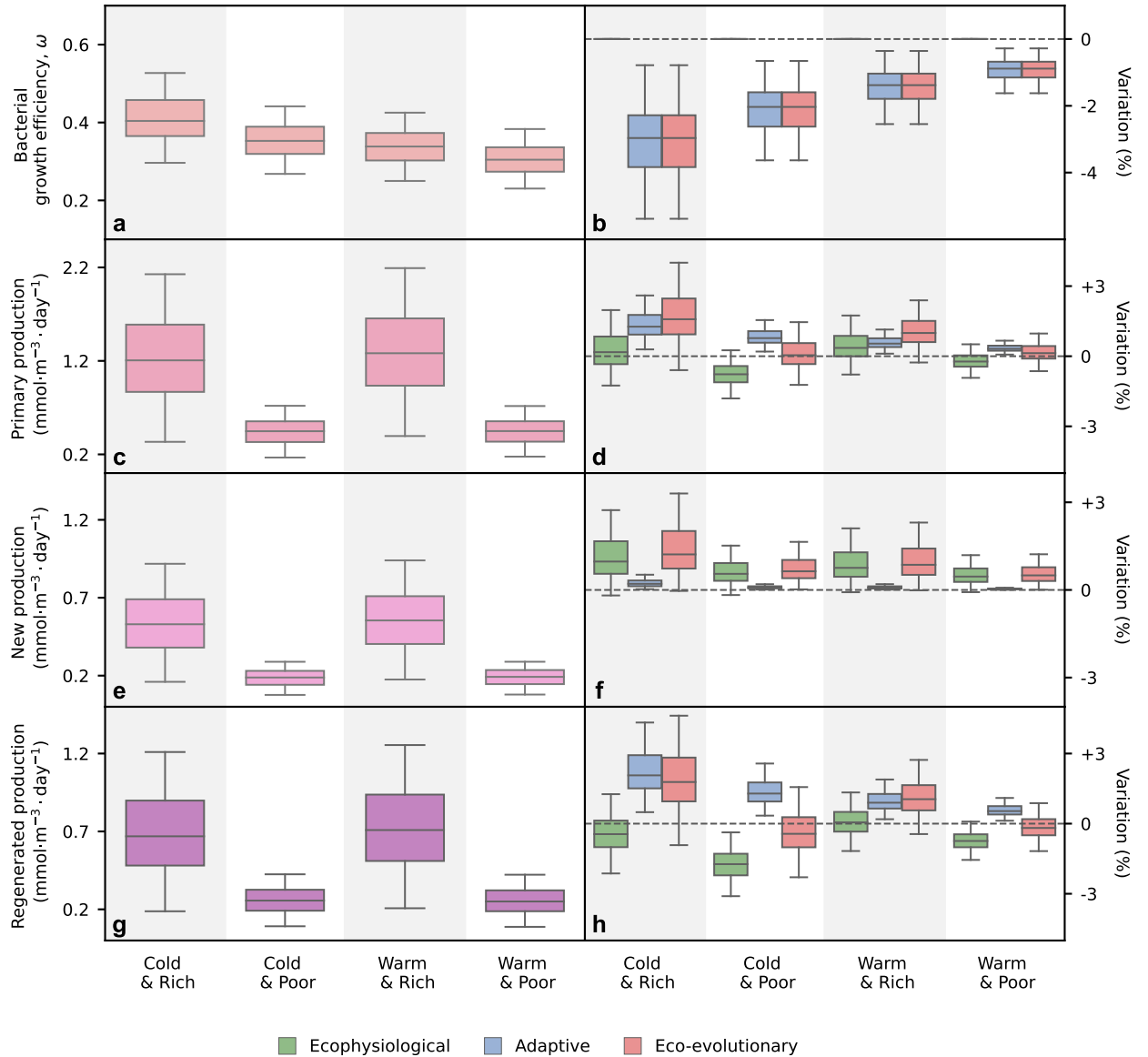


FIGURE 3.8: Initial ecosystem equilibrium and ecophysiological and eco-evolutionary responses to warming in four hypothetical biogeographic regions differing in water temperature (cold vs. warm) and nutrient availability (low vs. high). (a, c, e, g) Ecosystem equilibrium at initial temperature, T_0 . (b, d, f, h) Ecophysiological (green) and eco-evolutionary (red) responses to warming with the difference between the two quantifying the effects of adaptation through selection (blue). Initial temperature, T_0 , and nutrient input, ϕ , are fixed, respectively at 5°C or 20°C for cold vs. warm regions, and 0.03 day^{-1} or 0.1 day^{-1} for nutrient-poor vs. nutrient-rich regions. All other parameters vary in the default parameter ranges.

production (Figure 3.8e-h). The response of new production is similar in all regions (Figure 3.8f), and the contrast in primary production comes from regenerated production variation (Figure 3.8e). As seen before, the ecophysiological response of primary production is driven by regenerated production variation induced by nutrient availability—positive in nutrient-rich regions, negative in nutrient-poor regions. In contrast, the effect of bacterial adaptation is always positive (even if small on new production), but depends on the initial temperature of the environment: the effect is larger in initially cold environments, smaller in initially warm environments. This implies that the ecophysiological response of the system and the effect of bacterial adaptation add up in regions that are both cold and nutrient-rich, such as the Arctic Ocean, resulting in a strong increase in total primary production.

3.3 Conclusion and perspectives

Our study aims at improving our mechanistic understanding of nutrient cycling in the surface oceans and its response to climate warming. We asked how the rise of sea surface temperature alters the microbial loop efficiency and primary production, both ecophysiological and through bacterial adaptation. Nutrient limitation turns out to be the main control of the ecophysiological response of primary production to warming, controlling microbial loop efficiency and thus the balance between new and regenerated production. We show that bacterial adaptation is an equally important factor of the response of primary production to warming, especially in cold oceanic regions. Our results highlight the importance of two often underestimated components of biogeochemical ocean models, namely the dependence of ecosystem production on the microbial loop, and the adaptive potential of microbial populations [262, 198].

3.3.1 Ecophysiological vs. eco-evolutionary predictions

When used to resolve the ecophysiological response of the ecosystem to sea surface warming, our model predicts general trends such as a decrease bacterial, phytoplankton, and zooplankton biomass and an increase in top-down controls. This is consistent with other predictions suggesting that oceans may become more oligotrophic over time [234], with stronger top-down control by grazing [45]. Our model predicts that despite this general decrease in population biomass, primary production may either increase or decrease with warming, confirming that biomass measurements alone are poor predictors of changes in primary production [267].

Changes in the balance of top-down and bottom-up controls of phytoplankton abundance are thought to be important to assess the future of primary production in the face of climate warming [150]. Our ecophysiological model provides a simple framework to evaluate

this balance and predict the net response of primary production to warming. In agreement with existing data [30, 150], our model predicts nutrient-poor areas to be more prone to a decrease in primary production than richer regions, and provides a mechanistic explanation for this pattern. In nutrient-poor environments exposed to warming, regenerated production decreases faster than new production increases, resulting in an overall decrease in primary production. The decline in primary production is a result of a change in the balance between new and regenerated production due to a decrease in microbial loop efficiency, further confirming the important feedback of the recycling pathway in oligotrophic environments, as previously reported in Fenchel [96].

At ecosystem equilibrium, the f-ratio and the e-ratio are equal [236], meaning that new production equals export production. This allows us to predict the ecophysiological response of export production to sea-surface warming. Even though total primary production can decrease due to increasing temperatures in nutrient-poor environments, this response is fully driven by the decrease in regenerated production. New production increases across all simulated systems, which means that export production increases in all regions.

Due to their fast metabolic rates and short generation time [219] relative to the timescale of climate change, heterotrophic bacteria have a strong potential to evolve and adapt rapidly to their changing environment. Our model was designed to predict the optimal strategy of heterotrophic bacteria for resource allocation into growth in a given environment, or bacterial growth efficiency, under a trade-off with resource acquisition. As the environment changes, the optimal strategy changes, and the consequences for primary production can be evaluated. As sea surface temperature rises, the optimal BGE responds to two opposing selective pressures, namely increased bacterial mortality and the depletion of dissolved organic matter. While nutrient abundance is the main driver of ecophysiological responses to warming, environmental temperature shapes BGE adaptation. We find that increasing temperature favors a bottom-up control of BGE, with decreasing concentrations of DON driving the optimal BGE down. The DON decrease is stronger in cold regions, resulting in a stronger adaptive response of bacterial populations.

These results provide new insights into the ‘link or sink’ behavior of the microbial loop [96]. By recapturing otherwise lost organic matter and recycling or transferring it to higher trophic levels, the microbial loop can increase export production (the ‘link’ behavior). On the other hand, by fixing nutrients in bacterial biomass, the microbial loop can effectively decrease export production (the ‘sink’ behavior). Across all simulated systems, adaptation to warming drives BGE down and microbial loop efficiency decreases, with antagonistic consequences for export production. One effect is to decrease the export ratio (equal to the f-ratio in our model), acting as a sink. The opposing effect is to increase overall primary production, which increases export production, acting as a link. Both effects on export ratio and primary production are significant here, confirming the importance of taking both into account when assessing export production and its response to warming [151]. The increase in

primary production is larger than the decrease of f-ratio, which eventually makes the ‘link’ component of the microbial loop stronger.

We predict eco-evolutionary processes mediated by heterotrophic bacterial adaptation to shape contrasted biogeographical responses to warming, as bacterial optimal BGE follows a temperature gradient while ecophysiological responses follow a nutrient gradient. In nutrient-rich regions, bacterial adaptation and ecophysiological responses combine synergistically to increase both new and regenerated production. This is of particular significance in already productive cold and rich regions such as the Arctic Ocean [278], where productivity is expected to increase in the coming years [161]. Our model predicts an even larger increase due to bacterial adaptation. In nutrient-poor regions, the effects of bacterial adaptation oppose the ecophysiological decrease of primary production. In cold and poor regions, adaptation mitigates the decrease in primary production, going as far as to reverse it, whereas ecophysiology drives the overall response in regions that are both nutrient-poor and warm.

Our results underscore the need to take adaptive processes into account in predictive models of ocean productivity [271]. As BGE is often assumed to be independent of temperature for a given strain of bacteria [263, 167], it is usually set as constant in biogeochemical models, but we showed that natural selection acting on bacterial strains with varying BGE could impact our prediction of future primary production in the ocean.

3.3.2 Bridging eco-evolutionary modeling and sequence data

Our modeling approach derived from evolutionary game theory [210] is purely phenotypical in essence: BGE is treated as a quantitative character, heritable variation is assumed, and adaptation to a changing environment is predicted as the outcome of optimization under the constraint of a trade-off with resource acquisition. Under broad conditions [129, 90], the underlying genetic architecture of the traits and genetic mechanisms of their variation do not alter the phenotypic results. However, the study of microbial communities has benefited tremendously from the expansion of our molecular sequencing capability and genomic and other ‘omics’ analytical toolbox. These advances provide support for underlying hypotheses in our models and present new opportunities to evaluate our key predictions, as we briefly summarize hereafter.

‘Omics’ studies can support and inform phenotypic models by providing data on genes, transcripts, proteins and metabolites to infer phenotypic trait variation within and between populations, and uncover some of the underlying mechanisms such as selection and constraints. BGE is a challenging trait to extract from omics data [170] because it compounds multiple underlying traits related to cellular maintenance, protein synthesis, and metabolic and respiratory pathways [233, 193]. Saifuddin et al. [233] circumvent these difficulties and

predict BGE by using genome-scale metabolic modeling subject to flux balance analysis [246]. They resolve BGE variation across 200 bacterial taxa and provide support for the adaptive nature of this variation and for the growth efficiency—resource acquisition trade-off used in our model. This is in support of other studies combining comparative genomics with direct trait measurement by laboratory assays [193, 230].

Evidence from omics studies is also growing for the role of adaptive evolution in the response of whole microbial communities to environmental change [176, 199, 242]. New metagenomic computational pipelines hold much promise to extend pioneering evolutionary analyses done in small-scale systems such as the human gut microbiome [111, 282, 243] to ocean microbial communities. For example, bioinformatic pipelines for microbial community metagenome assembly such as GraftM [31] and MetaPop [117, 58] can resolve microbial metagenomic sequence data at intra-population level, identify Single-nucleotide polymorphisms (SNPs), calculate nucleotide diversity, and detect positive selection within populations. We expect such computational tools to greatly improve our ability to assess bacterial adaptive evolution within natural communities such as those involved in the ocean microbial loop.

Finally, ecosystem models that assume a simple relation between phenotypic traits and gene-encoded biochemical pathways [241] pave the way for the development of phenotype-based models of evolutionary adaptation that will directly simulate metagenomes and metatranscriptomes, hence opening the possibility to quantitatively test the predictions of models like ours with omics data.

3.3.3 Model extensions and conclusion

To our knowledge, this is the first model aimed to predict the effect of microbial adaptation on ocean productivity. Previous models of biological adaptation in warming oceans addressed the impact of adaptation through selection on phytoplankton community diversity [241, 255, 119, 238, 22]. Some of these studies suggest that adaptation may reduce community diversity especially in tropical regions, leading to a potential decrease in primary production in these regions [255]. Future work is warranted to probe the generality of this result, integrate bacterial and phytoplankton adaptation in a common framework, and extend the scope of potential adaptive responses to warming to a broader set of traits and trade-offs, and to other functional groups. We highlight two areas of interest.

Regarding the set of traits and trade-offs, our model focuses on the growth efficiency vs. resource acquisition trade-off, thus assuming that bacterial populations do not change along the stress-tolerance axis of life-history variation. This assumption could be lifted in future work. By using sequence data and computational tools to extract quantitative information about stress tolerance traits, we should be able to extend existing comparative genomic

analyses to obtain a more comprehensive and quantitative understanding of bacterial phenotypic variation in all three axes of life-history evolution: growth efficiency, resource acquisition, and stress tolerance [170]. Such information is needed to account for stress tolerance in predictive models of bacterial adaptation. Once done, it will be possible to address the specific ecophysiological and eco-evolutionary effects of stressors such as extreme climatic events on microbial loop efficiency, and their consequences for carbon and nutrient cycling.

Regarding the inclusion of other functional groups, viruses are of particular interest because of their dramatic direct ecological impact (e.g., the viral shunt of material fluxes [96, 277, 63]), their indirect role as physiological hijackers and selective agents of their hosts [33], and their own capacity for record fast evolution and adaptation to ecological and environmental change. Existing ecosystem models provide a solid foundation for such developments [274], which will contribute to a general workflow for integrating micro-organisms evolutionary adaptation in global earth system models. Meta-omics tools and analyses that have been developed specifically for marine viral communities [118] should help identify key adaptive traits and trade-offs that would be captured in eco-evolutionary models.

In conclusion, bacteria adaptation to warming can drive changes in ocean primary production of the same magnitude as the ecophysiological response, especially in the most productive areas such as the Arctic Ocean. While ecophysiological mechanisms may accurately predict short-term responses of ecosystem function to seasonal variation in temperature, we expect eco-evolutionary responses to be important on multi-annual timescales, over which bacterial populations may evolve and adapt to long-term trends in temperature. Our model provides a critical step towards the integration of microbial eco-evolutionary processes in ocean ecosystem models, necessary for improving our projections of ocean nutrient cycle in a warming world.

Chapter 4

Natural selection in Earth system models

With Anh Le-Duy Pham, Olivier Aumont and Régis Ferrière, in progress. Presented at AGU Fall Meeting 2021 [47].

‘Mutation: it is the key to our evolution. It has enabled us to evolve from a single-celled organism into the dominant species on the planet. This process is slow, and normally taking thousands and thousands of years. But every few hundred millennia, evolution leaps forward.’

Professor X, *X-Men* (2000)

Given the importance of the ocean-atmosphere coupling, predicting the future of biogeochemical cycles in the ocean is a major challenge for understanding climate change. Earth system models (ESMs) are general models designed to represent the interactions between the different ‘systems’ of the planet: physical evolution of climate, biogeochemistry and anthropogenic influence [103]. Developed to simulate the oceans and forecast its future state, they are successful at fitting past and current observations, but their forecasting capacity is limited by large levels of uncertainty. Even though significant efforts have been made to account for biological processes of increasing complexity in ESMs, these models remain agnostic to a fundamental ability of life: that of evolving and adapting in response to environmental change. This is especially true of microbial populations, with their remarkably large sizes and genetic diversity. As the ‘microbial engines’ of biogeochemical cycles evolve and adapt to changing environments, they may in return alter the global biogeochemistry of our planet. Predicting to what extent was the question at the core of this chapter.

To address this question, we implement eco-evolutionary processes in ESMs in a way that aim at computational efficiency and biological consistency. Our approach basically extends the selection gradient equation of adaptive dynamics to global ocean ecosystem models.

We test our approach in a low-dimensional proof-of-concept setting, and implement it in the NEMO-PISCES ESM by focusing on the adaptive evolution of bacterial growth efficiency (BGE) in heterotrophic bacteria. We find that BGE values exhibit a consistent biogeographical pattern that correlates with labile DOC concentrations, and that taking bacterial adaptation into account introduces a new layer of uncertainty in primary production forecasting.

4.1 Eco-evolutionary processes in ESMs, a current blindspot

4.1.1 The importance of adaptation for climate forecasting

The ocean plays a major role in the carbon cycle. It holds fifty times more carbon than the atmosphere [93] and absorbs more than a quarter of all anthropogenic emissions of carbon due to the sheer size of its surface [272]. Oceanic life in particular is central to biogeochemical cycles: half of all primary production in the world comes from phytoplankton [92], and oxygen minimum zones depend on the presence of aerobic bacteria [205].

Yet the future of ocean biogeochemical cycles under climate change is uncertain. The rise of carbon concentration can lead to acidification [225], and sea surface temperatures rising may cause weaker nutrient fluxes from the deep sea [30], deoxygenation [205], and sea-level rise [39]. Those changes may have dramatic consequences on ecosystems [23, 38], which may feed back to the atmosphere and further alter the Earth's climate.

General circulation models (GCMs) have been developed to understand and predict the dynamics of the ocean-atmosphere interface and forecast the future of the carbon cycle [91]. Improving predictions and forecasts requires constant complexification and refinements. Notably, biogeochemical cycles driven by oceanic life are now included in most models [102], turning GCMs into Earth system models (ESMs). However, the integration of biological and ecological processes remains fragmentary. In particular, heterotrophic bacteria and the microbial loop are represented in some models [132] but not others [15].

Ecosystem models are calibrated on data from past and current states, and forecasting assumes that species a hundred years from now will not be sensibly different from what they are now [137]. While this may be a reasonable approximation for organisms with long lifespans and generation times such as large vertebrates, this may not apply to the bulk of biodiversity: microorganisms that are known to evolve and adapt rapidly to changing environments [111, 282]. As microbial life is central to biogeochemical cycles [94], taking into account microbial adaptive capacity appears to be paramount for a better understanding and forecasting of our oceans and climate. [137, 187].

As the planetary environment changes, the ocean microbiome will evolve and adapt, and feed back to the global Earth system. The inclusion of such eco-evolutionary processes in

ESMs has been a research focus in recent years [271, 154], but difficulties remain that hampers implementation. There is a need for a mathematical and computational framework that is both simple and operational enough as to be run effectively, and biologically valid as to give meaningful predictions. In this chapter, we address this challenge by shifting from mechanistic models of eco-evolutionary processes to phenomenological descriptions relying on the macroscopic models of adaptive dynamics.

4.1.2 State of the art

Here we present a brief overview of existing frameworks and highlight the underlying common principle. A more comprehensive review is to be found in Ward et al. [271]; here we only focus on their methodological specificities.

A brief review of existing frameworks

The ‘brute force’ method to integrate eco-evolutionary processes in an Earth system model would be to implement an individual-based model (Figure 4.1a), where each individual is represented by their phenotype (typically a quantitative trait or suite of traits). When an individual reproduces, there is a non-zero probability that their offspring has a slightly different phenotype, caused by a mutation in the underlying genotype. On the long term, this process fuels the evolutionary adaptation of the population, in a feedback loop with its environment (see Chapter 1). Such a simulation approach, however, is computationally prohibitive, given the size of the microorganism populations that we focus on, and the computational demand of ESMs in and on itself. Consider cyanobacteria: a single milliliter of sea water contains about 100,000 individuals [104]. In a dynamic ocean where water masses flow and mix, the number of interactions integrated over the ocean would be literally astronomical. In order to circumvent this difficulty, several options are conceivable (Figure 4.1). Some models represent populations as densities on a continuous trait space (Figure 4.1b), and eco-evolutionary processes are implemented as a diffusion process [154]. But integrating over both the trait space and geographic space remains computationally unaffordable, and further approximations are needed. One may assume that the population trait density follows a normal law [154], leading to explicit mathematical expressions for the evolution of trait mean and variance (Figure 4.1c). This approach raises two issues: first, when two distributions from two water cells mix, the resulting distribution is far from a normal distribution, which may not be captured by this model; secondly, assuming trait densities other than Gaussian distributions could lead to drastically different results. Another approach is to discretize the trait space (Figure 4.1d), and thus constrain the number of possible phenotypes. Recurrently then, the less adapted phenotypes are replaced by new phenotypes, which are generated stochastically [58] or deterministically [158, 238]. Here a significant issue stems from the definition of

which phenotypes to replace: one might replace the least abundant [58] or merge the most similar [54], but either option remains somewhat arbitrary. Finally, one could do entirely without trait diversity, and focus on monomorphic populations (Figure 4.1e). New phenotypes would appear one at a time, with each invasion being resolved by determining which phenotype is fitter [148]. The limitation here lies in strong biological assumptions, such as populations at ecological equilibrium, new populations at initially very small densities or mutations appearing one at a time.

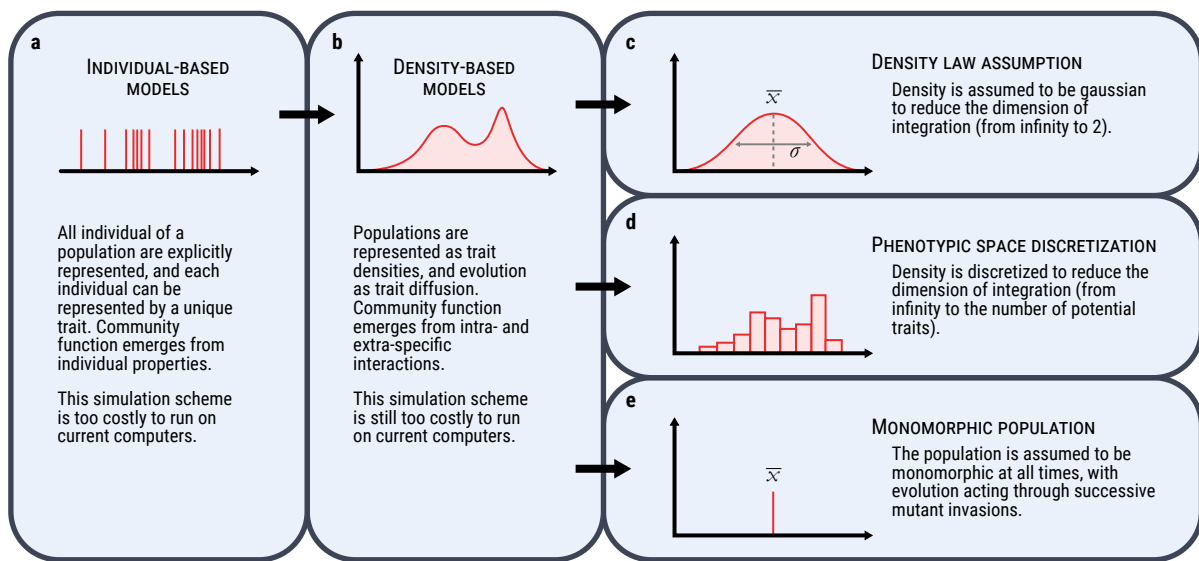


FIGURE 4.1: Current simplification schemes for integrating eco-evolutionary processes in Earth system models. Left to right, from the most complex to the simplest. (a) Individual-based models; (b) Density-based models; (c) Density law assumption; (d) Phenotypic space discretization; (e) Monomorphic population assumption.

Despite the important differences between the models we briefly described, they all share an underlying principle. At their core, all these models try to simplify individual-based models to make them computationally tractable through assumptions of large populations, small mutations or trait diffusion. All these models describe adaptive evolution as a stepwise process in a mechanistic way: first, new genotypes are generated, either through mutations or immigration; then, the fittest phenotypes are selected. Models may differ in the way they perform phenotype generation (stochastic vs. deterministic) or subsequent selection (as the outcome of explicitly modeled ecological interactions, or through a fitness function derived from the ecological model). These two steps represent what we call the ‘generation-selection’ cycle.

4.2 A proposed alternative: the selection gradient equations

Here, we propose an alternative modeling approach by departing from mechanistic models of the generation-selection cycle and favoring a phenomenological approach (Figure 4.2). If we assume that adapting populations follow a selection gradient, we can use eco-evolutionary theory to derive an equation governing the dynamics of population phenotypes, and then integrate them in ESMs. By doing so, we can avoid a large fraction of the computational cost of the more mechanistic models, while taking advantage of the body of eco-evolutionary theory.

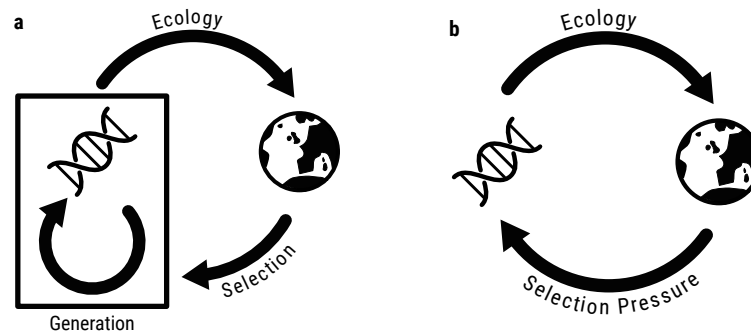


FIGURE 4.2: From the ‘generation-selection’ cycle (a) to the selection pressure (b): a paradigm shift.

4.2.1 Keeping the basic structure of current ESMs

The goal of our approach is to fit as seamlessly as possible into current ESMs by adopting their ecosystem modeling principles. This will facilitate the comparisons of our predictions with previous, non-evolutionary model output and thus to quantify the effect of eco-evolutionary processes on scenarios of future ecosystem and climate change.

One critical step of our approach is to avoid describing the diversity of phenotypes at any point in time within a population. The representation of trait diversity would fundamentally alter the algorithmic structure of current ESMs. Biogeochemical components of current ESMs such as PISCES [15] are compartment models in which metabolic traits are shared across organisms in each compartment (Figure 4.3). For instance, the same temperature dependency (represented by the Q_{10} trait) is shared amongst all diatoms in the PISCES model. This modeling strategy allows us to keep the original ecological models used in current ESMs intact, with eco-evolutionary processes implemented as a way to have dynamical parameter values. Instead of a set of individuals expressing potentially different trait values, we focus on the mean trait value and assume that the underlying mechanism of trait variation (i.e. genetic mutation) only causes small changes.

Describing the adaptation dynamics of the traits is done through a differential equation.

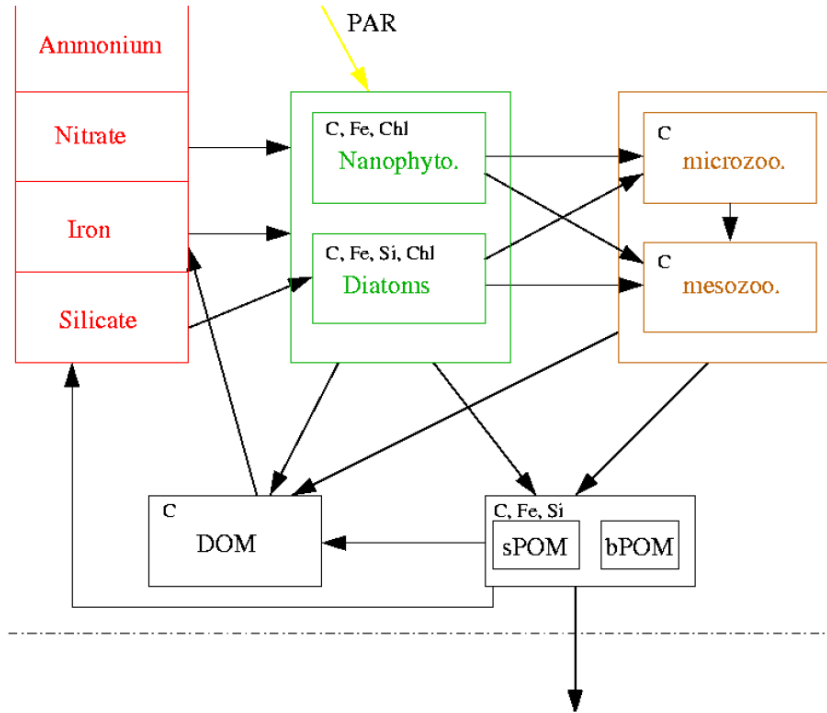


FIGURE 4.3: Architecture of PISCES. This figure only shows the ecosystem model omitting thus oxygen and the carbonate system. The elements which are explicitly modeled are indicated in the left corner of each box. Figure taken from Aumont et al. [15].

Hereafter we focus on a one-dimensional trait space, and explore higher dimensionality in the ‘further developments’ section. Although the one-dimensional trait case may appear limited in scope, it is rich in practical applications: for example, cell size is an integrative trait that influences many secondary traits in phytoplankton populations, and heterotrophic bacterial growth efficiency is an ‘effect trait’ of major significance for nutrient cycling and ecosystem function. We denote the one-dimensional trait by x and describe its adaptive evolution through the following equation:

$$\frac{dx}{dt} = \Sigma(x, E) \tag{4.1}$$

where E represents all relevant environmental parameters and $\Sigma(x, E)$ denotes the selection ‘pressure’.

Key to our modeling approach is to apply equation (4.1) to each single water cell. This allows us to keep our model consistent with the biogeochemical structure of current ESMs such as NEMO-PISCES [15], where biogeochemical fluxes are simulated exclusively through the use of oceanic tracers [123]. Tracers are properties of a water cell that can be physical (e.g. temperature), chemical (e.g. salinity) or biological (e.g. phytoplankton biomass) [236]. They can either be physically ‘extensive’ (such as biomass) or ‘intensive’ (such as temperature) depending on how they behave relative to water cell mixing. Defined as such, our trait x

cannot be considered a tracer – to keep track of its time dynamics, we need to define a new tracer that takes the trait into account. If x is the trait of a population with biomass P , we define the tracer $Tr(x) = x \times P$. We can then find the value of our trait x by dividing this new tracer by the population biomass. The resulting trait of two water masses mixing will be the weighted average of each trait relative to the population biomasses.

We emphasize that this solution is in and of itself an approximation, but argue that it may not cause much more error than methods that pre-define the shape (e.g. Gaussian) of a trait distribution [154]. Our approach amounts to approximate the trait of the average population by the weighted average of the traits, which is a reasonable approximation in most cases.

4.2.2 Defining the selection gradient

Based on the canonical equation of adaptive dynamics [79, 40], we propose the following analytical form for the selection pressure:

$$\Sigma(x, E) = \alpha \cdot N \cdot P(x, E) \quad (4.2)$$

where α is the adaptation capacity of a given taxon, N the population size and $P(x, E)$ the selection gradient. We assume that trait x can be represented by a certain unit u , such as $[x] = u$ and that population size N can be represented by a unit N (which can be biomass density, population count, etc...). Time is represented by an arbitrary unit T .

The α parameter represents the adaptive capacity when normalized for population size, with $[\alpha] = u \cdot T^{-1} \cdot N^{-1}$. In the absence of data on mutation rate and variance, the α parameter may be difficult to calibrate directly; calibration should be done instead based on the credibility of model outputs. We assume that rate of adaptation is proportional to population size: larger populations can generate more variation that fuels adaptation. Finally, we need to define the selection gradient P in the context of ESMs. Simple dimensional analysis tells us that this measure should be dimensionless, and there are three ingredients that should enter its derivation:

1. If the population stands at an evolutionary stable strategy x^* [98] for a given environment E , then $P(x, E) = 0$. A population reaching an evolutionary stable strategy may not evolve any further. Conversely, if the population is phenotypically far from its evolutionary stable strategy, selection should ‘push’ towards locally fitter traits.
2. It needs to be locally computable, both spatially and temporally. Some studies [72] calculate the expected attractor (point equilibrium) of adaptation a priori; then the selection gradient is modeled as a ‘restoring force’ which drives adaptation. Other studies

[227] average the gradient over time. These approaches are not computationally viable in a dynamic environment as spatially complex as the global oceans, and we need a measure that can be easily computed at each grid cell, at each time step. In addition, this is consistent with the fact that selection gradients act at all times, and in all environments locally.

3. The selection gradient model should be prone to biological interpretation. The model should be consistent with biology and not a an ad hoc mathematical construction. This is needed to allow biological interpretations of the process at all relevant spatial scales, from local to regional to global, and at each time step. For instance, this suggests that we should avoid deriving a model for the average trait from one that assumes forces a specific arbitrary mathematical form for phenotype space or trait distribution.

These criteria insure that our equation will stick as closely as possible to the biological reality of ecosystems while being computationally cheap.

We use the selection gradient P from the adaptive dynamics modeling approach, which is based on the concept of invasion fitness [98]. The invasion fitness measures the ability of a given phenotype to invade and replace a resident population that was at ecological equilibrium, and is defined as the initial growth rate of the invading population. The underlying assumption is that a phenotype that is able to grow (as a population) in an environment where a resident population is at equilibrium, will eventually outcompete the resident. If both phenotypes are close enough as to essentially share the same ecological niche, the competitive exclusion principle implies that the invasive population will replace the resident population [115].

We emphasize that the derivation of the selection gradient from invasion fitness does not assume an actual sequence of mutation, invasion and selection. The ‘mutation-invasion-selection’ cycle is a mathematical treatment (timescale separation) which allows to derive the selection gradient and thus obtain a model of the continuous-time dynamics of the adaptive trait.

Invasion fitness is usually defined for an ecosystem at ecological equilibrium, which is not the case here: we need an equivalent for non-stationary systems. For this equivalent, we use the instantaneous invasion fitness defined as the difference $\Delta r_{x',x}$ between the invading and resident population growth rates when the invading population is infinitesimally small compared to the resident. Similar approaches have been developed in other works, notably in Dercole et al. [74] for stationary but out-of-equilibrium ecologies, and Cortez and Ellner [60].

$$\bar{S}(x', x) := \Delta r_{x',x} \tag{4.3}$$

This quantity measures whether a new population is fitter than a population already established in that niche. When the resident population is at ecological equilibrium, this definition matches standard invasion fitness. For phenotypes that are close enough (and away from an evolutionary stable strategy), this quantity will be positive on only one side of the resident trait, thus giving the direction of evolution (Figure 4.4).

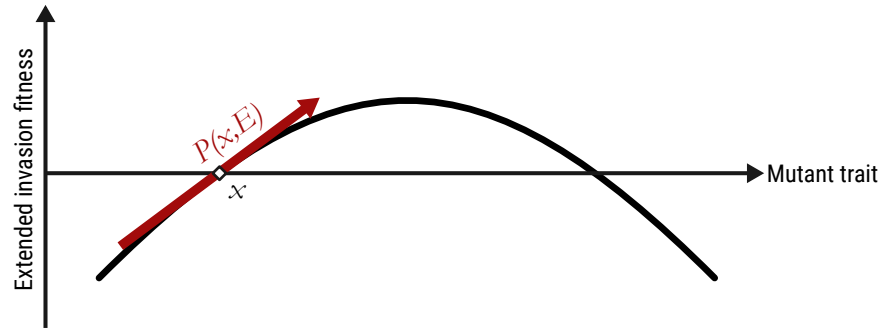


FIGURE 4.4: Computing the direction of evolution from the extended invasion fitness.

We then define P as the gradient of the instantaneous invasion fitness, representing the gradual change of population trait over time (normalized by $s_0 = 1$ for the sake of dimension consistency). Using the same notation as in the previous chapters, we find:

$$P(x, E) := \frac{d\bar{S}(x)}{s_0} \quad (4.4)$$

This measure captures both the direction and the strength of selection and fulfills our three criteria:

1. By definition of the gradient, selection ‘pushes’ population traits towards a convergent stable strategy.
2. The selection gradient stems from a growth rate, and is thus locally computable at any point in time.
3. It offers a biological interpretation, namely the differential of effective growth on either side of the resident trait.

Finally, we can write the complete selection gradient equation as follows:

$$\frac{dx}{dt} = \alpha \cdot N \cdot \frac{d\bar{S}(x)}{s_0} \quad (4.5)$$

4.2.3 Pros and cons of the method

A selection gradient modeling approach holds promises for the integration of evolutionary adaptation and eco-evolutionary feedbacks in global ecosystem models. Here we emphasize some caveats.

First, as mentioned before, this conceptual framework does not include phenotypic diversity within a population. This is at odds with previous eco-evolutionary studies in which phenotypic diversity is central: speciation [231], seasonal phenotypic variations [22] or phylogeny [176]. As we develop a framework to fit eco-evolutionary processes into current ESMs and study the future of biogeochemical cycles on long timescales, the lack of an explicit representation of phenotypic diversity may not be critical.

Similarly, since population adaptation works on timescales of multiple generations, this method is only fit for studies taking place on long timescales. As such, it is relevant for the study of biogeochemical cycles under climate change, but less so for the study of seasonal ocean dynamics, such as algal blooms.

Finally, our method only deals with population phenotypes without an explicit genotype-phenotype map. One drawback is to prevent linking models with omics data, that advancing technologies are generating at exponential rates [176]. Bridging the gap between 'omics data and our proposed framework for integrating eco-evolutionary processes into ESMs should be a research focus for the near future, following the path charted by studies such as Coles et al. [58].

In spite of these limitations, our method is cost-effective from a computational standpoint. It is algorithmically compatible with the current generation of ESMs and the model outputs lend themselves to biological interpretation, especially with respect to comparing ecosystem trajectories with and without adaptive trait variation and eco-evolutionary feedbacks.

4.2.4 Theoretical evaluation in a chemostat model

In order to evaluate our framework, we implemented the selection gradient equations in an ecosystem toy model with no spatial component. By comparing eco-evolutionary dynamics predicted by the selection gradient equation to individual-based simulations, we can assess the performance of the former.

Toy model and analysis

In this simple chemostat model (Fig 4.5), we consider a single bacterial population B and a single resource R , with an input and washout rate J . The state of the environment is mea-

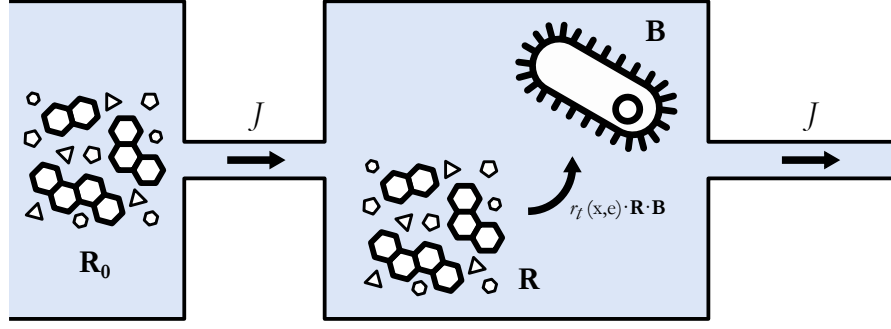


FIGURE 4.5: The one-compartment chemostat model. R_0 represents the constant resource concentration in the reservoir, R the resource concentration in the chemostat, B the bacterial biomass in the chemostat, J the washout rate, r_t the individual bacterial growth rate, x the bacterial trait and e the environmental parameter.

sured by a time-series E_t , which can be parametrized to be constant, or change linearly or randomly (e.g. as a Brownian motion) with time. The fitness of a population relative to the current environment can then be represented by a single trait x , and the individual growth rate depends on the distance between the trait and the environmental measure:

$$r_t(x) = \lambda \cdot \exp\left(-\left(\frac{x-E_t}{\sigma}\right)^2\right) \cdot R \quad (4.6)$$

The closest we can get to mechanistically represent adaptation in such a setting is through an individual-based model, that we implement with a rigorous Gillespie algorithm [42] by assigning a constant carbon content q to bacterial cells. We derive the selection gradient equation under the assumption of large populations (which allows us to treat population and resource abundance as density and concentration, respectively). Under this assumption, the density dynamics can be described by the following set of equations:

$$\begin{cases} \frac{dR}{dt} = J \cdot (R_0 - R) - r_t(x) \cdot B \\ \frac{dB}{dt} = r_t(x) \cdot B - J \cdot B \end{cases} \quad (4.7)$$

From this set of equations, we derive the selection gradient at each time step:

$$d\bar{S}(x) = -2 \times \frac{x - E_t}{\sigma^2} \times r_t(x) \quad (4.8)$$

The selection gradient equation is implemented with Newton's method at each timestep for different values of α . This allows us to compute the equation dynamically even in complex cases such as the environment fluctuating as a Brownian motion. We score the outputs of the selection gradient equation according to their \mathcal{L}^2 -distance to the mean trait of the individual-based model.

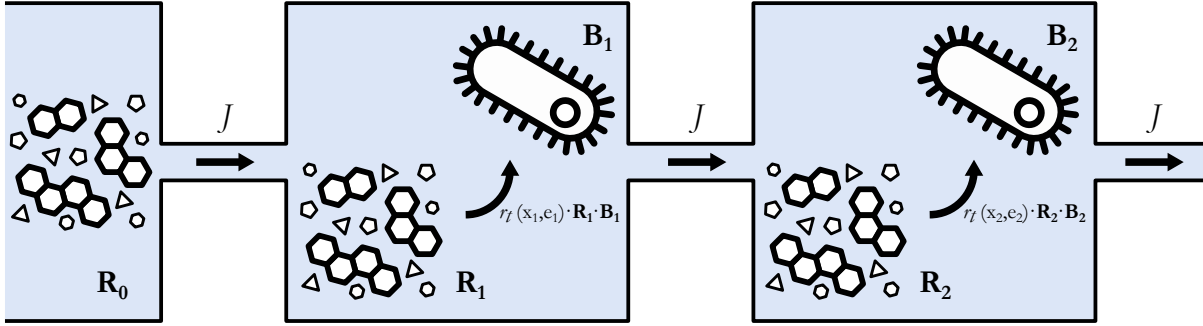


FIGURE 4.6: The two-compartment chemostat model. R_0 represents the constant resource concentration in the reservoir, R_i the resource concentration in the i -th chemostat, B_i the bacterial biomass in the i -th chemostat, J the washout rate, r_i the individual bacterial growth rate, x_i the bacterial trait and e_i the environmental parameter in the i -th chemostat. All parameters are defined in Table 4.1.

Finally, we implement the method for a two-compartment chemostat model in which each compartment has a different environmental parameter (Figure 4.6). Material from the first compartment drains into the second compartment, and we parametrize the model such as the main source of trait variation in the second compartment comes from mixing with the first. The α value is shared between both compartments.

Parameters used for the simulations are described in Table 4.1.

Parameter	Value	Unit
R_0	2.5	$\text{mmol} \cdot \text{m}^{-3}$
J	0.5	h^{-1}
λ	1	h^{-1}
σ	1	-
q	1E-3	mmol
α	variable	$\text{h}^{-1} \cdot \text{mmol}^{-1} \cdot \text{m}^3$

TABLE 4.1: Simulation parameters for the chemostat models.

Results and conclusions

When varying α logarithmically in the range $[2.5 \cdot 10^{-8}; 2.5 \cdot 10^{-3}] \text{h}^{-1} \cdot \text{mmol}^{-1} \cdot \text{m}^3$, we find values that yield a good approximation of the trait distribution mean regardless of the environmental dynamics (red lines in Fig. 4.7). When α is too low, the inertia is too strong and does not capture rapid adaptation to a new environment. Conversely, high values of α can lead to trait values sticking to the environmental value, showing the importance of parametrization.

We computed the selection gradient equations for different population sizes by varying

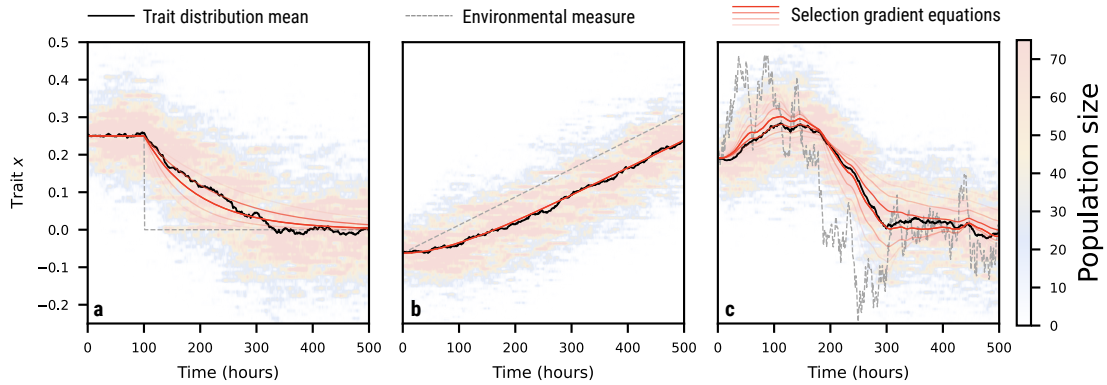


FIGURE 4.7: Comparing the selection gradient equations to individual-based simulations under three environmental conditions. (a) Discontinuous variation. (b) Linear variation. (c) Brownian motion. The mean of the trait distribution is represented in black, and the environmental parameter in dotted gray lines. The selection gradient equations (red lines) were computed for different values of α , and represented with different shades according to their distance (in the \mathcal{L}^2 sense) to the prediction from the individual-based model. All parameters are defined in Table 4.1.

bacterial content q by a factor 10 and increasing adaptation speeds through increasing mutation probabilities (Figure 4.8). The selection gradient equations are scored according to their distance to the mean trait of the individual-based model, with shades that are inversely proportional to their \mathcal{L}^2 -distance.

To compute these scores, we used the same parameters across simulations. For some simulations, a large number of outputs from the selection gradient equations with different α values stand out in the figure. This indicates that the simulations have trouble distinguishing which value fits the mean trait best. We conclude from this observation that the method is unfit for small populations, in which stochastic variations are much more important and cannot be captured by the selection gradient equation. However, the results are robust to different adaptation speeds when the population is large enough. In particular, fast adaptation can be captured by our model.

In order to test the influence of mixing, we examine the two-compartment chemostat model in which the environmental variation is driven by a Brownian environment in the first compartment while the environment is constant in the second compartment. Thus, the only trait variation in the second compartment comes from mixing, allowing us to evaluate the method for mixing water cells (Figure 4.9).

We find that even when trait variation comes exclusively from mixing with other water cells, the selection gradient equation can be parametrized to fit both a compartment where trait variation comes from natural selection (compartment 1) and a compartment where trait variation comes from mixing (compartment 2).

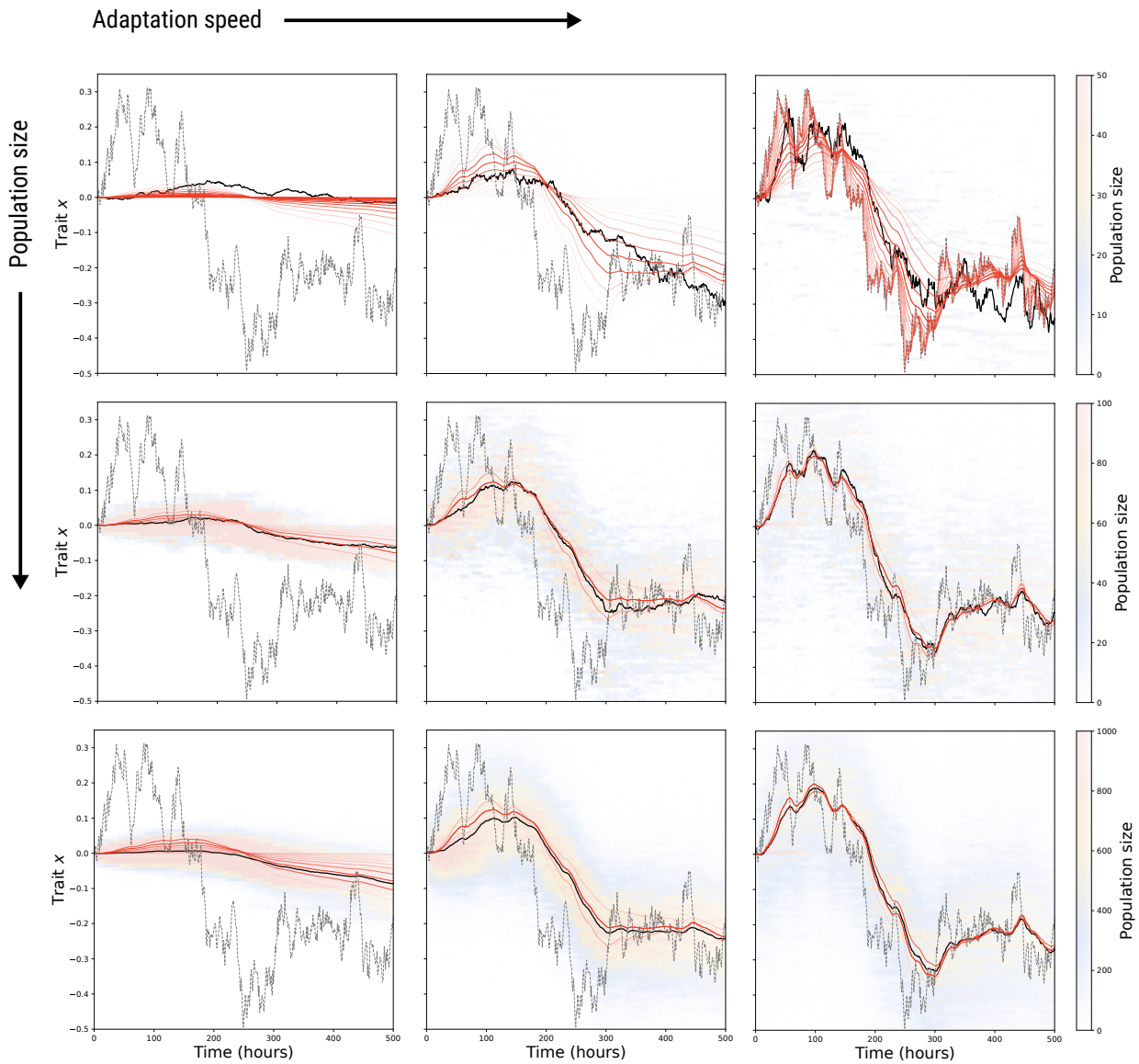


FIGURE 4.8: Comparing the selection gradient equations to individual based models for different population sizes (top to bottom) and adaptation speeds (left to right). The selection gradient equations were computed for different values of α , and represented with different shades according to their distance (in the \mathcal{L}^2 sense) to the ‘exact’ result from individual-based simulations.

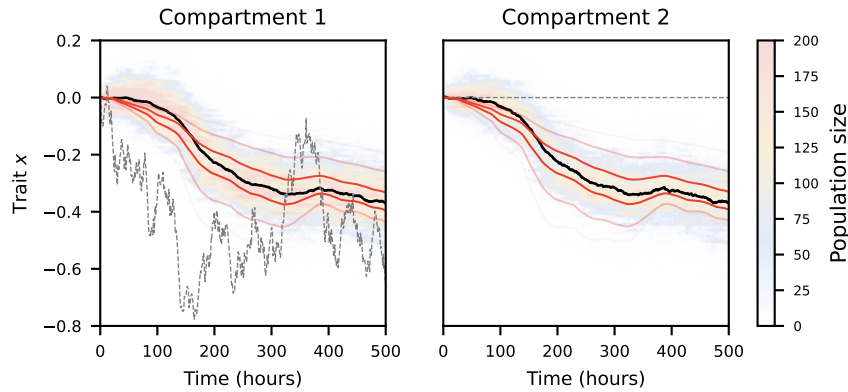


FIGURE 4.9: Comparing the selection gradient equations to individual based models in a two-compartment chemostat model. The mean of the trait distribution is represented in black, and the environmental parameter in dotted gray lines. The selection gradient equations (red lines) were computed for different values of α , and represented with different shades according to their distance (in the \mathcal{L}^2 sense) to the target result from the individual-based model.

4.3 Bacterial growth efficiency in NEMO-PISCES

In this section, we present a first effective integration of eco-evolutionary processes in an Earth system model. We implement the selection gradient equation in the NEMO-PISCES model to study the evolution of bacterial growth efficiency (BGE) and examine the consequences for bacterial biomass, LDOC concentrations and primary production.

Bacterial adaptation may have important consequences for the future of primary production [48]. As the environment changes, population-wide metabolic parameters shift due to natural selection. In return, this shift may alter the ecological state of the system, entangling environmental parameters and population metabolisms in an eco-evolutionary feedback loop [187]. Because of the role of heterotrophic bacteria in nutrient recycling, we expect bacterial adaptation to play a role in ocean productivity and ocean ecosystem function [269], potentially altering the balance between new and regenerated primary production. How much and where then become key questions, that we address in this section.

4.3.1 Methods

The NEMO-PISCES model

In this study, we integrate the selection gradient equation in the NEMO-PISCES coupled model used in Pham et al. [215], which is based on PISCESv2 [15]. We use the ORCA2-LIM configuration of NEMO for the dynamic state of the ocean, which has a horizontal resolution of at most 2° , with a resolution increasing to 0.5° at the equator, and 30 vertical levels of increasing depth (10m at the surface to 500m at 5000m depth).

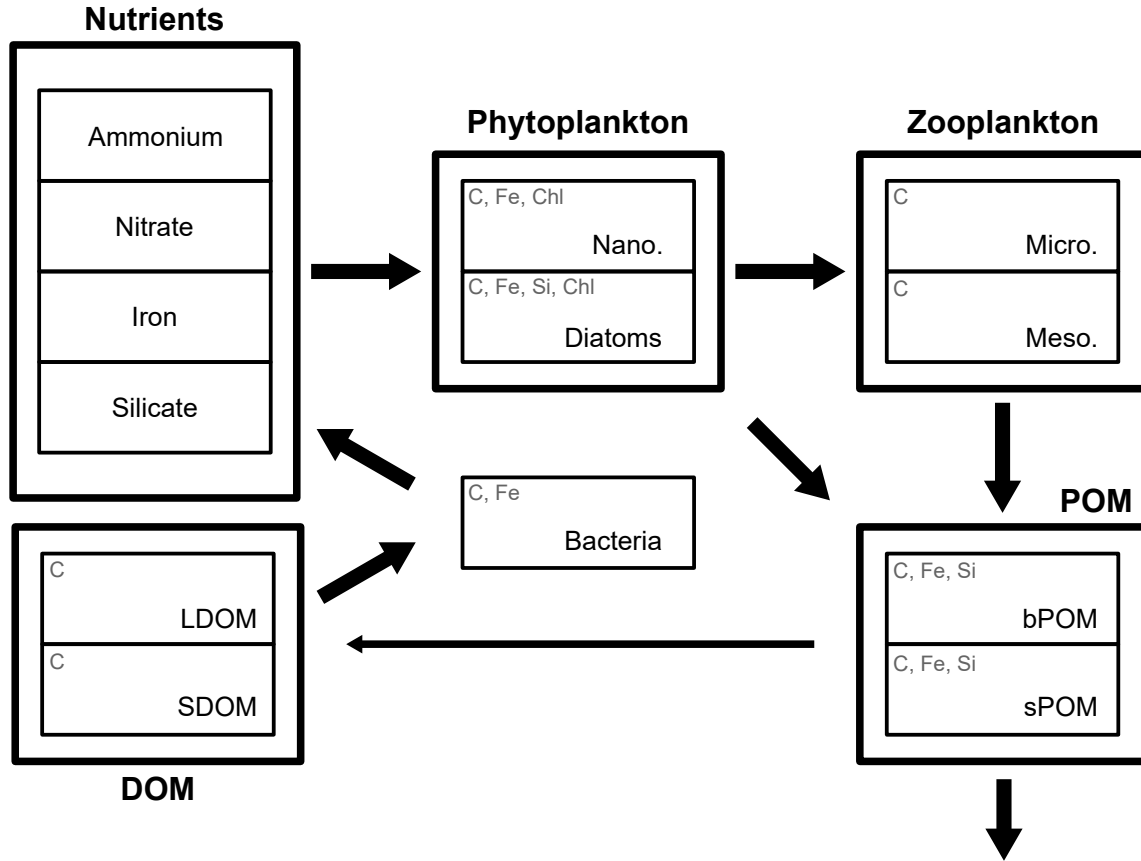


FIGURE 4.10: Schematic structure of the NEMO-PISCES biological model. All compartments are represented, with explicitly modeled elements represented in the upper left corner of the compartments. Arrows represent fluxes of biogeochemical elements, but do not aim to be comprehensive.

The biological model includes 26 compartments (Figure 4.10) and represents basic nutrients, two classes of phytoplankton and two of zooplankton, particulate and dissolved organic matter. Two compartments will be of particular interest, the bacterial biomass compartment B and the labile DOC compartment $LDOC$. Bacteria evolve according to the following dynamic equation:

$$\frac{\partial B}{\partial t} = \underbrace{(1 - \delta^B - \sigma^B)}_{\text{bacterial growth efficiency}} \times \mu^B B - m^B \frac{B}{K_m + B} B - sh \times w^B B^2 - g^Z(B) Z \quad (4.9)$$

where δ^B represents the exudation rate of heterotrophic bacteria, σ^B the respiration rate, μ^B the uptake rate, m^B the linear mortality rate, K_m an adjustment variable for regions of low bacterial abundance, sh the shear rate, w^B the aggregation term and $g^Z(B)$ grazing of bacteria by zooplankton.

There are two important terms here for our eco-evolutionary analysis. First, the ratio of resource consumed turned immediately into bacterial biomass (i.e. the bacterial growth efficiency):

$$\text{BGE} = 1 - \delta^B - \sigma^B. \quad (4.10)$$

This term is at the core of our eco-evolutionary framework (see next section), along with the maximal growth rate μ^B , which has the following expression:

$$\mu^B = \mu_{\max}^B f_B(T) \times \underbrace{\min \left(L_N^B, L_{PO_4}^B, L_{Fe}^B, \frac{LDOC}{LDOC + KLDOC} \right)}_{\text{nutrient limitation term}}. \quad (4.11)$$

Together, the BGE and maximal growth rate will allow us to compute the strength and direction of bacterial adaptation.

The evolutionary framework

Adapting the framework from Chapter 2 calls for some adjustments. For instance, the definition of bacterial growth efficiency used in NEMO-PISCES considers a constant exudation rate δ^B . Therefore, we do not work with BGE directly but with the respiration rate σ^B , which we allow to vary and from which we derive BGE values. In practical terms, we keep the exudation fraction δ^B fixed and allow the respiration fraction to vary, with the following dependency from equation (4.11):

$$KLDOC : \sigma^B \mapsto \left(\frac{\sigma_0}{\sigma^B} \right)^\theta \times KLDOC_0. \quad (4.12)$$

Here, σ_0 is a reference value for respiration rate σ^B , for which $KLDOC = KLDOC_0$. The sensitivity of the trade-off is measured by the parameter θ , which could be seen as the relative cost of resource acquisition compared to biomass growth. For instance, if $\theta > 1$ investing twice as much in bacterial growth divides resource acquisition capacity by more than a factor two.

The selection gradient equation

In order to implement equation (4.5) into NEMO-PISCES, we define the effective individual growth rate g of a bacterial population with respiration rate σ in the following way:

$$g : \sigma \mapsto (1 - \delta^B - \sigma) \mu^B(\sigma) - m^B \frac{B}{K_m + B} - sh \times w^B B - \frac{g^Z(B)}{B} Z \quad (4.13)$$

The instantaneous invasion fitness \bar{S} for an invading population σ' over a resident population σ is given by

$$\bar{S}(\sigma', \sigma) = g(\sigma') - g(\sigma) \quad (4.14)$$

In general, we could numerically compute the selection gradient $d\bar{S}(\sigma)$ in the following way, assuming a small BGE variation $\delta\sigma$:

$$d\bar{S}(\sigma) \approx \frac{g(\sigma + \delta\sigma/2) - g(\sigma - \delta\sigma/2)}{\delta\sigma} \quad (4.15)$$

For $\delta\sigma$ small enough compared to σ values, this approximation is acceptable.

In this simple case however, it is possible to calculate the selection gradient *a priori* if we assume that LDOC limitation is the main driver of selection. Indeed, g is differentiable with respect to σ , hence

$$d\bar{S}(\sigma) = \left(\theta \cdot \frac{(1 - \delta^B - \sigma)}{\sigma} \cdot \frac{KLDOC(\sigma)}{LDOC + KLDOC(\sigma)} - 1 \right) \times \mu^B(\sigma). \quad (4.16)$$

The sign of $d\bar{S}$ thus depends on the labile DOC concentration and metabolic parameters of the bacterial cell.

Model experiments

In order to explore the impact of a variable BGE on the global geochemical cycles, we simulate different scenarios. All parameters are chosen as in Pham et al. [215], with the added evolutionary parameters and constant iron quota as follows:

Parameter	Value	Unit
α	1E4	$\text{d}^{-1} \cdot \text{mmol C}^{-1} \cdot \text{m}^3$
θ	3	-
σ_0	0.6	-
$KLDOC_0$	2E-3	$\text{mmol C} \cdot \text{m}^{-3}$
Fe/C	15E-6	-

TABLE 4.2: Parameters for the standard run of NEMO-PISCES.

Two parameters are of major interest here: the adaptive capacity of a lineage α , and the trade-off parameter θ . Indeed, σ_0 and $KLDOC_0$ are taken from the parametrization found in Pham et al. [215], and are used as an evolutionary starting point.

We run the following experiments, and focus on the mean values of the surface ocean (down to 100m depth):

- **Control run:** the standard simulation, including bacterial adaptation and with initial parameters.
- **θ_i runs:** sensitivity runs for the θ and α parameters, where $\theta = i$ and $s \in \{\text{slow, standard, fast}\}$. Slow runs have an α parameter five times lower than in the standard run, and fast runs have it five times higher. With this formalism, the control run would be written as $\theta3_{\text{standard}}$. We run the simulation for $\theta \in \{1, 2, 3, 4\}$.
- **BGE $_i$ runs:** in these runs, we turn off bacterial adaptation (i.e. $\alpha = 0$) and keep BGE value constant all over the ocean at $i\%$. We run the simulation for $i \in \{10, \dots, 80\}$.
- **T0 run:** to compute the effect of bacterial adaptation on the response of the microbial loop to climate change, we run a scenario in which BGE values are taken equal to its yearly average for each grid cell for the initial temperature distribution.
- **ECO run:** we increase the temperature across the ocean by 5°C and run the model without adaptation, where BGE values match the **T0 run**. This run will give us the ecophysiological response of the ecosystem to climate warming.
- **ΔT run:** we run the standard parameter model with increased temperature and record BGE values to use in the eco-evolutionary scenario.
- **ECO-EVO run:** we run the model without adaptation, where BGE values match the yearly average values of the **ΔT run**. This run will give us the eco-evolutionary response of the ecosystem to climate warming.

Each experiment is run for 20 years using the same physical forcing as in Pham et al. [215] initialized with a homogeneous ocean, so that the surface ocean is at a quasi-steady state. A supplementary year is then run for each experiment, with results being averaged over each month. These data are then compared to the control run so that the influence of eco-evolutionary processes on global biogeochemical cycles can be evaluated.

4.3.2 Results

Model validation

The modifications made to the model developed in Pham et al. [215] based on PISCES v2 [15] are marginal, and amount to having a dynamic BGE in the system instead of a fixed one and a fixed iron quota. As such, the goal of this study is not to validate the whole model, which has already been done [215], but to investigate the global changes that the inclusion of eco-evolutionary processes causes. The only direct change made was on the bacterial component, with the aim of controlling that bacterial biomass (Figure 4.11b) and LDOC concentration (Figure 4.11c) are consistent with measurements [35] and previous simulations [215].

Both follow the expected trends, but bacterial biomass seem to be slightly overestimated and the LDOC concentration underestimated in our run.

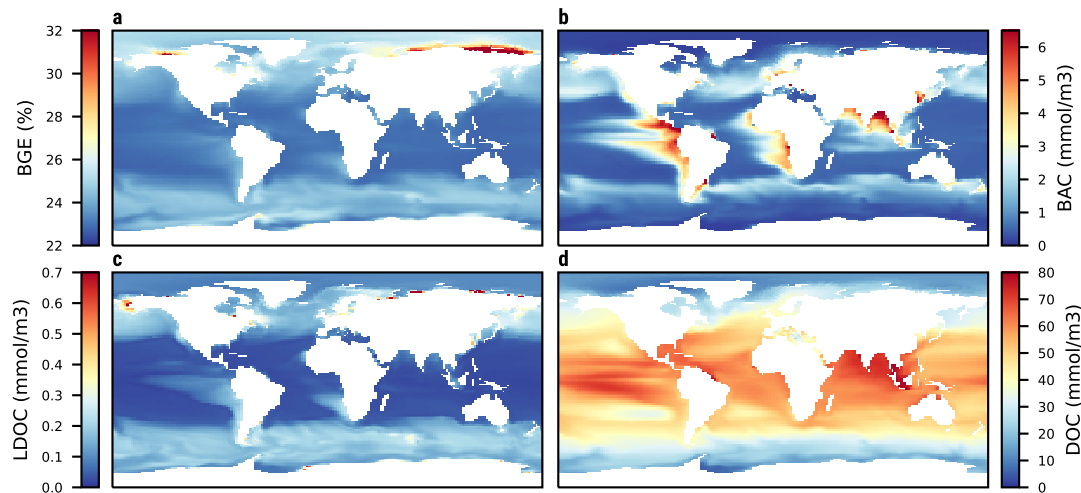


FIGURE 4.11: Distribution of key compartments in the control run. (a) Bacterial growth efficiency (BGE). (b) Bacterial biomass. (c) Labile DOC concentration. (d) DOC concentration.

BGE is notably hard to deduce from *in situ* data such as genomic data [170], but the values, located between roughly 20% and 30% are consistent with what is found in nature [18] and the general trends reproduce theoretical results [48]: lower values of BGE are found in nutrient-poor and warm waters, whereas the highest values are predicted at the poles.

Sensitivity to evolutionary parameters

The scale of BGE across the ocean is largely determined by the trade-off sensitivity θ rather than the adaptive capacity α (Figure 4.12). Higher values of trade-off sensitivity drive BGE values down, as it becomes costlier to invest in resource acquisition. At mid-latitudes, rapid adaptation results in stronger BGE gradients, with minimum values going lower than with slow adaptation (Figures 4.13a-b). At high latitudes, larger variations appear when adaptation is slow, but regions with the more extremes values are also regions where bacteria are least adapted (Figure 4.13c). Across the global oceans, bacteria are fitter relative to their local environment when adaptation capacity is high (Figures 4.13c-d).

What drives BGE variations? A comparison with fixed BGE values

We first performed a principal component analysis (PCA) on the surface system to quantify the correlations between variables (Figure 4.14). For the six variables analyzed, most of the variation (75.23%) can be explained by two dimensions. BGE is highly correlated to both DOC pools, positively to LDOC and negatively to DOC. Primary production and bacterial

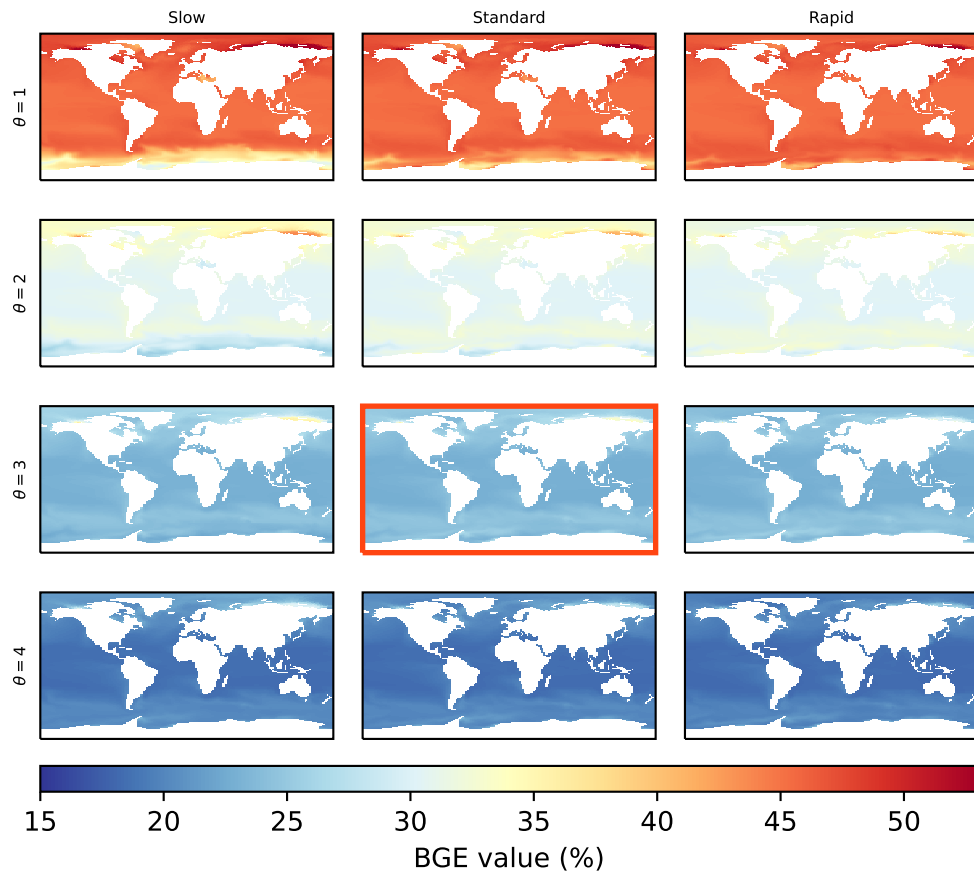


FIGURE 4.12: Sensitivity of bacterial growth efficiency to adaptive capacity and trade-off parameter θ (dimensionless). Adaptive capacity is twice as high (resp. low) in the rapid (resp. slow) scenario as in the standard run. The control run is framed in red.

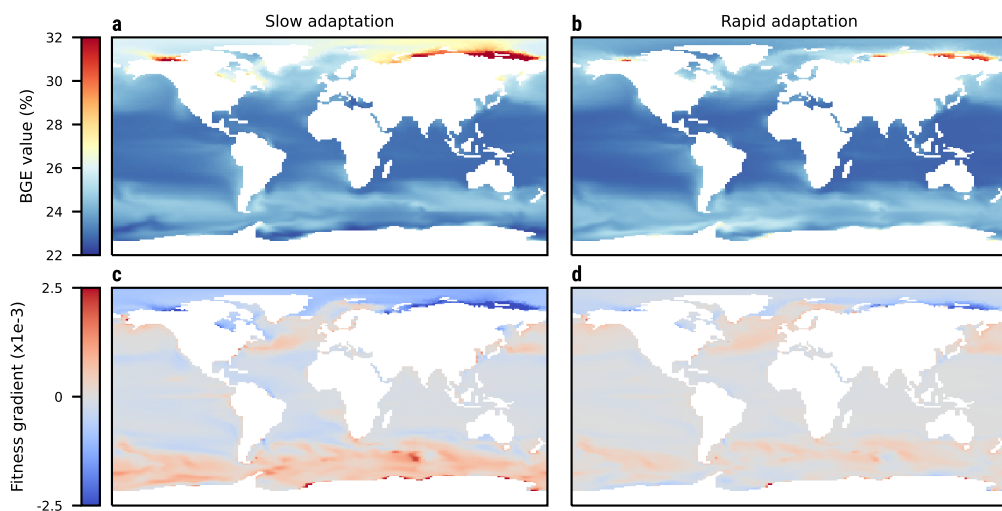


FIGURE 4.13: Sensitivity of bacterial growth efficiency to the population adaptive capacity. (a-b) BGE values for (a) slow and (b) rapid adaptation. (c-d) Fitness gradient at steady-state for (c) slow and (d) rapid adaptation.

biomass are highly correlated, probably due to the fact that environmental factors favoring bacteria also favor phytoplankton in general.

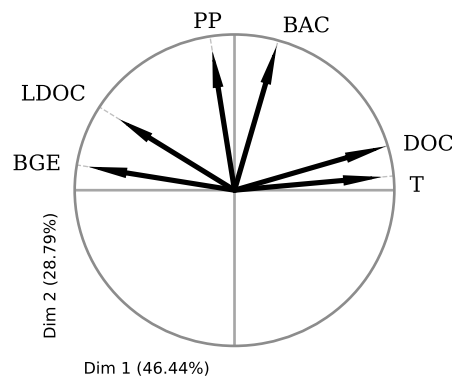


FIGURE 4.14: Principal Component Analysis of the surface data averaged over a year. The following quantities are represented: bacterial growth efficiency (BGE), primary production (PP), bacterial biomass (BAC), DOC, temperature (T) and labile DOC (LDOC).

BGE is mostly determined by LDOC concentrations (Figure 4.14 and equation 4.16) and its adaptation corresponds to a near LDOC-minimum at the global scale (Figures 4.15c-d). A common misconception regarding darwinian evolution is that populations ‘optimize’ a community-level characteristic such as biomass, which is not the case here (Figure 4.15a). In general, the best competitor is the population that exploits its environment the most, a fact often referred to as the ‘pessimization principle’ [180]. Our model provides a striking example, as bacterial adaptation leads, not to maximizing biomass (Figure 4.15a), but to minimizing the direct resource, labile DOC (Figure 4.15c). The difference between a global LDOC minimum and our simulations could come from the fact that in a spatially explicit environment, local adaptation may not lead to a globally optimized population, or from the hypothesis that bacteria are always LDOC-limited, which may not be the case in certain oceanic regions.

Impact of bacterial adaptation on productivity under ocean warming

The microbial loop is thought to process about half of all primary production [96, 142], recycling part of it to fuel regenerated production at the surface [236]. In our model, primary production depends linearly on BGE value (Figure 4.16), with a variation of BGE by 1% implying an opposite variation in total primary production across the ocean of 0.025 mol/m^2 . Under environmental change, bacterial adaptation could then mechanically impact ocean productivity through the variation of BGE: this effect of adaptation would add to the eco-physiological response of primary production, further increasing the uncertainty regarding its future.

In order to compute the effect of bacterial adaptation on sea-surface ecosystems under

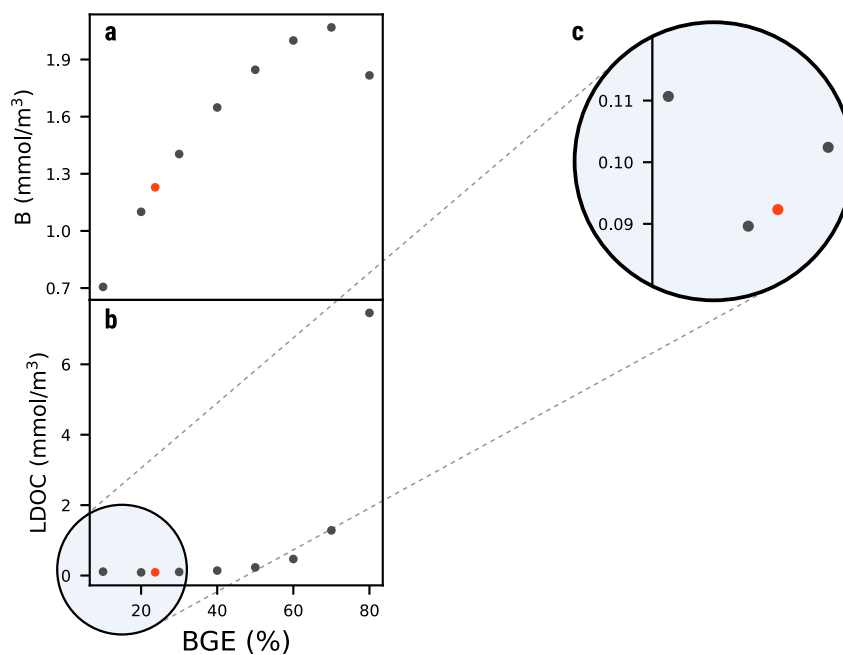


FIGURE 4.15: General statistics averages over the ocean with respect to BGE values. In gray, simulations of the BGE_i runs where BGE is kept constant at its initial value across the ocean. In red, the standard simulation. (a) Bacterial biomass. (b) Labile DOC concentration with respect to BGE. (c) Zoom on the first four data points of LDOC concentration.

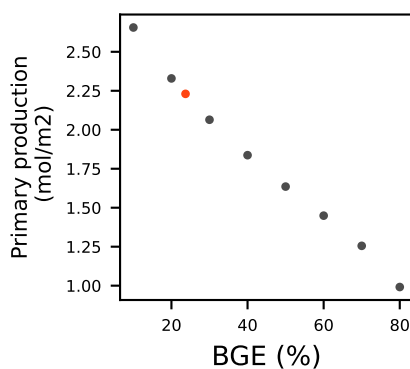


FIGURE 4.16: Surface primary productivity averaged over the year with respect to BGE values. In gray, simulations of the BGE_i runs where BGE is kept constant at its initial value across the ocean. In red, the standard simulation.

environmental change, the water temperature is increased by 5°C across the ocean. To isolate the macroscopic effect of bacterial adaptation, we use the yearly average of adapted BGE values to initial and increased temperatures as a forced input in the NEMO-PISCES model without adaptation (which is already done for temperature for instance). We then compare three runs: the **T0** run, with standard temperatures and BGE values adapted to the initial temperature, the **ECO** run, with increased temperatures and BGE values fixed to the values adapted to the initial temperatures, and the **ECO-EVO** run, with increased temperatures and BGE values adapted to the increased temperatures.

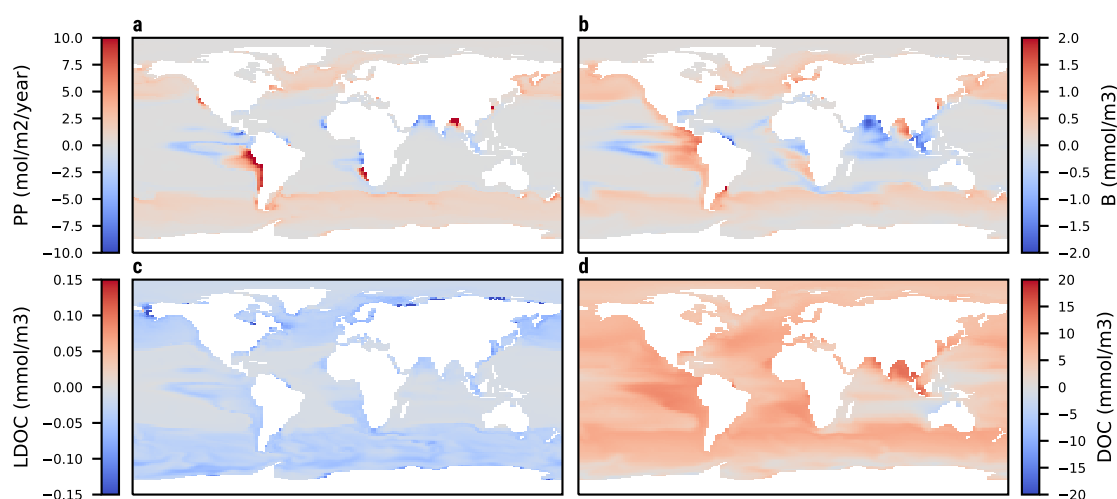


FIGURE 4.17: Effect of a 5°C increase of sea-surface temperature on oceanic ecosystems in absence of bacterial adaptation. Mean anomaly over the course of a year for (a) primary production; (b) bacterial biomass; (c) labile DOC concentration; (d) DOC concentration.

When bacterial adaptation is not taken into account, high latitudes and coastal areas from the southern hemisphere become more productive when temperature increases (Figure 4.17a). This results in a global productivity increase by 1.27 billion tons of carbon per year. Part of this captured carbon fuels bacterial biomass in the regions where productivity increases (Figure 4.17b), leading to a decrease in labile DOC concentration (Figure 4.17c). Global carbon stocks increase, with higher concentrations in DOC (Figure 4.17d).

These environmental changes drive bacterial adaptation. The decrease in labile DOC concentrations leads to an increase in the resource acquisition pressure for bacterial population. In response, bacterial adaptation results in decreasing BGE values in most of the biogeographical regions. The effect is spatially diverse, with strongest decreases observed in cold regions rich in labile DOC. When integrated over the global ocean, BGE decreases by a little over 0.2%.

The effect of this adaptation on primary production is spatially and seasonally diverse (Figure 4.19). In accordance with the conclusions from Chapter 3, productivity tends to increase across the ocean, with the largest increases occurring in already productive regions.

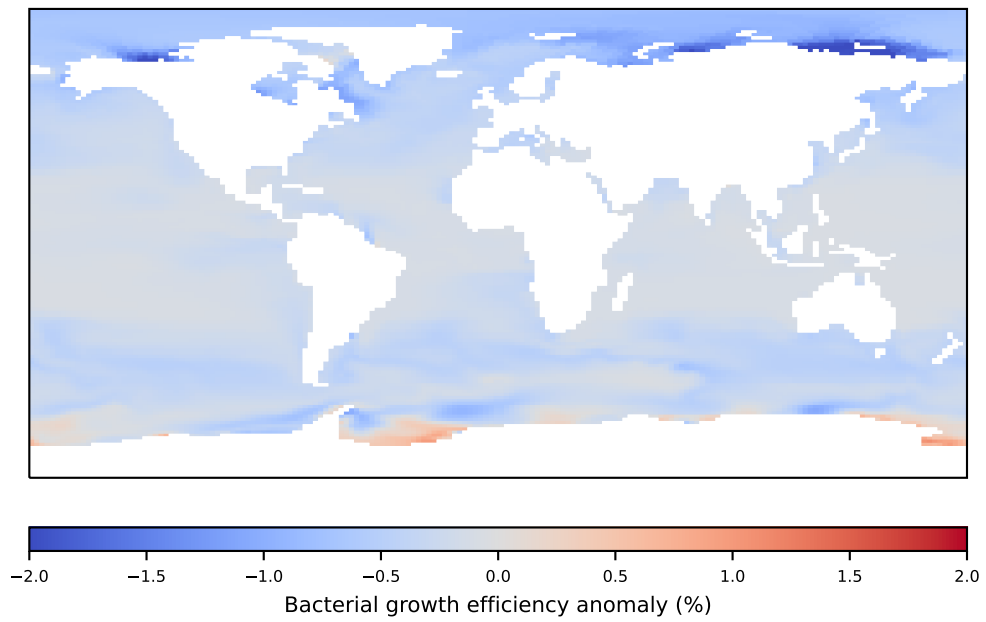


FIGURE 4.18: Adaptive effect of a 5°C increase of sea-surface temperature on bacterial growth efficiency.

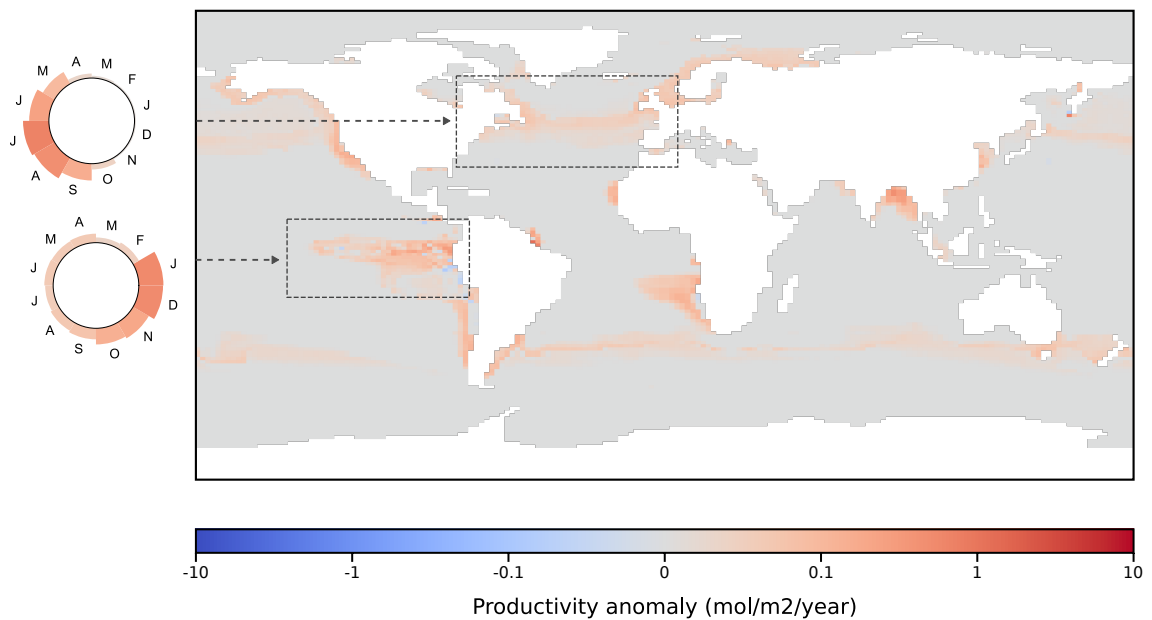


FIGURE 4.19: Effect of bacterial adaptation on primary production after a 5°C increase of sea-surface temperature. The scale is logarithmic, with all effects under 0.01 mol/m²/year clipped to 0. On the left, seasonal effect of bacterial adaptation on two specific regions, the Northern Atlantic and Eastern Pacific.

BGE values are constant over the course of a year, but the effects of bacterial adaptation can be seasonal: both in the Northern Atlantic and the Eastern Pacific, primary production decreases in the summer, their most productive period. The rest of the year, productivity stays constant in the Antarctic and increases slightly in the northern Atlantic.

Overall, bacterial adaptation results in a global primary production increase of 30.8 million tons of carbon per year. Compared to the 1.27 billion tons of carbon in absence of bacterial adaptation, we can conclude that including bacterial adaptation into primary production forecasts can alter predictions by over 2.4%, which adds to the uncertainty regarding the future of primary production [150]. Integrated over several decades, such a deviation could propagate and lead to drastically different predictions.

4.4 Conclusions

This study focused on a constant environment over the course of a year, where physical properties of the ocean were forced (temperature, salinity, currents, etc.). A proxy for climate change was used in the form of a temperature increase, but only quasi-steady states were compared. As of yet, there is no proper feedback from our system to global parameters of the Earth system; in particular, there is no coupling with atmospheric models. The next logical step would be to implement the selection gradient equation in a coupled model taking into account future scenarios of CO₂ emissions [191]. Indeed, here we focused on the impact of a temperature increase on microbial loop function in the sea surface, but other effects of global climate change might have similar or even stronger consequences: ocean stratification could reduce vertical mixing and expand nutrient poor zones, which would have important consequences on LDOC reservoirs. Changes in these reservoirs would likely have a large impact on BGE, which might then feed back to the system globally. There are no theoretical barriers to applying the selection gradient equation to climate scenarios, only practical matters of computational power and fine-tuning parameters.

At its core, the selection gradient equation is derived from evolutionary game theory [210], and is thus purely phenotypical. The trait is a quantitative characteristic of the cells, which can be inherited with or without variation from one generation to the next, and adaptation is represented as the outcome of an optimization process under the constraint of a trade-off. Despite the fact that genomic data are numerous and can be used to infer even complex functional traits such as BGE [230, 233], many studies such as ours still model ecosystems from a strictly phenotypical point of view. Integrating 'omics data into ecosystem models has become a research priority [147, 77, 61].

Models have been successful in reproducing the ecological state of a system and even biogeochemical fluxes [58] or displaying evidence of niche adaptation [183]. Advances such as metabolic modeling [213, 57], and community assembly inferred from metagenomics and

metatranscriptomics data [183] allow for a robust mapping of existing genotypes to phenotypes. But the reason why eco-evolutionary still rely on trait-based models [239, 141] stems from the relative simplicity of predicting variation of a functional trait compared to the genetic variations of an individual cell: trait-based models describe ecological systems at macroscopic scales while retaining the microscopic scale of individual variations. The outcomes of adaptation are predicted at the level of phenotypes; we now need model that take further steps towards delivering these predictions in ‘currencies’ that can be related to omics data. Models such as Coles et al. (2017 Science) pave the way in this direction, and further theoretical advances are being made [173], but much remains to be done, especially in the face of formidable computational challenges [265].

Our method relies on populations that can be described by a one-dimensional trait-space. While this is the case in many common evolutionary frameworks, where populations are described with one ‘master trait’ (e.g. phytoplankton described by their size [238]), it is not the only one. For instance, a general approach for multidimensional microbial adaptation is provided by the YAS framework (for Yield-resource Acquisition-Stress tolerance) Malik et al. [170]. Our approach focuses on the trade-off between yield and resource acquisition, but a new dimension could be added by considering resource allocation to stress tolerance.

In sum, we have achieved the first integration of eco-evolutionary processes into Earth system models using a trait-based model and a phenomenological model of adaptation. Applying our approach to simple, low-dimensional toy models shows that it works reasonably well. When applied to the PISCES-NEMO ESM, we obtain credible results that could be the basis for climate forecast. Uncertainties brought by microbial adaptation could be assessed on a large scale, and predictions for the future of oceanic ecosystems refined. Such endeavors are necessary for developing robust forecasts of the biological pump.

Chapter 5

Bacteriophages and the microbial loop

'Foxdie is a type of retrovirus that targets and kills only specific people. It contains smart enzymes, created through protein engineering. They are programmed to respond to specific genetic patterns in the cells.'

Naomi Hunter, *Metal Gear Solid* (1998)

In this chapter, we focus on the biogeochemical influence viruses have on oceanic ecosystems. How do lysis and the viral shunt influence microbial loop function and bacterial adaptation? We explain how to model bacteriophage influence on the microbial loop, and study the particular case of the microbial loop in the aphotic zone under ocean stratification.

5.1 Viruses, players at the heart of the microbial loop

Viruses are the most abundant type of cells in the ocean, with on average 10 viral cells for 1 bacterial cell [279], even if the ratio can typically range from 1:1 to 100:1 [276]. They are thought to cause about half of all bacterial mortality, the other half usually coming from grazing via zooplankton [33], and as such to play an important role in biogeochemical cycles, particularly in the microbial loop.

5.1.1 The biogeochemical importance of viral life cycles

Viruses are parasitic entities, as they need to hijack other cells to be able to reproduce. Marine viruses can be highly specialized in the type of host they target [279], and one strain of viruses will usually only infect one type of cells. Heterotrophic bacteria are infected by a

class of viruses called bacteriophages, whose life cycle we'll describe in this section (Figure 5.1). We can broadly divide the life of a virus in two phases: an extracellular phase in which a free-floating virus needs to encounter a host (i.e. a bacterial cell) in order to survive, and an intracellular phase in which viral DNA gets reproduced by bacterial mechanisms.

Bacteriophages do not have the ability to move by themselves and rely on diffusion to initiate contact with host cells. Contact is made in the form of protein interactions between the phage¹ and a particular location on the bacterial membrane called a *receptor*, where the adsorption takes place [52]. The viral genome enters the host cell through a mix of physical and biochemical means: the pressure gradient between a bacterial cell and the viral capsid can mechanically 'push' the genome in the host, while any leftover genetic material can be 'pulled' by specific enzymes [145, 184].

Once the genome enters the host cell, it can generally enter two phases, the *lytic phase* or the *lysogenic phase*. During the lytic phase, bacterial function is hijacked and host DNA can even be hydrolyzed all in order to produce more viral particles (or virions). Once a certain virion number threshold is met, the host cell literally bursts and releases viral particles in the environment. The lysogenic phase differs in the sense that it doesn't necessarily end in host death, as the viral genome is integrated in the bacterial DNA and benefits from host reproduction. Due to certain environmental or metabolic conditions [33], the cell can go in lytic phase after a lysogenic period.

For the remainder of the chapter, we will focus on the lytic phase of viral life cycles. Indeed, lysis induces a literal burst of the host cell, leading to all organic material inside the bacteria be released in the environment as DOM. This short-circuits the traditional food web and moves carbon from unicellular organisms (e.g. heterotrophic bacteria or phytoplankton) directly to the DOM pool. This carbon pathway is thought to be significant, with some estimates putting as much as 25% of all organic carbon flow moving through the viral shunt [277]. This viral shunt could help stimulate productivity in an ecosystem by making nutrients available that were otherwise already locked, as the DOM produced by lysis is readily available to heterotrophic bacteria [109] and can then be transferred to phytoplankton [247]. On the other hand, bacterial mortality caused by viruses could detract from the biological pump, decreasing overall export. Indeed, the two main sources of mortality for bacteria are grazing and lysis [109]. While grazing move carbon 'up' the biological pump, leading eventually to POM sinking in the deep ocean, lysis moves carbon 'down' by transferring organic carbon to the DOM pool. A study using data from the *Tara Oceans* expedition found that overall, carbon export in oligotrophic ocean was correlated to the presence of specific phages [125].

By moving carbon to the DOM pool, bacteriophages are at the heart of the microbial loop, stimulating nutrient recycling in spite of the induced mortality increase [274]. Bacte-

¹Short for 'bacteriophage'.

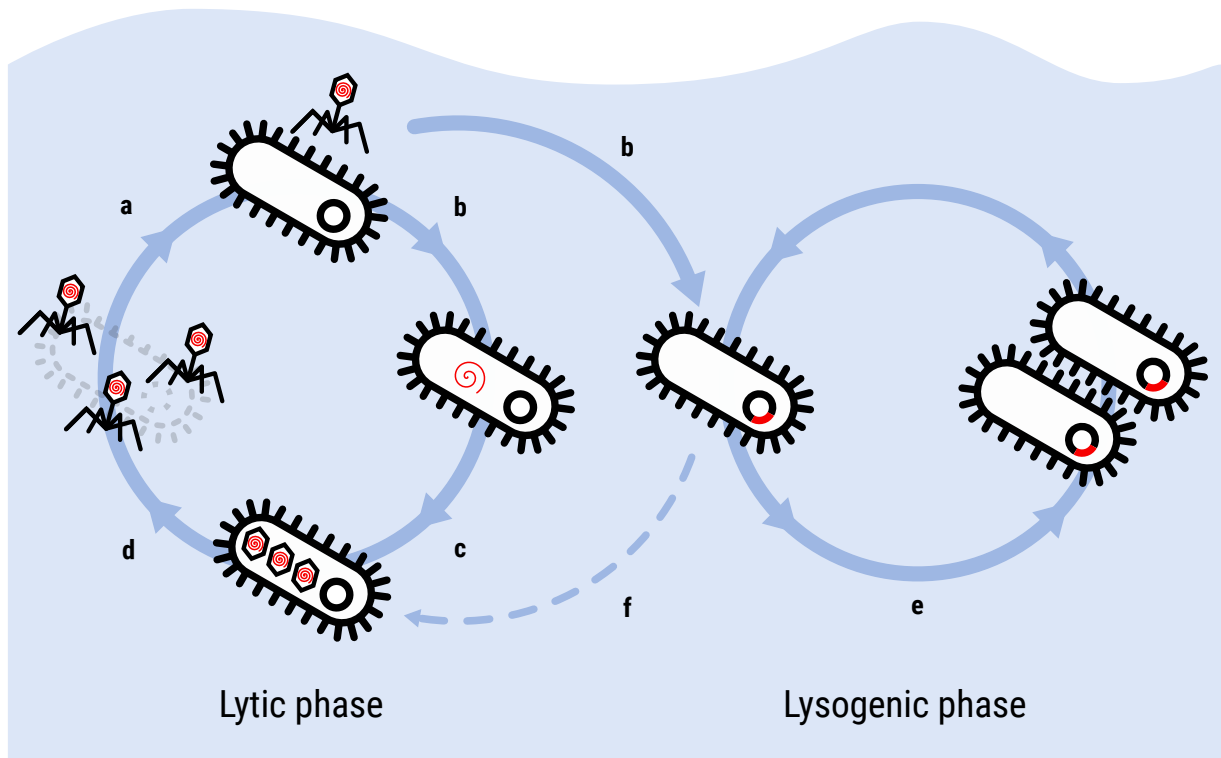


FIGURE 5.1: The life-cycle of a bacteriophage. Strands of viral DNA are represented in red. (a) Contact between a phage and a bacterial cell; (b) Infection; (c - Lytic phase) Replication; (d - Lytic phase) Lysis; (e - Lysogenic phase) Vertical transmission; (f - Lysogenic phase) Induction of the lytic phase.

riophages have two antagonistic effects on bacterial populations, increasing both their mortality rates and DOM availability. How these effects interact to influence bacterial adaptation through selection, and how this will affect microbial loop function is still unresolved. In order to address this question, we include bacteriophages in the microbial loop module from Chapter 2 and adapt the eco-evolutionary analysis to assess the impact of phages on bacterial adaptation: by comparing the bacterial ESS in three scenarios (without bacteriophages; with bacteriophages but without the viral shunt; and with both bacteriophages and the viral shunt) we isolate the effects of lysis and the viral shunt on the evolutionary equilibrium of bacterial populations.

5.1.2 Integrating bacteriophages in the microbial loop module

Ecological integration of bacteriophages in the microbial loop

The first step in including bacteriophages in the eco-evolutionary microbial loop module is to understand its ecological interaction with bacteria and DOM. In order to focus on the sole impact of the viral shunt and increased mortality, the choice was made to consider an instantaneous lysis upon successful infection. We do not consider the infected state of bacteria, which allows us to integrate bacteriophages in the microbial loop module with the

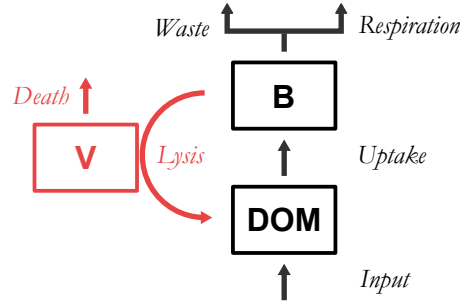


FIGURE 5.2: Theoretical microbial loop model with bacteriophages. B, bacterial biomass; V, phage biomass; DOM, dissolved organic matter concentration. In red, pools and fluxes added when compared to the module developed in Chapter 2.

inclusion of only one additional viral pool (Figure 5.2). All fluxes are modelled as follow for a general model \mathcal{M} , in which all pools are represented in biomass concentration:

- Fluxes relating to the microbial loop in absence of viruses are the same as the ones described in Chapter 2².
- I measures the incidence rate of contact between bacteria and viral particles. The difference in matter content between them being important for keeping track of the viral shunt, we model contact rates in terms of individual cells, not biomass. Thus, we introduce q_B (resp. q_V) as the matter content of bacterial cells (resp. bacteriophages): that way, B/q_B represents the number of bacterial cells and V/q_V the number of viral cells. We have:

$$I = \psi \cdot \frac{B}{q_B} \cdot \frac{V}{q_V} \quad (5.1)$$

- Each contact does not automatically end in an infection and subsequent (immediate) lysis. Indeed, we take into account inefficient infections [273], with interaction between a bacterial cell with a viral particle having a probability π to lead to an actual infection. Effective infection rate will thus be $\pi \times I$.
- Successful infections result in viral bursts of size β , and is measured in number of cells. Unsuccessful infections lead to the decay of the bacteriophage (the bacterial cell remains unchanged).
- All excess matter from lysis (the *viral shunt* VS) moves to the DOM pool. We have:

²Note that for instance, if viruses specific to phytoplankton are present in the model, the viral shunt from this taxonomy will show in the input term $In(\mathcal{M})$.

$$VS = \underbrace{(q_B - \beta q_V) \cdot \pi I}_{\text{excess nutrient released from lysis}} \quad (5.2)$$

- μ_V denote the mortality rate of phages. All matter derived from viral death exits the system³.

The dynamical evolution of the system can then be described by the following system of ordinary differential equations:

$$\left\{ \begin{array}{l} \frac{dDOM}{dt} = In(\mathcal{M}) + VS - U_B \\ \frac{dB}{dt} = \omega U_B - W(\mathcal{M}) - q_B \cdot \pi I \\ \frac{dV}{dt} = q_V \cdot \beta \pi I - q_V \cdot I - \mu_V V \end{array} \right. \quad (5.3)$$

Strictly speaking, the integration of bacteriophages did not call for modifying the microbial loop module, and this general integration was done for the purpose of clarity. Indeed, mortality induced by viruses can be integrated to the general waste term $W(\mathcal{M})$, with the individual bacterial waste term $w(\omega, \mathcal{M})$ expressed as:

$$w(\omega, \mathcal{M}) = \underbrace{\pi \cdot \psi \cdot \frac{V}{q_V}}_{\text{mortality induced by lysis}} + \text{other bacterial waste terms} \quad (5.4)$$

Then, the viral shunt VS can be integrated in the input term $In(\mathcal{M})$ to complete the integration in the module.

Evolutionary integration of bacteriophages in the microbial loop

In addition to influencing the ecosystem's population dynamics, bacteriophages impact bacterial adaptation. Here we discuss the implication of including bacteriophages on the **trait** and **trade-offs** defined in Chapter 2.

Phage infection is a major source of stress for bacterial populations, and they may invest part of their energy in defending themselves against infection. Bacteria have numerous means of stopping an infection, as reviewed in Azam and Tanji [16]. They can inhibit the adsorption by changing the receptor, limit the viral DNA injection by encoding specific genes, break viral DNA once injected or even stop its replication. All of those mechanisms can be

³As with bacterial mortality in Chapter 2, this exit can loop back as an input in the general model \mathcal{M} .

summarized in our model by the probability of successful infection π , and therefore we can define π to be a function of our trait ω , the BGE, in order to reflect those mechanisms:

$$\pi : \omega \mapsto \pi(\omega). \quad (5.5)$$

Here, the probability of a successful infection should decrease with the increase in respiration ($1 - \omega$), which is taken as a proxy of energy expenditure of the bacterial cell. π should therefore be an increasing function of ω . In this chapter, we use the following expression for the probability π , with π_0 being the maximum infection probability and θ_S the ‘stress tolerance’ trade-off constant:

$$\pi(\omega) = \omega^{\theta_S} \times \pi_0. \quad (5.6)$$

Alternate model of trait variation

A note should be made here that the choice to keep only one trait in this study is not the only possible one. This ‘mother trait’ approach (explained in details in Chapter 2) can be replaced by a direct application of Malik et al. [170] and its ‘YAS’ framework. If we directly apply the YAS framework, a trade-off between resource acquisition and stress tolerance may also exist, which is not the case here. Indeed, when yield (BGE) decreases, both resource acquisition and stress tolerance increase and vice-versa as respiration rates increase.

In order to introduce this second trade-off, the trait-space needs to be two-dimensional, with three non-independent traits y, a, s each representing the investment of resource consumed into respectively yield, resource acquisition and stress tolerance. In this framework, the different trade-offs would be (with θ_A the resource acquisition trade-off constant):

$$\omega = y \quad (5.7)$$

$$K_B(a) = \frac{1}{a^{\theta_A}} \times K_B^0 \quad (5.8)$$

$$\pi(s) = (1 - s)^{\theta_S} \times \pi_0 \quad (5.9)$$

$$y + a + s = 1. \quad (5.10)$$

This framework could be interesting for further studies taking phage-host coevolution, but for the purpose of this thesis we chose to follow the most straightforward approach in the study of biogeochemical cycles, and keep the trait unidimensional for potential future integration in ESMs.

5.1.3 The NB-V model in the aphotic zone

In this chapter, we compute the effect of bacteriophages on the microbial loop itself by focusing on the system in the aphotic zone, where the external DOM input is constant at a given depth [175]. This allows us to see the impact of bacteriophages on the system with minimal parameters while still modeling a relevant ecosystem.

We implement the microbial loop module in the microbial loop model of the aphotic zone (NB) with viruses (V) to develop the $\mathcal{M}_{\text{NB-V}}$ model. The viral shunt is entirely redirected to the DOM pool (Figure 5.3).

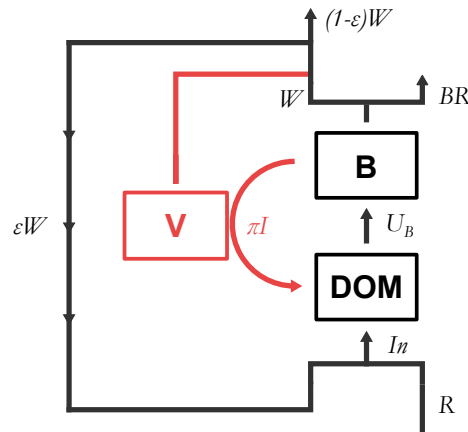


FIGURE 5.3: Model $\mathcal{M}_{\text{NB-V}}$ of the microbial loop in the aphotic zone. B, bacterial biomass; V, phage biomass; DOM, dissolved organic matter concentration. In red, pools and fluxes added when compared to the module developed in the case-study from Chapter 2.

All fluxes can be found in the case-study from Chapter 2, with the added viral fluxes described in this chapter. It should be noted that the general waste product W now takes viral death into account, and the waste from contact between phage and bacteria:

$$W = \underbrace{\mu_B B + \mu_V V}_{\text{cell mortality and egestion}} + \underbrace{q_V \cdot I}_{\text{waste of viral capsid after contact}} \quad (5.11)$$

As all other fluxes are identical to the previous case-study, we can derive the following system of differential equations to describe the dynamics of the system:

$$\left\{ \begin{array}{l} \frac{dDOM}{dt} = R + \epsilon \cdot W + VS - U_B \\ \frac{dB}{dt} = \omega U_B - \mu_B B - q_B \cdot \pi I \\ \frac{dV}{dt} = q_V \cdot \beta \pi I - q_V \cdot I - \mu_V V \end{array} \right. \quad (5.12)$$

Ecological equilibrium

In order to compute the effect of phages and the viral shunt on the system, it is useful to compare the system in presence and in absence of viruses. For reference, we recall the equilibrium values of the \mathcal{M}_{NB} model without viruses:

$$\bar{B}_{NB} = \frac{\omega R}{(1 - \omega \epsilon) \cdot \mu_B} \quad (5.13)$$

$$\overline{DOM}_{NB} = \frac{\mu_B}{\omega \lambda_B - \mu_B} \cdot K_B \quad (5.14)$$

Let's now assume that an equilibrium is possible in presence of viruses. We can derive the value of the bacterial biomass \bar{B} at steady-state through the dynamics of phages. We find:

$$\bar{B} = q_B \cdot \frac{\mu_V}{(\pi \beta - 1) \cdot \psi}. \quad (5.15)$$

This value only depends on viral parameters, and no longer on resource parameters. The inclusion of viruses shifts the system from a 'bottom-up' state (where the limitation for population growth is nutrient limitation) to a 'top-down' state (where the limitation for population growth is mortality and predation). A consequence of this shift is that an equilibrium with viruses may not be possible if the limitation induced by DOM uptake is stronger than the phage-induced limitation. We can therefore define the maximum bacterial biomass $\bar{B}_{MAX} = \bar{B}_{NB}$, and state that an equilibrium with viruses will only be possible if $\bar{B} < \bar{B}_{MAX}$.

In that case, a little algebra yields the following value for viral equilibrium:

$$\bar{V} = \frac{(1 - \omega \epsilon) \cdot \mu_B}{\left((1 - \omega) \cdot \frac{q_B}{q_V} + \omega \cdot (1 - \epsilon) \beta \right) \cdot \frac{\pi}{\pi \beta - 1} \cdot \mu_V} (\bar{B}_{MAX} - \bar{B}). \quad (5.16)$$

$\bar{V} > 0$ if and only if $\bar{B} < \bar{B}_{MAX}$. For the remainder of the chapter, we assume that the parameters are chosen such as if an equilibrium exists, it will be a stable one and no cycles

appear⁴. This leads to the following expression for DOM concentration:

$$\overline{DOM} = \frac{R + \epsilon \bar{W} + VS}{\lambda_B \bar{B} - (R + \epsilon \bar{W} + VS)} \cdot K_B \quad (5.17)$$

Evolutionary equilibrium

By substituting the appropriate expressions of equation (2.14) and tailor it to the \mathcal{M}_{NB-V} model, we find the following selection gradient:

$$\begin{aligned} dS(\omega) = & \frac{\mu_B + \pi(\omega)\psi \frac{\bar{V}}{q_V}}{\omega} \\ & - \theta_A \cdot \frac{\omega}{1 - \omega} \cdot \frac{K(\omega)}{K(\omega) + \overline{DOM}} \cdot \lambda_B \frac{\overline{DOM}}{K(\omega) + \overline{DOM}} \\ & - \theta_S \cdot \frac{\pi(\omega)}{\omega} \cdot \psi \frac{\bar{V}}{q_V}. \end{aligned} \quad (5.18)$$

5.2 Bacteriophage influence in a constant environment

Adding a viral compartment to the aphotic zone model changes the steady-state concentrations and fluxes, but also the ESS value for BGE for a given environment. In this section, we assess the impact of bacteriophages on the evolutionary stable strategy and subsequent effects on microbial loop function.

5.2.1 Shifting the evolutionary stable strategy

The inclusion of viruses shifts the evolutionary equilibrium from the \mathcal{M}_{NB} model, which affects the whole system. Expressing the selection gradient as a function of the selection gradient $dS_{NB}(\omega)$ in absence of viruses allows us to compare the two evolutionary stable strategies:

⁴Numerical validation of the stability of the equilibrium will be performed when appropriate.

$$\begin{aligned}
 dS(\omega) = & dS_{NB}(\omega) \\
 & + \theta_A \cdot \frac{\omega}{1-\omega} K_B(\omega) \cdot \lambda_B \left(\frac{\overline{DOM}_{NB}}{(K_B(\omega) + \overline{DOM}_{NB})^2} - \frac{\overline{DOM}}{(K_B(\omega) + \overline{DOM})^2} \right) \\
 & + (1 - \theta_S) \frac{\pi(\omega)}{\omega} \cdot \psi \frac{\bar{V}}{q_V}.
 \end{aligned} \tag{5.19}$$

To assess how the new evolutionary equilibrium ω^* compares to the evolutionary equilibrium ω_{NB}^* in absence of phages, we compute the value of $dS(\omega_{NB}^*)$: this value is positive if and only if $\omega^* > \omega_{NB}^*$. We find:

$$\begin{aligned}
 dS(\omega_{NB}^*) = & \theta_A \cdot \frac{\omega_{NB}^*}{1-\omega_{NB}^*} K_B(\omega_{NB}^*) \cdot \lambda_B \left(\frac{\overline{DOM}_{NB}}{(K_B(\omega_{NB}^*) + \overline{DOM}_{NB})^2} - \frac{\overline{DOM}}{(K_B(\omega_{NB}^*) + \overline{DOM})^2} \right) \\
 & + (1 - \theta_S) \frac{\pi(\omega_{NB}^*)}{\omega_{NB}^*} \cdot \psi \frac{\bar{V}}{q_V}.
 \end{aligned} \tag{5.20}$$

The two terms in this expression correspond to the effect of DOM variation in presence of bacteriophages, and to the effect of induced mortality by lysis itself. The former could be seen as the effect of the *resource acquisition pressure* A_p and the latter of the *stress tolerance pressure* S_p . Let us first focus on the stress tolerance pressure:

$$S_p = (1 - \theta_S) \frac{\pi(\omega_{NB}^*)}{\omega_{NB}^*} \cdot \psi \frac{\bar{V}}{q_V}. \tag{5.21}$$

The stress tolerance pressure is positive if and only if $\theta_S < 1$. Since θ_S is the stress tolerance trade-off sensitivity constant, its value with respect to 1 informs us on which function is more metabolically ‘expensive’. For $\theta_S < 1$, every marginal investment in stress tolerance measured by a decreasing yield ω will decrease the probability of successful infection $\pi(\omega)$ by a smaller amount: increasing bacterial defence against phages costs more than increasing yield. In this case, the increase in mortality due to viral particles will be handled more effectively by increasing yield than by increasing stress tolerance: the lytic pressure is positive, and drives BGE values up.

We now focus on the resource acquisition pressure A_p :

$$A_p = \theta_A \cdot \frac{\omega_{NB}^*}{1-\omega_{NB}^*} K_B(\omega_{NB}^*) \cdot \lambda_B \left(\frac{\overline{DOM}_{NB}}{(K_B(\omega_{NB}^*) + \overline{DOM}_{NB})^2} - \frac{\overline{DOM}}{(K_B(\omega_{NB}^*) + \overline{DOM})^2} \right). \tag{5.22}$$

The sign of the resource acquisition pressure depends on the respective values of the following function f applied to DOM concentration equilibrium values:

$$f : x \mapsto \frac{x}{(K_B(\omega_{NB}^*) + x)^2}. \quad (5.23)$$

This function is increasing on $[0, K_B(\omega_{NB}^*)]$ and decreasing afterwards. Two broad cases can be distinguished: DOM-poor environments, in which DOM concentrations with and without viruses are below the threshold value $K_B(\omega_{NB}^*)$; and DOM-rich environments, where both concentrations are above. Fringe cases in which concentrations are on either side of the threshold value are not included, as in those cases $\overline{DOM} \approx \overline{DOM}_{NB}$. Finally, the presence of viruses increases the equilibrium concentration of DOM for a given value of BGE ω . The inclusion of viruses shifts the structure of the system from a ‘bottom-up’ limited to a ‘top-down’ limited system, which by relieving pressure on the resource mechanically increases its equilibrium concentration. Therefore, we can conclude that $\overline{DOM}_{NB} < \overline{DOM}$.

When faced with stress-induced mortality, individuals have two potential responses: they either increase their efficiency in using the resource they gather (increasing yield), or they increase their capacity to consume resources (increasing resource acquisition). The same increase in resource concentration will result in a higher gain in individual growth rate in nutrient-poor environment than in nutrient-rich environments (Figure 5.4). In the former, investing in resource acquisition will therefore be more advantageous than investing in yield inducing a BGE decrease, and vice-versa in the latter.

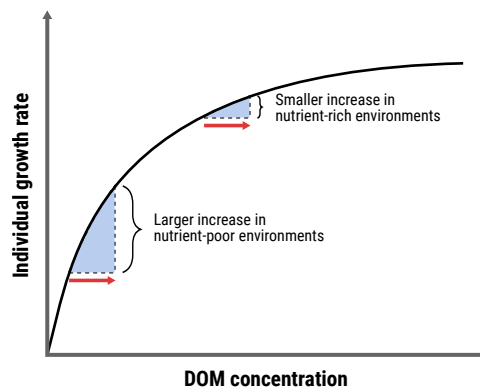


FIGURE 5.4: Effect of an increase in DOM concentration on individual growth rate in nutrient-poor and nutrient-rich environments. Individual growth rate follows a type-I response (Monod function) to DOM concentration. In red, the same increase of equilibrium DOM concentration due to bacteriophages in poor and rich environments.

To isolate the effect of the viral shunt on the system, we focus on the ecological equilibrium state, particularly equation (5.17). The effect of the viral shunt is to increase DOM concentration at its steady-state, which increases the difference between \overline{DOM} and \overline{DOM}_{NB} :

all other things being equal, the viral shunt will intensify the effect of viruses on the resource acquisition pressure – increasing BGE in rich environments and decreasing it in poor ones.

To summarize, the effect of bacteriophages on the evolutionary stable strategy is twofold. First, by increasing bacterial mortality, phages induce BGE adaptation by either increasing yield or stress tolerance, depending on their relative costs. Second, by increasing DOM availability to bacteria, phages can induce an increase in BGE values in DOM-rich environments, and a decrease in DOM-poor ones, a phenomenon intensified by the viral shunt.

5.2.2 Phages increase DOM recycling

In order to assess the role of each parameter on DOM recycling in presence of bacteriophages, we perform a sensitivity analysis of the system. The DOM input was set to represent the remineralization rate of POM at a depth of 100m according to the Martin curve [175] with a flux $F_{100} = 5 \text{ molC/m}^2/\text{year}$ and a b parameter such as $b = 1$. A set of baseline parameters was derived from Bendtsen et al. [25] and adjusted for the results to represent a credible water-column ecosystem (Table 5.1). We then perform 1,000 simulations following a Latin hypercube where each parameter is varied by a maximum of $\pm 20\%$.

Parameter	Baseline value	Unit
T	15	$^{\circ}\text{C}$
R	0.1	$\text{mmol}\cdot\text{m}^{-3}\cdot\text{day}^{-1}$
λ_B^0	1	day^{-1}
K_B^0	1	$\text{mmol}\cdot\text{m}^{-3}$
θ_A	2	
μ	0.01	day^{-1}
ϵ	0.5	
E_A	0.6	eV
q_B	1	q
q_V	5E-3	q
β	70	cells
θ_S	1	
ψ	0.2	$q\cdot(\text{mmol}\cdot\text{m}^{-3})^{-1}\cdot\text{day}^{-1}$

TABLE 5.1: Baseline simulation parameters of the $\mathcal{M}_{\text{NB-V}}$ model.

We first compare key outputs in their steady states under three different scenarios: one without phages (the \mathcal{M}_{NB} model), one with phages but where the viral shunt exits the system instead of returning to the DOM pool, and the complete $\mathcal{M}_{\text{NB-V}}$ model with viral shunt.

Most of the effect of phages on the equilibrium state of the system (Figure 5.5) comes from the inclusion of phages rather than the viral shunt, even a slight positive effect can be

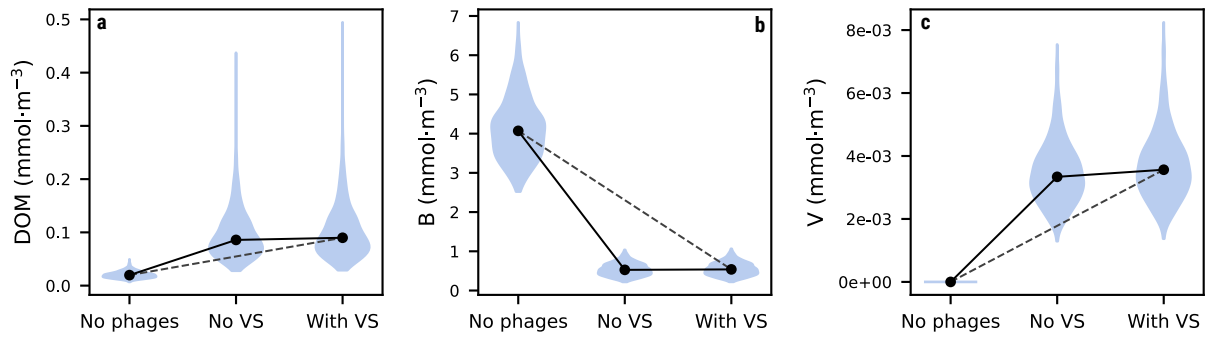


FIGURE 5.5: Influence of bacteriophages and the viral shunt on equilibrium concentrations. The median values of the distributions are represented as black dots, connected to clearly show the trend of the inclusion of different subsystems. The position of the dotted line relative to the solid lines informs us on the relative strength of viral inclusion and viral shunt. VS, viral shunt; (a) DOM concentration; (b) Bacterial biomass; (c) Viral biomass.

seen on DOM concentration and viral biomass. The added input of DOM doesn't compare to the systemic shift from a 'bottom-up' to 'top-down' limited system induced by the sole inclusion of a viral compartment.

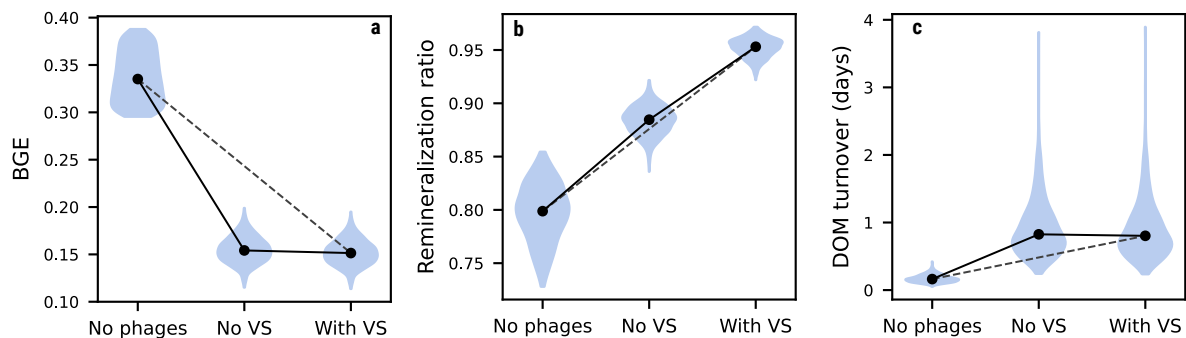


FIGURE 5.6: Influence of bacteriophages and the viral shunt key microbial loop outputs. (a) bacterial growth efficiency; (b) remineralization ratio; (c) DOM turnover rate. The median values of the distributions are represented as black dots, connected to clearly show the trend of the inclusion of different subsystems. The position of the dotted line relative to the solid lines informs us on the relative strength of viral inclusion and viral shunt. VS, viral shunt.

Just as predicted in the previous section, including viruses to the microbial loop in a DOM-poor environment induced a BGE decrease (Figure 5.6a). Once again, the effect of the viral shunt is too weak to produce a significant result.

Both the inclusion of a viral compartment and the viral shunt have a strong effect on the remineralization ratio (Figure 5.6b). The effect of the viral shunt is straightforward to explain: all excess matter from the lysis stays in the system and has a chance to end up respired.

On the other hand, we could expect that the inclusion of a viral compartment without the viral shunt would decrease the remineralization ratio by killing bacteria faster and keeping the community biomass down. The increase in remineralization ratio comes from adaptive mechanisms, not ecological ones: phages drive BGE values down (Figure 5.6a), and as such increase the individual respiration rate enough to make up for all other factors.

Bacteriophages tend to slow down DOM turnover (Figure 5.6c). By increasing the size of the DOM pool and limiting the growth of bacteria, phages decrease the uptake pressure on the environment's resource. The viral shunt has very little effect on DOM turnover however.

To summarize, for most state variables and functions of the microbial loop, the inclusion of a viral compartment is far more important than the viral shunt itself. By shifting the limitation from 'bottom-up' to 'top-down', bacteriophages limit bacterial growth, increase the pressure for stress tolerance and resource acquisition and overall induce faster cycling of the nutrients through the microbial loop. This is especially true of the remineralization ratio, which is even further increased by the viral shunt. Faster cycling of nutrients imply a stronger recycling pathway, but how does this pathway vary under climate change?

5.3 Bacteriophage influence under ocean stratification

In this section, we compute the eco-evolutionary response of the microbial loop to ocean stratification, which is represented by a 20% decrease in external DOM input R and analyze the potential extinction of phages due to bacterial adaptation.

5.3.1 Eco-evolutionary response of the system

In the absence of viruses, ocean stratification has little effect on bacterial adaptation (Figure 5.7 and section 2.3). The inclusion of bacteriophages not only changes the initial value of BGE, it also influences its response to ocean stratification: BGE increases by approximately 1% (Figure 5.7). This will impact nutrient remineralization (Figure 5.8) and DOM turnover (Figure 5.9).

The ecophysiological response of the remineralization ratio is sensitive to ocean stratification with opposite effects depending on the viral shunt (Figure 5.8). In the absence of the viral shunt, an increase in ocean stratification stimulates the remineralization. Reduced DOM input implies a lower viral biomass: the main source of bacterial mortality decreases, which mechanically increases the relative importance of respiration compared to mortality. When the viral shunt is active, the decrease in viral mortality represents a net loss of potential recycled DOM which could eventually be respired, leading to the remineralization ratio.

The interaction between bacterial adaptation and the viral shunt is also quite complex.

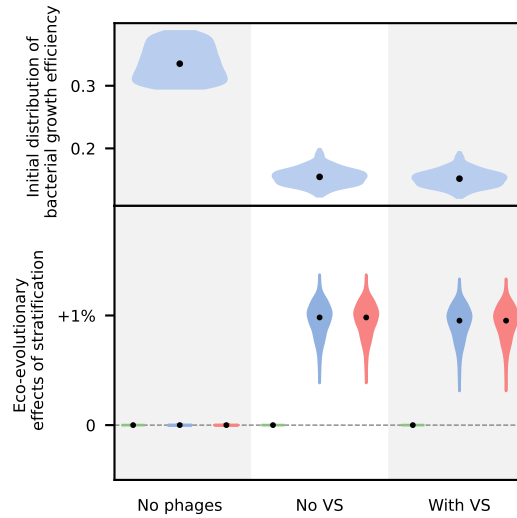


FIGURE 5.7: Influence of phages on bacterial adaptation to ocean stratification. The top row represents the distribution of values in the initial environment (Figure 5.6a), and the bottom row the ecophysiological response of the system (in green), the effect of bacterial adaptation (in blue) and the total eco-evolutionary response of the system. VS, viral shunt.

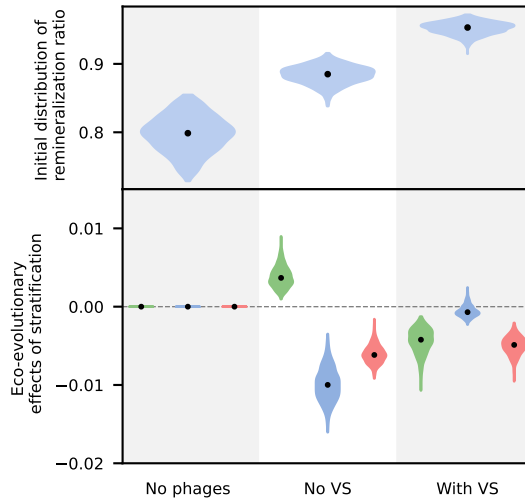


FIGURE 5.8: Influence of phages on remineralization ratio variations ocean stratification. The top row represents the distribution of values in the initial environment (Figure 5.6b), and the bottom row the ecophysiological response of the system (in green), the effect of bacterial adaptation (in blue) and the total eco-evolutionary response of the system. VS, viral shunt.

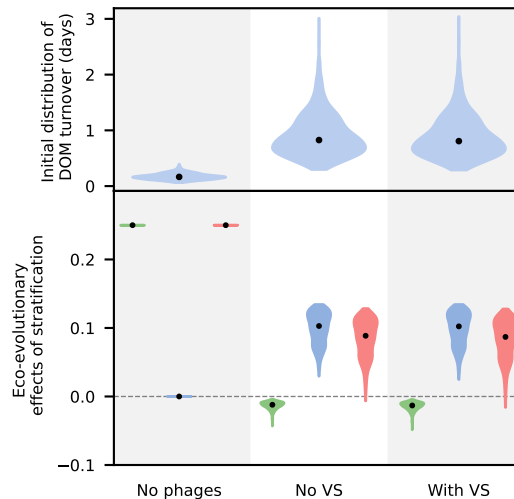


FIGURE 5.9: Influence of phages on DOM turnover variations to ocean stratification. The top row represents the distribution of values in the initial environment (Figure 5.6c), and the bottom row the ecophysiological response of the system (in green), the effect of bacterial adaptation (in blue) and the total eco-evolutionary response of the system. VS, viral shunt.

Indeed, the increase in BGE is equal in presence and absence of the viral shunt, but the effect of this increase is significantly different in both cases when it comes to the remineralization ratio. Without the viral shunt, an increase in BGE results in a decrease of the remineralization ratio, as the respiration rate decreases. But with the viral shunt, this increase can in some cases stimulate remineralization: looking at the correlation between this effect and the model parameters, we find that it is most positively correlated to the trade-off constant θ_S ($r = 0.60$) and negatively correlated to burst size β ($r = -0.55$). The model is sensitive to the relative cost of stress tolerance compared to yield: when stress tolerance costs more than yield ($\theta_S < 1$), the effect of a BGE increase will weaken the defences of bacteria to phages relatively more and increase infection rates. Since in the presence of the viral shunt, lysis actually stimulates remineralization as we've seen, remineralization ratio increases. For the same reasons, a high viral burst detracts from the viral shunt, as less matter gets redirected to the DOM pool, leading to a decrease in overall remineralization.

An interesting feature that emerges is that the total eco-evolutionary effect of ocean stratification is equivalent in both the presence and absence of viral shunt, but nothing indicates that this is a structural result of the model, and may rely on this specific parametrization.

Without of bacterial adaptation, DOM turnover decreases when stratification increases: stratification implies a decrease in DOM concentration (equation 5.17), which results in faster turnover. The effect is reversed by bacterial adaptation, because increasing BGE decreases the uptake rate, which results in an overall increase in DOM turnover.

5.3.2 Can ocean stratification lead to phage extinction?

Coexistence between bacteria and phages is possible only under the condition expressed by equations (5.13) and (5.15):

$$\bar{B} < \bar{B}_{\text{MAX}} \quad (5.24)$$

In the case of ocean stratification, two parameters shift, DOM input R and BGE value ω , which may result in bacterial biomass to cross the threshold and lead to phage extinction.

In the absence of bacterial adaptation, ocean stratification leads to a decrease of \bar{B}_{MAX} . If we call ω_0 the initial BGE value (i.e. before ocean stratification), we find that phages go extinct if the DOM input decreases below the threshold nutrient input R_R defined by:

$$R_{\text{EXT}} = q_B \cdot \frac{\mu_V \cdot \mu_B \cdot (1 - \omega_0)}{\omega_0 (\pi(\omega_0) \beta - 1) \cdot \psi}. \quad (5.25)$$

We now assume that the decrease in R is not enough to drive phages to extinction. From equations (5.13) and (5.15), we find that \bar{B}_{MAX} is an increasing function of ω whereas \bar{B} is a decreasing function of ω for $\omega > \omega_{\text{INF}}$ such as $\pi(\omega_{\text{INF}}) \beta = 1$. Let us prove that there exists a minimum value ω_{EXT} below which phages can't thrive, meaning such as $\bar{B}_{\text{MAX}}(\omega_{\text{EXT}}) = \bar{B}(\omega_{\text{EXT}})$. On one hand, we have

$$\lim_{\omega \rightarrow \omega_{\text{INF}}^+} \bar{B}(\omega) = +\infty. \quad (5.26)$$

On the other hand, $\bar{B}_{\text{MAX}}(\omega_{\text{INF}})$ is bounded. By our initial assumption of a system with bacteria-phages coexistence, we have $\bar{B}(\omega_0) < \bar{B}_{\text{MAX}}(\omega_0)$. By virtue of the intermediate value theorem, we conclude that there exists a value ω such as $\bar{B}(\omega) = \bar{B}_{\text{MAX}}(\omega)$, which we call ω_{EXT} (Figure 5.10).

The value of ω_{EXT} is given by the crossing point of \bar{B}_{MAX} and \bar{B} :

$$\frac{\omega_{\text{EXT}} \cdot R}{(1 - \omega_{\text{EXT}} \cdot \epsilon) \cdot \mu_B} = q_B \cdot \frac{\mu_V}{(\pi(\omega_{\text{EXT}}) \beta - 1) \cdot \psi}. \quad (5.27)$$

Computing the sign of selection gradient $dS(\omega)$ for $\omega = \omega_{\text{EXT}}$ indicates the position of ω^* relative to ω_{EXT} , as $dS(\omega_{\text{EXT}}) < 0$ if and only if $\omega_{\text{EXT}} < \omega^*$. For $\omega = \omega_{\text{EXT}}$, $\overline{DOM} = \overline{DOM}_{\text{NB}}$ and $\bar{V} = 0$. This leads to the following relationship:

$$dS(\omega_{\text{EXT}}) = dS_{\text{NB}}(\omega_{\text{EXT}}). \quad (5.28)$$

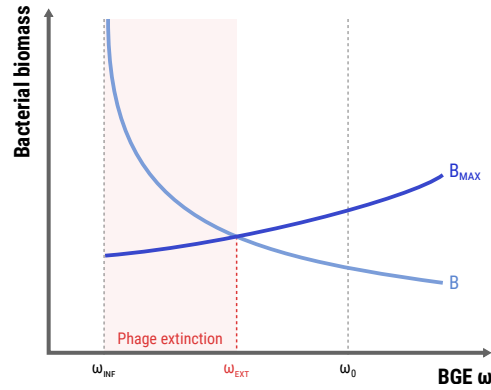


FIGURE 5.10: Existence of a threshold value ω_{EXT} below which bacteriophages go to extinction. \bar{B}_{MAX} , bacterial biomass in absence of phages; \bar{B} , bacterial biomass in presence of phages; ω_{INF} , lower bound of the valid domain in presence of phages; ω_0 , initial value of the system for which bacteria and phages coexist.

Equation (5.28) indicates that both ω^* and ω_{NB}^* are on the same side of ω_{EXT} , so that $\omega^* < \omega_{EXT}$ if and only if $\omega_{NB}^* < \omega_{EXT}$. In other words, bacterial adaptation may lead bacteriophages to extinction if the evolutionary equilibrium lies in the phage extinction zone. The ESS ω_{NB}^* in absence of bacteriophages does not depend on DOM input R (equation 2.24), whereas ω_{EXT} increases with a DOM input decrease (equation 5.27): there could be a point at which ω_{EXT} increases past the constant ω_{NB}^* , which would drive phages to extinction. Bacterial adaptation in response to ocean stratification could drive a population of specialized phages to extinction.

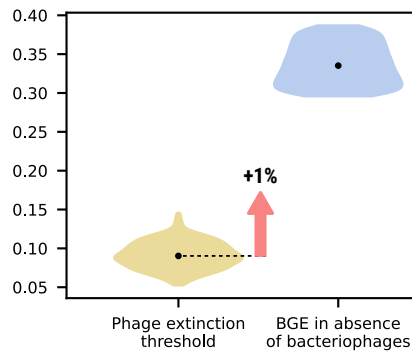


FIGURE 5.11: Distribution of the extinction threshold relative to bacterial growth efficiency and eco-evolutionary effect of ocean stratification. The red arrow represents the median eco-evolutionary effect of a 20% decrease in external DOM input due to ocean stratification.

With the considered parametrization, the extinction threshold is still not reached after the DOM input decrease, but the gap narrows (Figure 5.11), and deep in the water column in oligotrophic regions, this threshold could be passed. Based on the analysis from this section, phage extinction would lead to lower nutrient remineralization, faster DOM turnover and higher bacterial biomass concentration across the oceans.

5.4 Conclusion and perspectives

This chapter focused on the integration of bacteriophages to the microbial loop, and how the viral shunt influences its function. Its effect on the system in the aphotic zone was extensively analyzed, and in order to complete the study a closer look needs to be taken on sea-surface ecosystems. This work was already pursued in Weitz et al. [274] for the integration of phages in a constant environment, and the study from this chapter will allow us to extrapolate its future under a changing ocean.

In their study, Weitz et al. [274] develop a model close to the NPZ-B model discussed in this thesis (see Chapter 3), with some notable differences: there are two classes of phytoplankton (eukaryotes and cyanobacteria) and only one class of dissolved inorganic nitrogen (whereas we made the distinction between nitrate and ammonium to track new and regenerated production). Each unicellular organism has a specific class of viruses attached, and the viral shunt drives nitrogen from all unicellular pool to the dissolved organic nitrogen pool. While the system exhibited the shift from a ‘bottom-up’ to a ‘top-down’ limitation with the decrease in zooplankton biomass and an increase in organic and inorganic nutrients that was expected, the inclusion of viruses proved to actually increase total biomass of unicellular organisms. This change in ecosystem structure came with a change in ecosystem function, with increased remineralization (as was the case in the $\mathcal{M}_{\text{NB-V}}$ model) and subsequent increased primary production. The decrease in trophic transfer (and as such, in overall export) shows that this productivity increase comes from increased regenerated production.

The shift in evolutionary stable strategy (section 5.2.1) would also take place in a sea-surface ecosystem model: BGE values would increase in nutrient-rich regions and decrease in nutrient-poor regions compared to a system without phages. When bacteriophages are not taken into account, BGE values are already positively correlated to the richness of the environment (Chapter 3), so the inclusion of a viral compartment would increase the biogeographical differences in bacterial growth efficiencies. We expect regeneration to increase in productive zones, driving primary production up.

Under the surface, our model predicts that ocean stratification could lead to the extinction specialized bacteriophages. However unlikely, such a scenario would be a ‘tipping element’ for ocean ecosystems [159]. Tipping elements represent Earth subsystems that are continental or subcontinental in scale and for which small variations in the environment could result in dramatic shifts in function. A paramount example of a tipping element in the Earth system is the melting of the polar caps: if the ice sheets at the poles melt over a certain point, the albedo of the Earth would change significantly leading to even more warming and no possibility to go back to full covering of the poles [253]. Considering the significance of bacteriophages to the marine food web, the remodeling of ecological communities by adaptation-driven phage extinction might shift biogeochemical cycles in the ocean to a new state. Bacteriophage extinction due to bacterial adaptation could lead to lower DOM

regeneration and primary production [274] and increased bacterial biomass, reinforcing the ‘sink’ aspect of the microbial loop [96]. Nonetheless, the prediction of an ecological shift in viral abundance and diversity below some critical depth underlines the limits of our model: data shows that viral counts increase relative to bacteria deep in the water-column in oxygen minimum zones [133], showing the importance of mechanisms not captured by our model. In order to test the predictions and results of this chapter, an implementation in an ESM such as the NEMO-PISCES model [15] would be the next logical step.

In addition to exerting a strong biogeochemical control on the microbial loop, bacteriophages also impact the adaptation of heterotrophic bacteria by altering their metabolism [34], increasing their mutation rate [208] or promoting genetic innovation through integration [200] (more thorough reviews can be found in Breitbart et al. [33] and Chevallereau et al. [52]). Transduction, a phage-mediated horizontal-gene transfer mechanism is of particular interest for our thesis. It is thought to have permitted the apparition of entire metabolic pathways [185], and allows the rapid spread of innovation in general [128]). In the next chapter, we shall thus focus on the impact of transduction on bacterial adaptation.

Chapter 6

Transduction, a viral mechanism influencing bacterial adaptation

With Sylvie Méléard and Régis Ferrière, in preprint [50]. Presented at Virtual Evolution 2021 [51].

‘A fly got into the transmitter pod with me that first time, when I was alone. The computer got confused - there weren’t supposed to be two separate genetic patterns - and it decided to, uh, splice us together.’

Seth Brundle, *The Fly* (1986)

In addition to their ecological and biogeochemical importance, bacteriophages influence bacterial adaptation through genetic mechanisms such as transduction. Transduction is a horizontal gene transfer mechanism (HGT) in which phage particles transfer genetic material from one bacterial cell to another. Depending on the allele transferred (whether it is beneficial or deleterious), transduction may accelerate or hinder bacterial adaptation. In this chapter, we resolve the conflicting effects of transduction on bacterial adaptation in a simple eco-evolutionary model for large populations characterized by a quantitative (resource-use) trait with a single evolutionary optimum.

6.1 Introduction

Bacteria can transfer genetic material ‘vertically’ to daughter cells as well as ‘horizontally’ between cells. The process of horizontal gene transfer allows bacterial species to successfully conquer and adapt to new ecological niches [68, 202, 153] by driving the rapid spread of evolutionary innovation [128, 131]. Well-studied mechanisms of horizontal gene transfer (HGT)

between bacterial cells are transformation, conjugation, and transduction. Of the three, transduction by bacterial viruses, or phages, is generally regarded as the most important [46]. Transduction is the process whereby host DNA is packaged into phage particles which then deliver the bacterial DNA as they infect other cells. Through transduction, viruses can influence the genotypic composition of host populations, hence potentially their hosts' evolution. For example, phages are notorious for their role in the transfer of pathogenicity islands and antibiotic resistance genes.

While transduction may contribute substantially to the evolution of major ecological innovations in prokaryotes, very little is known about the role that transduction plays in the adaptation of bacterial populations to small or gradual, quantitative, rather than large, qualitative, changes in their environment [223, 257]. The conventional view is that, as a mechanism that facilitates the spread of genetic elements among host cells, transduction may accelerate bacterial adaptation to a changing environment [7]. But if bacteria can acquire advantageous mutations through transduction, they may also receive deleterious ones [224, 27]. In addition, if a high rate of transduction comes at the cost of a high rate of viral infection, the adaptive benefit of spreading beneficial mutations may be further eroded by the overall mortality cost of infection. Our goal here is to resolve these conflicting effects of transduction on bacterial adaptation by developing and analysing a simple mathematical model.

Different mechanisms of transduction have been described, depending on the phage life cycle and the region of host DNA that can be transferred [101, 66]. Specialized transduction and lateral transduction involve temperate phages, i.e. phages that can enter either the lytic or lysogenic life cycles. Specialized transduction occurs when a prophage (phage in lysogeny) excises incorrectly from the host bacterial genome and ends up packaging some of the flanking regions of host DNA. The recently described lateral transduction [46] also involves temperate phages, whose late excision and *in situ* replication leads to highly efficient packaging of host DNA over several hundred kilobases downstream of the integration site. Finally, generalized transduction can involve phages that are temperate as well as virulent, i.e. that can only replicate via the lytic cycle. In generalized transduction, phages randomly package host DNA instead of their own and thus can transfer any fragment of the bacterial genome. Phages packed with host DNA, or transducing particles, are released during lysis, together with functional virions. Transducing particles have the ability to adsorb to bacterial surface receptors and inject their DNA. However, as they lack viral genes, transducing particles cannot trigger lysis. Instead, the injected bacterial DNA might be integrated into the recipient cell's genome by recombination. In this study, we focus on generalized transduction by virulent phages, which allows us to keep the mathematical framework simple and tractable.

In our model the phenotype of asexually reproducing bacterial cells is characterized by a quantitative trait which measures the cell's ability to acquire a single resource. We use a sim-

ple genotype-phenotype map based on an infinite-site, infinite allele model in which mutations occur upon cell division and cause small, random phenotypic change. The mutated DNA of a mutant cell may be transferred to recipient cells and integrated in their genome via generalized transduction due to a non-evolving virulent phage. To model selection on bacterial trait variation, we take an eco-evolutionary approach in which the intensity and direction of selection is not given *a priori* [78]. Rather, selection results from the ecological process of cells competing for their resources, with competition being more intense among cells that are phenotypically more similar.

Starting with an individual-level model of bacteria competing among themselves and susceptible to infection by a virulent phage, we extend the model to track the effect of generalized transduction on the cells' genotype and phenotype. Assuming the existence of a single trait value that maximizes individual resource acquisition (i.e., a single evolutionary optimum), the adaptation process unfolds as the bacterial population moves in its one-dimensional phenotypic space. By assuming that the process is mutation-limited, we derive the general equation driving the adaptive trait dynamics. We combine the mathematical analysis of this equation with numerical simulations of the individual-based process to resolve the effect of generalized transduction on (i) the speed of adaptation away from the evolutionary optimum, (ii) the dynamics of adaptation near the optimum, (iii) the maintenance of phenotypic diversity that may result from disruptive selection around the optimum.

6.2 A mathematical model for transduction

Our model of generalized transduction is summarized in Figure 6.1. During the reproduction and encapsulation of the viral genome, DNA 'mispackaging' may occur resulting in viral particles that contain part of the host genome instead of viral DNA [257]. These viral particles, that we call *Gene Transducing Particles*, or GTP, may no longer cause the lysis of the cells they infect. Instead, they pass genetic material from the previous host on to the receiving cell, where it may be integrated in the genome by recombination. As a consequence, the phenotype of the receiving cell, and its offspring lineage, may be altered (Figure 6.1a).

6.2.1 Individual-level model of infection and transduction

To describe the genotypic and phenotypic effects of transduction, we focus on a quantitative character, or trait, a , and introduce a simple model of the genotype-phenotype map. We make the following assumptions:

1. The trait is under the control of many loci of small, additive effects.

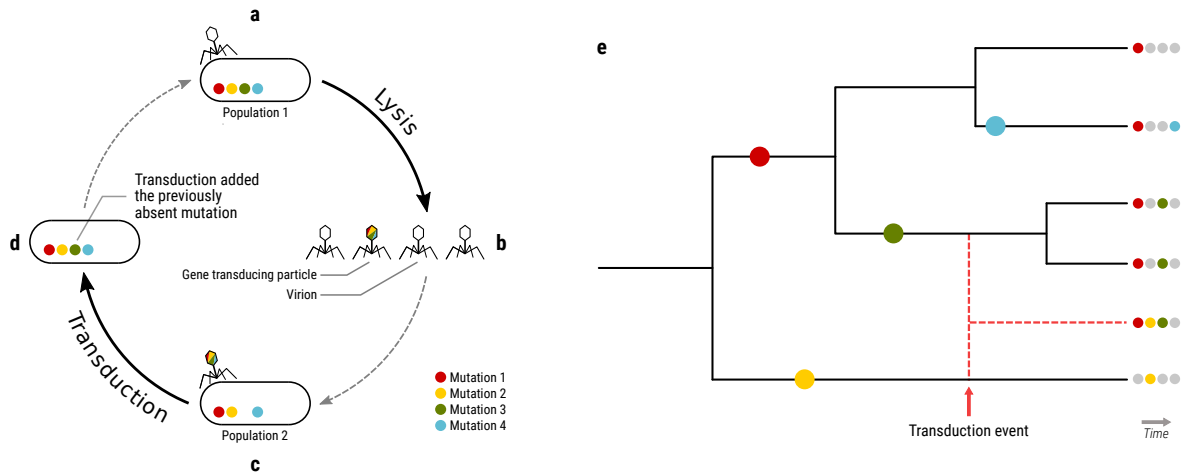


FIGURE 6.1: Transduction moves mutant alleles among individuals and create new genotypes. Infection by a lytic virus (a) causes a viral burst. Some of the viral particles released from the burst are gene transducing particles (b) that may transfer a mutated allele from the previous host to a new host (c). With a given probability of transduction, the mutated allele is integrated by recombination into the new host's genome (d). Mutations that occur in different lineages are vertically inherited (e). When a transduction event occurs, a new lineage is created (e, dashed red lines).

2. We use the principle of an infinite site model, so that no two mutations will impact the same locus.
3. Alleles at the different loci can be moved by transduction. Transduced DNA is integrated by non-homologous end joining [221], i.e. the new DNA fragment is *added* to the host genome, and does not replace the resident allele.
4. We assume no dosage effect, meaning that the number of occurrences of an allele does not influence the level of expression of the gene.
5. Mispackaging of host DNA in a new viral particle (GTP), the delivery of the previous host's DNA by the GTP, and the integration of transferred genetic material into the newly infected host's genome, are stochastic events. Each event occurs with a certain probability.
6. The integration step of the transduction process is more likely if the phenotypes are more similar. The reason is that the underlying genotypic difference between more similar phenotypes is likely smaller, which may facilitate recombination.

Per assumptions 3 and 4, when a cell receives a copy of a mutation it already carries, two copies of the same mutated sequence will occur in the genotype, but assumption 4 implies that the phenotype will not be altered by the second copy of the mutation. Only the presence or absence of an allele influences the cell's phenotype. The genotype-phenotype map can

thus be described as follows. By n we denote the number of mutations that have occurred in a population at time t . Since each mutation occurs on a different site (assumption 1), we can define $\mathbb{M}_i \subseteq \{1, \dots, n\}$ the subset of mutations that individual i carries. The phenotypic effect of each mutation (indexed by m , varying from 1 to n) is a small perturbation ϵ_m . As a consequence, the trait a_i for individual i is

$$a_i = a_0 + \sum_{m \in \mathbb{M}_i} \epsilon_m \quad (6.1)$$

where a_0 is the initial value of the trait in an isogenic population.

Now if i and j designate two individuals respectively carrying the mutation sets \mathbb{M}_i and \mathbb{M}_j , let us consider the case where individual i encounters a GTP originating from individual j , thus carrying \mathbb{M}_j . By injecting DNA from individual j into the individual i , the GTP transfers individual j 's specific mutations to the recipient cell's genotype without altering the mutations already carried by i . Thus, i 's mutation set will change from \mathbb{M}_i to $\mathbb{M}_i \cup \mathbb{M}_j$, and its phenotype will be altered accordingly. The population coalescent (Figure 6.1b) shows that when a transduction event takes place between two distinct lineages, a new lineage results from the recombination of the two original genetic material. In that sense, transduction can be seen as driving 'sparse sexual reproduction events' [19]. Note that modeling the phenotypic effect of transduction cannot be based solely on individuals' phenotypes; the explicit tracking of genotypes is required. Indeed, if \mathbb{M}_i as expressed as phenotype a_i and \mathbb{M}_j as a_j , there is no inferring phenotype $a_{i \cup j}$ solely from phenotypes a_i and a_j .

We now consider the simplest case of a resident population in which a mutant appears. The mutation set of the resident population is the empty set \emptyset , and the mutation set of the mutant is $\{1\}$, i.e., $\mathbb{M}_{res} = \emptyset$ and $\mathbb{M}_{mut} = \{1\}$. Then the following transduction events may occur:

- Interaction between a cell and a GTP carrying DNA of the same genotype: no genotypic or phenotypic change.
- Interaction between a resident cell and a GTP carrying mutant DNA: since $\emptyset \cup \{1\} = \{1\}$, the resident cell acquires the mutation set of the mutant and changes to the mutant phenotype.
- Interaction between a mutant cell and GTP carrying resident DNA: since $\{1\} \cup \emptyset = \{1\}$, the mutation set of the mutant is unchanged and there is no phenotypic change.

Thus, whether they interact with resident or mutant bacteria, resident GTPs do not alter the phenotype of the recipient cells, while mutant GTPs may change the phenotype of resident cells into the mutant phenotype. As a consequence, the bacterial population remains dimorphic (i.e., transduction does not create a third phenotype) and the resident GTP population has no effect on the overall population dynamics.

6.2.2 Phage-bacteria population dynamics with mutation and transduction

We use a multitype logistic model of birth and death [149] to model the population dynamics of resident bacteria with trait value a and mutant bacteria with trait value A (population sizes X and Y , respectively), viruses (population size V), and GTP carrying mutant DNA (population size U). The order of magnitude of the bacterial population size is denoted by K . Bacteria reproduce asexually at rate b and die at rate d . Both rates may depend on the population size and trait value; for simplicity, we will focus on the case where the negative demographic effect of competition for limited resources is borne out by the death rate. Viruses form a homogeneous population, and GTPs are defined by the genotype and phenotype of their host of origin. Virions die at rate μ_v , and interactions between resident bacteria and viral particles carrying mutant DNA occur at the individual rate $\psi(a)$. An interaction between a bacterium and an active virus results in instant lysis and a viral burst whereby β new viral particles are created, each having a probability γ of being a GTP. When a bacterium with trait a and a GTP from a cell with trait a' come into contact, with probability $\eta(a, a')$ the foreign DNA fragment is integrated by recombination into the recipient bacterial genome; the smaller the difference between a and a' , the larger $\eta(a, a')$ is [257].

In the large population limit (large K), population sizes X, Y, V, U can be rescaled into population densities x, y, v, u whose time dynamics are governed by the following deterministic equations [178] :

$$\left\{ \begin{array}{l} \frac{dx}{dt} = (b(a) - d_{DD}(a, x, A, y)x - \psi(a)v - \psi(a)\eta(a, A)u)x \\ \frac{dy}{dt} = (b(A) - d_{DD}(A, y, a, x)y - \psi(A)v + \psi(a)\eta(a, A)u)x \\ \frac{dv}{dt} = (1 - \gamma)\beta(\psi(a)x + \psi(A)y)v - (\mu_v + \psi(a)x + \psi(A)y)v \\ \frac{du}{dt} = \gamma\beta\psi(A)yv - (\mu_v + \psi(a)x + \psi(A)y)u \end{array} \right. \quad (6.2)$$

Competition among cells is assumed to result in a density-dependent (DD) death rate which increases linearly with density, given by

$$\begin{aligned} d_{DD}(a, x, A, y) &= d(a) + c(a, a)x + c(A, a)y \\ d_{DD}(A, y, a, x) &= d(A) + c(A, A)y + c(a, A)x \end{aligned} \quad (6.3)$$

where $d(a)$ (respectively $d(A)$) is the intrinsic death rate of individuals with trait value a (resp. A) and c measures the intensity of competition between individual cells as a function of their trait values. In a monomorphic population with trait value a , transduction alone has no effect on bacteria's phenotype, hence the phage-bacteria population equilibrium:

$$\begin{cases} \bar{x}(a) = \frac{\mu_v}{\psi(a)((1-\gamma)\beta - 1)} \\ \bar{v}(a) = \frac{1}{\psi(a)} \left(r(a) - \frac{\mu_v}{\psi(a)((1-\gamma)\beta - 1)} c(a, a) \right) \end{cases} \quad (6.4)$$

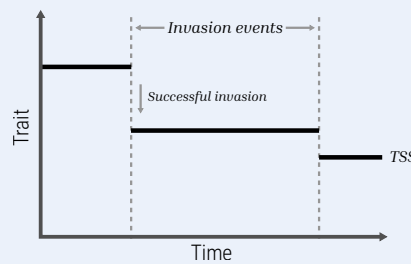
In our numerical simulations, for the chosen range of parameter values (see Table 6.1), this equilibrium was always found to be globally stable. Virus-bacteria population cycles or the extinction of one or both populations were never detected over our range of trait values.

6.2.3 Mutant invasion, Trait Substitution Sequence, and canonical equation of adaptive dynamics

We assume that the adaptation process is mutation-limited (mutation occurs rarely on the timescale of population dynamics) and that mutations have small phenotypic effects. Those are key assumptions under which the adaptation process in very large populations can be described as a *Trait Substitution Sequence* (TSS) [181, 40].

Toolbox 6.1 *Trait Substitution Sequence*

In the TSS model, a mutant either invades and replaces the resident type, or goes to extinction – provided the population has not come too close to a potential evolutionary optimum [116, 115]. This means that no two populations of resident and mutant bacteria that are phenotypically similar may coexist, except possibly near an evolutionary optimum.



The population evolves adaptively by making small phenotypic ‘jumps’ in the trait space as in the figure above, each jump corresponding to the invasion of a successful mutant into the former resident-trait population.

The invasion success of a mutant A in a resident population of trait value a is determined by the mutant’s invasion fitness, i.e. the mutant population growth rate from initially very small density in a resident population at ecological equilibrium. This is obtained from the previous dynamical system for population densities (equation 6.2). In this paper, we use S

and p to denote respectively the invasion fitness and invasion probability in the absence of transduction, and S_T and p_T to denote invasion fitness and invasion probability with transduction.

To infer the probability of invasion and characteristic invasion time while taking the population finiteness into account, we link the deterministic dynamical system describing the dynamics of large populations to the stochastic individual-level process of birth and death events driving the dynamics of small populations (initial mutant population, resident population upon complete invasion). Once the probability $p(a, A)$ of invasion of a mutant trait A in a resident population of trait a is known, we derive the ‘jump rate’ of the adaptation process with transduction. To this end, we rescale time by $K \cdot r_M$, where K is the order of population size and r_M is the mutation rate. On this new timescale, the population evolves adaptively in trait space according to the TSS model, jumping from trait a to trait A at rate

$$p(A, a) \bar{x}(a) b(a) m(a, dA) \quad (6.5)$$

where $\bar{x}(a)$ is the equilibrium population density of the resident trait a , and $m(a, dA)$ is the mutation kernel from trait a to trait A , taken as $m(a, dA) = m(A - a)dA$.

Taking the limit of arbitrarily small mutations happening fast (relative to the new timescale), the TSS converges towards a process driven by the so-called ‘canonical equation of adaptive dynamics’ [79, 41, 44]. In the absence of transduction, this limit process is deterministic and the canonical equation reads

$$da_t = \sigma_0^2(a_t) \bar{x}(a_t) b(a_t) \partial_1 p(a_t, a_t) \quad (6.6)$$

where a_t denotes the trait value evolving as a function of time t , mutational phenotypic effects are symmetrical, and σ_0 is the standard deviation of the distribution of mutational effects (mutation kernel, m). The direction of selection is given by the invasion probability gradient $\partial_1 p(a, a)$, i.e. the derivative of invasion probability p with respect to its first variable, evaluated for a mutant trait value equal to the resident’s, a . In the general case without transduction, the probability gradient can be expressed as the selection gradient $\partial_1 S(a, a)$ divided by the birth rate $b(a)$. Thus, at any time t the rate of adaptation is a function of the selection gradient, population size, and mutation size at that time.

‘Evolutionary singularities’ are trait values at which the selection gradient vanishes [182]. An evolutionary singularity, denoted by a^* , can be ‘attractive’ in the phenotype space, in which case the TSS of a population whose phenotypic state is some distance away from a^* will evolve under directional selection towards a^* . If selection around the singularity a^* is stabilizing, the TSS remains in a neighborhood of a^* . Selection may also turn disruptive around a^* . Whether selection is stabilizing or disruptive is predicted by the criterion for evolutionary branching [79, 44].

6.2.4 Simulations

We performed individual-level simulations of populations and trait dynamics by implementing a rigorous Gillespie algorithm, based on [40]. The speed of adaptation was estimated from simulations of the TSS and compared to our mathematical approximations. All simulations were carried out using constant rates of birth, intrinsic death, and infection, respectively equal to b_0, d_0, ψ_0 . We used the following form for the competition term

$$c(a, A) := \frac{\exp\left(-\left(\frac{a-A}{\sigma_C}\right)^2\right)}{K_0 \exp\left(-\left(\frac{a-a^*}{\sigma_K}\right)^2\right)} \quad (6.7)$$

where σ_C measures competition sensitivity to phenotypic difference ($a - A$), K_0 represents the maximal carrying capacity of the environment, σ_K represents the sensitivity of the population carrying capacity to the distance of trait a to the phenotypic optimum a^* . We use the following form for the transduction probability

$$\eta(a, A) := \eta_0 \exp\left(-\left(\frac{a-A}{\sigma_\eta}\right)^2\right) \quad (6.8)$$

where η_0 is the maximal transduction probability and σ_η measures the sensitivity of ψ to the phenotypic difference ($a - A$). Default values for all parameters are listed in Table 6.1.

6.3 Results

6.3.1 Dynamics of bacterial adaptation without transduction

First we consider the baseline scenario in which the evolving bacterial population is exposed to viral infection but no transduction occurs, $\eta_0 = 0$. Here the invasion fitness $S(A, a)$ of a mutant trait A in a resident population of trait a is

$$S(A, a) = r(A) - c(a, A)\bar{x}(a) - \psi(A)\bar{v}(a). \quad (6.9)$$

The term $r(A) - c(a, A)\bar{x}(a)$ is the invasion fitness in the absence of viral infection. The additional term $-\psi(A)\bar{v}(a)$ measures the negative effect of infection on bacterial fitness. As expected, this negative effect is stronger if the equilibrium viral population, $\bar{v}(a)$, or the infection rate, $\psi(A)$, is larger. From equation (6.9) it follows that the invasion probability is $p(A, a) = [S(A, a)]_+ / b(A)$, with a characteristic time of invasion of the order of $\log(K)$ [27].

The direction of selection is given by the selection gradient $\partial_1 S(a, a)$ and the rate of adaptation, by the canonical equation

Parameter	Expression	Numerical values
Population size order	K constant	$K = 200$
Trait range	$]a_{\text{INF}}, a_{\text{SUP}}[$	$a_{\text{INF}} = -1.5$ $a_{\text{SUP}} = 1.5$
Birth rate	$b(a) = b_0$ constant	$b_0 = 4 \text{ day}^{-1}$
Death rate	$d(a) = d_0$ constant	$d_0 = 0.5 \text{ day}^{-1}$
Competition rate	$c(A, a) = \frac{\exp\left(-\left(\frac{a-A}{\sigma_C}\right)^2\right)}{K_0 \exp\left(-\left(\frac{a-a^*}{\sigma_K}\right)^2\right)}$	$\sigma_C = 5$ $K_0 = 5K$ $a^* = 0$ $\sigma_K = 1$
Infection rate	$\psi(a) = \psi_0$ constant	ψ_0 variable
Viral death rate	μ_v constant	$\mu_v = 5 \text{ day}^{-1}$
Burst size	V constant	$V = 100$
Probability of GTP release	γ constant	$\gamma = 0.01$
Transduction probability	$\eta(a, A) = \eta_0 \exp\left(-\left(\frac{a-A}{\sigma_\eta}\right)^2\right)$	η_0 variable $\sigma_\eta = 1$
Mutation standard deviation	h constant	$h = 0.01$

TABLE 6.1: Default simulation parameters.

$$da_t = \sigma_0^2(a_t) \bar{x}(a_t) b(a_t) \partial_1 p(a_t, a_t). \quad (6.10)$$

We assume that the functions r , c and ψ are such that there is a single evolutionary singularity, a^* . For the model specifications used in our numerical simulations, a^* exists and is always globally attractive; selection around a^* is stabilizing if $\sigma_K < \sigma_C$, or disruptive, with evolutionary branching, if $\sigma_K > \sigma_C$. These conditions are identical to those obtained in the absence of infection [82].

6.3.2 Mutant invasion with transduction

With transduction ($\eta_0 > 0$), invasion fitness $S_T(A, a)$ of a mutant trait value A in a resident population of trait a is given by the following expression (see supplementary section A for the mathematical derivation):

$$S_T(A, a) = S(A, a) + \frac{\gamma}{1-\gamma} \psi(A) \bar{v}(a) \eta(a, A). \quad (6.11)$$

Transduction alters invasion fitness by adding the positive term $\frac{\gamma}{1-\gamma} \psi(A) \bar{v}(a) \eta(a, A)$. Thus, invasion fitness with transduction is always greater than invasion fitness without transduction: $S_T(A, a) > S(A, a)$ (Figures 6.2a-b). We can further decompose the additive term into three factors: $\psi(A) \bar{v}(a)$, $\frac{\gamma}{1-\gamma}$, and $\eta(a, A)$. The first factor represents the rate at which mutant bacteria interact with the viral population at ecological equilibrium with the resident bacterial population, each of these interactions being a potential opportunity for the release of GTPs. The second factor measures the abundance of GTPs released by a mutant infection relative to active viruses. Taken together, the two factors measure the strength of potential transduction events compared to infection events. The last term represents the proportion of these potential transduction events that result in actual genetic transfer. The three factors together thus quantify the intensity of transduction.

As a consequence, mutants that are selected against (negative invasion fitness, $S < 0$) in the absence of transduction may be favored and invade when transduction is strong enough, resulting in $S_T > 0$ (Figure 6.2b). Also, irrespective of the intensity of transduction, negatively selected mutants ($S < 0$) that are phenotypically close to the resident phenotype always invade. In fact, with transduction, any mutant of sufficiently small effect is predicted to invade.

Transduction also affects the mutant-resident dynamics following mutant invasion. The potential for ‘back invasion’ by the resident population once rare is determined by the ‘back invasion fitness’ (see supplementary section A):

$$\tilde{S}_T(a, A) = S(a, A) - \frac{\gamma}{1-\gamma} \psi(a) \bar{v}(A) \eta(a, A) \quad (6.12)$$

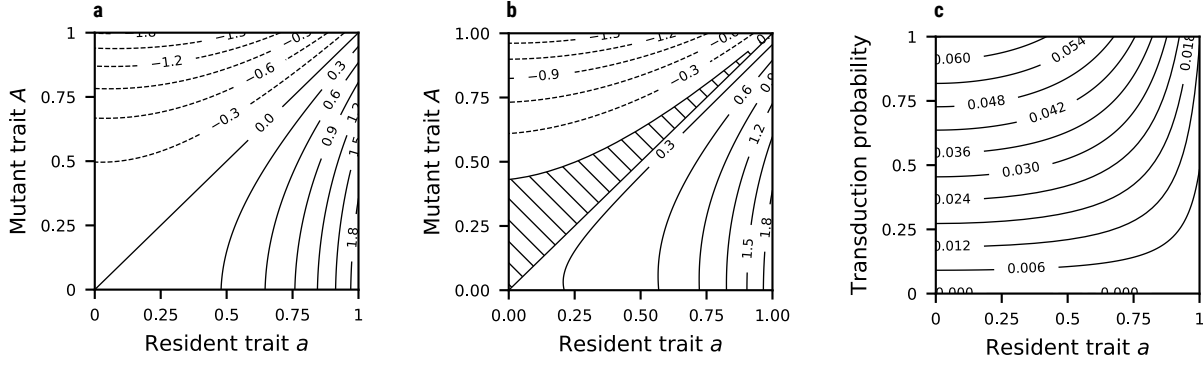


FIGURE 6.2: Influence of transduction on invasion fitness and the probability of invasion. (a) Contours of invasion fitness $S(A, a)$ in the absence of transduction. (b) Contours of invasion fitness $S_T(A, a)$ with transduction ($\psi_0 = 1.0$ and $\psi_0 = 10^{-5}$). The hatched area highlights trait values of a and A for which $S(A, a) < 0$ and $S_T(A, a) > 0$. (c) Invasion probability $p_T(a, a)$ of a mutant that is phenotypically identical to the resident strain, as a function of the resident trait value and transduction probability. Other parameters are set to their default values (see Supplementary Table 1).

By making a negative contribution to the right-hand side of equation (6.12), transduction generally hampers back invasion. In particular, for any mutation of small effect ($S(A, a) \approx 0$), transduction always begets invasion ($S_T(A, a) \approx \frac{\gamma}{1-\gamma} \psi(A) \bar{v}(a) \eta(a, A) > 0$) and always prevents back invasion ($\tilde{S}_T(a, A) \approx -\frac{\gamma}{1-\gamma} \psi(a) \bar{v}(A) \eta(a, A) < 0$).

Transduction always increases the invasion probability of a mutant (supplementary section B). For small transduction rates (which is the case when mutations have small phenotypic effects) and large viral burst sizes ($V \gg 1$, which is expected in natural systems), the probability of invasion with transduction is given by the following approximation (supplementary section B):

$$p_T(A, a) \approx [S_T(A, a)]_+ / b(A). \quad (6.13)$$

Of note, equations (6.11) and (6.13) imply $S_T(a, a) > 0$ and $p_T(a, a) > 0$ for any trait value a . Thus, a mutant that is phenotypically identical to the resident type has positive invasion fitness (Figure 6.2b), as opposed to zero invasion fitness in models without transduction (Figure 6.2a). This is due to our explicit genotype-phenotype map: albeit phenotypically identical to the resident type, the mutant type is genetically different (by definition, it carries a new mutation) and our model of transduction accounts for this. Using notations introduced earlier, we have $\mathbb{M}_{res} = \emptyset$ and $\mathbb{M}_{mut} = \{1\}$, and our model predicts $S_T(\mathbb{M}_{mut}, \mathbb{M}_{res}) > 0$. However, $S_T(\mathbb{M}_{res}, \mathbb{M}_{res}) = 0$, which is consistent with the expectation that a mutant strain that is identical, both genetically and phenotypically, to the resident strain should have zero invasion fitness.

The invasion probability for mutants that are phenotypically identical to their resident progenitor, $p(a, a)$, provides an approximation for the invasion probability of mutations of

small phenotypic effect. The probability $p_T(a, a)$ is higher near the evolutionary singularity a^* (Figure 6.2c). Thus, due to transduction, the invasion probability of any mutation of small effect increases as the adaptation process brings the population closer to the evolutionary singularity.

6.3.3 Rate of adaptation with transduction

Here we assume that mutations have small phenotypic effects. By rescaling time appropriately, we derive a macroscopic model for the dynamics of adaptation similar to the canonical equation. With transduction, however, the macroscopic model retains a stochastic component and takes the form of a stochastic differential equation or integro-differential equation, depending on the shape of the mutation kernel. The models, hence the dynamics of adaptation that they capture, critically depend on whether the mutation kernel is symmetrical around zero (unbiased mutational effects) or not (biased mutational effects), and determine whether adaptation will be deterministic or stochastic (see all mathematical derivations in supplementary section C).

Case of unbiased mutation

With unbiased mutation the rate of adaptation is controlled by

$$da_t = u(a_t) \partial_1 p_T(a_t, a_t) dt + \sqrt{u(a_t) p_T(a_t, a_t)} dW_t \quad (6.14)$$

where $u(a_t) = \sigma_0^2(a_t) b(a_t) \bar{x}(a_t)$ and W_t is a Brownian motion. The Brownian component arises because transduction causes $p_T(a, a) > 0$. The mean adaptation rate with transduction is given by the deterministic part of the stochastic canonical equation (6.14). To assess the effect of transduction on adaptation speed away from the evolutionary optimum, we compare this deterministic part to the similar term in the canonical equation without transduction, equation (6.10). Under our simulation assumptions (*i.e.* birth rate, infection rate, and mutation size independent of the trait), $u(a_t)$ is constant, and the rate of adaptation is solely determined by the invasion probability $p_T(a_t, a_t)$ and its first derivative $\partial_1 p_T(a_t, a_t)$.

The adaptation rate is always higher with transduction, all the more so as the maximum transduction rate, η_0 , is larger (Figures 6.3a-c). As evolutionary trajectories come closer to the optimum, the (absolute) difference in adaptation rate with vs. without transduction becomes smaller (Figure 6.3b), but this effect is largely driven by the general tendency for adaptation to slow down near the optimum. When controlling for the slow down by computing the relative difference in adaptation rates, the accelerating effect of transduction remains (Figure 6.3c). Numerical simulations of the TSS agree with these analytical results (Figures 6.4a-c).

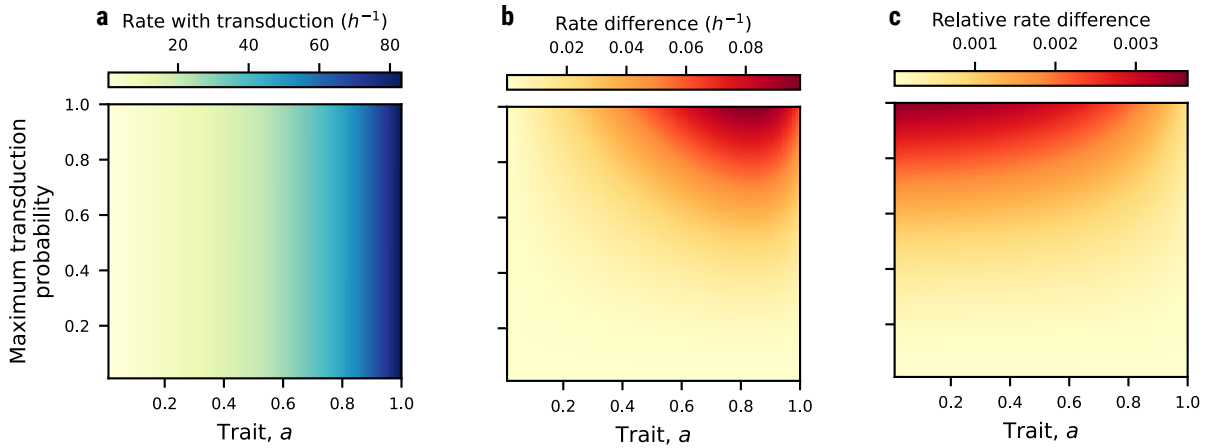


FIGURE 6.3: Influence of transduction on adaptation rates. (a) Rate of adaptation with transduction as a function of trait value a , for a given maximum transduction probability, η_0 . (b) Absolute and (c) relative difference between rates of adaptation with and without transduction. The evolutionary optimum is at $a^* = 0$, and parameters are set at their default values (see Table 6.1).

Because the invasion probability $p_T(a, a)$ increases as trait a approaches a^* (Figures 6.2c), we expect the dynamics of adaptation to become more stochastic as the population evolves closer to the singularity a^* . This is confirmed by numerical simulations of the TSS (Figures 6.4a-c). Thus, transduction increases both adaptation speed away from the optimum, and stochasticity near the optimum. To quantify the net effect of these antagonistic influences on adaptation, we use an index of adaptation, I , defined as the ratio of the speed of adaptation without transduction relative to the mean sojourn time of the population in a small phenotypic neighborhood around the evolutionary optimum (defined as all trait values a for which $1/c(a, a) > 0.99K_0$). $I \ll 1$ means that the stochastic component of adaptation pushes the process away from the evolutionary optimum faster than the deterministic driver can pull it back. In this case, the population remains in a maladapted state, i.e. away from the predicted optimum. Conversely, $I \gg 1$ means that the deterministic driver of adaptation brings the population near its evolutionary optimum faster than the stochastic component upsets adaptation. In this case, adaptation trajectories can be approximated with exponential functions of time t of the form $C \exp(-\alpha t)$. The parameter α then provides a measure of convergence speed that can be compared across models with and without transduction.

We used numerical simulations to evaluate how the adaptation index, I , and adaptation convergence speed, α , respond to two key parameters of the bacteria-phage interaction, the rate of infection, ψ_0 , and the maximum probability of transduction, η_0 (Figures 6.4d-f). If either one of the infection rate, ψ_0 , or transduction probability, η_0 , is very low (less than ca. 0.01), then $I \gg 1$ and the adaptation trait dynamics closely follows its predicted deterministic path towards a^* (Figures 6.4a,d). If both ψ_0 and η_0 are large enough (product larger than ca. $5 \cdot 10^{-4}$), then $I \ll 1$, meaning that even though convergence towards an evolution-

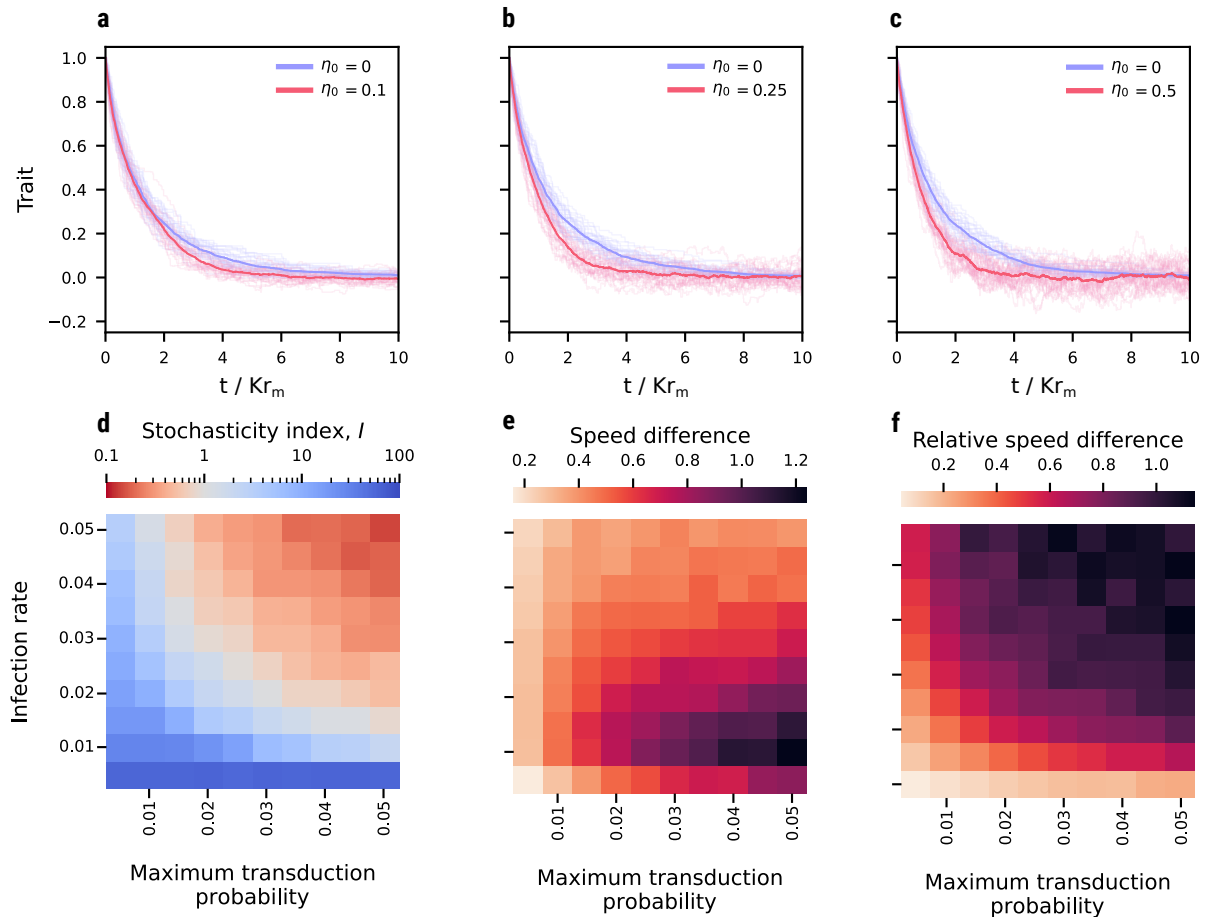


FIGURE 6.4: Influence of transduction on adaptation rates. (d-f) Simulated Trait Substitution Sequences (TSS) for $\psi_0 = 10^{-5}$ and (d) $\eta_0 = 0.01$, (e) $\eta_0 = 0.25$, and (f) $\eta_0 = 0.5$. 30 simulation runs for each ψ_0 value were performed (light blue and light red lines) with a time normalization by a factor of Km . The thick dark lines represent the mean trajectory for each set of simulations. (g) Adaptation index, I . Blue and red shades respectively indicate $I > 1$ (the dominant effect of transduction is to accelerate adaptation away from the optimum) and $I < 1$ (the dominant effect of transduction is stochasticity around the optimum). (h) Absolute and (i) relative difference in convergence adaptation speed, α , with vs. without transduction, calculated from 100 simulation runs for each pair of transduction probability and infection rate. Other parameters are set to their default values (see Table 6.1). See text for definitions of I and α .

ary optimum is expected, the adaptation trajectories strongly fluctuate around the optimum without ever settling down (Figures 6.4b-d). Increasing the transduction probability generally increases the adaptation convergence speed (Figures 6.4a-c,e). The absolute effect, in comparison with the convergence speed without transduction, is sensitive to the infection rate, being strongest at low infection rates (Figure 6.4e). This is because the mortality cost of infection tends to attenuate the accelerating effect of transduction on adaptation. When measuring the effect of transduction on the convergence speed relatively to the speed without transduction (*relative* convergence speed, Figure 6.4e), we find that the larger the infection rate, the stronger the positive effect of transduction on the speed of adaptation.

Case of biased mutation

With biased mutation, the average mutational effect is nonzero and given by

$$m_0(a) = \int_{-1}^1 h m(a, h) dh$$

Then the characteristic timescale over which adaptation proceeds is set by t/ϵ , where t is the baseline timescale over which the cells' population dynamics unfold. The t/ϵ timescale is much shorter than the t/ϵ^2 timescale over which adaptation proceeds with unbiased mutation, i.e. adaptation occurs much more rapidly with biased mutation. On this faster timescale, the stochasticity of the adaptation process with transduction is smoothed out, and the adaptation dynamics are governed by a deterministic ordinary equation

$$da_t = m_0(a_t) \frac{\gamma}{1-\gamma} \eta_0 \psi(a_t) \bar{x}(a_t) \bar{v}(a_t) dt. \quad (6.15)$$

In this case, the long-term adaptation dynamics takes steps of the order of the average mutational bias, measured by $m_0(a)$, at a rate given by the population rate of transduction events, equal to $\frac{\gamma}{1-\gamma} \eta_0 \psi(a_t) \bar{x}(a_t) \bar{v}(a_t)$.

6.3.4 Effect of transduction on bacterial adaptive diversification

Without transduction, the model predicts conditions under which selection turns from directional to disruptive around the evolutionary singularity a^* , resulting in a case of evolutionary branching (Figure 6.5a). A full mathematical investigation of evolutionary branching with transduction goes beyond the scope of this paper. Instead we gained some insights into the effect of transduction on bacterial adaptive diversification from a large set of numerical simulations. The simulations consistently show that even the lowest level of transduction widens the trait range over which a mutant can invade in a neighborhood of the evolutionary singularity (Figures 6.5b-f). Nonetheless, evolutionary branching occurs under the con-

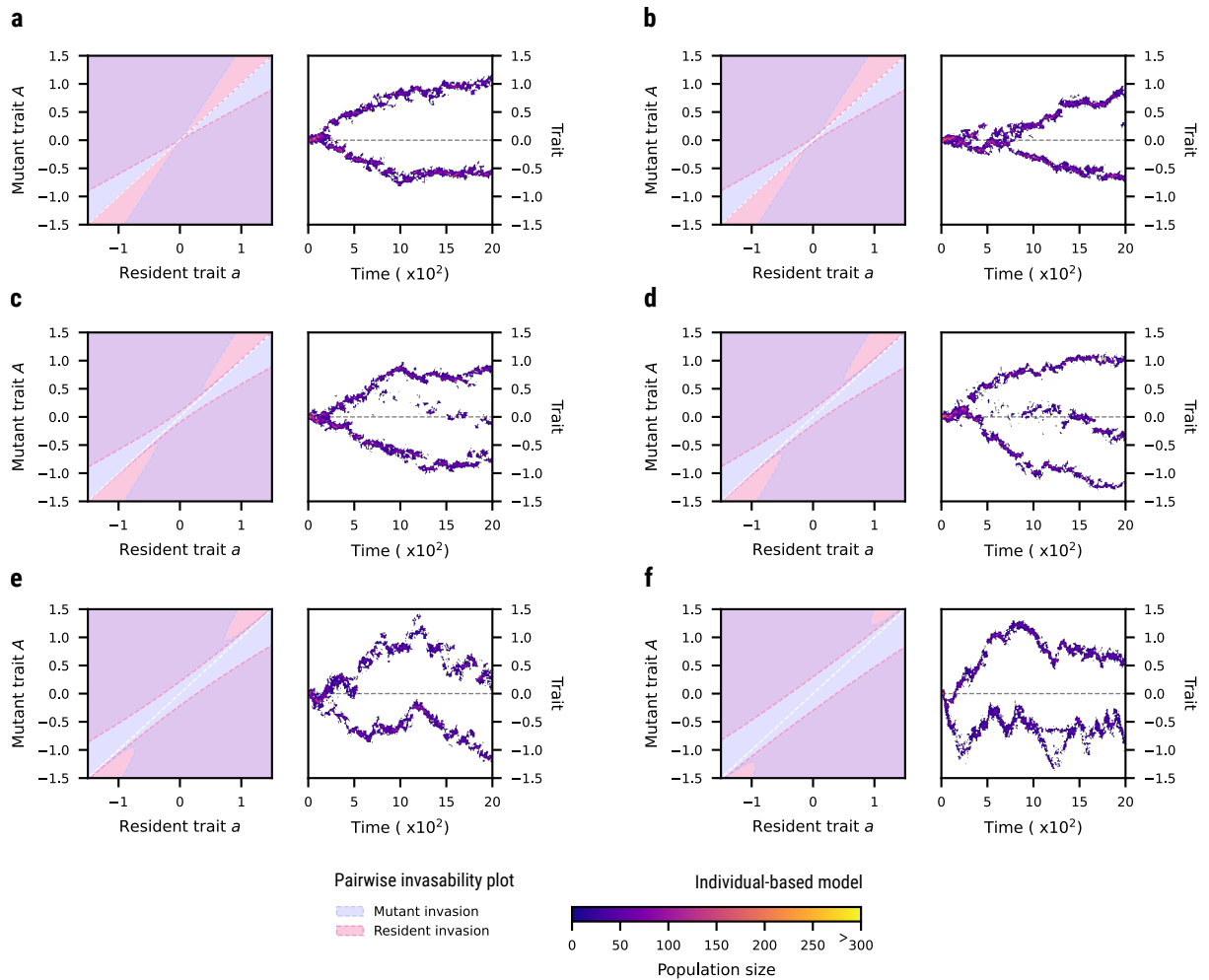


FIGURE 6.5: Pairwise invasibility plots and example simulations of trait distribution dynamics. The transduction probability, η_0 , takes the following values: (a) 0; (b) 0.01; (c) 0.05; (d) 0.1; (e) 0.25; (f) 0.5. For each value of η_0 , the left pane shows regions of resident and mutant trait values for which mutant invasion fitness is positive (blue) or resident invasion fitness is positive (red). In the region of overlap (purple), the mutant and resident populations may coexist. Right panes show trait distribution dynamics simulated by making use of a Gillespie algorithm. Parameter values: $\psi_0 = 10^{-5}$, $\sigma_K = 2$, $\sigma_C = 1$, and other parameters set to their default values (see Table 6.1).

ditions predicted in the absence of transduction, and the fact that back invasion fitness is always negative does not seem to slow the process.

At low transduction rate (low η_0), a third, intermediate branch can evolve and station around the evolutionary singularity, which is a fitness minimum (Figures 6.5b-d). This branch emerges from the mixing of genomes in the two outer branches (as explained in Figure 6.1) and follows either one of these branches. This is because they only persist thanks to horizontal gene transfer, and would go extinct without the flux of individuals coming from the original branch. Thus, competition exerted by individuals in the intermediate branch select for further divergence of the outer branches (Figure 6.5d). In sum, transduction at low rates tends to increase the genetic and phenotypic diversity and phenotypic range that evolves in the population.

At higher transduction rates, large stochastic variations manifest in the outer two branches, which then tend to outcompete any middle branch (Figures 6.5e,f). Large stochastic excursions of one branch away from the evolutionary singularity may allow the other branch to stay closer to the singularity (Figures 6.5e,f). Thus, transduction makes it possible for a sub-population to station around an evolutionary optimum which is a fitness minimum. When this happens, competition exerted by this sub-population prevents any third branch from even sprouting (Figures 6.5e,f). See Supplementary figure 1 for additional example simulations.

6.4 Conclusions

Horizontal gene transfer is expected to have conflicting effects on bacterial adaptation: the transfer of beneficial mutations may facilitate and accelerate adaptation, while the transfer of deleterious mutations might hold adaptation back. Transduction by virulent phages adds a direct demographic factor to these conflicting effects, since the frequency of gene transfer is tied to viral infection hence to cell mortality. To resolve the effect of transduction on bacterial adaptation, we extended the trait-based approach of adaptive dynamics modeling to include a simple genotype-phenotype map and capture the mobility of genetic elements between host cells and their potential phenotypic effects. Our hybrid – genetic and trait-based – approach uses an infinite-site, infinite-allele model with small additive effects of mutations. Our model applies to generalized transduction by virulent phages and assumes that ‘back transduction’ of a descendant allele recombining at the progenitor locus is a very unlikely event, which is consistent with the non-homologous end joining transduction mechanism [221].

In the absence of transduction, the mortality cost of viral infection tends to slow bacterial adaptation down. A key of transduction is to increase the invasion fitness of any mutant, irrespective of their fitness effect (deleterious or beneficial) in the absence of transduction. This

makes it possible for deleterious alleles to invade, and for beneficial alleles to invade faster. Far from an evolutionary optimum, the positive fitness effect on deleterious mutations (of a given mutational effect size) is small relative to the effect on beneficial mutations. As a consequence, adaptation can be much faster with transduction than without. Close to an evolutionary optimum, transduction tends to reduce the fitness difference between deleterious and beneficial mutants and both can have relatively high positive invasion fitness. This can generate strong stochastic fluctuations in the adaptive trajectories. If the evolutionary optimum is a fitness minimum in the absence of transduction, thus turning selection from directional to disruptive, the expected phenotypic polymorphism and divergence also occurs with transduction. At low transduction rates, a subpopulation may even persist near the optimum, driving further phenotypic divergence of the other coexisting subpopulations. At high transduction rates, stochasticity drives large fluctuations in phenotypic branches, including recurrent incursions near the optimum.

Previous studies (e.g. Moradigaravand and Engelstädter [188]) have modeled and discussed this ‘bad gene effect’ of HGT. Non-homologous end joining transduction is distinct in the sense that the bad gene effect never consistently reverts the direction of selection, as it may in the case of conjugation [27]. Rather, it tends to broaden the range of selection outcomes. As the transfer term of invasion fitness $S(A, a)$ is positive for any mutant trait that arises in the resident population, not only may deleterious trait values invade, but beneficial trait values have even greater invasion fitness than they would have in the absence of transduction, implying a larger probability of invasion and a shorter invasion time. Quantitatively, these effects can be substantial (Figure 6.2b). This prediction is consistent with previous theoretical results on HGT [56] and experimental data showing that horizontal gene transfer can facilitate adaptation by accelerating the fixation of beneficial alleles [19].

With transduction, any small phenotypical variant has positive invasion fitness. As a consequence, even though directionality towards the evolutionary optimum remains favored (as shown by the deterministic term in the canonical equation (6.14)), random jumps of the TSS in the opposite direction are possible at any mutation event. This broad range of invading mutants around the evolutionary optimum fuels wide stochastic fluctuations in the adaptation process. Stochastic fluctuations of the adaptation trajectory due to transduction are most pronounced near the evolutionary optimum, a^* , thereby hampering convergence to the evolutionary optimum and preventing the stabilization of adaptive trajectories around it. This is a consequence of the ‘top-down’ control of the bacterial population by viruses, which means that for traits closer to the evolutionary optimum, the population of viruses (not bacteria) becomes larger, resulting in a higher rate of transduction and eventually a wider range of mutant phenotypes with positive invasion fitness around a^* .

Stochasticity in adaptive evolution is generally associated with genetic drift in finite (small) population size. In contrast, the adaptation stochasticity evidenced here occurs in spite of the large population size, and its long-term effect on the adaptive trait dynamics is captured

by the stochastic canonical equation (6.14). This equation can be compared with the canonical equation for finite populations [43]. Both equations contain a stochastic term proportional to the square root of the invasion probability of a neutral trait. Classically, the non-zero value of this term reflects the effect of genetic drift in finite populations. Here, the population is virtually infinite and the non-zero value comes from the stochasticity of transduction events. Although the root cause of stochasticity is profoundly different, this outcome is qualitatively similar: deleterious alleles can invade and go to fixation.

The fact that trait fluctuations still occur near the evolutionary optimum implies that the host population will never be fully adapted to a static environment: by facilitating the fixation of *any* mutant, transduction lowers the mean fitness of the population. This is in line with previous studies showing that HGT is not a facilitator of adaptation in static environments [223]. In contrast, transduction is expected to accelerate adaptation in response to environmental change that changes the evolutionary optimum, all the more so as the shift in optimum is greater.

Our results also shed new light on the effect of horizontal gene transfer on genetic and phenotypic diversity [196]. Transduction events add new lineages to the population (Figure 6.1), with two contrasting outcomes that are revealed by individual-level simulations (Supplementary figure 1), either enhanced diversification or apparent optimization. At low transduction rates, the genome-mixing effect of transduction dominates and trait diversity increases. At higher transduction rates, the stochasticity of transduction events scale up and cause the stochastic motion of evolutionary branches; this may result in ‘apparent optimization’ whereby one branch (sub-population) remains close to the evolutionary optimum, thus causing extinction of some or all the other branches, hence a reduction in trait diversity.

Our analysis highlights the influence of transduction rate parameters on the rate and dynamics of bacterial adaptation. These parameters are: the infection rate, ψ , the gene transducing particles (GTP) production fraction, γ , and the maximum transduction probability, η_0 . The latter two, that are specific to the transduction process, remain poorly constrained. Laurenceau et al. [152] provided evidence suggesting that generalized transduction is the dominant mode of transduction in *Prochlorococcus*, the most abundant phototrophs in the open ocean. By examining the mispackaging of host DNA by different cyanophages, they described a mechanism to explain the production of GTPs, which paves the way toward quantifying GTP production. Interestingly, their proposed mechanism suggests that GTP production might respond to environmental conditions and vary with ocean depth, latitude, and season. Quantitative data are also lacking for the maximum transduction probability, η_0 . It is known that multiple barriers exist to prevent the recombination of exogenous DNA in the recipient cell [220, 203], and here too, a better understanding of the mechanism should help estimating this critical parameter. The development of new sequencing-based methodology, e.g. Kleiner et al. [144] transductomics approach, will inform these efforts by providing insights into real-time ongoing HGT in complex microbial communities.

Our model is focused on generalized transduction by virulent phages. Future developments will aim at extending the model to temperate (lysogenic) phages, which can also drive specialized and lateral transduction. This will broaden the scope of our framework to questions involving the evolution of transduction-related traits in both bacterial host and phage populations. All three transduction parameters may be under the genetic control of both phage and host – the infection rate by virulent genes and resistant genes, respectively; the GTPs production rate and transduction probability by viral genes that control DNA excision and packaging and host genes that control DNA integration. With temperate phages that can transfer bacterial DNA without killing recipient cells, positive selection pressures may exist on genes that benefit both hosts and phages [100, 275] and result in high-frequency transduction [46].

Adaptation acceleration could have numerous implications for marine ecosystems, and transduction is expected to have an important role in shaping genetic diversity in the oceans: the number of transduction events in Tampa Bay, Gulf of Mexico alone has been estimated at 10^{14} per year [139]. In the context of rapidly changing marine environments due to climate warming, a better understanding of bacterial response due to transduction is a step towards integrating this important mechanism in global biogeochemical models of the oceans.

For transduction involves the transfer and integration of alleles between hosts, models that keep track of the individuals' phenotype (but not genotype) are insufficient to describe the adaptive trait dynamics of a host population in which transduction occurs. Our modeling approach goes beyond previous population-genetic models of HGT [196, 174, 195] to track the genealogy of mutations together with phenotypic trait values, which influence demographic performance and ecological interactions among individuals and their environment. Beyond the question of how transduction affect host adaptation, the mathematical method used here could pave the way to further advance the integration of transmission genetics in trait-based models of adaptation.

A Deriving the invasion fitness with transduction

We assume the system to be at this equilibrium when the mutant with trait A appears. We then have to see how the system evolves when the initial conditions are given by

$$(x(t=0), y(t=0), v(t=0), u(t=0)) = (\bar{x}(a), \epsilon_y, \bar{v}(a), \epsilon_u)$$

where $\epsilon_y, \epsilon_u > 0$ are infinitely small. We then place ourselves at $t = 0^+$. At the first order, $x(t)$ and $v(t)$ are constant, therefore the dynamics of the invading population are driven by the linear system

$$\begin{cases} \left. \frac{dy}{dt} \right|_{t=0^+} = (b(A) - d(A) - c(a, A)\bar{x}(a) - \psi(A)\bar{v}(a))\epsilon_y + \psi(a)\eta(a, A)\bar{x}(a)\epsilon_u \\ \left. \frac{du}{dt} \right|_{t=0^+} = \gamma\beta\psi(A)\bar{v}(a)\epsilon_y - (d_v + \psi(a)\bar{x}(a))\epsilon_u. \end{cases} \quad (6.16)$$

Invasion success is determined by the eigenvalues of this linear system. If both values are real and negative, the resident equilibrium is stable, and invasion fails. On the contrary, if both values are real (being conjugated) and one is positive, invasion succeeds. The eigenvalues, denoted by λ_+ and λ_- , are given by

$$\lambda_{\pm} = \frac{1}{2} \left(S(A, a) - (d_v + \psi(a)\bar{x}(a)) \pm \sqrt{\Delta} \right) \quad (6.17)$$

where

$$S(A, a) = r(A) - c(a, A)\bar{x}(a) - \psi(A)\bar{v}(a) \quad (6.18)$$

and

$$\Delta = (S(A, a) + (d_v + \psi(a)\bar{x}(a)))^2 + 4(\gamma\psi(a)\psi(A)\eta(a, A)\beta\bar{x}(a)\bar{v}(a)).$$

Here, $S(A, a)$ represents the invasion fitness in the absence of transduction, meaning when $\eta(a, A) = 0$. As expected intuitively, invasion fitness is higher if the mutant intrinsic growth rate is larger, or the competition or infection pressure experienced by the mutant from the resident population is weaker.

Since both of its terms are positive, $\Delta \geq 0$ (i.e. all eigenvalues are real). Both eigenvalues being real, we can focus on the greater of the two, which is λ_+ . There are two cases that emerge then: either λ_+ is negative, implying that the resident equilibrium will be stable, or it is positive, and then we can conclude that the resident equilibrium will be unstable, and that invasion will succeed.

If $\Delta > (S(A, a) - (d_v + \psi(a)\bar{x}(a)))^2$, then $\lambda_+ > 0$. By rewriting Δ as

$$\Delta = (S(A, a) - (d_v + \psi(a)\bar{x}(a)))^2 + 4((d_v + \psi(a)\bar{x}(a))S(A, a) + \gamma\psi(a)\psi(A)\eta(a, A)\beta\bar{x}(a)\bar{v}(a)).$$

we can then conclude that $\lambda_+ > 0$ if

$$S(A, a) + \frac{\gamma}{1-\gamma} \times \psi(A)\bar{v}(a) \times \eta(a, A) > 0. \quad (6.19)$$

Reciprocally, if $\lambda_+ > 0$, either $S(A, a) - (d_v + \psi(a)\bar{x}(a)) > 0$ and then in particular $S(A, a) > 0$ and (6.19) is satisfied, or $-\sqrt{\Delta} < S(A, a) - (d_v + \psi(a)\bar{x}(a)) < 0$, and after some algebra we can conclude that (6.19) is also satisfied.

We then obtain invasion Fitness with transduction, denoted by $S_T(A, a)$:

$$S_T(A, a) := S(A, a) + \frac{\gamma}{1-\gamma} \psi(A)\bar{v}(a)\eta(a, A). \quad (6.20)$$

If $S_T(A, a) > 0$, a mutant individual with trait A can invade a resident population with trait a , otherwise invasion does not occur.

Back invasion

Now that we know the conditions under which a mutant population can invade a resident population, let us see how the resident population bodes when it ‘invades back’ a mutant population. This case is useful to determine whether an invasion by the mutant will result in a coexistence equilibrium between mutant and resident, or if we can work under the *invasion implies fixation* hypothesis.

The same calculations as before show us that we can define the backward invasion fitness \tilde{S}_T as such:

$$\tilde{S}_T(a, A) = S(a, A) - \frac{\gamma}{1-\gamma} \psi(a) \bar{v}(A) \eta(a, A). \quad (6.21)$$

B Deriving the invasion probability with transduction

In the previous section, we have looked at the condition a mutant bacterium of trait A must satisfy in order to be able to invade the resident bacterium of trait a . But due to the stochastic nature of the process, even when a mutant bacterium satisfies (6.19), the invasion is not guaranteed. In this section, we compute the probability invasion of a mutant bacteria and the characteristic time it takes for an invasion to unfold. We largely base our work on Champagnat, Ferrière, and Méléard [42] to derive the probability invasion.

Coupling of the process with a simple branching process

We put ourselves at the resident equilibrium (6.4), with the notation $(\bar{x}(a) \cdot K, 0, \bar{v}(a) \cdot K, 0)$ and study the individual-based process (X^K, Y^K, V^K, U^K) . We introduce a small perturbation (Y_0, U_0) , negligible in front of the other values. Let us introduce $\epsilon > 0$.

Let us divide an invasion event in 3 distinct phases for K large enough, as it is done in [40] (we work under the assumption that the mutation is small enough so that no cohabitation between mutant and resident populations is possible):

1. The mutant population Y^K either reaches the threshold size of ϵ or becomes extinct.
2. If the mutant population is not extinct, a new equilibrium will be reached following the deterministic approximation until the resident population reaches the threshold size of ϵ .
3. The resident population becomes extinct.

The idea here is the following: we want to prove that when $K \rightarrow +\infty$, the behavior of the invading population (Y^K, U^K) tends to a branching process until the total population reaches a threshold size ϵ for $\epsilon > 0$, while X^K, V^K stay relatively constant at their dynamical equilibrium.

The ecological equilibrium of the resident population

Let us first show that we can assume that the resident bacteria population and virion population stay at ecological equilibrium during the first phase. During this phase, mutant population Y^K hasn't reached the threshold ϵ yet. If we refer to the dynamical equation, this means that, at the first order with respect to ϵ , resident bacteria and virion populations stay at ecological equilibrium $(\bar{x}(a) \cdot K, \bar{v}(a) \cdot K)$. The jumps of the stochastic process are of order $O(1/K)$. Since we work under large values of K and that the ecological equilibrium $(\bar{x}(a) \cdot K, \bar{v}(a) \cdot K)$ is term-by-term nonzero, we can conclude that at order $O(1/K)$, resident bacteria and virion populations stay at ecological equilibrium $(\bar{x}(a) \cdot K, \bar{v}(a) \cdot K)$.

In conclusion, we can assume that during the first phase, resident bacteria and virion population remain constant in size at ecological equilibrium.

Trajectorial representation of the invading population for the first phase

Let us define the following Poisson point measures:

- **Birth of a mutant:** $\mathcal{N}_1(ds, du)$ on $\mathbb{R}_+ \times \mathbb{R}_+$ with intensity measure $dsdu$
- **Death of a mutant:** $\mathcal{N}_2(ds, du)$ on $\mathbb{R}_+ \times \mathbb{R}_+$ with intensity measure $dsdu$
- **Infection of a mutant:** $\mathcal{N}_3(ds, du)$ on $\mathbb{R}_+ \times \mathbb{R}_+$ with intensity measure $dsdu$
- **Transduction of a resident:** $\mathcal{N}_4(ds, du)$ on $\mathbb{R}_+ \times \mathbb{R}_+$ with intensity measure $dsdu$
- **Death of a GTP:** $\mathcal{N}_5(ds, du)$ on $\mathbb{R}_+ \times \mathbb{R}_+$ with intensity measure $dsdu$

We then can describe our mutant process through the following trajectorial representation:

$$\begin{aligned}
 \begin{pmatrix} Y_t^K \\ U_t^K \end{pmatrix} &= \begin{pmatrix} Y_0^K \\ U_0^K \end{pmatrix} + \int_0^t \int_{\mathbb{R}} \begin{pmatrix} +1/K \\ 0 \end{pmatrix} \mathbb{1}_{u \leq Y_s^K - b(A)} \mathcal{N}_1(ds, du) \\
 &+ \int_0^t \int_{\mathbb{R}} \begin{pmatrix} -1/K \\ 0 \end{pmatrix} \mathbb{1}_{u \leq Y_s^K - (d(A)+c(a,A)\bar{x}(a)+c(A,A)Y_s^K)} \mathcal{N}_2(ds, du) \\
 &+ \int_0^t \int_{\mathbb{R}} \sum_{i=0}^{\beta} \begin{pmatrix} -1/K \\ i/K \end{pmatrix} \mathbb{1}_{Y_s^K - \sum_{j=0}^{i-1} p_i^{(\beta,\gamma)} \psi(A)\bar{v}(a) < u \leq Y_s^K - \sum_{j=0}^i p_i^{(\beta,\gamma)} \psi(A)\bar{v}(a)} \mathcal{N}_3(ds, du) \\
 &+ \int_0^t \int_{\mathbb{R}} \begin{pmatrix} +1/K \\ -1/K \end{pmatrix} \mathbb{1}_{u \leq U_s^K - \psi(A)\bar{v}(a)} \mathcal{N}_4(ds, du) \\
 &+ \int_0^t \int_{\mathbb{R}} \begin{pmatrix} 0 \\ -1/K \end{pmatrix} \mathbb{1}_{u \leq U_s^K - (d_\nu + \psi(A)Y_s^K)} \mathcal{N}_5(ds, du).
 \end{aligned}$$

Bounding our process with branching processes

Let us now show that we can find two branching processes $(\tilde{Y}^{K,1}, \tilde{U}^{K,1}), (\tilde{Y}^{K,2}, \tilde{U}^{K,2})$ such as

$$\forall t \in \mathbb{R}, \quad \begin{aligned} \tilde{Y}_t^{K,1} &\leq Y_t^K \leq \tilde{Y}_t^{K,2} \\ \tilde{U}_t^{K,1} &\leq U_t^K \leq \tilde{U}_t^{K,2}. \end{aligned} \tag{6.22}$$

Using the same Poisson point measures and the same initial condition, let us define the following processes, we define

$$\begin{aligned}
 \begin{pmatrix} \tilde{Y}_t^{K,1} \\ \tilde{U}_t^{K,1} \end{pmatrix} &= \begin{pmatrix} Y_0^K \\ U_0^K \end{pmatrix} + \int_0^t \int_{\mathbb{R}} \begin{pmatrix} +1/K \\ 0 \end{pmatrix} \mathbb{1}_{u \leq \tilde{Y}_s^{K,1} - b(A)} \mathcal{N}_1(ds, du) \\
 &+ \int_0^t \int_{\mathbb{R}} \begin{pmatrix} -1/K \\ 0 \end{pmatrix} \mathbb{1}_{u \leq \tilde{Y}_s^{K,1} - (d(A)+c(a,A)\bar{x}(a)+c(A,A)\epsilon)} \mathcal{N}_2(ds, du) \\
 &+ \int_0^t \int_{\mathbb{R}} \sum_{i=0}^{\beta} \begin{pmatrix} -1/K \\ i/K \end{pmatrix} \mathbb{1}_{\tilde{Y}_s^{K,1} - \sum_{j=0}^{i-1} p_i^{(\beta,\gamma)} \psi(A)\bar{v}(a) < u \leq \tilde{Y}_s^{K,1} - \sum_{j=0}^i p_i^{(\beta,\gamma)} \psi(A)\bar{v}(a)} \mathcal{N}_3(ds, du) \\
 &+ \int_0^t \int_{\mathbb{R}} \begin{pmatrix} +1/K \\ -1/K \end{pmatrix} \mathbb{1}_{u \leq \tilde{U}_s^{K,1} - \psi(A)\bar{v}(a)} \mathcal{N}_4(ds, du) \\
 &+ \int_0^t \int_{\mathbb{R}} \begin{pmatrix} 0 \\ -1/K \end{pmatrix} \mathbb{1}_{u \leq \tilde{U}_s^{K,1} - (d_\nu + \psi(A)\epsilon)} \mathcal{N}_5(ds, du)
 \end{aligned}$$

and

$$\begin{pmatrix} \tilde{Y}_t^{K,2} \\ \tilde{U}_t^{K,2} \end{pmatrix} = \begin{pmatrix} Y_0^K \\ U_0^K \end{pmatrix} + \int_0^t \int_{\mathbb{R}} \begin{pmatrix} +1/K \\ 0 \end{pmatrix} \mathbb{1}_{u \leq \tilde{Y}_s^{K,2} - b(A)} \mathcal{N}_1(ds, du)$$

$$\begin{aligned}
 & + \int_0^t \int_{\mathbb{R}} \begin{pmatrix} -1/K \\ 0 \end{pmatrix} \mathbb{1}_{u \leq \tilde{Y}_s^{K,2}} (d(A)+c(a,A)\bar{x}(a)) \mathcal{N}_2(ds, du) \\
 & + \int_0^t \int_{\mathbb{R}} \sum_{i=0}^{\beta} \begin{pmatrix} -1/K \\ i/K \end{pmatrix} \mathbb{1}_{\tilde{Y}_s^{K,2} \sum_{j=0}^{i-1} p_i^{(\beta,\gamma)} \psi(A) \bar{v}(a) < u \leq \tilde{Y}_s^{K,2} \sum_{j=0}^i p_i^{(\beta,\gamma)} \psi(A) \bar{v}(a)} \mathcal{N}_3(ds, du) \\
 & + \int_0^t \int_{\mathbb{R}} \begin{pmatrix} +1/K \\ -1/K \end{pmatrix} \mathbb{1}_{u \leq \tilde{U}_s^{K,2}} \psi(A) \bar{v}(a) \mathcal{N}_4(ds, du) \\
 & + \int_0^t \int_{\mathbb{R}} \begin{pmatrix} 0 \\ -1/K \end{pmatrix} \mathbb{1}_{u \leq \tilde{U}_s^{K,2}} d_v \mathcal{N}_5(ds, du).
 \end{aligned}$$

The only differences come from the deaths of a mutant and the death of a GTP. The second order terms have been either replaced by ϵ (for the lower bound: indeed, by definition of the first phase, $Y_t^K \leq \epsilon$) or completely removed (for the upper bound).

Let us now verify that we indeed have

$$\begin{aligned}
 \forall t \in \mathbb{R}, \quad \tilde{Y}_t^{K,1} &\leq Y_t^K \leq \tilde{Y}_t^{K,2}, \\
 \tilde{U}_t^{K,1} &\leq U_t^K \leq \tilde{U}_t^{K,2}.
 \end{aligned}$$

Let us show that if at time $t_1 \in \mathbb{R}_+$, (6.22) is verified, then it shall be verified for all the times $t > t_1$.

Let us call T the first event that occurs after t_1 . Since the Poisson point measures are the same, we can conclude that we will be studying the same point in one of the PPM \mathcal{N}_i for $i \in 1, \dots, 5$. Let us see the different possibilities:

- **Birth of a mutant:** thanks to the hypothesis, we know that

$$\tilde{Y}_{T^-}^{K,1} \leq Y_{T^-}^K \leq \tilde{Y}_{T^-}^{K,2}$$

so

$$\tilde{Y}_{T^-}^{K,1} b(A) \leq Y_{T^-}^K b(A) \leq \tilde{Y}_{T^-}^{K,2} b(A)$$

which means that a jump of $+1/K$ for $\tilde{Y}^{K,1}$ (i.e. $u \leq \tilde{Y}^{K,1} b(A)$) would imply a jump for Y^K which would imply a jump for $\tilde{Y}^{K,2}$. No matter what, the order is respected.

- **Death of a mutant:** here, we can't use the same argument as before. Indeed, let us look closer at the relationship between $\tilde{Y}_{T^-}^{K,1}$ and $Y_{T^-}^K$. We know that

$$\tilde{Y}_{T^-}^{K,1} \leq Y_{T^-}^K$$

but

$$d(A) + c(a, A)\bar{x}(a) + c(A, A)\epsilon \geq d(A) + c(a, A)\bar{x}(a) + c(A, A)Y_{T^-}^K \tag{6.23}$$

so there could be instances where Y^K would jump of $-1/K$ but not $\tilde{Y}^{K,1}$. We then need to make difference between two cases:

- If $Y_{T^-}^K > \tilde{Y}_{T^-}^{K,1}$ then we know that $Y_{T^-}^K - 1/K \geq \tilde{Y}_{T^-}^{K,1}$, since $Y^K, \tilde{Y}^{K,1} \in \mathbb{N}/K$, so the order is kept.
- If $Y_{T^-}^K = \tilde{Y}_{T^-}^{K,1}$, then since (6.23) we can infer

$$\tilde{Y}_{T^-}^{K,1}(d(A) + c(a, A)\bar{x}(a) + c(A, A)\epsilon) \geq Y_{T^-}^K(d(A) + c(a, A)\bar{x}(a) + c(A, A)Y_{T^-}^K)$$

so a jump for Y^K would here imply a jump for $\tilde{Y}^{K,1}$. The order is yet again respected.

The same arguments can be made between Y^K and $\tilde{Y}^{K,2}$, so we can conclude that the order is respected.

- **Other events:** the three other events that can occur are dealt with in the same way that we just did on the first two cases.

Since we have the same initial condition, we can conclude that (6.22) is verified for $t = 0$, meaning we have it verified for all $t > 0$.

By construction, we indeed have found two branching processes such as

$$\begin{aligned} \forall t \in \mathbb{R}, \tilde{Y}_t^{K,1} \leq Y_t^K \leq \tilde{Y}_t^{K,2} \\ \tilde{U}_t^{K,1} \leq U_t^K \leq \tilde{U}_t^{K,2}. \end{aligned}$$

Conclusion

What we have just proven is that for every $K \in \mathbb{N}^*$, every $\epsilon > 0$ and especially every ω (ω being the realization of the Poisson point measures) we have

$$\begin{aligned} \forall t \in \mathbb{R}, \tilde{Y}_t^{K,1} \leq Y_t^K \leq \tilde{Y}_t^{K,2} \\ \tilde{U}_t^{K,1} \leq U_t^K \leq \tilde{U}_t^{K,2} \end{aligned}$$

where $\forall t \in \mathbb{R}, \lim_{\epsilon \rightarrow 0} \tilde{Y}_t^{K,1} = \tilde{Y}_t^{K,2}$ (resp. for $\tilde{U}^{K,i}$).

We can then conclude, when K is large, and when $\epsilon \rightarrow 0$, the process $(Y^K, U^K)_t$ converges with high probability towards the two-type branching process with the following transitions:

Next state	Rate	Event
$(Y + 1, U)$	$b(A)Y$	<i>Birth</i>
$(Y - 1, U)$	$(d(A) + c(a, A)\bar{x}(a))Y$	<i>Death</i>
$(Y + 1, U - 1)$	$\psi(a)\eta(a, A)\bar{x}(a)U$	<i>Transduction</i>
$(Y - 1, U + k)$	$\psi(A)\bar{v}(a)p_k^{(\beta, \gamma)}Y$	<i>Infection</i>
$(Y, U - 1)$	$d_v U + \psi(a)(1 - \eta(a, A))\bar{x}(a)U$	<i>Death</i>

The same reasoning can be applied to the third phase with individuals of type Y, V, U being at ecological equilibrium and individual of type X going to extinction. We then find a simple birth and death branching process which we will study further down this paper.

Probability of invasion

Once the process reaches the threshold size of ϵ , the large population limits allows us to conclude that the invasion is successful (since $S_T(A, a) > 0$). Hence, the probability of invasion of the mutant populations can be determined by the probability that the coupled two-type branching process described above diverges towards infinity.

Let us call $u_{i,j} = \mathbb{P}((Y, U) \text{ will become extinct } | Y = i, U = j)$ and note $u_1 = u_{1,0}$ and $u_2 = u_{0,1}$. We have

$$\forall i, j \geq 0, u_{i,j} = (u_1)^i \times (u_2)^j. \quad (6.24)$$

When analysing the process, we find that (u_1, u_2) verifies

$$\begin{cases} u_1 &= q_1 u_1^2 + \sum_{k=0}^{\beta} q_2 p_k^{(\beta, \gamma)} (u_2)^k + (1 - q_1 - q_2) \\ u_2 &= q_3 u_1 + (1 - q_3) \end{cases} \quad (6.25)$$

where

$$q_1 = \frac{b(A)}{b(A) + d(A) + c(a, A)\bar{x}(a) + \psi(A)\bar{v}(a)}$$

$$q_2 = \frac{\psi(A)\bar{v}(a)}{b(A) + d(A) + c(a, A)\bar{x}(a) + \psi(A)\bar{v}(a)}$$

$$q_3 = \frac{\psi(a)\eta(a, A)\bar{x}(a)}{\psi(a)\bar{x}(a) + d_v} = \frac{\eta(a, A)}{(1 - \gamma)\beta}.$$

Bacteria-phage coexistence implies $(1 - \gamma)\beta > 1$, which assures us that $q_3 < 1$.

A typical invasion starting off with only one mutant bacterium, we introduce the probability of invasion as $p_T(A, a) = 1 - u_1$. We take the first line of (6.25), which is equal to

$$u_1 = q_1 u_1^2 + q_2 (1 - \gamma + \gamma u_2)^\beta + (1 - q_1 - q_2).$$

We note that $u_2 = 1 - q_3(1 - u_1) = 1 - q_3 p_T(A, a)$ and replace u_1 by $1 - p_T(A, a)$. We then find that $p_T(A, a)$ satisfies the following equation:

$$b(A) \times p_T(A, a)^2 - S(A, a) \times p_T(A, a) + \psi(A)\bar{v}(a) \left(1 - \frac{\gamma\eta(a, A)}{(1 - \gamma)\beta} \times p_T(A, a) \right)^\beta - \psi(A)\bar{v}(a) = 0.$$

For readability purposes, we will continue to use q_3 for the remainder of this proof.

It is interesting to see that when transduction does not occur (i.e. $\eta(a, A) = 0$), we have $q_3 = 0$ and the result becomes:

$$p(A, a) = \frac{[S(A, a)]_+}{b(A)}. \quad (6.26)$$

We can see that the result is akin to the one found when studying a simple branching process. Indeed, since the GTP population will have no impact whatsoever when $\eta(a, A) = 0$, we can restrain ourselves to the study of said branching process.

We shall now focus on proving the existence and uniqueness of a root $p \in (0; 1)$ to the following polynomial under the condition $S_T(A, a) > 0$, $S_T(A, a)$ being defined in (6.11):

$$Q = b(A) \times X^2 - S(A, a) \times X + \psi(A)\bar{v}(a)(1 - \gamma q_3 \times X)^\beta - \psi(A)\bar{v}(a).$$

To do this, we shall use the *Descartes' Rule of Signs* [75], which states that if the terms of a single-variable polynomial with real coefficients are ordered by descending variable exponent, then the number of positive

roots of the polynomial is either equal to the number of sign differences between consecutive nonzero coefficients, or is less than it by an even number.

For this approach, we will use the following switch in variables:

$$\xi = 1 - \gamma q_3 \times X.$$

It is important to note that, since $\gamma < 1$, $q_3 < 1$, we know that $X \in [0; 1]$ if and only if $\xi \in [1 - \gamma q_3; 1] \subset [0; 1]$. This leads to the new following polynomial:

$$\tilde{Q} = \psi(A) \bar{v}(a) \xi^\beta + \frac{b(A)}{\gamma^2 q_3^2} \xi^2 + \frac{1}{\gamma q_3} \left(S(A, a) - \frac{2b(A)}{\gamma q_3} \right) \xi - \psi(A) \bar{v}(a) - \frac{S(A, a)}{\gamma q_3} + \frac{b(A)}{\gamma^2 q_3^2}.$$

We ordered \tilde{Q} in decreasing exponents, and we can clearly see that the first two coefficients are non-negative. Since the polynom has only four coefficients, there can be at most two switches of signs between consecutive coefficients (between the second and third, and between the third and fourth). Descartes' rule of signs then assures us that there will be **at most 2** positive roots of \tilde{Q} .

Let us now show that we can find **at least 2** roots of \tilde{Q} in $[1 - \gamma q_3; 1]$ under the condition $S(A, a) > 0$. This would assure us that there are exactly 2 positive roots of \tilde{Q} , and that they are both in $[1 - \gamma q_3; 1]$.

First of all, let us note that

$$\tilde{Q}(1) = 0$$

Then, we can calculate than

$$\tilde{Q}(1 - \gamma q_3) = d(A) + c(a, A) \bar{x}(a) + \psi(A) \bar{v}(a) (1 - \gamma q_3)^\beta > 0$$

And at last, we have

$$\tilde{Q}'(1) = S(A, a) + \psi(A) \bar{v}(a) \beta \gamma q_3 = S(A, a)$$

which is positive by hypothesis.

We can then conclude easily that there is a root of \tilde{Q} in $(1 - \gamma q_3; 1)$. Since 1 is also a root, we have found at least 2 roots of \tilde{Q} in $[1 - \gamma q_3; 1]$, meaning we have exactly 2 positive roots, both in $[1 - \gamma q_3; 1]$.

From there, we can switch back to Q in order to conclude that there are exactly 2 roots in $[0; 1]$ when $S_T(A, a) > 0$, one of which is 0 and the other one $p_T(A, a)$.

We can then define $p_T(A, a)$ as the non trivial root of the following equation:

$$b(A) \times p_T(A, a)^2 - S(A, a) \times p_T(A, a) + \psi(A) \bar{v}(a) \left(1 - \frac{\gamma \eta(a, A)}{(1 - \gamma)^\beta} \times p_T(A, a) \right)^\beta - \psi(A) \bar{v}(a) = 0. \quad (6.27)$$

Comparing p_T and p

Let us now compare this root to $p(A, a)$, defined in (6.26).

If $S(A, a) \leq 0$, $p(A, a) = 0$ and then $p_T(A, a) \geq p(A, a)$.

If $S(A, a) > 0$, then $p(A, a) = \frac{S(A, a)}{b(A)}$. When evaluating Q at $p(A, a)$, we find:

$$Q(p(A, a)) = \psi(A) \bar{v}(a) (1 - \gamma q_3 \times p(A, a))^\beta - \psi(A) \bar{v}(a) < 0$$

Since $Q'(0) < 0$, we conclude that $p_T(A, a) > p(A, a)$.

In conclusion, we have shown that transduction always increases the probability of invasion of a mutant.

A useful approximation

It is interesting to consider that $\beta \gg 1$, which would lead to this interpretation of the defining equation of $p_T(A, a)$:

$$b(A) \times p_T(A, a)^2 - S(A, a) \times p_T(A, a) + \psi(A) \bar{v}(a) \exp\left(-\frac{\gamma}{1-\gamma} \eta(a, A) p_T(A, a)\right) - \psi(A) \bar{v}(a) = 0.$$

Then, if we consider that $\gamma \eta(a, A) p_T(A, a) \ll 1$ (which is reasonable for values as high as a tenth of a unit for two or three of the three factors), we have yet another approximation:

$$b(A) \times p_T(A, a)^2 - \underbrace{\left(S(A, a) + \frac{\gamma}{1-\gamma} \eta(a, A) \psi(A) \bar{v}(a)\right)}_{=S_T(A, a)} \times p_T(A, a) = 0.$$

Which leads us to this explicit definition of the approximation $\tilde{p}_T(A, a)$:

$$\tilde{p}_T(A, a) = \frac{[S_T(A, a)]_+}{b(A)}. \quad (6.28)$$

It is noteworthy to see that we find a somewhat classical form to the invasion probability, being the invasion fitness divided by the mutant birth rate, as can be found in Billiard et al. [27] for example.

C Convergence towards the stochastic canonical equation

Let us call \mathcal{D} the trait domain for which bacteria-phage coexistence is possible and stable. We define $\mathcal{N}(du, dA, ds)$ the Poisson point measure on $\mathbb{R}_+ \times \mathcal{D} \times \mathbb{R}_+$ with intensity measure $du dA ds$. The trait substitution sequence can then be expressed in the following way:

$$a_t = a_0 + \int_0^t \int_{\mathcal{D}} \int_{\mathbb{R}_+} (A - a_{s^-}) \mathbb{1}_{u \leq \bar{x}(a_{s^-}) b(a_{s^-}) p_T(A, a_{s^-}) m(a_{s^-}, dA)} \mathcal{N}(du, dA, ds)$$

To derive the canonical equation, we assume that the mutations step are very small, of order ϵ , i.e.:

$$\forall A \in \mathcal{D}, |A - a| > \epsilon \implies m(A - a) = 0.$$

By defining $\mathcal{N}(du, dh, ds)$ the Poisson point measure on $\mathbb{R}_+ \times [-1; 1] \times \mathbb{R}_+$ with intensity measure $du dh ds$, we can express the TSS the following way:

$$a_t^\epsilon = a_0^\epsilon + \int_0^t \int_{-1}^1 \int_{\mathbb{R}_+} h \epsilon \cdot \mathbb{1}_{u \leq \bar{x}(a_s^\epsilon) b(a_s^\epsilon) p_T(a_s^\epsilon + h \epsilon, a_s^\epsilon) m(a_s^\epsilon, dh)} \mathcal{N}(du, dh, ds)$$

This process is a semi-martingale [178] which can be re-written as

$$a_t^\epsilon = a_0^\epsilon + \epsilon \int_0^t \int_{-1}^1 h \bar{x}(a_s^\epsilon) b(a_s^\epsilon) m(a_s^\epsilon, h) p_T(a_s^\epsilon + \epsilon h, a_s^\epsilon) dh ds + M_t^\epsilon$$

where

$$\langle M^\epsilon \rangle_t = \epsilon^2 \int_0^t \int_{-1}^1 h^2 \bar{x}(a_s) b(a_s) m(a_s^\epsilon, h) p_T(a_s^\epsilon + \epsilon h, a_s^\epsilon) dh ds.$$

Symmetrical mutation kernel m

When decomposing p to the first order, we find:

$$\begin{aligned} a_t^\epsilon &= a_0^\epsilon + \epsilon \int_0^t \int_{-1}^1 h \bar{x}(a_s^\epsilon) b(a_s^\epsilon) m(h) (p_T(a_s^\epsilon, a_s^\epsilon) + \epsilon h \partial_1 p_T(a_s^\epsilon, a_s^\epsilon) + o(\epsilon)) dh ds + M_t^\epsilon \\ &= a_0^\epsilon + \epsilon \int_0^t \bar{x}(a_s^\epsilon) b(a_s^\epsilon) p_T(a_s^\epsilon, a_s^\epsilon) \underbrace{\int_{-1}^1 h m(a_s^\epsilon, h) dh}_{=0 \text{ since } m \text{ is symmetrical}} ds \\ &\quad + \epsilon^2 \int_0^t \bar{x}(a_s^\epsilon) b(a_s^\epsilon) \partial_1 p_T(a_s^\epsilon, a_s^\epsilon) \int_{-1}^1 h^2 m(a_s^\epsilon, h) dh ds + o(\epsilon^2) + M_t^\epsilon \\ &= a_0^\epsilon + \epsilon^2 \int_0^t \bar{x}(a_s^\epsilon) b(a_s^\epsilon) \partial_1 p_T(a_s^\epsilon, a_s^\epsilon) \sigma_0^2(a_s^\epsilon) ds + o(\epsilon^2) + M_t^\epsilon \end{aligned}$$

with, for the martingale part:

$$\langle M^\epsilon \rangle_t = \epsilon^2 \int_0^t \int_{-1}^1 h^2 \bar{x}(a_s) b(a_s) m(a_s^\epsilon, h) p_T(a_s^\epsilon, a_s^\epsilon) dh ds + o(\epsilon^2).$$

This leads to rescale time according to

$$\xi_t^\epsilon = a_{t/\epsilon^2}^\epsilon, \tag{6.29}$$

leading to

$$\xi_t^\epsilon = \xi_0^\epsilon + \int_0^t \bar{x}(\xi_{s'}^\epsilon) b(\xi_{s'}^\epsilon) \partial_1 p_T(\xi_{s'}^\epsilon, \xi_{s'}^\epsilon) \sigma_0^2(\xi_{s'}^\epsilon) ds' + \tilde{M}_t^\epsilon + o(1)$$

with

$$\langle \tilde{M}^\epsilon \rangle_t = \int_0^t \bar{x}(\xi_{s'}) b(\xi_{s'}) p_T(\xi_{s'}, \xi_{s'}) \sigma_0^2(\xi_s) ds' + o(1). \quad (6.30)$$

When $\epsilon \rightarrow 0$, we have $\langle \tilde{M}^\epsilon \rangle \rightarrow \int_0^t \sigma_0^2(\xi_s) b(\xi_s) \bar{x}(\xi_s) p_T(\xi_s, \xi_s) ds$ which is non-zero, from where the stochastic part of the canonical equation comes from. As we stated before, this particularity stems from the fact that $\forall a \in \mathcal{D}, p_T(a, a) > 0$.

Other than this one particularity, we find ourselves in the case studied in [44]. We shall then refer to this paper for the final part of the convergence proof. We do find the following expression for the canonical equation:

$$da_t = u(a_t) \partial_1 p_T(a_t, a_t) dt + \sqrt{u(a_t) p_T(a_t, a_t)} dW_t$$

where $u(a_t) = \sigma_0^2(a_t) b(a_t) \bar{x}(a_t)$ and W_t is a Brownian motion.

Asymmetrical mutation kernel

For this particular case, we define:

$$m_0(a) := \int_{-1}^1 h m(a, h) dh$$

which is nonzero by hypothesis. When going through the same steps as before, we find

$$a_t^\epsilon = a_0^\epsilon + \epsilon \int_0^t \bar{x}(a_s^\epsilon) b(a_s^\epsilon) p_T(a_s^\epsilon, a_s^\epsilon) m_0(a_s^\epsilon) ds + o(\epsilon) + M_t^\epsilon$$

with

$$\langle M^\epsilon \rangle_t = \epsilon^2 \int_0^t \int_{-1}^1 h^2 \bar{x}(a_s) b(a_s) m(a_s, h) p_T(a_s^\epsilon, a_s^\epsilon) dh ds + o(\epsilon^2).$$

We now see that the appropriate rescaling is

$$\tilde{\xi}_t^\epsilon = a_{t/\epsilon}^\epsilon. \quad (6.31)$$

Contrary to the prior rescaling, this one smoothes out the stochastic part, which is of order ϵ^2 . The limit then is the solution to the following ordinary equation

$$\tilde{\xi}_t = \tilde{\xi}_0 + \int_0^t \bar{x}(\tilde{\xi}_s) b(\tilde{\xi}_s) p_T(\tilde{\xi}_s, \tilde{\xi}_s) m_0(\tilde{\xi}_s) ds. \quad (6.32)$$

In this case, the long-term adaptation dynamics are driven deterministically by selection.

Concluding remarks

‘ - Jon, wait, before you leave... I did the right thing, didn't I? It all worked out in the end.

‘ - "In the end"? Nothing ends, Adrian. Nothing ever ends.’

Ozymandias & Dr. Manhattan, *Watchmen* (1986)

The goal of this thesis was to assess and quantify the potential role of heterotrophic bacterial adaptation in the response of the microbial loop to climate change. To the best of our knowledge, such an eco-evolutionary study of heterotrophs had not been conducted before for ocean ecosystems (and only recently had it been for terrestrial soil ecosystems). This research thus extends a body of theory and modeling previously focused on phototrophs (phytoplankton) and their capacity for rapid adaptation and importance in carbon sequestration.

In **Chapter 1** we summarized the importance of the ocean in regulating global climate and highlighted the role of microorganisms in capturing carbon from the atmosphere. Particular attention was given to the microbial loop and its capacity to recycle dissolved organic matter into nutrients. We presented the threats climate change poses to oceanic ecosystems and their potential feedback to the carbon cycle, and current modeling efforts to predict climate through Earth system models (ESMs). The current generation of ESMs do not include microorganism adaptation through natural selection, which might have a significant impact on the response of the biological pump to climate change. Finally, we presented the evolutionary framework and global scope of the thesis, which is to develop an eco-evolutionary modeling framework for the microbial loop and resolve its potential responses to climate change.

Chapter 2 was devoted to the development of the microbial loop module used for most of the eco-evolutionary study. We used a trait-based, ecosystem model that includes one bacterial biomass compartment and one dissolved organic matter compartment. This module was designed for integration in a larger class of ecosystem models. Bacterial growth is assumed to vary across bacterial strains, constrained by a trade-off with resource acquisition and stress tolerance. Under some assumptions on ecological stability, we were able to calcu-

late the evolutionary stable strategy of bacterial populations. We finally integrated the module in a simple model of the microbial loop in the aphotic zone: the system is limited by DOM input, and the total remineralization power of the microbial loop is greater than the sum of the individual contributions. Ocean warming decreases DOM concentration at steady-state, selecting bacterial strains that invest more in resource acquisition, which decreases bacterial biomass but increases total remineralization. Ocean stratification decreases total remineralization and increases DOM turnover time, without inducing an adaptive response from bacterial populations.

We coupled the microbial loop model to a sea-surface ecosystem model in **Chapter 3** to predict the response of primary production to ocean warming. We found that the ecophysiological response of primary production to warming is driven by a decrease in regenerated production which depends on nutrient availability. In nutrient-poor environments, the loss of regenerated production to warming is due to decreasing microbial loop activity. However, this ecophysiological response can be opposed or even reversed by bacterial adaptation through selection, especially in cold environments: heterotrophic bacteria with lower bacterial growth efficiency are selected, which strengthens the 'link' behavior of the microbial loop, increasing both new and regenerated production. In cold and rich environments such as the Arctic Ocean, the effect of bacterial adaptation on primary production exceeds the ecophysiological response.

To generate quantitative predictions of the influence of bacterial adaptation on the oceanic carbon cycle, we developed a novel method for integrating eco-evolutionary processes with Earth system models in **Chapter 4**. To circumvent the computational cost of simulating the mechanistic process of evolution and the resulting trait diversity, we relied on a phenomenological description of trait adaptation at the community level. Applying this framework to the study of bacterial growth efficiency adaptation yielded a trait distribution close to the predictions made from the sea-surface ecosystem model. When sea-surface temperatures are increased, we find that bacterial adaptation can add significant uncertainty to primary production forecasts: in our simulation, the increase in primary production was 2.8% higher due to eco-evolutionary processes. These results call for the integration of the framework in forecast scenarios, and the application to phytoplankton adaptation.

In **Chapter 5** and **Chapter 6** we pave the way to integrate bacterial viruses, or bacteriophages, in eco-evolutionary models of the microbial loop. In **Chapter 5**, we address the ecological and biogeochemical influence of bacteriophages on bacterial adaptation and the microbial loop. By switching the system from a 'bottom-up' to a 'top-down' limitation, phages decrease bacterial biomass and increase DOM concentration. In DOM-poor environments, the increase in steady-state DOM concentrations favors the resource-acquisition strategy in bacteria, driving BGE down. Depending on which function is metabolically more expensive between yield and stress tolerance, lysis can either drive yield investment up (i.e. a BGE increase) or stress tolerance investment up (i.e. a BGE decrease). Overall, the effects of bac-

terio-phages in a constant environment increase DOM remineralization. Ocean stratification decreases both remineralization ratio and total remineralization of DOM, and could potentially drive specialized phage populations to low abundance and even extinction.

In **Chapter 6**, we address the genetic effect of transduction, the main mechanism of horizontal transfer of genetic material between bacteria, on bacterial adaptation. We developed an individual-based model of transduction to resolve the effect of bacteriophages on bacterial adaptation speed. Under directional selection (away from the optimum), the effect of transferring beneficial alleles dominates and transduction tends to accelerate adaptation. When stabilizing selection is expected (near the optimum), transduction generates large stochastic fluctuations in the population's adaptive trajectory, thus hindering adaptation. Under disruptive selection, transduction may either limit (as sexual recombination would) or promote phenotypic diversification. Similarly to genetic drift in finite populations, transduction confers a positive probability of fixation to any allele (positively or negatively selected) even though the bacterial population is very large. Transduction, like other HGT mechanisms, is expected to facilitate adaptation in response to environmental change, when the population stands far enough from its evolutionary optimum, despite the negative demographic effect of viral infection.

Overall, this thesis proved the importance of the recycling pathway in ocean productivity by giving a first assessment of the potential eco-evolutionary feedback loop mediated by the microbial loop. Because of increased temperatures and intensified stratification, climate change leads to more oligotrophic oceans, selecting heterotrophic bacteria that invest more in resource gathering mechanisms. This leads to increased respiration, fueling the recycling pathway: in the surface ocean, this causes an increase in regenerated production; deeper in the water column, increased remineralization could mitigate the effect of stratification by increasing the upward flux of nitrate. Bacteriophages tend to reinforce the recycling power of the microbial loop and its response to climate change. By increasing remineralization and fueling new and regenerated production, the microbial loop feeds back negatively to climate change. But at the same time, increasing the concentration of dissolved inorganic carbon in the ocean could intensify acidification, simultaneously generating a positive feedback.

Quantifying the relative strengths of the positive and negative feedbacks calls for further studies to integrate them in Earth system models. The 'selection gradient equations' framework developed in this thesis could provide a basis for such studies. Phytoplankton adaptation could also be studied within this framework, and eventually one could aim for an integration taking adaptation into account across microbial primary producers and decomposers. Bacteriophage adaptation was not discussed in this thesis despite the importance of coevolution mechanisms for bacterial community structure, but this topic offers a promising direction for future work. Potential phage extinction discussed here could be averted by evolutionary rescue, and the consequences for the viral shunt and microbial loop function should be further explored.

Humans may have become the strongest evolutionary force on the planet. How microbial communities evolve and adapt in response to anthropogenic climate change is a major frontier of global ecology and evolutionary biology. Our work provides a theoretical basis to assess and predict the significance of these responses and their impact on the Earth's carbon cycle. This research calls for extending the theory, validating the models, and continuing their integration in global climate-ecosystem forecasting frameworks.

Bibliography

- [1] Elsa Abs and Régis Ferrière. “Modeling Microbial Dynamics and Heterotrophic Soil Respiration: Effect of Climate Change”. In: *Biogeochemical Cycles: Ecological Drivers and Environmental Impact*. Ed. by Katerina Dontsova, Zsuzsanna Balogh-Brunstad, and Gaël Le Roux. American Geophysical Union, 2020. Chap. 5, pp. 103–131.
- [2] Elsa Abs, Hélène Leman, and Régis Ferrière. “A multi-scale eco-evolutionary model of cooperation reveals how microbial adaptation influences soil decomposition”. In: *Communications biology* 3.1 (2020), pp. 1–13.
- [3] Alistair Adcroft, Chris Hill, Jean-Michel Campin, John Marshall, and Patrick Heimbach. “Overview of the formulation and numerics of the MIT GCM”. In: *Proceedings of the ECMWF seminar series on Numerical Methods, Recent developments in numerical methods for atmosphere and ocean modelling*. 2004, pp. 139–149.
- [4] Alice L Alldredge and Mary W Silver. “Characteristics, dynamics and significance of marine snow”. In: *Progress in oceanography* 20.1 (1988), pp. 41–82.
- [5] Steven D Allison, Matthew D Wallenstein, and Mark A Bradford. “Soil-carbon response to warming dependent on microbial physiology”. In: *Nature Geoscience* 3.5 (2010), pp. 336–340.
- [6] Charlotte J Alster, Peter Baas, Matthew D Wallenstein, Nels G Johnson, and Joseph C von Fischer. “Temperature sensitivity as a microbial trait using parameters from macromolecular rate theory”. In: *Frontiers in microbiology* 7 (2016), p. 1821.
- [7] Cheryl P Andam, Sarah M Carver, and Sean T Berthrong. “Horizontal gene flow in managed ecosystems”. In: *Annual Review of Ecology, Evolution, and Systematics* 46 (2015), pp. 121–143.
- [8] David Archer, Haroon Kheshgi, and Ernst Maier-Reimer. “Dynamics of fossil fuel CO₂ neutralization by marine CaCO₃”. In: *Global Biogeochemical Cycles* 12.2 (1998), pp. 259–276.
- [9] Damian L Arevalo-Martínez, Annette Kock, CR Löscher, Ruth A Schmitz, and Hermann W Bange. “Massive nitrous oxide emissions from the tropical South Pacific Ocean”. In: *Nature Geoscience* 8.7 (2015), pp. 530–533.

- [10] C Arnosti. “Microbial extracellular enzymes and their role in dissolved organic matter cycling”. In: *Aquatic Ecosystems*. Elsevier, 2003, pp. 315–342.
- [11] C Arnosti, S Durkin, and WH Jeffrey. “Patterns of extracellular enzyme activities among pelagic marine microbial communities: implications for cycling of dissolved organic carbon”. In: *Aquatic microbial ecology* 38.2 (2005), pp. 135–145.
- [12] Carol Arnosti. “Microbial extracellular enzymes and the marine carbon cycle”. In: *Annual review of marine science* 3 (2011), pp. 401–425.
- [13] Carol Arnosti. “Patterns of microbially driven carbon cycling in the ocean: links between extracellular enzymes and microbial communities”. In: *Advances in Oceanography* 2014 (2014).
- [14] Carol Arnosti, Greta Reintjes, and R Amann. “A mechanistic microbial underpinning for the size-reactivity continuum of dissolved organic carbon degradation”. In: *Marine Chemistry* 206 (2018), pp. 93–99.
- [15] Olivier Aumont, Christian Éthé, Alessandro Tagliabue, Laurent Bopp, and Marion Gehlen. “PISCES-v2: An ocean biogeochemical model for carbon and ecosystem studies.” In: *Geoscientific Model Development Discussions* 8.2 (2015).
- [16] Aa Haeruman Azam and Yasunori Tanji. “Bacteriophage-host arm race: an update on the mechanism of phage resistance in bacteria and revenge of the phage with the perspective for phage therapy”. In: *Applied microbiology and biotechnology* 103.5 (2019), pp. 2121–2131.
- [17] Farooq Azam, Tom Fenchel, J G_ Field, JS Gray, LA Meyer-Reil, and F Thingstad. “The ecological role of water-column microbes in the sea”. In: *Marine ecology progress series* (1983), pp. 257–263.
- [18] Farooq Azam and Francesca Malfatti. “Microbial structuring of marine ecosystems”. In: *Nature Reviews Microbiology* 5.10 (2007), pp. 782–791.
- [19] David A Baltrus, Karen Guillemin, and Patrick C Phillips. “Natural transformation increases the rate of adaptation in the human pathogen *Helicobacter pylori*”. In: *Evolution: International Journal of Organic Evolution* 62.1 (2008), pp. 39–49.
- [20] Anthony D Barnosky, Nicholas Matzke, Susumu Tomiya, Guinevere OU Wogan, Brian Swartz, Tiago B Quental, et al. “Has the Earth’s sixth mass extinction already arrived?” In: *Nature* 471.7336 (2011), pp. 51–57.
- [21] James E Bauer, Peter M Williams, and Ellen RM Druffel. “¹⁴C activity of dissolved organic carbon fractions in the north-central Pacific and Sargasso Sea”. In: *Nature* 357.6380 (1992), pp. 667–670.
- [22] Aike Beckmann, C-Elisa Schaum, and Inga Hense. “Phytoplankton adaptation in ecosystem models”. In: *Journal of theoretical biology* 468 (2019), pp. 60–71.

- [23] Michael Behrenfeld. “Uncertain future for ocean algae”. In: *Nature Climate Change* 1.1 (2011), pp. 33–34.
- [24] J Michael Beman, Cheryl-Emiliane Chow, Andrew L King, Yuanyuan Feng, Jed A Fuhrman, Andreas Andersson, et al. “Global declines in oceanic nitrification rates as a consequence of ocean acidification”. In: *Proceedings of the National Academy of Sciences* 108.1 (2011), pp. 208–213.
- [25] Jørgen Bendtsen, Claus Lundsgaard, Mathias Middelboe, and David Archer. “Influence of bacterial uptake on deep-ocean dissolved organic carbon”. In: *Global Biogeochemical Cycles* 16.4 (2002), pp. 74–1.
- [26] Albert F Bennett, Khoi M Dao, and Richard E Lenski. “Rapid evolution in response to high-temperature selection”. In: *Nature* 346.6279 (1990), pp. 79–81.
- [27] Sylvain Billiard, Pierre Collet, Régis Ferrière, Sylvie Méléard, and Viet Chi Tran. “The effect of competition and horizontal trait inheritance on invasion, fixation, and polymorphism”. In: *Journal of theoretical biology* 411 (2016), pp. 48–58.
- [28] NL Bindoff, WWL Cheung, JG Kairo, J Arístegui, VA Guinder, R Hallberg, et al. “Changing Ocean, Marine Ecosystems, and Dependent Communities”. In: *IPCC Special Report on the Ocean and Cryosphere in a Changing Climate* (2021).
- [29] Zachary D Blount, Christina Z Borland, and Richard E Lenski. “Historical contingency and the evolution of a key innovation in an experimental population of *Escherichia coli*”. In: *Proceedings of the National Academy of Sciences* 105.23 (2008), pp. 7899–7906.
- [30] Laurent Bopp, Laure Resplandy, James C Orr, Scott C Doney, John P Dunne, M Gehlen, et al. “Multiple stressors of ocean ecosystems in the 21st century: projections with CMIP5 models”. In: *Biogeosciences* 10.10 (2013), pp. 6225–6245.
- [31] Joel A Boyd, Ben J Woodcroft, and Gene W Tyson. “GraftM: a tool for scalable, phylogenetically informed classification of genes within metagenomes”. In: *Nucleic Acids Research* 46.10 (2018), e59–e59.
- [32] Timothy P Boyer, John I Antonov, Olga K Baranova, Carla Coleman, Hernan E Garcia, Alexandra Grodsky, et al. “World Ocean Database 2013.” In: (2013).
- [33] Mya Breitbart, Chelsea Bonnain, Kema Malki, and Natalie A Sawaya. “Phage puppet masters of the marine microbial realm”. In: *Nature microbiology* 3.7 (2018), pp. 754–766.
- [34] MYA Breitbart, Luke R Thompson, Curtis A Suttle, and Matthew B Sullivan. “Exploring the vast diversity of marine viruses”. In: *Oceanography* 20.2 (2007), pp. 135–139.
- [35] ET Buitenhuis, WKW Li, MW Lomas, DM Karl, MR Landry, and Stéphan Jacquet. “Picoheterotroph (Bacteria and Archaea) biomass distribution in the global ocean”. In: *Earth System Science Data* 4.1 (2012), pp. 101–106.

- [36] DK Button. “Biochemical basis for whole-cell uptake kinetics: specific affinity, oligotrophic capacity, and the meaning of the Michaelis constant”. In: *Appl. Environ. Microbiol.* 57.7 (1991), pp. 2033–2038.
- [37] Craig A Carlson, Paul A Del Giorgio, and Gerhard J Herndl. “Microbes and the dissipation of energy and respiration: from cells to ecosystems”. In: *Oceanography* 20.2 (2007), pp. 89–100.
- [38] Ricardo Cavicchioli, William J Ripple, Kenneth N Timmis, Farooq Azam, Lars R Bakken, Matthew Baylis, et al. “Scientists’ warning to humanity: microorganisms and climate change”. In: *Nature Reviews Microbiology* 17.9 (2019), pp. 569–586.
- [39] Anny Cazenave and William Llovel. “Contemporary sea level rise”. In: *Annual review of marine science* 2 (2010), pp. 145–173.
- [40] Nicolas Champagnat. “A microscopic interpretation for adaptive dynamics trait substitution sequence models”. In: *Stochastic processes and their applications* (2006).
- [41] Nicolas Champagnat, R Ferrière, and G Ben Arous. “The canonical equation of adaptive dynamics: a mathematical view”. In: *Selection* 2.1-2 (2002), pp. 73–83.
- [42] Nicolas Champagnat, Régis Ferrière, and Sylvie Méléard. “Unifying evolutionary dynamics: From individual stochastic processes to macroscopic models”. In: *Theoretical Population Biology* (2006).
- [43] Nicolas Champagnat and Amaury Lambert. “Evolution of discrete populations and the canonical diffusion of adaptive dynamics”. In: *The Annals of Applied Probability* 17.1 (2007), pp. 102–155.
- [44] Nicolas Champagnat and Sylvie Méléard. “Polymorphic evolution sequence and evolutionary branching”. In: *Probability Theory and Related Fields* 151.1-2 (2011), pp. 45–94.
- [45] Bingzhang Chen, Michael R Landry, Bangqin Huang, and Hongbin Liu. “Does warming enhance the effect of microzooplankton grazing on marine phytoplankton in the ocean?” In: *Limnology and oceanography* 57.2 (2012), pp. 519–526.
- [46] John Chen, Nuria Quiles-Puchalt, Yin Ning Chiang, Rodrigo Bacigalupe, Alfred Fillol-Salom, Melissa Su Juan Chee, et al. “Genome hypermobility by lateral transduction”. In: *Science* 362.6411 (2018), pp. 207–212.
- [47] Philippe Cherabier, Anh Le-Duy Pham, Olivier Aumont, and Régis Ferrière. “The Selection Gradient Equations: Integrating Microbial Evolutionary Processes in General Circulation Models.” In: *AGU Fall Meeting 2021*. AGU. 2021.
- [48] Philippe Cherabier and Régis Ferrière. “Eco-evolutionary responses of the microbial loop to surface ocean warming and consequences for primary production”. In: *The ISME journal* (2021), pp. 1–10.

- [49] Philippe Cherabier and Régis Ferrière. “Eco-evolutionary responses of the microbial loop to surface ocean warming and consequences for primary production”. In: (2021).
- [50] Philippe Cherabier, Sylvie Méléard, and Régis Ferrière. “Viral transduction and the dynamics of bacterial adaptation”. In: *bioRxiv* (2021).
- [51] Philippe Cherabier, Sylvie Méléard, and Régis Ferrière. “Viral transduction and the dynamics of bacterial adaptation”. In: *Virtual Evolution 2021*. 2021.
- [52] Anne Chevallereau, Benoît J Pons, Stineke van Houte, and Edze R Westra. “Interactions between bacterial and phage communities in natural environments”. In: *Nature Reviews Microbiology* 20.1 (2022), pp. 49–62.
- [53] Ryszard J Chróst. “Microbial ectoenzymes in aquatic environments”. In: *Aquatic microbial ecology*. Springer, 1990, pp. 47–78.
- [54] James R Clark, Stuart J Daines, Timothy M Lenton, Andrew J Watson, and Hywel TP Williams. “Individual-based modelling of adaptation in marine microbial populations using genetically defined physiological parameters”. In: *Ecological modelling* 222.23-24 (2011), pp. 3823–3837.
- [55] Corentin Clerc, Olivier Aumont, and Laurent Bopp. “Should we account for mesozooplankton reproduction and ontogenetic growth in biogeochemical modeling?” In: *Theoretical Ecology* 14.4 (2021), pp. 589–609.
- [56] Elisheva Cohen, David A Kessler, and Herbert Levine. “Analytic approach to the evolutionary effects of genetic exchange”. In: *Physical Review E* 73.1 (2006), p. 016113.
- [57] John A Cole, Lars Kohler, Jamila Hedhli, and Zaida Luthey-Schulten. “Spatially-resolved metabolic cooperativity within dense bacterial colonies”. In: *BMC systems biology* 9.1 (2015), pp. 1–17.
- [58] VJ Coles, MR Stukel, MT Brooks, A Burd, BC Crump, MA Moran, et al. “Ocean biogeochemistry modeled with emergent trait-based genomics”. In: *Science* 358.6367 (2017), pp. 1149–1154.
- [59] Sinéad Collins, Björn Rost, and Tatiana A Ryneerson. “Evolutionary potential of marine phytoplankton under ocean acidification”. In: *Evolutionary applications* 7.1 (2014), pp. 140–155.
- [60] Michael H Cortez and Stephen P Ellner. “Understanding rapid evolution in predator-prey interactions using the theory of fast-slow dynamical systems”. In: *The American Naturalist* 176.5 (2010), E109–E127.
- [61] Domenico d’Alelio, Damien Eveillard, Victoria J Coles, Luigi Caputi, Maurizio Ribera d’Alcalà, and Daniele Iudicone. “Modelling the complexity of plankton communities exploiting omics potential: From present challenges to an integrative pipeline”. In: *Current opinion in systems biology* 13 (2019), pp. 68–74.

- [62] Eric A D'Asaro. "Turbulence in the upper-ocean mixed layer". In: *Annual review of marine science* 6 (2014), pp. 101–115.
- [63] Roberto Danovaro, Cinzia Corinaldesi, Antonio Dell'Anno, Jed A Fuhrman, Jack J Middelburg, Rachel T Noble, et al. "Marine viruses and global climate change". In: *FEMS microbiology reviews* 35.6 (2011), pp. 993–1034.
- [64] Charles Darwin. *Journal and Remarks (The Voyage of the Beagle)*. John Murray, 1839.
- [65] Charles Darwin. *On the origin of species*. John Murray, 1859.
- [66] Alan R Davidson. "A common trick for transferring bacterial DNA". In: *Science* 362.6411 (2018), pp. 152–153.
- [67] Carla CCR De Carvalho. "Marine biofilms: a successful microbial strategy with economic implications". In: *Frontiers in marine science* 5 (2018), p. 126.
- [68] Fernando De la Cruz and Julian Davies. "Horizontal gene transfer and the origin of species: lessons from bacteria". In: *Trends in microbiology* 8.3 (2000), pp. 128–133.
- [69] Casimir De Lavergne, Jaime B Palter, Eric D Galbraith, Raffaele Bernardello, and Irina Marinov. "Cessation of deep convection in the open Southern Ocean under anthropogenic climate change". In: *Nature Climate Change* 4.4 (2014), pp. 278–282.
- [70] Paul A Del Giorgio and Jonathan J Cole. "Bacterial growth efficiency in natural aquatic systems". In: *Annual Review of Ecology and Systematics* 29.1 (1998), pp. 503–541.
- [71] Paul A Del Giorgio and Carlos M Duarte. "Respiration in the open ocean". In: *Nature* 420.6914 (2002), pp. 379–384.
- [72] David Demory, Anne-Claire Baudoux, Adam Monier, Nathalie Simon, Christophe Six, Pei Ge, et al. "Picoeukaryotes of the *Micromonas* genus: sentinels of a warming ocean". In: *The ISME journal* 13.1 (2019), pp. 132–146.
- [73] Fabio Dercole, Fabio Della Rossa, and Pietro Landi. "The transition from evolutionary stability to branching: A catastrophic evolutionary shift". In: *Scientific reports* 6.1 (2016), pp. 1–8.
- [74] Fabio Dercole, R Ferriere, Alessandra Gragnani, and Sergio Rinaldi. "Coevolution of slow–fast populations: evolutionary sliding, evolutionary pseudo-equilibria and complex Red Queen dynamics". In: *Proceedings of the Royal Society B: Biological Sciences* 273.1589 (2006), pp. 983–990.
- [75] René Descartes. *Discours de la méthode – La Géométrie*. 1637.
- [76] Tim DeVries, Mark Holzer, and Francois Primeau. "Recent increase in oceanic carbon uptake driven by weaker upper-ocean overturning". In: *Nature* 542.7640 (2017), pp. 215–218.
- [77] Gregory J Dick. "Embracing the mantra of modellers and synthesizing omics, experiments and models". In: (2017).

- [78] Ulf Dieckmann and Régis Ferrière. “Adaptive dynamics and evolving biodiversity”. In: (2004).
- [79] Ulf Dieckmann and Richard Law. “The dynamical theory of coevolution: a derivation from stochastic ecological processes”. In: *Journal of mathematical biology* 34.5-6 (1996), pp. 579–612.
- [80] Odo Diekmann. “A beginners guide to adaptive dynamics”. In: *Summer school on mathematical biology* (2002), pp. 63–100.
- [81] Dimensions. *Blue Whales Dimensions*. 2022. URL: <https://www.dimensions.com/element/blue-whale> (visited on 02/11/2022).
- [82] Michael Doebeli and Ulf Dieckmann. “Evolutionary branching and sympatric speciation caused by different types of ecological interactions”. In: *The american naturalist* 156.S4 (2000), S77–S101.
- [83] Scott C Doney, Victoria J Fabry, Richard A Feely, and Joan A Kleypas. “Ocean acidification: the other CO₂ problem”. In: *Annual review of marine science* 1 (2009), pp. 169–192.
- [84] Guilhem Doucier. “Evolution of Collective-level Darwinian Properties”. PhD thesis. Université Paris sciences et lettres, 2019.
- [85] Knut Drescher, Carey D Nadell, Howard A Stone, Ned S Wingreen, and Bonnie L Bassler. “Solutions to the public goods dilemma in bacterial biofilms”. In: *Current Biology* 24.1 (2014), pp. 50–55.
- [86] John P Dunne, Jasmin G John, Elena Shevliakova, Ronald J Stouffer, John P Krasting, Sergey L Malyshev, et al. “GFDL’s ESM2 global coupled climate–carbon earth system models. Part II: carbon system formulation and baseline simulation characteristics”. In: *Journal of Climate* 26.7 (2013), pp. 2247–2267.
- [87] Anh Le-Duy Pham, Olivier Aumont, Lavenia Ratnarajah, and Alessandro Tagliabue. “Examining the interaction between free-living bacteria and iron in the global ocean”. In: (*preprint*) (2021).
- [88] Eric S Egleston, Christopher L Sabine, and François MM Morel. “Revelle revisited: Buffer factors that quantify the response of ocean chemistry to changes in DIC and alkalinity”. In: *Global Biogeochemical Cycles* 24.1 (2010).
- [89] NOAA National Centers for Environmental information. *Climate at a Glance: Global Time Series*. 2022. URL: <https://www.ncdc.noaa.gov/cag/global/time-series/globe/ocean/ytd/12/1880-2017> (visited on 02/28/2022).
- [90] Ilan Eshel, Marcus W Feldman, and Aviv Bergman. “Long-term evolution, short-term evolution, and population genetic theory”. In: *Journal of Theoretical Biology* 191.4 (1998), pp. 391–396.

- [91] Veronika Eyring, Sandrine Bony, Gerald A Meehl, Catherine A Senior, Bjorn Stevens, Ronald J Stouffer, et al. “Overview of the Coupled Model Intercomparison Project Phase 6 (CMIP6) experimental design and organization”. In: *Geoscientific Model Development* 9.5 (2016), pp. 1937–1958.
- [92] Paul Falkowski. “Ocean science: the power of plankton”. In: *Nature* 483.7387 (2012), S17–S20.
- [93] Paul Falkowski, RJ Scholes, EEA Boyle, Josep Canadell, D Canfield, James Elser, et al. “The global carbon cycle: a test of our knowledge of earth as a system”. In: *Science* 290.5490 (2000), pp. 291–296.
- [94] Paul G Falkowski, Tom Fenchel, and Edward F Delong. “The microbial engines that drive Earth’s biogeochemical cycles”. In: *science* 320.5879 (2008), pp. 1034–1039.
- [95] Michael JR Fasham, Hugh W Ducklow, and Stuart M McKelvie. “A nitrogen-based model of plankton dynamics in the oceanic mixed layer”. In: *Journal of Marine Research* 48.3 (1990), pp. 591–639.
- [96] Tom Fenchel. “The microbial loop–25 years later”. In: *Journal of Experimental Marine Biology and Ecology* 366.1-2 (2008), pp. 99–103.
- [97] Régis Ferrière and Stéphane Legendre. “Eco-evolutionary feedbacks, adaptive dynamics and evolutionary rescue theory”. In: *Philosophical Transactions of the Royal Society B: Biological Sciences* 368.1610 (2013), p. 20120081.
- [98] Régis Ferrière and J-F Le Galliard. “Invasion fitness and adaptive dynamics in spatial population models”. In: (2001).
- [99] Christopher B Field, Michael J Behrenfeld, James T Randerson, and Paul Falkowski. “Primary production of the biosphere: integrating terrestrial and oceanic components”. In: *science* 281.5374 (1998), pp. 237–240.
- [100] Alfred Fillol-Salom, Ahlam Alsaadi, Jorge A Moura de Sousa, Li Zhong, Kevin R Foster, Eduardo PC Rocha, et al. “Bacteriophages benefit from generalized transduction”. In: *PLoS pathogens* 15.7 (2019), e1007888.
- [101] PC Fineran, NK Petty, and GPC Salmond. “Transduction: host DNA transfer by bacteriophages”. In: (2009).
- [102] Gregory Flato, Jochem Marotzke, Babatunde Abiodun, Pascale Braconnot, Sin Chan Chou, William Collins, et al. “Evaluation of climate models”. In: *Climate change 2013: the physical science basis. Contribution of Working Group I to the Fifth Assessment Report of the Intergovernmental Panel on Climate Change*. Cambridge University Press, 2014, pp. 741–866.
- [103] Gregory M Flato. “Earth system models: an overview”. In: *Wiley Interdisciplinary Reviews: Climate Change* 2.6 (2011), pp. 783–800.

- [104] Pedro Flombaum, José L Gallegos, Rodolfo A Gordillo, José Rincón, Lina L Zabala, Nianzhi Jiao, et al. “Present and future global distributions of the marine Cyanobacteria *Prochlorococcus* and *Synechococcus*”. In: *Proceedings of the National Academy of Sciences* 110.24 (2013), pp. 9824–9829.
- [105] World Wildlife Foundation. *Blue Whales*. 2022. URL: <https://www.worldwildlife.org/species/blue-whale> (visited on 02/11/2022).
- [106] PJS Franks, JS Wroblewski, and GR Flierl. “Behavior of a simple plankton model with food-level acclimation by herbivores”. In: *Marine Biology* 91.1 (1986), pp. 121–129.
- [107] Thomas L Frölicher, Luca Ramseyer, Christoph C Raible, Keith B Rodgers, and John Dunne. “Potential predictability of marine ecosystem drivers”. In: *Biogeosciences* 17.7 (2020), pp. 2061–2083.
- [108] Weiwei Fu, James T Randerson, and J Keith Moore. “Climate change impacts on net primary production (NPP) and export production (EP) regulated by increasing stratification and phytoplankton community structure in the CMIP5 models”. In: *Biogeosciences* 13.18 (2016), pp. 5151–5170.
- [109] Jed A Fuhrman. “Marine viruses and their biogeochemical and ecological effects”. In: *Nature* 399.6736 (1999), pp. 541–548.
- [110] Theodore Garland. “Trade-offs”. In: *Current Biology* 24.2 (2014), R60–R61.
- [111] Nandita R Garud, Benjamin H Good, Oskar Hallatschek, and Katherine S Pollard. “Evolutionary dynamics of bacteria in the gut microbiome within and across hosts”. In: *PLoS biology* 17.1 (2019), e3000102.
- [112] George Francis Gause. *Vérifications expérimentales de la théorie mathématique de la lutte pour la vie*. Vol. 277. Hermann et Cie, 1935.
- [113] AN Geerts, Joost Vanoverbeke, Bram Vanschoenwinkel, Wendy Van Doorslaer, Hei-drun Feuchtmayr, David Atkinson, et al. “Rapid evolution of thermal tolerance in the water flea *Daphnia*”. In: *Nature Climate Change* 5.7 (2015), pp. 665–668.
- [114] Katerina Georgiou, Rose Z Abramoff, John Harte, William J Riley, and Margaret S Torn. “Microbial community-level regulation explains soil carbon responses to long-term litter manipulations”. In: *Nature Communications* 8.1 (2017), pp. 1–10.
- [115] Stefan AH Geritz. “Resident-invader dynamics and the coexistence of similar strategies”. In: *Journal of Mathematical Biology* 50.1 (2005), pp. 67–82.
- [116] Stefan AH Geritz, Mats Gyllenberg, Frans JA Jacobs, and Kalle Parvinen. “Invasion dynamics and attractor inheritance”. In: *Journal of Mathematical Biology* 44.6 (2002), pp. 548–560.

- [117] Ann C Gregory, Kenji Gerhardt, Zhi-Ping Zhong, Benjamin Bolduc, Ben Temperton, Konstantinos T Konstantinidis, et al. “MetaPop: a pipeline for macro-and micro-diversity analyses and visualization of microbial and viral metagenome-derived populations”. In: *bioRxiv* (2020).
- [118] Ann C Gregory, Ahmed A Zayed, Nádia Conceicao-Neto, Ben Temperton, Ben Bolduc, Adriana Alberti, et al. “Marine DNA viral macro-and microdiversity from pole to pole”. In: *Cell* 177.5 (2019), pp. 1109–1123.
- [119] Ghjuvan Micaelu Grimaud, Valérie Le Guennec, Sakina-Dorothee Ayata, Francis Mairet, Antoine Sciandra, and Olivier Bernard. “Modelling the effect of temperature on phytoplankton growth across the global ocean”. In: *IFAC-PapersOnLine* 48.1 (2015), pp. 228–233.
- [120] Ghjuvan Micaelu Grimaud, Francis Mairet, and Olivier Bernard. “Modelling thermal adaptation in microalgae: an adaptive dynamics point of view”. In: *IFAC Proceedings Volumes* 47.3 (2014), pp. 4376–4381.
- [121] Jo P Grime. “Evidence for the existence of three primary strategies in plants and its relevance to ecological and evolutionary theory”. In: *The american naturalist* 111.982 (1977), pp. 1169–1194.
- [122] John Philip Grime. “Vegetation classification by reference to strategies”. In: *Nature* 250.5461 (1974), pp. 26–31.
- [123] NEMO TOP Working Group. *Tracers in Ocean Paradigm (TOP) – The NEMO passive tracers engine*. Scientific Notes of Climate Modelling Center 28. Zenodo. DOI: [10 . 5281/zenodo.1471700](https://doi.org/10.5281/zenodo.1471700).
- [124] Nicolas Gruber, Dominic Clement, Brendan R Carter, Richard A Feely, Steven Van Heuven, Mario Hoppema, et al. “The oceanic sink for anthropogenic CO₂ from 1994 to 2007”. In: *Science* 363.6432 (2019), pp. 1193–1199.
- [125] Lionel Guidi, Samuel Chaffron, Lucie Bittner, Damien Eveillard, Abdelhalim Larhlimi, Simon Roux, et al. “Plankton networks driving carbon export in the oligotrophic ocean”. In: *Nature* 532.7600 (2016), pp. 465–470.
- [126] Lionel Guidi, Louis Legendre, Gabriel Reygondeau, Julia Uitz, Lars Stemann, and Stephanie A Henson. “A new look at ocean carbon remineralization for estimating deepwater sequestration”. In: *Global Biogeochemical Cycles* 29.7 (2015), pp. 1044–1059.
- [127] Edward K Hall, Claudia Neuhauser, and James B Cotner. “Toward a mechanistic understanding of how natural bacterial communities respond to changes in temperature in aquatic ecosystems”. In: *The ISME journal* 2.5 (2008), pp. 471–481.
- [128] James PJ Hall, Michael A Brockhurst, and Ellie Harrison. “Sampling the mobile gene pool: innovation via horizontal gene transfer in bacteria”. In: *Philosophical Transactions of the Royal Society B: Biological Sciences* 372.1735 (2017), p. 20160424.

- [129] Peter Hammerstein. “Darwinian adaptation, population genetics and the streetcar theory of evolution”. In: *Journal of mathematical biology* 34.5 (1996), pp. 511–532.
- [130] Dennis A Hansell and Craig A Carlson. *Biogeochemistry of marine dissolved organic matter*. Academic Press, 2014.
- [131] Weilong Hao and G Brian Golding. “The fate of laterally transferred genes: life in the fast lane to adaptation or death”. In: *Genome Research* 16.5 (2006), pp. 636–643.
- [132] Hiroyasu Hasumi and Toshi Nagata. “Modeling the global cycle of marine dissolved organic matter and its influence on marine productivity”. In: *Ecological modelling* 288 (2014), pp. 9–24.
- [133] Lei He, Kedong Yin, and Xiangcheng Yuan. “Double maximum ratios of viruses to bacteria in the water column: implications for different regulating mechanisms”. In: *Frontiers in Microbiology* 10 (2019), p. 1593.
- [134] David A Hutchins and Feixue Fu. “Microorganisms and ocean global change”. In: *Nature microbiology* 2.6 (2017), pp. 1–11.
- [135] David A Hutchins, Nathan G Walworth, Eric A Webb, Mak A Saito, Dawn Moran, Matthew R McIlvin, et al. “Irreversibly increased nitrogen fixation in *Trichodesmium* experimentally adapted to elevated carbon dioxide”. In: *Nature communications* 6.1 (2015), pp. 1–7.
- [136] E.U. Copernicus Marine Service Information. *Global Analysis Forecast Bio 001 028*. 2022. URL: https://resources.marine.copernicus.eu/product-detail/GLOBAL_ANALYSIS_FORECAST_BIO_001_028/INFORMATION (visited on 02/28/2022).
- [137] Andrew J Irwin, Zoe V Finkel, Frank E Müller-Karger, and Luis Troccoli Ghinaglia. “Phytoplankton adapt to changing ocean environments”. In: *Proceedings of the National Academy of Sciences* 112.18 (2015), pp. 5762–5766.
- [138] Amal Jayakumar, Xuefeng Peng, and Bess B Ward. “Community composition of bacteria involved in fixed nitrogen loss in the water column of two major oxygen minimum zones in the ocean”. In: *Aquatic microbial ecology* 70.3 (2013), pp. 245–259.
- [139] Sunny C Jiang and John H Paul. “Gene transfer by transduction in the marine environment”. In: *Applied and environmental microbiology* 64.8 (1998), pp. 2780–2787.
- [140] Peng Jin, Kunshan Gao, and John Beardall. “Evolutionary responses of a coccolithophorid *Gephyrocapsa oceanica* to ocean acidification”. In: *Evolution* 67.7 (2013), pp. 1869–1878.
- [141] Thomas Kiørboe, André Visser, and Ken H Andersen. “A trait-based approach to ocean ecology”. In: *ICES Journal of Marine Science* 75.6 (2018), pp. 1849–1863.
- [142] David L Kirchman, Xosé Anxelu G Morán, and Hugh Ducklow. “Microbial growth in the polar oceans—role of temperature and potential impact of climate change”. In: *Nature Reviews Microbiology* 7.6 (2009), pp. 451–459.

- [143] Georgiy Kirillin, Hans-Peter Grossart, and Kam W Tang. “Modeling sinking rate of zooplankton carcasses: effects of stratification and mixing”. In: *Limnology and Oceanography* 57.3 (2012), pp. 881–894.
- [144] Manuel Kleiner, Brian Bushnell, Kenneth E Sanderson, Lora V Hooper, and Breck A Duerkop. “Transductomics: sequencing-based detection and analysis of transduced DNA in pure cultures and microbial communities”. In: *Microbiome* 8.1 (2020), pp. 1–17.
- [145] Sarah Köster, Alex Evilevitch, Meerim Jeembaeva, and David A Weitz. “Influence of internal capsid pressure on viral infection by phage λ ”. In: *Biophysical journal* 97.6 (2009), pp. 1525–1529.
- [146] IZUMI Koujima, H Hayashi, K Tomochika, A Okabe, and Y Kanemasa. “Adaptational change in proline and water content of *Staphylococcus aureus* after alteration of environmental salt concentration”. In: *Applied and environmental microbiology* 35.3 (1978), pp. 467–470.
- [147] Jan-Ulrich Kreft, Caroline M Plugge, Clara Prats, Johan HJ Leveau, Weiwen Zhang, and Ferdi L Hellweger. “From genes to ecosystems in microbiology: modeling approaches and the importance of individuality”. In: *Frontiers in microbiology* 8 (2017), p. 2299.
- [148] Colin T Kremer and Christopher A Klausmeier. “Species packing in eco-evolutionary models of seasonally fluctuating environments”. In: *Ecology Letters* 20.9 (2017), pp. 1158–1168.
- [149] Amaury Lambert et al. “The branching process with logistic growth”. In: *The Annals of Applied Probability* 15.2 (2005), pp. 1506–1535.
- [150] Charlotte Laufkötter, Meike Vogt, Nicolas Gruber, Maki Aita-Noguchi, Olivier Aumont, Laurent Bopp, et al. “Drivers and uncertainties of future global marine primary production in marine ecosystem models”. In: *Biogeosciences* 12.23 (2015), pp. 6955–6984.
- [151] Charlotte Laufkötter, Meike Vogt, Nicolas Gruber, Olivier Aumont, Laurent Bopp, Scott C Doney, et al. “Projected decreases in future marine export production: the role of the carbon flux through the upper ocean ecosystem”. In: *Biogeosciences* 13.13 (2016), pp. 4023–4047.
- [152] Raphaël Laurenceau, Nicolas Raho, Mathieu Forget, Aldo A Arellano, and Sallie W Chisholm. “Frequency of mispackaging of *Prochlorococcus* DNA by cyanophage”. In: *The ISME journal* 15.1 (2021), pp. 129–140.
- [153] Jeffrey G Lawrence. “Gene transfer in bacteria: speciation without species?” In: *Theoretical population biology* 61.4 (2002), pp. 449–460.

- [154] Guillaume Le Gland, Sergio M Vallina, S Lan Smith, and Pedro Cermeño. “SPEAD 1.0—Simulating Plankton Evolution with Adaptive Dynamics in a two-trait continuous fitness landscape applied to the Sargasso Sea”. In: *Geoscientific Model Development* 14.4 (2021), pp. 1949–1985.
- [155] Karine Leblanc, Javier Arístegui, Leanne Armand, Phillip Assmy, Beatriz Beker, Antonio Bode, et al. “A global diatom database—abundance, biovolume and biomass in the world ocean”. In: *Earth System Science Data* 4.1 (2012), pp. 149–165.
- [156] Glenn Ledder. “The basic dynamic energy budget model and some implications”. In: *Letters in Biomathematics* 1.2 (2014), pp. 221–233.
- [157] ZhongPing Lee, Alan Weidemann, John Kindle, Robert Arnone, Kendall L Carder, and Curtiss Davis. “Euphotic zone depth: Its derivation and implication to ocean-color remote sensing”. In: *Journal of Geophysical Research: Oceans* 112.C3 (2007).
- [158] Olof Leimar, Michael Doebeli, and Ulf Dieckmann. “Evolution of phenotypic clusters through competition and local adaptation along an environmental gradient”. In: *Evolution: International Journal of Organic Evolution* 62.4 (2008), pp. 807–822.
- [159] Timothy M Lenton, Hermann Held, Elmar Kriegler, Jim W Hall, Wolfgang Lucht, Stefan Rahmstorf, et al. “Tipping elements in the Earth’s climate system”. In: *Proceedings of the national Academy of Sciences* 105.6 (2008), pp. 1786–1793.
- [160] Marina Lévy, Laurent Bopp, Pierre Karleskind, Laure Resplandy, Christian Éthé, and Françoise Pinsard. “Physical pathways for carbon transfers between the surface mixed layer and the ocean interior”. In: *Global Biogeochemical Cycles* 27.4 (2013), pp. 1001–1012.
- [161] KM Lewis, GL Van Dijken, and Kevin R Arrigo. “Changes in phytoplankton concentration now drive increased Arctic Ocean primary production”. In: *Science* 369.6500 (2020), pp. 198–202.
- [162] Richard C Lewontin. “The units of selection”. In: *Annual review of ecology and systematics* 1.1 (1970), pp. 1–18.
- [163] Futian Li, John Beardall, Sinéad Collins, and Kunshan Gao. “Decreased photosynthesis and growth with reduced respiration in the model diatom *Phaeodactylum tricorutum* grown under elevated CO₂ over 1800 generations”. In: *Global Change Biology* 23.1 (2017), pp. 127–137.
- [164] Guancheng Li, Lijing Cheng, Jiang Zhu, Kevin E Trenberth, Michael E Mann, and John P Abraham. “Increasing ocean stratification over the past half-century”. In: *Nature Climate Change* 10.12 (2020), pp. 1116–1123.
- [165] Guanlin Li, Michael H Cortez, Jonathan Dushoff, and Joshua S Weitz. “When to be temperate: on the fitness benefits of lysis vs. lysogeny”. In: *Virus Evolution* 6.2 (2020), veaa042.

- [166] Enhui Liao, Wenfang Lu, Xiao-Hai Yan, Yuwu Jiang, and Autumn Kidwell. “The coastal ocean response to the global warming acceleration and hiatus”. In: *Scientific reports* 5.1 (2015), pp. 1–10.
- [167] Ángel López-Urrutia and Xosé Anxelu G Morán. “Resource limitation of bacterial production distorts the temperature dependence of oceanic carbon cycling”. In: *Ecology* 88.4 (2007), pp. 817–822.
- [168] André Lwoff. “Lysogeny”. In: *Bacteriological reviews* 17.4 (1953), pp. 269–337.
- [169] Gurvan Madec and NEMO System Team. *NEMO ocean engine*. Scientific Notes of Climate Modelling Center 27. Zenodo. DOI: [10.5281/zenodo.1464816](https://doi.org/10.5281/zenodo.1464816).
- [170] Ashish A Malik, Jennifer BH Martiny, Eoin L Brodie, Adam C Martiny, Kathleen K Treseder, and Steven D Allison. “Defining trait-based microbial strategies with consequences for soil carbon cycling under climate change”. In: *The ISME journal* 14.1 (2020), pp. 1–9.
- [171] Shruti Malviya, Eleonora Scalco, Stéphane Audic, Flora Vincent, Alaguraj Veluchamy, Julie Poulain, et al. “Insights into global diatom distribution and diversity in the world’s ocean”. In: *Proceedings of the National Academy of Sciences* 113.11 (2016), E1516–E1525.
- [172] Syukuro Manabe and Kirk Bryan. “Climate calculations with a combined ocean-atmosphere model”. In: *J. Atmos. Sci* 26.4 (1969), pp. 786–789.
- [173] Susanna Manrubia, José A Cuesta, Jacobo Aguirre, Sebastian E Ahnert, Lee Altenberg, Alejandro V Cano, et al. “From genotypes to organisms: State-of-the-art and perspectives of a cornerstone in evolutionary dynamics”. In: *Physics of Life Reviews* 38 (2021), pp. 55–106.
- [174] Junwen Mao and Ting Lu. “Population-dynamic modeling of bacterial horizontal gene transfer by natural transformation”. In: *Biophysical journal* 110.1 (2016), pp. 258–268.
- [175] John H Martin, George A Knauer, David M Karl, and William W Broenkow. “VERTEX: carbon cycling in the northeast Pacific.” In: *Deep-Sea Research* 34.2 (1987), pp. 267–285.
- [176] Christopher J Marx. “Can you sequence ecology? Metagenomics of adaptive diversification”. In: *PLoS biology* 11.2 (2013), e1001487.
- [177] V Masson-Delmotte, P Zhai, A Pirani, SL Connors, C Péan, S Berger, et al. “IPCC, 2021: Climate Change 2021: The Physical Science Basis. Contribution of Working Group I to the Sixth Assessment Report of the Intergovernmental Panel on Climate Change”. In: (2021).
- [178] Sylvie Méléard and Vincent Bansaye. *Stochastic models for structured populations*. Springer, 2015.

- [179] Barbara A Methé, Karen E Nelson, Jody W Deming, Bahram Momen, Eugene Melamud, Xijun Zhang, et al. “The psychrophilic lifestyle as revealed by the genome sequence of *Colwellia psychrerythraea* 34H through genomic and proteomic analyses”. In: *Proceedings of the National Academy of Sciences* 102.31 (2005), pp. 10913–10918.
- [180] JAJ Metz. “Adaptive dynamics”. In: (2012).
- [181] Johan AJ Metz, Stefan AH Geritz, Géza Meszéna, Frans JA Jacobs, and Joost S Van Heerwaarden. “Adaptive dynamics: a geometrical study of the consequences of nearly faithful reproduction”. In: (1995).
- [182] Johan AJ Metz, Sido D Mylius, and Odo Diekmann. “When does evolution optimize? On the relation between types of density dependence and evolutionarily stable life history parameters”. In: (1996).
- [183] Thomas Mock, Robert P Otilar, Jan Strauss, Mark McMullan, Pirita Paaanen, Jeremy Schmutz, et al. “Evolutionary genomics of the cold-adapted diatom *Fragilariopsis cylindrus*”. In: *Nature* 541.7638 (2017), pp. 536–540.
- [184] Ian J Molineux and Debabrata Panja. “Popping the cork: mechanisms of phage genome ejection”. In: *Nature Reviews Microbiology* 11.3 (2013), pp. 194–204.
- [185] Adam Monier, Antònio Pagarete, Colomban de Vargas, Michael J Allen, Jean-Michel Claverie, and Hiroyuki Ogata. “Horizontal gene transfer of an entire metabolic pathway between a eukaryotic alga and its DNA virus”. In: *Genome research* 19.8 (2009), pp. 1441–1449.
- [186] Jacques Monod. “The growth of bacterial cultures”. In: *Annual review of microbiology* 3.1 (1949), pp. 371–394.
- [187] J Grey Monroe, David W Markman, Whitney S Beck, Andrew J Felton, Megan L Vahsen, and Yamina Pressler. “Ecoevolutionary dynamics of carbon cycling in the anthropocene”. In: *Trends in ecology & evolution* 33.3 (2018), pp. 213–225.
- [188] Danesh Moradigaravand and Jan Engelstädter. “The impact of natural transformation on adaptation in spatially structured bacterial populations”. In: *BMC evolutionary biology* 14.1 (2014), p. 141.
- [189] Mary Ann Moran, Elizabeth B Kujawinski, William F Schroer, Shady A Amin, Nicholas R Bates, Erin M Bertrand, et al. “Microbial metabolites in the marine carbon cycle”. In: *Nature Microbiology* 7.4 (2022), pp. 508–523.
- [190] Hélène Morlon, Todd L Parsons, and Joshua B Plotkin. “Reconciling molecular phylogenies with the fossil record”. In: *Proceedings of the National Academy of Sciences* 108.39 (2011), pp. 16327–16332.
- [191] Richard H Moss, Jae A Edmonds, Kathy A Hibbard, Martin R Manning, Steven K Rose, Detlef P Van Vuuren, et al. “The next generation of scenarios for climate change research and assessment”. In: *Nature* 463.7282 (2010), pp. 747–756.

- [192] Marco Mühlenbruch, Hans-Peter Grossart, Falk Eigemann, and Maren Voss. “Mini-review: Phytoplankton-derived polysaccharides in the marine environment and their interactions with heterotrophic bacteria”. In: *Environmental microbiology* 20.8 (2018), pp. 2671–2685.
- [193] Mario E Muscarella, Xia Meng Howey, and Jay T Lennon. “Trait-based approach to bacterial growth efficiency”. In: *Environmental Microbiology* 22.8 (2020), pp. 3494–3504.
- [194] Toshi Nagata. “Organic matter-bacteria interactions in seawater”. In: *Microbial ecology of the oceans* 2 (2008), pp. 207–241.
- [195] Phillip Nazarian, Frances Tran, and James Q Boedicker. “Modeling multispecies gene flow dynamics reveals the unique roles of different horizontal gene transfer mechanisms.” In: *Frontiers in microbiology* 9 (2018), p. 2978.
- [196] Rene Niehus, Sara Mitri, Alexander G Fletcher, and Kevin R Foster. “Migration and horizontal gene transfer divide microbial genomes into multiple niches”. In: *Nature communications* 6 (2015), p. 8924.
- [197] Philipp Noll, Lars Lilge, Rudolf Hausmann, and Marius Henkel. “Modeling and exploiting microbial temperature response”. In: *Processes* 8.1 (2020), p. 121.
- [198] Jon Norberg, Mark C Urban, Mark Vellend, Christopher A Klausmeier, and Nicolas Loeuille. “Eco-evolutionary responses of biodiversity to climate change”. In: *Nature climate change* 2.10 (2012), pp. 747–751.
- [199] Siobhán O’Brien, David J Hodgson, and Angus Buckling. “The interplay between microevolution and community structure in microbial populations”. In: *Current opinion in biotechnology* 24.4 (2013), pp. 821–825.
- [200] Nancy Obeng, Akbar Adjie Pratama, and Jan Dirk van Elsas. “The significance of mutualistic phages for bacterial ecology and evolution”. In: *Trends in microbiology* 24.6 (2016), pp. 440–449.
- [201] Ingrid Obernosterer, M Fourquez, and S Blain. “Fe and C co-limitation of heterotrophic bacteria in the naturally fertilized region off the Kerguelen Islands”. In: *Biogeosciences* 12.6 (2015), pp. 1983–1992.
- [202] Howard Ochman, Jeffrey G Lawrence, and Eduardo A Groisman. “Lateral gene transfer and the nature of bacterial innovation”. In: *nature* 405.6784 (2000), p. 299.
- [203] Pedro H Oliveira, Marie Touchon, and Eduardo PC Rocha. “Regulation of genetic flux between bacteria by restriction–modification systems”. In: *Proceedings of the National Academy of Sciences* 113.20 (2016), pp. 5658–5663.
- [204] Melissa M Omand, Rama Govindarajan, Jing He, and Amala Mahadevan. “Sinking flux of particulate organic matter in the oceans: Sensitivity to particle characteristics”. In: *Scientific reports* 10.1 (2020), pp. 1–16.

- [205] Andreas Oschlies, Peter Brandt, Lothar Stramma, and Sunke Schmidtko. “Drivers and mechanisms of ocean deoxygenation”. In: *Nature Geoscience* 11.7 (2018), pp. 467–473.
- [206] Daniel Padfield, Genevieve Yvon-Durocher, Angus Buckling, Simon Jennings, and Gabriel Yvon-Durocher. “Rapid evolution of metabolic traits explains thermal adaptation in phytoplankton”. In: *Ecology letters* 19.2 (2016), pp. 133–142.
- [207] Evgeny A Pakhomov, Leonid K Pshenichnov, Anatoly Krot, Valery Paramonov, Ilia Slypko, and Pavel Zabroda. “Zooplankton Distribution and Community Structure in the Pacific and Atlantic Sectors of the Southern Ocean during Austral Summer 2017–18: A Pilot Study Conducted from Ukrainian Long-Liners”. In: *Journal of Marine Science and Engineering* 8.7 (2020), p. 488.
- [208] Csaba Pal, Marià D Macià, Antonio Oliver, Ira Schachar, and Angus Buckling. “Co-evolution with viruses drives the evolution of bacterial mutation rates”. In: *Nature* 450.7172 (2007), pp. 1079–1081.
- [209] Christos Panagiotopoulos, Mireille Pujo-Pay, Mar Benavides, France Van Wambeke, and Richard Sempéré. “The composition and distribution of semi-labile dissolved organic matter across the southwest Pacific”. In: (2019).
- [210] Geoffrey A Parker and J Maynard Smith. “Optimality theory in evolutionary biology”. In: *Nature* 348.6296 (1990), pp. 27–33.
- [211] Uta Passow and Craig A Carlson. “The biological pump in a high CO₂ world”. In: *Marine Ecology Progress Series* 470 (2012), pp. 249–271.
- [212] Xuefeng Peng, Sarah E Fawcett, Nicolas Van Oostende, Martin J Wolf, Dario Marconi, Daniel M Sigman, et al. “Nitrogen uptake and nitrification in the subarctic North Atlantic Ocean”. In: *Limnology and Oceanography* 63.4 (2018), pp. 1462–1487.
- [213] Octavio Perez-Garcia, Gavin Lear, and Naresh Singhal. “Metabolic network modeling of microbial interactions in natural and engineered environmental systems”. In: *Frontiers in microbiology* 7 (2016), p. 673.
- [214] Thomas Pfeiffer, Stefan Schuster, and Sebastian Bonhoeffer. “Cooperation and competition in the evolution of ATP-producing pathways”. In: *Science* 292.5516 (2001), pp. 504–507.
- [215] Anh Le-Duy Pham, Olivier Aumont, Lavenia Ratnarajah, and Alessandro Tagliabue. “Examining the interaction between free-living bacteria and iron in the global ocean”. In: *Earth and Space Science Open Archive* (2021), p. 52.
- [216] Eric R Pianka. “On r- and K-selection”. In: *The American Naturalist* 104.940 (1970), pp. 592–597.
- [217] Martin F Polz and Otto X Cordero. “Bacterial evolution: genomics of metabolic trade-offs”. In: *Nature microbiology* 1.11 (2016), pp. 1–2.

Bibliography

- [218] Lawrence R Pomeroy. “The ocean’s food web, a changing paradigm”. In: *Bioscience* 24.9 (1974), pp. 499–504.
- [219] Lawrence R Pomeroy, PETER J leB. WILLIAMS, Farooq Azam, and John E Hobbie. “The microbial loop”. In: *Oceanography* 20.2 (2007), pp. 28–33.
- [220] Ovidiu Popa and Tal Dagan. “Trends and barriers to lateral gene transfer in prokaryotes”. In: *Current opinion in microbiology* 14.5 (2011), pp. 615–623.
- [221] Ovidiu Popa, Einat Hazkani-Covo, Giddy Landan, William Martin, and Tal Dagan. “Directed networks reveal genomic barriers and DNA repair bypasses to lateral gene transfer among prokaryotes”. In: *Genome research* 21.4 (2011), pp. 599–609.
- [222] HO Pörtner, DC Roberts, M Tignor, ES Poloczanska, K Mintenbeck, A Alegría, et al. “IPCC, 2022: Climate Change 2022: Impacts, Adaptation, and Vulnerability. Contribution of Working Group II to the Sixth Assessment Report of the Intergovernmental Panel on Climate Change”. In: (2022).
- [223] Yoav Raz and Emmanuel Tannenbaum. “The influence of horizontal gene transfer on the mean fitness of unicellular populations in static environments”. In: *Genetics* 185.1 (2010), pp. 327–337.
- [224] Rosemary J Redfield. “Evolution of bacterial transformation: is sex with dead cells ever better than no sex at all?” In: *Genetics* 119.1 (1988), pp. 213–221.
- [225] Ulf Riebesell and Jean-Pierre Gattuso. “Lessons learned from ocean acidification research”. In: *Nature Climate Change* 5.1 (2015), pp. 12–14.
- [226] Ulf Riebesell, Arne Körtzinger, and Andreas Oschlies. “Sensitivities of marine carbon fluxes to ocean change”. In: *Proceedings of the National Academy of Sciences* 106.49 (2009), pp. 20602–20609.
- [227] Jörgen Ripa and Ulf Dieckmann. “Mutant invasions and adaptive dynamics in variable environments”. In: *Evolution* 67.5 (2013), pp. 1279–1290.
- [228] Richard B Rivkin and Louis Legendre. “Biogenic carbon cycling in the upper ocean: effects of microbial respiration”. In: *Science* 291.5512 (2001), pp. 2398–2400.
- [229] Beltran Rodriguez-Brito, LinLin Li, Linda Wegley, Mike Furlan, Florent Angly, Mya Breitbart, et al. “Viral and microbial community dynamics in four aquatic environments”. In: *The ISME journal* 4.6 (2010), pp. 739–751.
- [230] Benjamin RK Roller, Steven F Stoddard, and Thomas M Schmidt. “Exploiting rRNA operon copy number to investigate bacterial reproductive strategies”. In: *Nature microbiology* 1.11 (2016), pp. 1–7.
- [231] Howard D Rundle and Patrik Nosil. “Ecological speciation”. In: *Ecology letters* 8.3 (2005), pp. 336–352.

- [232] Christopher L Sabine, Richard A Feely, Nicolas Gruber, Robert M Key, Kitack Lee, John L Bullister, et al. “The oceanic sink for anthropogenic CO₂”. In: *science* 305.5682 (2004), pp. 367–371.
- [233] Mustafa Saifuddin, Jennifer M Bhatnagar, Daniel Segrè, and Adrien C Finzi. “Microbial carbon use efficiency predicted from genome-scale metabolic models”. In: *Nature communications* 10.1 (2019), pp. 1–10.
- [234] Hugo Sarmiento, José M Montoya, Evaristo Vázquez-Domínguez, Dolors Vaqué, and Josep M Gasol. “Warming effects on marine microbial food web processes: how far can we go when it comes to predictions?” In: *Philosophical Transactions of the Royal Society B: Biological Sciences* 365.1549 (2010), pp. 2137–2149.
- [235] Jorge L Sarmiento and Nicolas Gruber. “Sinks for anthropogenic carbon”. In: *Physics today* 55.8 (2002), pp. 30–36.
- [236] Jorge L Sarmiento and Nicolas Gruber. *Ocean biogeochemical dynamics*. Princeton University Press, 2006.
- [237] Boris Sauterey, Benjamin Charnay, Antonin Affholder, Stéphane Mazevet, and Régis Ferrière. “Co-evolution of primitive methane-cycling ecosystems and early Earth’s atmosphere and climate”. In: *Nature communications* 11.1 (2020), pp. 1–12.
- [238] Boris Sauterey, Ben Ward, Jonathan Rault, Chris Bowler, and David Claessen. “The implications of eco-evolutionary processes for the emergence of marine plankton community biogeography”. In: *The American Naturalist* 190.1 (2017), pp. 116–130.
- [239] Boris Sauterey, Ben A Ward, Michael J Follows, Chris Bowler, and David Claessen. “When everything is not everywhere but species evolve: an alternative method to model adaptive properties of marine ecosystems”. In: *Journal of plankton research* 37.1 (2015), pp. 28–47.
- [240] C Schaum, Samuel Barton, Elvire Bestion, Angus Buckling, Bernardo Garcia-Carreras, Paula Lopez, et al. “Adaptation of phytoplankton to a decade of experimental warming linked to increased photosynthesis”. In: *Nature Ecology & Evolution* 1.4 (2017), pp. 1–7.
- [241] Matias Scheinin, Ulf Riebesell, Tatiana A Rynearson, Kai T Lohbeck, and S Collins. “Experimental evolution gone wild”. In: *Journal of the Royal Society Interface* 12.106 (2015), p. 20150056.
- [242] Thomas Scheuerl, Meirion Hopkins, Reuben W Nowell, Damian W Rivett, Timothy G Barraclough, and Thomas Bell. “Bacterial adaptation is constrained in complex communities”. In: *Nature Communications* 11.1 (2020), pp. 1–8.
- [243] Siegfried Schloissnig, Manimozhiyan Arumugam, Shinichi Sunagawa, Makedonka Mitreva, Julien Tap, Ana Zhu, et al. “Genomic variation landscape of the human gut microbiome”. In: *Nature* 493.7430 (2013), pp. 45–50.

- [244] Sunke Schmidtko, Lothar Stramma, and Martin Visbeck. “Decline in global oceanic oxygen content during the past five decades”. In: *Nature* 542.7641 (2017), pp. 335–339.
- [245] Oswald J Schmitz. “Global climate change and the evolutionary ecology of ecosystem functioning”. In: *Annals of the New York Academy of Sciences* 1297.1 (2013), pp. 61–72.
- [246] Daniel Segre, Dennis Vitkup, and George M Church. “Analysis of optimality in natural and perturbed metabolic networks”. In: *Proceedings of the National Academy of Sciences* 99.23 (2002), pp. 15112–15117.
- [247] Emma J Shelford and Curtis A Suttle. “Virus-mediated transfer of nitrogen from heterotrophic bacteria to phytoplankton”. In: *Biogeosciences* 15.3 (2018), pp. 809–819.
- [248] Meinhard Simon, Hans-Peter Grossart, Bernd Schweitzer, and Helle Ploug. “Microbial ecology of organic aggregates in aquatic ecosystems”. In: *Aquatic microbial ecology* 28.2 (2002), pp. 175–211.
- [249] JMPGR Smith and George R Price. “The logic of animal conflict”. In: *Nature* 246.5427 (1973), pp. 15–18.
- [250] Stephen C Stearns. “Trade-offs in life-history evolution”. In: *Functional ecology* 3.3 (1989), pp. 259–268.
- [251] Jan Taucher and Andreas Oschlies. “Can we predict the direction of marine primary production change under global warming?” In: *Geophysical Research Letters* 38.2 (2011).
- [252] Core Writing Team, RK Pachauri, and LA Meyer. “IPCC, 2014: Climate Change 2014: Synthesis Report. Contribution of Working Groups I, II and III to the Fifth Assessment Report of the Intergovernmental Panel on Climate Change”. In: (2021).
- [253] Marco Tedesco, Sarah Doherty, Xavier Fettweis, Patrick Alexander, Jeyavinoth Jeyaratnam, and Julienne Stroeve. “The darkening of the Greenland ice sheet: trends, drivers, and projections (1981–2100)”. In: *The Cryosphere* 10.2 (2016), pp. 477–496.
- [254] Roger Temam. *Navier-Stokes equations: theory and numerical analysis*. Vol. 343. American Mathematical Soc., 2001.
- [255] Mridul K Thomas, Colin T Kremer, Christopher A Klausmeier, and Elena Litchman. “A global pattern of thermal adaptation in marine phytoplankton”. In: *Science* 338.6110 (2012), pp. 1085–1088.
- [256] L Tjhuis, Mark CM Van Loosdrecht, and Jv Heijnen. “A thermodynamically based correlation for maintenance Gibbs energy requirements in aerobic and anaerobic chemotrophic growth”. In: *Biotechnology and bioengineering* 42.4 (1993), pp. 509–519.
- [257] Marie Touchon, Jorge A Moura De Sousa, and Eduardo PC Rocha. “Embracing the enemy: the diversification of microbial gene repertoires by phage-mediated horizontal gene transfer”. In: *Current opinion in microbiology* 38 (2017), pp. 66–73.

- [258] Sachia J Traving, Uffe H Thygesen, Lasse Riemann, and Colin A Stedmon. “A model of extracellular enzymes in free-living microbes: which strategy pays off?” In: *Appl. Environ. Microbiol.* 81.21 (2015), pp. 7385–7393.
- [259] Kevin E Trenberth, Lesley Smith, Taotao Qian, Aiguo Dai, and John Fasullo. “Estimates of the global water budget and its annual cycle using observational and model data”. In: *Journal of Hydrometeorology* 8.4 (2007), pp. 758–769.
- [260] Anastasios Tsoularis and James Wallace. “Analysis of logistic growth models”. In: *Mathematical biosciences* 179.1 (2002), pp. 21–55.
- [261] Jefferson T Turner. “Zooplankton fecal pellets, marine snow, phytodetritus and the ocean’s biological pump”. In: *Progress in Oceanography* 130 (2015), pp. 205–248.
- [262] Mark C Urban, Luc De Meester, Mark Vellend, Robby Stoks, and Joost Vanoverbeke. “A crucial step toward realism: responses to climate change from an evolving meta-community perspective”. In: *Evolutionary Applications* 5.2 (2012), pp. 154–167.
- [263] Evaristo Vázquez-Domínguez, Dolors Vaque, and Josep M Gasol. “Ocean warming enhances respiration and carbon demand of coastal microbial plankton”. In: *Global Change Biology* 13.7 (2007), pp. 1327–1334.
- [264] M Vichi and S Masina. “Skill assessment of the PELAGOS global ocean biogeochemistry model over the period 1980–2000”. In: *Biogeosciences* 6.11 (2009), pp. 2333–2353.
- [265] JAGM de Visser. “Genotype-phenotype maps and the predictability of evolution. Comment on ‘From genotypes to organisms: State-of-the-art and perspectives of a cornerstone in evolutionary dynamics’ by Susanna Manrubia et al.” In: *Physics of Life Reviews* 39 (2021), pp. 79–81.
- [266] Tyler Volk and Martin I Hoffert. “Ocean carbon pumps: Analysis of relative strengths and efficiencies in ocean-driven atmospheric CO₂ changes”. In: *The carbon cycle and atmospheric CO₂: natural variations Archean to present* 32 (1985), pp. 99–110.
- [267] Sophia Walther, Maximilian Voigt, Tea Thum, Alemu Gonsamo, Yongguang Zhang, Philipp Köhler, et al. “Satellite chlorophyll fluorescence measurements reveal large-scale decoupling of photosynthesis and greenness dynamics in boreal evergreen forests”. In: *Global change biology* 22.9 (2016), pp. 2979–2996.
- [268] Nathan G Walworth, Michael D Lee, Fei-Xue Fu, David A Hutchins, and Eric A Webb. “Molecular and physiological evidence of genetic assimilation to high CO₂ in the marine nitrogen fixer *Trichodesmium*”. In: *Proceedings of the National Academy of Sciences* 113.47 (2016), E7367–E7374.
- [269] Nathan G Walworth, Emily J Zakem, John P Dunne, Sinéad Collins, and Naomi M Levine. “Microbial evolutionary strategies in a dynamic ocean”. In: *Proceedings of the National Academy of Sciences* 117.11 (2020), pp. 5943–5948.

Bibliography

- [270] Peter J Wangersky. “Lotka-Volterra population models”. In: *Annual Review of Ecology and Systematics* 9.1 (1978), pp. 189–218.
- [271] Ben A Ward, Sinead Collins, Stephanie Dutkiewicz, Samantha Gibbs, Paul Bown, Andy Ridgwell, et al. “Considering the role of adaptive evolution in models of the ocean and climate system”. In: *Journal of advances in modeling earth systems* 11.11 (2019), pp. 3343–3361.
- [272] Andrew J Watson, Ute Schuster, Jamie D Shutler, Thomas Holding, Ian GC Ashton, Peter Landschützer, et al. “Revised estimates of ocean-atmosphere CO₂ flux are consistent with ocean carbon inventory”. In: *Nature communications* 11.1 (2020), pp. 1–6.
- [273] Joshua Weitz. *Quantitative viral ecology*. Princeton University Press, 2016.
- [274] Joshua S Weitz, Charles A Stock, Steven W Wilhelm, Lydia Bourouiba, Maureen L Coleman, Alison Buchan, et al. “A multitrophic model to quantify the effects of marine viruses on microbial food webs and ecosystem processes”. In: *The ISME journal* 9.6 (2015), pp. 1352–1364.
- [275] Carolin C Wendling, Dominik Refardt, and Alex R Hall. “Fitness benefits to bacteria of carrying prophages and prophage-encoded antibiotic-resistance genes peak in different environments”. In: *Evolution* 75.2 (2021), pp. 515–528.
- [276] Charles H Wigington, Derek Sonderegger, Corina PD Brussaard, Alison Buchan, Jan F Finke, Jed A Fuhrman, et al. “Re-examination of the relationship between marine virus and microbial cell abundances”. In: *Nature microbiology* 1.3 (2016), pp. 1–9.
- [277] Steven W Wilhelm and Curtis A Suttle. “Viruses and nutrient cycles in the sea: viruses play critical roles in the structure and function of aquatic food webs”. In: *Bioscience* 49.10 (1999), pp. 781–788.
- [278] Richard G Williams and Michael J Follows. *Ocean dynamics and the carbon cycle: Principles and mechanisms*. Cambridge University Press, 2011.
- [279] K Eric Wommack and Rita R Colwell. “Virioplankton: viruses in aquatic ecosystems”. In: *Microbiology and molecular biology reviews* 64.1 (2000), pp. 69–114.
- [280] L Zakharova, KM Meyer, and M Seifan. “Trait-based modelling in ecology: a review of two decades of research”. In: *Ecological Modelling* 407 (2019), p. 108703.
- [281] Jan Zalasiewicz, Colin Waters, and Mark Williams. “The anthropocene”. In: *Geologic Time Scale 2020*. Elsevier, 2020, pp. 1257–1280.
- [282] Shijie Zhao, Tami D Lieberman, Mathilde Poyet, Kathryn M Kauffman, Sean M Gibbons, Mathieu Groussin, et al. “Adaptive evolution within gut microbiomes of healthy people”. In: *Cell host & microbe* 25.5 (2019), pp. 656–667.

Appendix A

Acronyms

BGE	Bacterial growth efficiency
BP	Bacterial production
BR	Bacterial respiration
DIC	Dissolved inorganic carbon
DIN	Dissolved inorganic nitrogen
DOC	Dissolved organic carbon
DOM	Dissolved organic matter
DON	Dissolved organic nitrogen
ESM	Earth system model
ESS	Evolutionary stable strategy
GCM	Global circulation model
GTP	Gene transducing particle
HGT	Horizontal gene transfer
IBM	Individual-based model
LDOC	Labile dissolved organic carbon
MLE	Microbial loop efficiency
NP	New production
NPP	Net primary production
POM	Particulate organic matter
PP	Primary production
RCP	Representative Concentration Pathways
RP	Regenerated production
TSS	Trait substitution sequence

Appendix B

Résumé long

L'objectif de cette thèse est d'évaluer et de quantifier le rôle potentiel de l'adaptation des bactéries hétérotrophes dans la réponse de la boucle microbienne au changement climatique. A notre connaissance, une telle étude éco-évolutive des bactéries n'avait pas été menée auparavant dans l'océan, contrairement aux écosystèmes terrestres tels que les sols. En océanographie, l'accent est généralement mis sur le phytoplancton en raison de leur capacité d'adaptation aussi rapide que les bactéries hétérotrophes et de leur importance dans la séquestration du carbone.

Nous détaillons l'importance de l'océan dans la régulation du climat mondial dans le Chapitre 1 et soulignons le rôle des microorganismes dans la capture du carbone atmosphérique. Un intérêt particulier est porté à la boucle microbienne et à leur capacité à recycler la matière organique dissoute (DOM) en nutriments. Nous présentons les menaces que le changement climatique fait peser sur les écosystèmes océaniques et leur rétroaction potentielle sur le cycle du carbone, ainsi que les efforts actuels de modélisation pour prédire le climat au moyen de modèles du système terrestre. La génération actuelle de modèles n'inclut pas l'adaptation des micro-organismes par la sélection naturelle qui pourrait pourtant avoir un impact important sur la réponse de la pompe biologique au changement climatique. Nous présentons enfin le cadre évolutif et la portée globale de la thèse, qui est de développer un modèle éco-évolutif de la boucle microbienne et de résoudre sa réponse au changement climatique.

Le Chapitre 2 est consacré au développement du module de la boucle microbienne utilisé pour la majeure partie de l'étude éco-évolutive. Nous utilisons un modèle à compartiments basé sur les traits fonctionnels, composé d'un réservoir de biomasse bactérienne et d'un réservoir de matière organique dissoute. Ce module est conçu pour être intégré dans une classe plus large de modèles. L'efficacité de croissance bactérienne (BGE) est soumise à la sélection naturelle, limitée par un compromis entre l'acquisition de ressources et la tolérance au stress. Si un équilibre écologique stable est possible dans le modèle plus large,

il est possible de déterminer localement une stratégie évolutive stable des populations bactériennes. Nous intégrons enfin le module dans un modèle simple de la boucle microbienne dans la zone aphotique : le système est limité par l'apport de DOM, et le pouvoir de reminéralisation total de la boucle microbienne est supérieur à la somme des contributions individuelles. Le réchauffement de l'océan diminue la concentration de DOM à l'état d'équilibre, forçant les bactéries à investir davantage dans l'acquisition de ressources, ce qui diminue la biomasse bactérienne mais augmente la reminéralisation totale. La stratification de l'océan diminue la reminéralisation totale et augmente le temps de renouvellement de la DOM, sans induire une réponse adaptative des populations bactériennes.

Nous couplons le modèle de boucle microbienne à un modèle d'écosystème de surface de la mer dans le Chapitre 3 pour prédire la réponse de la production primaire au réchauffement de l'océan. Nous trouvons que la réponse écophysologique de la production primaire au réchauffement est conduite par une diminution de la production régénérée qui dépend de la disponibilité des nutriments. Dans les environnements pauvres en nutriments, la perte de la production régénérée est due à la diminution de l'activité de la boucle microbienne. Cependant, cette réponse écophysologique peut être opposée voire inversée par l'adaptation bactérienne, en particulier dans les environnements froids : les bactéries hétérotrophes ayant une efficacité de croissance plus faible sont sélectionnées, ce qui renforce le comportement de "liaison" de la boucle microbienne, augmentant à la fois la production nouvelle et la production régénérée. Dans les environnements froids et riches comme l'océan Arctique, l'effet de l'adaptation bactérienne sur la production primaire dépasse la réponse écophysologique.

Afin de générer des prédictions quantitatives de l'influence de l'adaptation bactérienne sur le cycle du carbone océanique, nous développons une nouvelle méthode d'intégration des processus éco-évolutifs aux modèles du système terrestre dans le Chapitre 4. Pour contourner le coût de calcul d'une simulation complète de l'évolution, nous nous appuyons sur une description phénoménologique de l'adaptation des traits au niveau de la communauté. L'application de ce cadre à l'étude de l'adaptation de l'efficacité de la croissance bactérienne permet d'obtenir une distribution de la BGE proche des prédictions du modèle d'écosystème de la surface océanique. Sous une augmentation de la température océanique, nous constatons que l'adaptation bactérienne peut ajouter une incertitude significative aux prévisions de la production primaire : dans notre simulation, l'augmentation de la production primaire était 2,8% plus élevée en raison de processus éco-évolutifs.

Les bactériophages sont introduits dans le Chapitre 5 pour étudier lequel leur influence écologique et biogéochimique sur l'adaptation bactérienne et la boucle microbienne. En faisant passer le système d'une limitation de type "bottom-up" à une limitation de type "top-down", les virus diminuent la biomasse bactérienne et augmentent la concentration de DOM. Dans les environnements pauvres en DOM, l'augmentation des concentrations de DOM à l'état d'équilibre favorise la stratégie d'acquisition de ressources des bactéries, entraî-

nant une baisse des valeurs de BGE. Selon le coût relatif du rendement de croissance par rapport à la tolérance au stress, la lyse peut soit augmenter l'investissement dans le rendement (c'est-à-dire une augmentation du BGE), soit augmenter l'investissement dans la tolérance au stress (c'est-à-dire une diminution du BGE). Globalement, les effets des bactériophages dans un environnement constant augmentent la reminéralisation du DOM. La stratification de l'océan diminue à la fois le ratio de reminéralisation et la reminéralisation totale de la DOM, et pourrait potentiellement conduire les populations spécialisées de phages à l'extinction.

Dans le Chapitre 6, nous développons un modèle individu-centré de la transduction, un mécanisme de transfert horizontal de gènes médié par les bactériophages, pour résoudre l'effet des bactériophages sur la vitesse d'adaptation des bactéries. En cas de sélection directionnelle (éloignée de l'optimum), l'effet du transfert d'allèles bénéfiques domine et la transduction tend à accélérer l'adaptation. Lorsque l'on s'attend à une sélection stabilisante (près de l'optimum), la transduction aplatit le "fitness landscape" et génère une grande quantité de stochasticité dans la trajectoire adaptative de la population, ce qui entrave l'adaptation. En cas de sélection perturbatrice, la transduction peut soit limiter (comme le ferait la recombinaison sexuelle), soit promouvoir la diversification phénotypique. Comme la dérive génétique dans les populations finies, la transduction confère une probabilité positive de fixation à tout allèle (sélectionné positivement ou négativement) même si la population bactérienne est très grande. Comme d'autres modèles de transfert horizontal de gènes, la transduction devrait faciliter l'adaptation en réponse aux changements environnementaux, lorsque la population est suffisamment éloignée de son optimum évolutif, malgré l'effet écologique négatif de l'infection virale.

Dans l'ensemble, cette thèse prouve l'importance de la voie de recyclage des nutriments dans la productivité des océans en donnant une première évaluation de la boucle de rétroaction éco-évolutive induite par la boucle microbienne. En raison de l'augmentation des températures et de l'intensification de la stratification, le changement climatique conduit à des océans plus oligotrophes, poussant les bactéries hétérotrophes à investir davantage dans les mécanismes de collecte des ressources. Cela entraîne une augmentation de la respiration, alimentant la voie du recyclage : dans l'océan de surface, cela conduit à une augmentation de la production régénérée ; plus profondément dans la colonne d'eau, une reminéralisation accrue pourrait atténuer l'effet de la stratification en augmentant le flux ascendant de nitrate. Les bactériophages tendent à renforcer le pouvoir de recyclage de la boucle microbienne et sa réponse au changement climatique. En augmentant la reminéralisation et en alimentant une production nouvelle et régénérée, la boucle microbienne génère une boucle de rétroaction négative au changement climatique. Mais en même temps, l'augmentation de la concentration de carbone inorganique dissous dans l'océan pourrait intensifier l'acidification, fournissant une boucle de rétroaction positive à cette partie du système.